Synthesis of Diblock Copolymer Nanoparticles via Polymerisation-Induced Self-Assembly

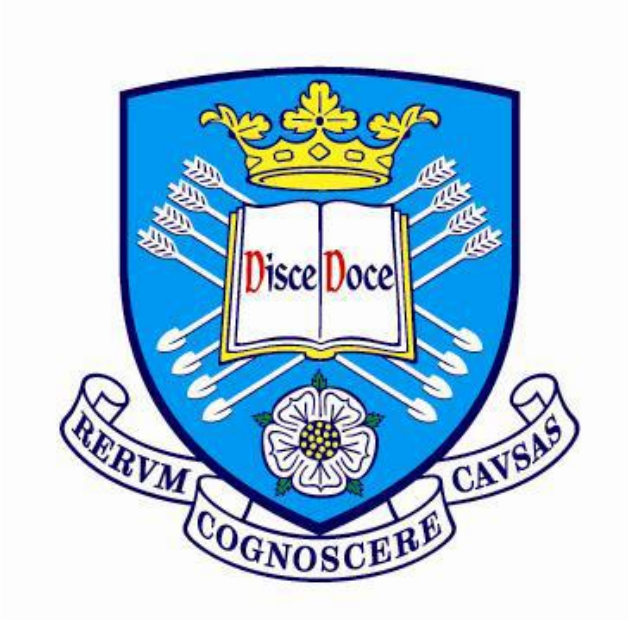

Victoria Jane Cunningham

Department of Chemistry
The University of Sheffield

Submitted to the University of Sheffield

In fulfilment of the requirements for the award of

Doctor of Philosophy

June 2016

Declaration

The work described in this thesis was carried out at the University of Sheffield between October 2012 and June 2016 and has not been submitted, either wholly or in part, for this or any other degree. All work is the original work of the author, except where acknowledged by references.

Signature: _____

V. J. Cunningham June 2016

Acknowledgements

First of all I'd like to thank my supervisor, Prof. Steve Armes. Your ideas, knowledge and memory are incredible. Thank you for all the opportunities since joining the Armes group as a Masters student; including a placement in Australia and attending multiple international conferences. Thank you for always having time to read any piece of work given to you and for improving my writing skills.

Thank you to the EPSRC for funding my PhD and to my industrial sponsors Ashland. I'd like to thanks Osama Musa for his ideas and discussions during all our telecom meetings as well as providing a very interesting monomer to work with. Alan Fernyhough, Sheila Murphy and Annie Lu are also thanked for their help at various stages during my PhD.

For all their help with analysis techniques, Sue Bradshaw (NMR) and Svetomir Tzokov (TEM). Yin Ning for SEM imaging and Abdullah Alswieleh for the surface patterning work and AFM.

A big thank you to all Armes group members past and present, you have all been amazing. The Summer BBQs, Christmas meals, Armes group bake off and ArmesFest500 would not be the same without you all. Liam Ratcliffe for introducing me to the world of RAFT and for allowing me to share your fume cupboard for 3 years! Nick Warren for answering all my stupid questions and always being on hand to fix a GPC! The latest doctors of the group Joe Lovett and Matt Derry, you both beat me to it but we all kept each other going from our first day. Mark Williams for reintroducing me to netball, as well as passing on your Pickering emulsion knowledge. Charlotte Morse (Mable, Maybel…), Amy Cockram and Kate Kirkham for always being there for a chat, I always know the corner of F3 I can go for a welcomed distraction from work. Lizzy Jones and Sarah Canning a massive thank you for all the dinners, cocktails, theatre trips, netball matches etc. over the last four years.

Alex, Caitlin, Chrissie, Laura and Joe for being the best housemates during my first four years at university. Without the enjoyment of my undergraduate studies with you all I wouldn't have stayed another four years!

Finally, my family, thank you for everything. My amazing sister Sarah who is always there for a chat, giggle or dance around the kitchen (providing you're in the country!). My brother Chris for encouraging me to do science, Michelle and the boys for all the fun and games when I come to visit. My Grandparents for all their kind words of support and Auntie Pip for offering me a place to stay on the other side of the world! The biggest thank you goes to my parents; there was a time when you didn't even think I'd get GCSEs! Your continued support, help and encouragement has motivated me to always 'try my best' and to you both I dedicate this thesis.

Publications

Primary publications resulting from work in this thesis

"Poly(glycerol monomethacrylate)-poly(benzyl methacrylate) diblock copolymer nanoparticles via RAFT emulsion polymerisation: synthesis, characterisation and interfacial activity" V. J. Cunningham, A. M. Alswieleh, K. L. Thompson, M. Williams, G. J. Leggett, S. P. Armes and O. M. Musa, *Macromolecules*, **2014**, *47*, 5613-5623.

"Synthesis, characterisation and Pickering emulsifier performance of poly(stearyl methacrylate)-poly(*N*-2-(methacryloyloxy)ethyl pyrrolidone) diblock copolymer nano-objects *via* RAFT dispersion polymerisation" V. J. Cunningham, S. P. Armes and O. M. Musa, *Polymer Chemistry*, **2016**, *7*, 1882-1891.

"RAFT aqueous dispersion polymerization of *N*-(2-(methacryloyloxy)ethyl)pyrrolidone: a convenient low viscosity route to high molecular weight water-soluble copolymers" V. J. Cunningham, M. J. Derry, L. A. Fielding, S. P. Armes and O. M. Musa, *Macromolecules*, **2016**, *49*, 4520-4533.

"Poly(*N*-2-(methacryloyloxy)ethyl pyrrolidone)-poly(benzyl methacrylate) diblock copolymer nano-objects via RAFT alcoholic dispersion polymerisation in ethanol" V. J. Cunningham, Y. Ning, S. P. Armes and O. M. Musa, *Polymer*, **2016**, http://dx.doi.org/10.1016/j.polymer.2016.07.072.

Secondary publications resulting from work in the thesis

"Are block copolymer worms more effective Pickering emulsifiers than block copolymer spheres?" K. L. Thompson, C. J. Mable, A. Cockram, N. J. Warren, V. J. Cunningham, E. R. Jones, R. Verber, S. P. Armes, *Soft Matter*, **2014**, *10*, 8615-8626.

Other publications

"Tuning the critical gelation temperature of thermoresponsive diblock copolymer worm gels" V. J. Cunningham, L. P. D. Ratcliffe, A. Blanazs, N. J. Warren, A. J. Smith, O. O. Mykhaylyk, S. P. Armes, *Polymer Chemistry*, **2014**, *5*, 6307-6317.

"Determining the effective density and stabilizer layer thickness of sterically-stabilized nanoparticles" B. Akpinar, L. A. Fielding, V. J. Cunningham, Y. Ning, O. O. Mykhaylyk, P. W. Fowler and S. P. Armes, *Macromolecules*, **2016**, 49, 5160-5171.

Patent Applications

1. 'Synthesis and characterisation of poly(stearyl methacrylate)-poly(*N*-2-(methacryloyloxy)ethyl pyrrolidone) diblock copolymer nano-objects via RAFT dispersion polymerisation in *n*-dodecane'

Inventors: Osama M. Musa, Victoria J. Cunningham and Steven P. Armes

Provisional patent filed in the USA, ISP-3897, 62/277240, 11-Jan-2016

2. 'RAFT aqueous dispersion polymerization of *N*-2-(methacryloyloxy)ethyl pyrrolidone: a convenient low-viscosity route to high molecular weight water-soluble copolymers'

Inventors: Osama M. Musa, Victoria J. Cunningham and Steven P. Armes

Provisional patent filed in the USA, ISP-3902, 62/323121, 15-Apr-2016

3. 'Poly(*N*-2-(methacryloyloxy)ethyl pyrrolidone)-poly(benzyl methacrylate) diblock copolymer nano-objects via RAFT alcoholic dispersion polymerisation in ethanol'

Inventors: Osama M. Musa, Victoria J. Cunningham and Steven P. Armes

Provisional patent filed in the USA, ISP-3928, 62/346719, 07-Jun-2016

Conferences

June 2013	*Poster presentation* at Macro Group UK Young Researcher Meeting, Nottingham, UK.
August 2013	*Poster presentation* at 10th IUPAC International Conference on Advanced Polymers via Macromolecular Engineering, Durham, UK.
July 2014	*Oral presentation* and *poster presentation* at UK Colloids 2014, London, UK.
August 2014	*Oral presentation* at the 248th National Meeting of the ACS, San Francisco, USA.
January 2015	*Poster presentation* at COOPOL - Intensifying a 100 Year Old Process: Control of Emulsion Polymerisation, Frankfurt, Germany.
May 2015	*Poster presentation* at Frontiers of Polymer Science, Lake Garda, Italy.
August 2015	*Oral presentation* at the 250th National Meeting of the ACS, Boston, USA.
February 2016	*Oral presentation* at the 30th Australian Colloid and Surface Science Student Conference, Kiola, Australia.

Abstract

Reversible addition-fragmentation chain transfer (RAFT) polymerisation has been used to synthesise a range of amphiphilic diblock copolymers. These diblock copolymers undergo polymerisation-induced self-assembly (PISA) to form spherical, worm-like or vesicular nano-objects, depending on the target diblock composition and the reaction conditions.

Firstly, a poly(glycerol monomethacrylate) macromolecular chain transfer agent (PGMA macro-CTA) was utilised to polymerise benzyl methacrylate (BzMA) via RAFT aqueous emulsion polymerisation. The core-forming PBzMA block was systematically varied from 62 to 1235 to form a series of $PGMA_{63}$-$PBzMA_x$ diblock copolymer spheres with mean particle diameters ranging from 28 to 230 nm at up to 50% w/w solids. BzMA conversions of at least 98% were achieved within 6 h at 70 °C. These spherical nanoparticles were used to prepare stable oil-in-water Pickering emulsions at various copolymer concentrations. The cis-diol functionality on the PGMA stabiliser chains enabled pH-selective adsorption of $PGMA_{63}$-$PBzMA_{124}$ nanoparticles onto patterned phenylboronic acid-functionalised planar silicon wafers.

A poly(stearyl methacrylate) (PSMA) macro-CTA was prepared via RAFT solution polymerisation in toluene. This $PSMA_{14}$ macro-CTA was then employed in the RAFT dispersion polymerisation of *N*-2-(methacryloyloxy)ethyl pyrrolidone (NMEP), in *n*-dodecane at 90 °C. ^{1}H NMR studies confirmed that the rate of NMEP polymerisation was significantly faster than that of a non-polar monomer (BzMA) under the same conditions. A series of $PSMA_{14}$-$PNMEP_x$ diblock copolymer spheres, worms or vesicles could be prepared via PISA, depending on the target degree of polymerisation (DP) of the core-forming PNMEP block and the solids content. This enabled construction of a phase diagram which allowed pure copolymer morphologies to be reproducibly targeted. $PSMA_{14}$-$PNMEP_{49}$ spheres were evaluated as Pickering emulsifiers: either water-in-oil or oil-in-water Pickering emulsions could be obtained depending on the shear rate employed for homogenisation. Further investigation suggested that high shear rates lead to *in situ* inversion of the initial *hydrophobic* $PSMA_{14}$-$PNMEP_{49}$ spheres to form *hydrophilic* $PNMEP_{49}$-$PSMA_{14}$ spheres.

The RAFT solution polymerisation of NMEP was conducted in ethanol at 70 °C. Reducing the CTA/initiator molar ratio from 10.0 to 3.0 when targeting $PNMEP_{100}$ led to a three-fold enhancement in the rate of polymerisation, which led to higher final monomer conversions. A $PNMEP_{50}$ macro-CTA was chain-extended with BzMA via RAFT alcoholic dispersion polymerisation. Electron microscopy studies indicated that the full range of diblock copolymer morphologies could be obtained. A $PNMEP_{45}$-$PBzMA_{232}$ diblock copolymer was also synthesised via a convenient 'one-pot' protocol in ethanol involving the initial RAFT solution polymerisation of NMEP followed by the RAFT dispersion polymerisation of BzMA. TEM analysis of aliquots extracted during the diblock copolymer synthesis indicated a gradual evolution in copolymer morphology from spherical micelles to pure vesicles via worms.

Finally, a PGMA macro-CTA with a mean DP of 63 was chain-extended with NMEP under RAFT aqueous dispersion polymerisation conditions. The target PNMEP DP was systematically varied from 100 up to 6000 to generate a series of $PGMA_{63}$-$PNMEP_x$ diblock copolymers in the form of highly-solvated particles, as judged by ^{1}H NMR. Kinetic studies confirmed that the RAFT aqueous dispersion polymerisation of NMEP was approximately four times faster than the RAFT solution polymerisation of NMEP in ethanol when targeting the same DP in each case. Spontaneous dissolution of the $PGMA_{63}$-$PNMEP_x$ particles occurs on cooling from 70 °C to 20 °C as the weakly hydrophobic core-forming PNMEP block passes through its LCST and becomes hydrophilic. Thus this RAFT aqueous dispersion polymerisation formulation offers an interesting and efficient route to a high molecular weight water-soluble polymer in a convenient low-viscosity form.

Abbreviations

4VP	4-Vinylpyridine
a_0	Cross-sectional area of the hydrophilic block
ACVA	4,4'-Azobis(4-cyanovaleric acid)
AIBN	2,2'-Azobisisobutyronitrile
AN	Acrylonitrile
ARGET	Activator (re)generated by electron transfer
ATRP	Atom transfer radical polymerisation
bmim	1-Butyl-3-methylimidazolium
BzMA	Benzyl methacrylate
$CaCl_2$	Calcium chloride
CDB	Cumyl dithiobenzoate
CGT	Critical gelation temperature
CMC	Critical micelle concentration
CPADB	4-Cyanopentanoic acid dithiobenzoate
CPDB	2-Cyano-2-propyldithiobenzoate
CTA	Chain transfer agent
CTAB	Cetryltriammonium bromide
CTPPA	4-Cyano-4-thiothiopropylsulfanyl pentanoic acid
DB	Dithiobenzoate
DDMAT	2-(Dodecylthiocarbonothioyl)-2-methylpropionic acid
DEGMA	Di(ethylene glycol) methyl ether methacrylate
DLS	Dynamic light scattering
DMAc	*N*,*N*-dimethyl acrylamide
DMAP	*N*,*N*-dimethylaminopyridine
DMF	Dimethylformamide
DP	Degree of polymerisation
DSS	4,4-Dimethyl-4-silapentane-1-sulfonic acid
EGDMA	Ethylene glycol dimethacrylate
f	Initiator efficiency
f_A	Volume fraction of block A
f_B	Volume fraction of block B
FOMA	1*H*,1*H*,2*H*,2*H*-per-flurooctyl methacrylate
GMA	Glycerol monomethacrylate
GPC	Gel permeation chromatography

HEMA	2-Hydroxyethyl methacrylate
HHHs	Hexagonally-packed hollow hoops
HPMA	2-Hydroxypropyl methacrylate
i	Total number of species
ICAR	Initiator for continuous activator regeneration
IUPAC	International Union of Pure and Applied Chemistry
kT	Thermal energy
LAM	Less activated monomer
l_c	Length of the hydrophobic block
LCMs	Large compound micelles
LCST	Lower critical solution temperature
LMA	Lauryl methacrylate
M	Molecular weight of the monomer repeat unit
MA	Methyl acrylate
MAA	Methacrylic acid
Macro-CTA	Macromolecular chain transfer agent
MAM	More activated monomer
MEA	2-Methoxyethyl acrylate
MMA	Methyl methacrylate
M_n	Number-average molecular weight
MPC	2-(Methacryloyloxy)ethyl phosphorylcholine
M_w	Weight-average molecular weight
M_w/M_n	Dispersity
MWD	Molecular weight distribution
n	Total number of monomer repeat units
N	Degree of polymerisation
$NaHCO_3$	Sodium bicarbonate
*n*BA	*n*-Butyl acrylate
*n*BMA	*n*-Butyl methacrylate
NIPAm	*N*-isopropyl acrylamide
NMEP	*N*-2-(methacryloyloxy)ethyl pyrrolidone
NMI	*N*-phenylmaleimide
NMP	Nitroxide-mediated polymerisation
NMR	Nuclear magnetic resonance
NPPOC	2-nitrophenylpropyloxycarbonyl
NVP	*N*-vinyl pyrrolidone

O/W	Oil-in-water
OEGMA	Oligoethylene glycol methacrylate
P	Packing parameter
P4VP	Poly(4-vinylpyridine)
PAA	Poly(acrylic acid)
PBzMA	Poly(benzyl methacrylate)
PDI	Polydispersity index
PDMAc	Poly(*N*,*N*-dimethyl acrylamide)
PDMS	Polydimethylsiloxane
PEG	Poly(ethylene glycol)
PEGA	Poly(ethylene glycol) methyl ether acrylate
PEGMA	Poly(ethylene glycol) methyl ether methacrylate
PEHA	Poly(2-ethylhexylacrylate)
PEO	Poly(ethylene oxide)
PEOMA	Poly(ethylene oxide) methyl ether methacrylate
PETTC	4-Cyano-4-(2-phenylethane sulfanylthiocarbonyl) sulfanylpentanoic acid
PF_6	Hexaflurophosphate
PGMA	Poly(glycerol monomethacrylate)
PHEMA	Poly(2-hydroxyethyl methacrylate)
PHPMA	Poly(2-hydroxypropyl methacrylate)
PISA	Polymerisation-induced self-assembly
PLMA	Poly(lauryl methacrylate)
PMA	Poly(methyl acrylate)
PMAA	Poly(methacrylic acid)
PMAG	Poly(2-(methacrylamido)-glycopyranose
PMEA	Poly(2-methoxyethyl acrylate)
PMMA	Poly(methyl methacrylate)
PMPC	Poly(2-(methacryloyloxy)ethyl phosphorylcholine)
P*n*BA	Poly(*n*-butylacrylate)
PNIPAm	Poly(*N*-isopropyl acrylamide)
PNMEP	Poly(*N*-2-(methacryloyloxy)ethyl pyrrolidone)
PNVP	Poly(*N*-vinyl pyrrolidone)
POEGMA	Poly(oligoethylene glycol) methacrylate
PPMA	3-Phenylpropyl methacrylate
PPPMA	Poly(3-phenylpropyl methacrylate)
PRE	Persistent radical effect

PS	Polystyrene
PSMA	Poly(stearyl methacrylate)
PTFEMA	Poly(2,2,2-trifluroethyl methacrylate)
PVAc	Poly(vinyl acetate)
RAFT	Reversible addition-fragmentation chain transfer
R_d	Rate of decomposition
RDRP	Radical deactivation radical polymerisation
R_i	Rate of initiation
R_p	Rate of propagation
R_t	Rate of termination
S	Styrene
SAXS	Small angle X-ray scattering
$scCO_2$	Supercritical carbon dioxide
SCPDB	4-Cyano-4-((thiobenzoyl)sulfanyl) pentanoic succinimide ester
SDS	Sodium dodecyl sulfate
SEM	Scanning electron microscopy
SMA	Stearyl methacrylate
TEM	Transmission electron microscopy
TEMPO	2,2,6,6-Tetramethylpiperidinyl-1-oxy
TFEMA	2,2,2-Trifluoroethyl methacrylate
T_g	Glass transition temperature
THF	Tetrahydrofuran
TTC	Trithiocarbonate
TTCA	2-(Dodecylthiocarbonothioylthio)-2-methylpropanoic acid
UV	Ultra-violet
V	Volume of the hydrophobic block
VAc	Vinyl acetate
W/O	Water-in-oil
χ	Flory-Huggins parameter
χN	Degree of segregation

Contents

Chapter 1

Introduction

1.1 Polymer Science

Polymers are found everywhere in modern life, from everyday objects such as a toothbrush to high-tech applications such as bulletproof vests. A polymer consists of many covalently-bonded repeat units called monomers. The mean number of repeat units per chain is known as the degree of polymerisation (DP). Staudinger first postulated the existence of macromolecules almost a century ago. This insight eventually earnt him the Nobel prize in Chemistry in 1953.[1] Polymers can be characterised in various ways depending on their origin, structure, formation and properties. Polymers can either be natural (e.g. cellulose) or synthetic (e.g. polystyrene). They can be linear, branched or crosslinked and can be formed by either addition or condensation reactions. They can have many important applications as plastics, elastomers or resins.[2] This shows the true diversity of the ever-growing field of polymer chemistry.

Unlike small molecules, polymers do not have a finite molecular weight. Instead they have a distribution of molecular weights (Figure 1.1), since each polymer chain can have a different number of monomer repeat units. This molecular weight distribution (MWD) means that most experimental measurements of molecular weight report only an average value. The two most common molecular weight averages are the number-average molecular weight (M_n) and the weight-average molecular weight (M_w).

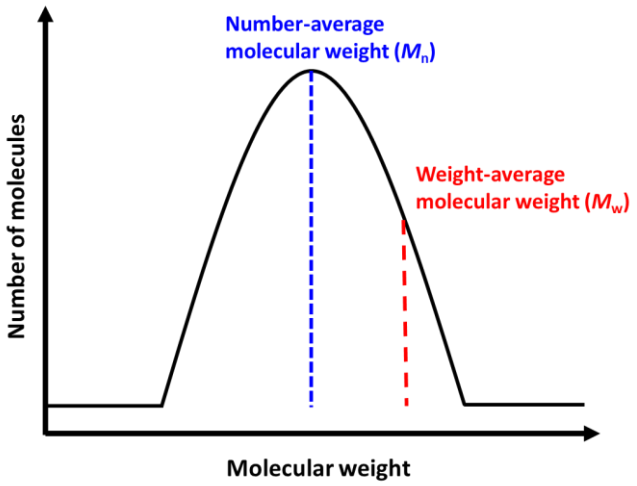

Figure 1.1 Schematic representation of a molecular weight distribution curve for a polymer indicating the number-average molecular weight (M_n) and weight-average molecular weight (M_w).[3,4]

M_n is defined by Equation 1:

$$M_n = \frac{\Sigma n_i M_i}{\Sigma n_i} \quad (1)$$

Where n is the total number of monomer repeat units, M is the molecular weight of the monomer repeat unit and i is the total number of species.

M_w is defined by Equation 2:

$$M_w = \frac{\Sigma n_i {M_i}^2}{\Sigma n_i M_i} \quad (2)$$

As shown in Figure 1.1, M_w tends to be skewed towards a higher molecular weight than M_n. The M_w/M_n ratio can be used to assess the breadth of the MWD. This parameter is also known as the dispersity. If all polymer chains were the same length, M_w and M_n would be identical resulting in a dispersity of unity. As this is not the case and M_w is biased towards higher molecular weights, M_w/M_n is always greater than unity.[3] M_n and M_w can be measured by gel permeation chromatography (GPC) if appropriate calibration standards are available.

1.2 Free Radical Polymerisation

Free radical polymerisation is a type of chain growth polymerisation. It is one of the most simple and versatile types of polymerisation, since it is applicable to a wide range of functional vinyl monomers. More-over, this technique can be used over a broad range of operating conditions (solution, emulsion, dispersion, suspension etc.).

There are three key steps in free radical polymerisation; initiation, propagation and termination. These are shown in Figure 1.2. Initiation can be broken down into two stages. Firstly, the decomposition of the initiator to produce free radicals. This is usually achieved by thermal homolysis of the initiator to form a pair of radicals (R$^{\bullet}$).

The radical then reacts with a monomer unit M, to produce a monomer-radical adduct ($M_1^{\bullet}$). Successive monomer addition then occurs during propagation until finally chain termination occurs. Termination can occur in one of two ways, either by combination or disproportionation. If termination occurs by combination, two polymer radicals combine to form a single chain, which has a molecular weight equal to the sum of the two polymer radicals. Alternatively, termination can occur by disproportionation, whereby a hydrogen atom is transferred from one polymer radical

to another, resulting in a terminal vinyl group on one chain and a hydrogen-capped chain on the other.

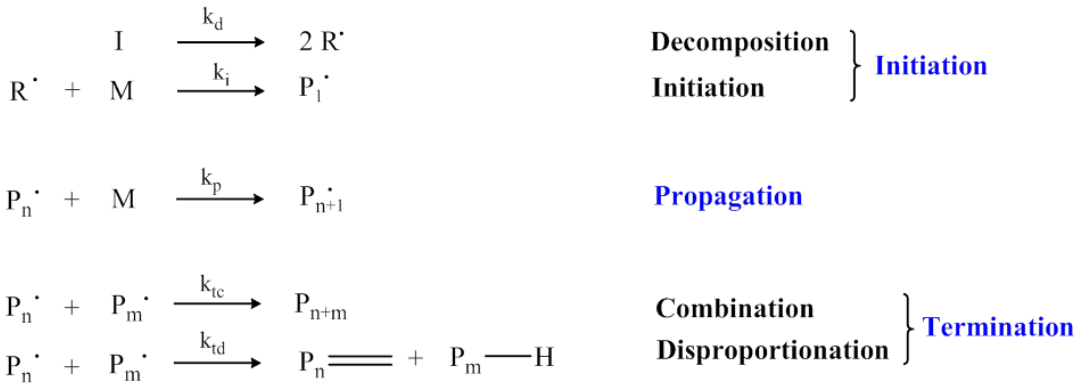

Figure 1.2 Reaction mechanism for free radical polymerisation showing initiation, propagation and termination steps.[4]

Decomposition, initiation, propagation and termination can be described by equations 3 to 6, where R_d is the rate of decomposition, R_i is the rate of initiation, R_p is the rate of propagation and R_t is the rate of termination (where $k_t = k_{tc} + k_{td}$). The ability of the radical to react with the monomer is defined as the initiator efficiency, *f*.

$$R_d = -\frac{d[I]}{dt} = k_d[I] \quad (3)$$

$$R_i = -\frac{d[R\cdot]}{dt} = 2k_d f[I] \quad (4)$$

$$R_p = -\frac{d[M]}{dt} = k_p[P\cdot][M] \quad (5)$$

$$R_t = -\frac{d[P\cdot]}{dt} = 2k_t[P\cdot]^2 \quad (6)$$

In a free radical polymerisation, the rate of initiation is limited by the relatively slow rate of initiator decomposition. Therefore, the rate-determining step is initiation, rather than propagation. Once the polymerisation has been initiated, high molecular weight polymers are formed almost immediately. In addition to initiation, propagation and termination side reactions can also occur in a free radical polymerisation. These undesirable side reactions include chain transfer to polymer, monomer, initiator or solvent. These side reactions are depicted generically in Figure 1.3 in which X represents the chain transfer species.

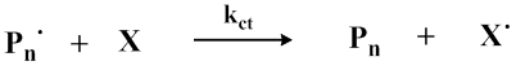

Figure 1.3 Chain transfer during free radical polymerisation.

One disadvantage of free radical polymerisation is that the reactivity of the polymer radical species makes it difficult to control the molecular weight distribution of the resulting polymer. The short lifetime of the propagating radical also makes it impossible to make certain copolymer architectures such as block copolymers.

1.3 Living Anionic Polymerisation

Living anionic polymerisation has no intrinsic termination step, which allows the synthesis of narrow MWD polymers with a given target molecular weight.[5] In a living polymerisation, the rate of initiation must be much faster than the rate of propagation.[6] Under these conditions, all chains are initiated at the same time and then grow uniformly.[7] There is no termination because carbanions cannot react with each other. These reaction conditions lead to a narrow MWD. 'Living' polymerisations are usually characterised by a linear increase in molecular weight with conversion. In contrast, high molecular weights are formed at the start of a free radical polymerisation (Figure 1.4).[8] Living anionic polymerisation offers a convenient route to the synthesis of well-defined block copolymers by sequential monomer addition since the chains remain active after all the initial monomer has been consumed.

The first reported example of living anionic polymerisation was by Szwarc in 1956.[9] A sodium-napthalene complex was used to initiate the polymerisation of styrene at -80 °C. Subsequent additions of styrene confirmed the 'living' nature of the polymerisation. Styrene has since been used for many living anionic polymerisations.[10,11] Organolithium compounds such as *n*-butyl lithium are often used as suitable initiators; they react with styrene to form a 'living' polystyrene chain that maintains its reactivity even after complete monomer consumption (see Figure 1.5).[11]

The main disadvantage of living anionic polymerisation is its intolerance towards impurities and monomer functionality. Living anionic polymerisations require extensive purification of both monomer and solvent as well as rigorous cleaning of

the glassware. Reactions are also often conducted at relatively low temperatures (< -50 °C).[12]

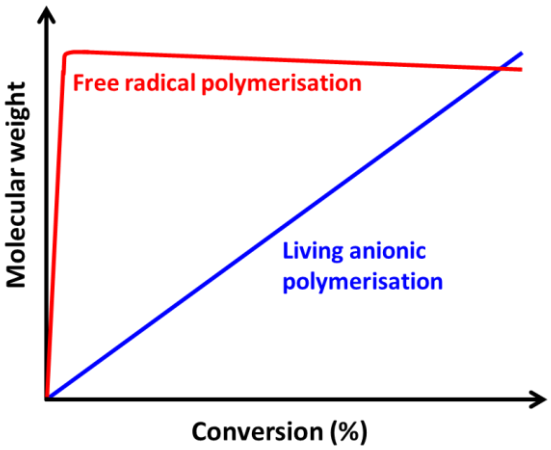

Figure 1.4 Molecular weight versus conversions for a free radical polymerisation and a living anionic polymerisation.

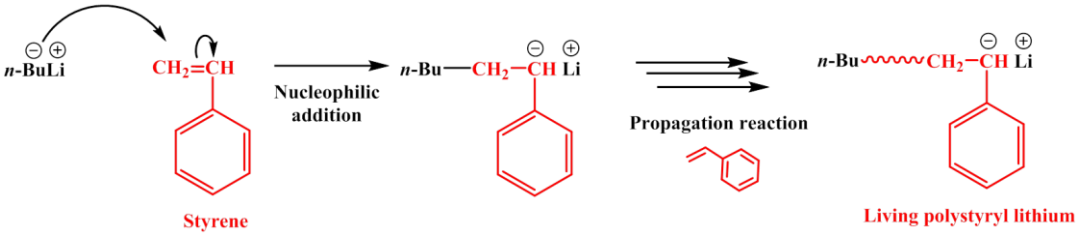

Figure 1.5 Living anionic polymerisation of styrene.[11]

1.4 Controlled/'Living' Radical Polymerisation

Controlled/living radical polymerisation is a 'pseudo-living' technique. Such polymerisations are characterised by the suppression of termination relative to propagation. This is achieved by the rapid equilibrium between active and dormant chains. Active polymer radicals are reversibly deactivated to minimise the probability of termination.[6] There is some disagreement over the nomenclature used for controlled/living radical polymerisation because termination is merely suppressed, rather than eliminated. Therefore the International Union of Pure and Applied Chemistry (IUPAC) has recommended using the term 'reversible deactivation radical polymerisation' (RDRP).[6]

RDRP combines the high levels of control conferred by living anionic polymerisation with the tolerance towards functionality and impurities that characterises free radical polymerisation. Advantages of RDRP include reliable

targeting of molecular weights, narrow molecular weight distributions and ease of implementation. RDRP is well-suited for the synthesis of functional block copolymers and other copolymer architectures are also possible, as shown in Figure 1.6.[13]

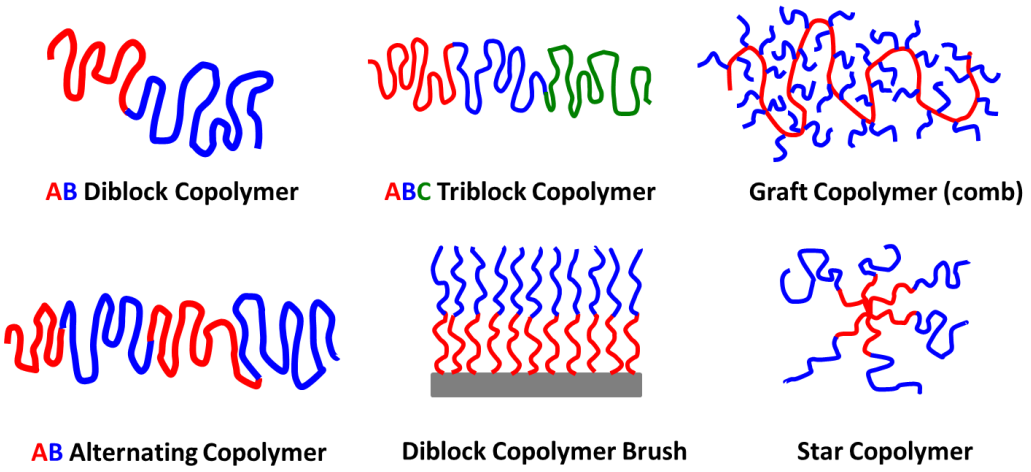

Figure 1.6 Block copolymer architectures reported in literature.[14-16]

Two main RDRP mechanisms are the persistent radical effect (PRE) and degenerative transfer.[13,17] Both involve an equilibrium between an active and dormant species, see Figure 1.7.

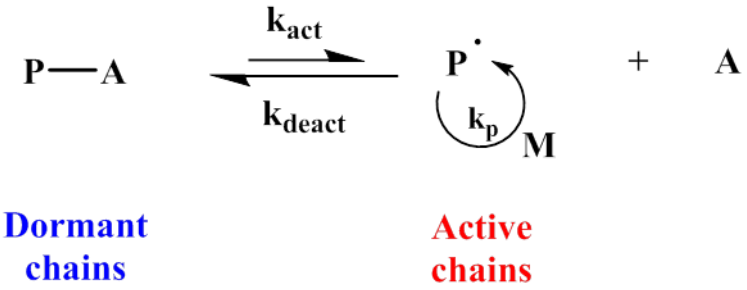

Figure 1.7 General dormant-active species equilibrium in reversible deactivation radical polymerisations.[13]

The three most widely used types of RDRP are nitroxide-mediated polymerisation (NMP), atom transfer radical polymerisation (ATRP) and reversible addition-fragmentation chain transfer (RAFT) polymerisation. Each polymerisation technique will be discussed in detail in the following sections. ATRP and NMP follow the PRE mechanism, whereas RAFT follows the degenerative transfer mechanism. The PRE does not require the addition of a radical initiator because the activation step generates a propagating radical. A capping species which is unable to undergo

termination, known as a 'persistent radical', can only react with the propagating polymer radical, P˙. This increases the lifetime of the dormant species relative to the active species. The rate of deactivation is much higher than that of activation, causing an increasing concentration of the dormant species and a concomitant reduction in P˙, which leads to a reduced rate of termination. In contrast, RAFT follows the degenerative transfer mechanism. This follows the same initiation and termination steps as free radical polymerisation and requires a radical initiator. An equilibrium between a chain transfer agent (CTA) and a propagating radial is established, in which the CTA forms a dormant species.[17] This mechanism will be discussed further in section 1.5.2.

1.4.1 Nitroxide-Mediated Polymerisation (NMP)

Initially, NMP syntheses were based on the use of a nitroxide (e.g. 2,2,6,6-tetramethylpiperidinyl-1-oxy (TEMPO)) and a thermal initiator (e.g. 2,2'-azobisisobutyronitrile (AIBN)) but this has since been developed to enable use of a unimolecular alkoxyamine initiator. This alkoxyamine decomposes to form both the nitroxide and the initiating radical.[18] Such unimolecular initiators lead to better control over polymer molecular weights and dispersities.[19,20]

NMP is based on the PRE. Figure 1.8 shows the mechanism using either (a) an alkoxyamine or (b) a nitroxide and an initiator; both methods involve a dynamic equilibrium between an active and dormant state. During the active state, monomer adds to the growing polymer radical.

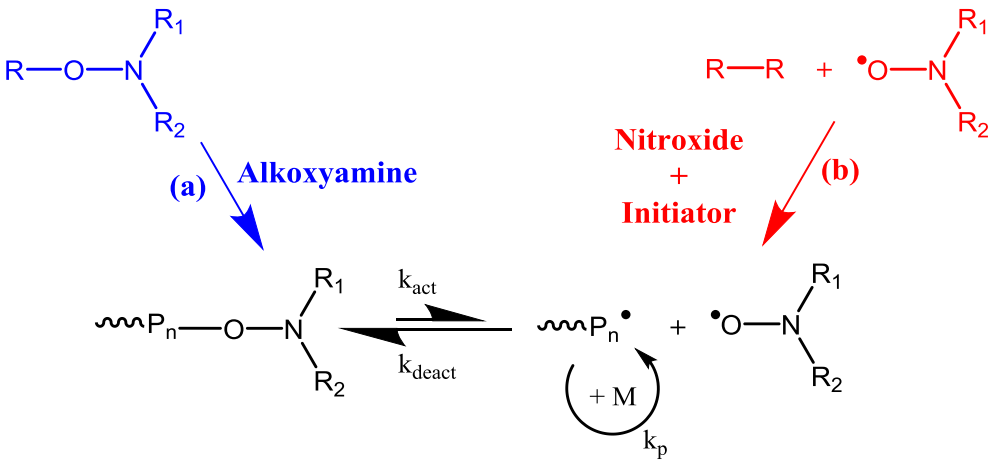

Figure 1.8 The activation-deactivation equilibrium in nitroxide-mediated polymerisation, (a) using a unimolecular initiator or (b) using a two-component system.[18]

Nitroxides and alkoxyamines have high bond dissociation energies and therefore NMP is typically conducted at high temperatures (> 120 °C when using TEMPO).[21] NMP is useful for a wide range of monomers, including styrene, acrylates, acrylamides, dienes and acrylonitrile but unfortunately it cannot be used for methacrylates. Compared with other RDRP techniques, NMP is a relatively environmentally-friendly technique because of its lack of a metal catalyst (ATRP) or malodorous sulfur compounds (RAFT).

1.4.2 Atom Transfer Radical Polymerisation (ATRP)

ATRP was developed independently by Sawamoto[22] and Matyjaszewski[23] and their co-workers in 1995. ATRP requires the use of a metal catalyst complex and an alkyl halide initiator. Figure 1.9 outlines the mechanism: the metal catalyst cleaves the alkyl halide bond, causing the metal catalyst to attain a higher oxidation state and generate an alkyl radical. The latter species is then able to react with free monomer to generate a polymer radical.[21]

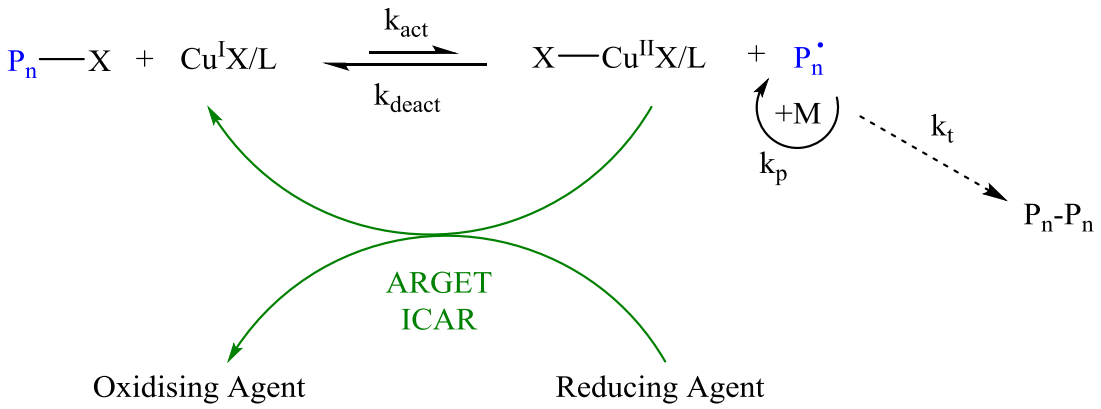

Figure 1.9 ARGET and ICAR ATRP using a copper catalyst.[21]

The most efficient and therefore most common ATRP catalysts involve copper. Their oxygen sensitivity, together with their cost of removal, made early ATRP syntheses uneconomic for industry. Since 1995, new ATRP formulations have been developed, such as activator (re)generated by electron transfer (ARGET) ATRP and initiator for continuous activator regeneration (ICAR). These ATRP formulations enable regeneration of the metal catalyst. Consequently, less catalyst is required, which reduces both the overall cost and also the oxygen sensitivity of the polymerisation. One disadvantage of ATRP is that its toxic metal catalyst requires removal at the end of the polymerisation for almost all applications.

ATRP has a high tolerance of monomer functionality and can be used for (meth)acrylates, (meth)acrylamides and styrenes. However, ATRP cannot be used for acidic monomers or dienes.[21,24] Acidic monomers can protonate ligands and destroy the catalyst, whereas dienes displace ligands and generate less redox-active species.

1.5 Reversible Addition-Fragmentation Chain Transfer (RAFT) Polymerisation

RAFT polymerisation is a type of living radical polymerisation that can produce well-defined block copolymers. It was first reported by Rizzardo and co-workers[25] in 1998 and over the past two decades RAFT has become a huge area of interest with hundreds of papers being published each year.[8,26-28]

RAFT polymerisation follows a degenerative chain transfer mechanism and uses a CTA to confer control over the molecular weight, with low dispersities being routinely achievable (typically $M_w/M_n < 1.20$).[29] RAFT is a highly versatile technique that can be used to polymerise a wide range of functional vinyl monomers. These include styrene, (meth)acrylates, (meth)acrylamides and vinyl acetate. The initiator type and concentration can also play a vital role in RAFT polymerisations. Typically, thermal initiators are used (e.g. AIBN and 4,4'-azobis(4-cyanovaleric acid) (ACVA)) but UV[30] and gamma source[31] initiation have also been reported in the literature. High CTA/initiator molar ratios are normally associated with well-controlled polymerisations, resulting in narrow dispersities. However, this can lead to prolonged reaction times, leading to greater loss of the RAFT end-group.[32] Thus a careful balance is required, particularly when targeting diblock copolymers to ensure high chain-end fidelity while maintaining narrow dispersities.

RAFT polymerisations have been conducted in a wide range of reaction media, from organic solvents such as benzene[25] to protic solvents, for example alcohols[33] and water.[34] RAFT has also been conducted in less conventional solvents such as ionic liquids[35] or supercritical carbon dioxide.[36] One important consideration for selecting a solvent is that the RAFT CTA must be soluble in the reaction medium.[32] RAFT agent selection will be discussed further in section 1.5.1.

1.5.1 Selection of a suitable RAFT chain transfer agent

The choice of RAFT CTA is essential for a successful RAFT polymerisation.[27,37] The generic chemical structure of a RAFT CTA is shown in Figure 1.10. The effectiveness of the RAFT CTA depends on the selection of appropriate Z and R groups for a given monomer, as well as the reaction conditions.

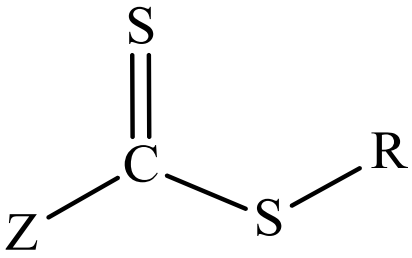

Figure 1.10 Generic chemical structure of a RAFT chain transfer agent, where R is a good leaving group and Z is a stabilising group.

The Z group should activate the C=S bond towards radical addition and also stabilise the transition state formed on addition of the propagating radical. Typical Z groups include aryl and alkyl groups.[25] The R group must be a good radical leaving group, but should also be capable of re-initiating polymerisation. Examples of suitable R groups include cumyl and cyanoisopropyl groups.

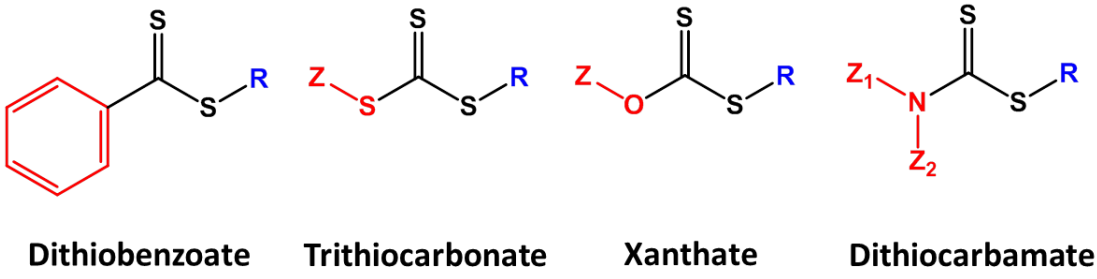

Figure 1.11 Dithiobenzoate, trithiocarbonate, xanthate and dithiocarbamate RAFT chain transfer agents.

Four classes of RAFT CTAs have been reported: dithiobenzoates (DB), trithiocarbonates (TTC), xanthates (dithiocarbonates) and dithiocarbamates (see Figure 1.11).[8] Careful selection of the RAFT CTA is required; dithiobenzoates have very high transfer constants but may cause retardation when used at high concentrations. In contrast, xanthates have lower transfer constants and are more effective with less activated monomers (LAMs) such as vinyl acetate.[8]

Moad and co-workers have reported guidelines for selection of an appropriate RAFT agent for a given monomer (Figure 1.12).[8] Solid lines indicate where good RAFT control is achieved, whereas dashed lines indicate only partial RAFT control. In general, more activated monomers (MAMs) such as methacrylates give better results when using a dithiobenzoate or trithiocarbonate RAFT agent whereas LAMs (e.g. *N*-vinyl pyrrolidone, NVP) perform better when using a xanthate or dithiocarbamate. Incorrect pairing of the monomer and CTA can inhibit or significantly limit the polymerisation leading to low monomer conversions.

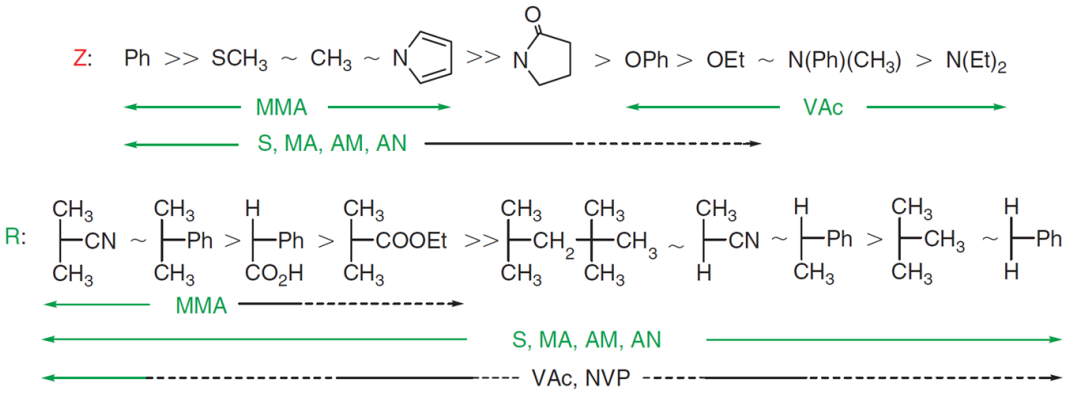

Figure 1.12 Guidelines for the selection of an appropriate RAFT agent for various monomers. Solid lines indicate that good control can be achieved, whereas dashed lines indicate only partial control.[8]

More recently, the development of so-called 'universal' RAFT agents such as *N*-(4-pyridinyl)-*N*-methyldithiocarbamate have enabled the polymerisation of both LAMs and MAMs (Figure 1.13).[38] Therefore allowing diblock copolymers to be synthesised in which one block comprises a MAM and the other is composed of a LAM. Benaglia and co-workers initially protonated the above universal RAFT agent using 4-toluenesulfonic acid, which enabled the polymerisation of methyl methacrylate (MMA). The resulting PMMA macromolecular chain transfer agent (macro-CTA) was neutralised by adding a stoichiometric amount of *N*,*N*-dimethylaminopyridine (DMAP). This neutral PMMA macro-CTA was chain-extended with a LAM, vinyl acetate (VAc), to form a PMMA-PVAc diblock copolymer. GPC analysis indicated a relatively high blocking efficiency compared to the PMMA macro-CTA but a relatively broad molecular weight distribution (M_w/M_n = 1.39) for the diblock copolymer.

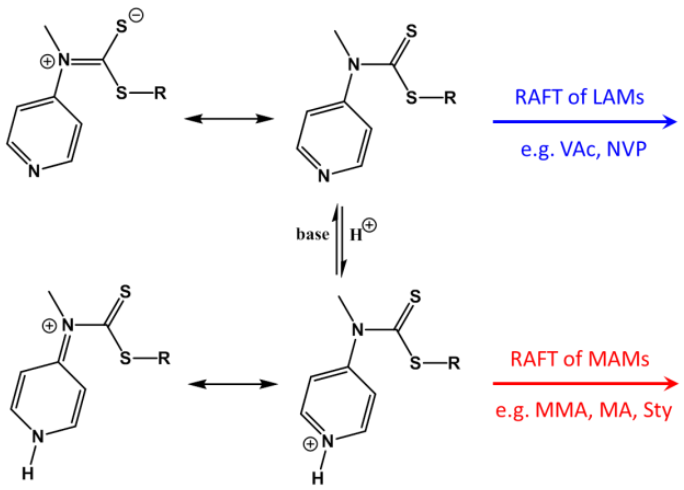

Figure 1.13 A 'universal' RAFT agent, *N*-(4-pyridinyl)-*N*-methyldithiocarbamate.[38]

One disadvantage of RAFT polymerisation is that it produces intrinsically coloured and often malodorous polymers, both of which are attributed to the sulfur-based RAFT CTA.[39] However, this problem has been significantly reduced by Moad and co-workers, who reported efficient removal of the RAFT CTA from the polymer chain-ends.[40,41] The most common methods of RAFT end-group removal are outlined in Figure 1.14. Reacting the thiocarbonylthio compound with a nucleophile (e.g. amines[42]) results in the formation of a thiol.[37,41] This is perhaps the most established RAFT end-group modification method. Thermal decomposition of the RAFT agent offers a solvent-free route and completely removes the sulfur from the polymer chain-end to leave an unsaturated chain-end.[43] Other methods include the use of radicals[40] or dienes.[44]

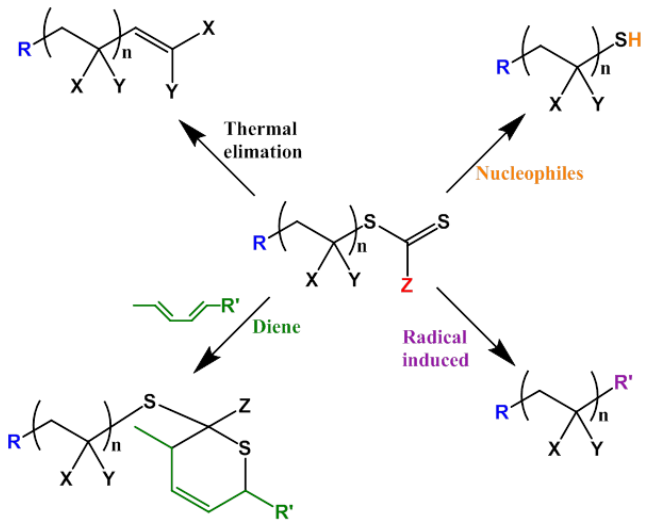

Figure 1.14 Schematic representation of the main methods of RAFT end group removal/modification.[37,40]

1.5.2 Mechanism of RAFT polymerisation

The mechanism of RAFT polymerisation[8,25-28] is based on the same three steps of polymerisation as free radical polymerisation (initiation, propagation and termination). However, propagation is slightly different from that in conventional free radical polymerisation (Figure 1.15). Initiation involves a conventional free radical initiator such as an azo or peroxide compound to generate radicals, which are then able to react with the monomer to generate a polymer radical ($P_n^{\bullet}$).

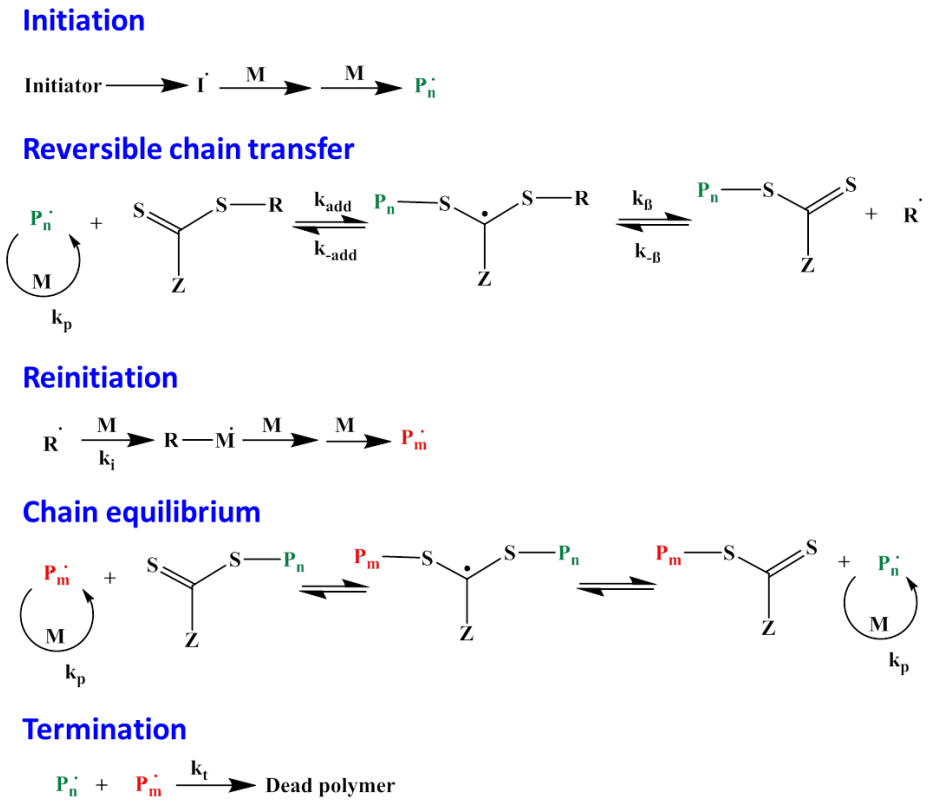

Figure 1.15 The accepted mechanism for RAFT polymerisation according to Rizzardo and co-workers.[8]

RAFT also has the additional kinetic steps of reversible chain transfer, reinitiation and chain equilibrium, as shown in Figure 1.15. Reversible chain transfer involves the growing polymer radical ($P_n^{\bullet}$) reacting with the RAFT CTA (or macro-CTA). Fragmentation of the intermediate radical leaves a polymeric thiocarbonylthio compound and a new radical ($R^{\bullet}$). $R^{\bullet}$ then reinitiates the polymerisation, reacting with monomer units to form a new polymer radical ($P_m^{\bullet}$). $P_m^{\bullet}$ can reversibly add to the macro-CTA produced in the reversible chain transfer step. This is the chain equilibrium step that produces controlled chain growth. Rapid equilibrium between active polymer radicals ($P_n^{\bullet}$ and $P_m^{\bullet}$) and the dormant polymeric thiocarbonylthio

compound provides an equal opportunity for the chains to grow. This allows targeting of molecular weight and gives narrow MWDs.

The final stage is the combination of two polymer radicals to form a dead polymer chain. RAFT suppresses termination of polymer chains relative to propagation, but a small amount of termination is still present.[28] The probability of termination and chain-end deactivation increases as the monomer concentration is reduced (monomer-starved conditions). Therefore RAFT polymerisations are often quenched prior to full conversion to allow the RAFT CTA to remain attached to the polymer chain for subsequent chain extension, if desired.

1.6 Emulsion Polymerisation

Conventional emulsion polymerisation involves four key components; a water-immiscible monomer, water-soluble initiator, surfactant and water. The use of water as the reaction medium has several advantages, including low viscosity, a cheap environmentally-friendly solvent and the efficient removal of heat from the polymerisation.[45] Consequently, this has led to emulsion polymerisation being heavily used in industry for the manufacture of paints, adhesives and coatings.[45,46] One disadvantage to conventional emulsion polymerisation is the use of high levels of surfactant. This is required for smaller latexes but it can have a negative effect on important polymer properties, such as film formation.

Conventional emulsion polymerisation involves three key stages; intervals I, II and III.[45-48] For simplicity, conventional emulsion polymerisation will be discussed, but the same principles apply to RAFT emulsion polymerisation with the surfactant being replaced with a hydrophilic macro-CTA.

Interval I begins with micrometre-sized surfactant-stabilised monomer droplets and surfactant micelles in solution.[48] The initiator generates radicals in the aqueous phase; these radicals are then able to react with a small amount of water-soluble monomer to form oligoradicals. Notwithstanding the low aqueous solubility of the monomer, a relatively small amount is present in the aqueous phase. Up to a critical chain length, oligoradicals are also soluble in the aqueous phase (Figure 1.16; Interval I). Once this critical chain length is reached, oligoradicals can either undergo homogeneous nucleation or heterogeneous nucleation.[49] Homogeneous nucleation

uses free surfactant present in solution to generate new micelles. Conversely, heterogeneous nucleation involves the oligoradical entering a preformed surfactant micelle. Heterogeneous nucleation is the primary route taken when the surfactant concentration is above the critical micelle concentration (CMC). Below the CMC, no surfactant micelles are present and therefore homogeneous nucleation occurs. During interval I, rapid polymerisation occurs with an increase in both polymerisation rate and number of particles with time (see Figure 1.17). Interval I is complete when all surfactant micelles have become monomer-swollen latex particles.

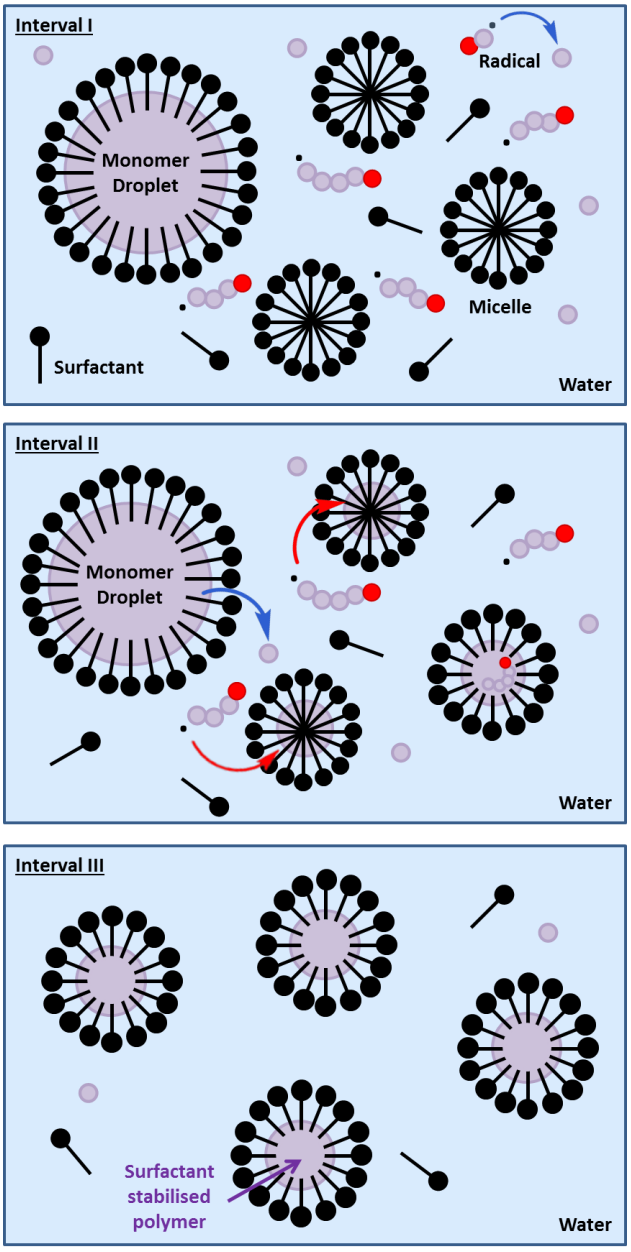

Figure 1.16 Schematic representation of the three primary intervals (I, II, III) in conventional emulsion polymerisation.[45,48]

Surfactant-stabilised monomer droplets and monomer-swollen nascent particles are present in interval II. During interval II, the monomer concentration in solution remains relatively constant. Monomer from the surfactant-stabilised monomer droplets replaces dissolved monomer in aqueous solution as it enters the monomer-swollen latexes, resulting in a constant polymerisation rate (Figure 1.17). When all monomer droplets have been consumed and only monomer-swollen latexes are present, interval II is complete.[48]

A reduction in the polymerisation rate occurs during interval III as the monomer concentration decreases within the monomer-swollen latexes (Figure 1.17). Interval III continues until all monomer is consumed and only colloidally-stable latex particles remain.[48]

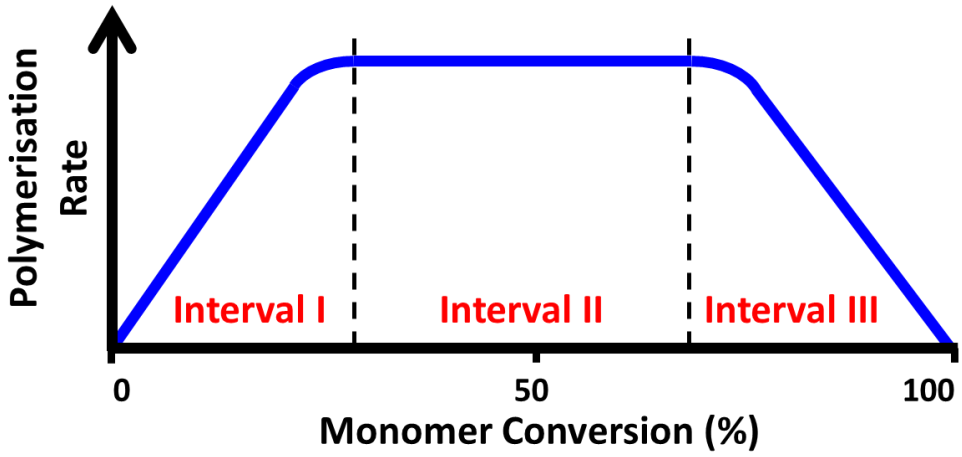

Figure 1.17 Rate of polymerisation versus monomer conversion for an emulsion polymerisation, illustrating intervals I, II and III.[46]

In addition to surfactant-stabilised emulsion polymerisations, so-called 'surfactant-free' emulsion polymerisations can also be performed. The final latex particles are usually stabilised by either surface charge or by a polymeric surfactant such as a poly(ethylene oxide)-based macromonomer (Figure 1.18).[48] For example, using an ionic initiator such as ammonium persulfate for the emulsion polymerisation of styrene initially leads to the formation of anionic sulfate-capped styrene oligomers in the aqueous phase. Given their surfactant-like character, these oligomers undergo *in situ* self-assembly to form micelles, which act as the locus for the ensuing styrene polymerisation – much like a conventional surfactant-stabilised emulsion polymerisation.

When a polymeric surfactant is used, such as a hydrophilic macro-CTA in RAFT aqueous emulsion polymerisation, the water-immiscible monomer polymerises from the macro-CTA, which remains soluble in the reaction solution up to a critical DP. At this point, the hydrophobic oligomer becomes insoluble and self-assembles into micelles where the hydrophilic macro-CTA acts as a steric stabiliser for the nanoparticles.

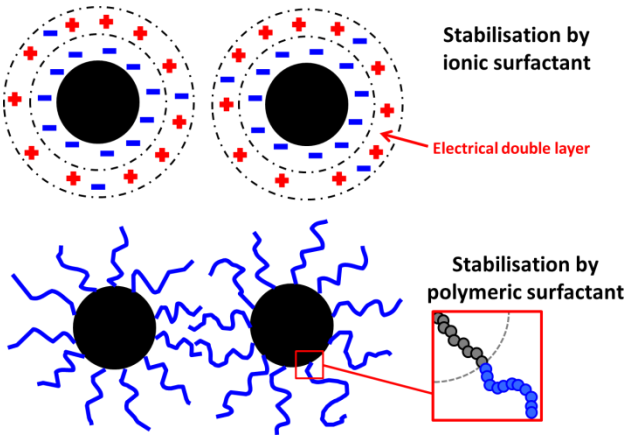

Figure 1.18 Stabilisation of polymer latexes by either an ionic surfactant or a polymeric surfactant.[48]

1.7 Dispersion Polymerisation

In a dispersion polymerisation, the monomer, initiator and stabiliser are fully soluble in the solvent of choice. One essential criterion for dispersion polymerisation is that the monomer is soluble in the reaction mixture, whereas the resulting polymer is insoluble.[50,51] This somewhat limits the monomer/solvent combinations possible for aqueous dispersion polymerisations and as a result, has led to much of the literature being focussed on non-aqueous formulations.[50] Dispersion polymerisation can be used to form near-monodisperse particles in the range of 0.1 to 15 μm.[51] Commercial applications of such latexes include inkjet printing, electronic displays and solvent coatings.[50]

The mechanism of a dispersion polymerisation can be separated into six key steps (Figure 1.19).[50] Initially, the monomer, (polymeric) stabiliser and initiator are all soluble in the reaction solution. The reaction mixture is then heated, causing thermal decomposition of the initiator to form radicals. In step 2, the initiator radicals react with monomer and begin to form oligomers. These oligomers are soluble in the solvent up to a certain critical molecular weight. They then precipitate to form small

unstable particles or nascent nuclei, as indicated in step 3. In this step, the stabiliser starts to adsorb onto the unstable particles, which begin to aggregate and increase in size (step 4). Further adsorption of the stabiliser eventually leads to colloidally stable particles (step 5). The particles continue to grow as the remaining monomer and oligomers enter the particles. At this stage, no new nuclei are formed. Finally, in step 6 the monomer is depleted and only sterically-stabilised particles remain. This indicates the end of the polymerisation.

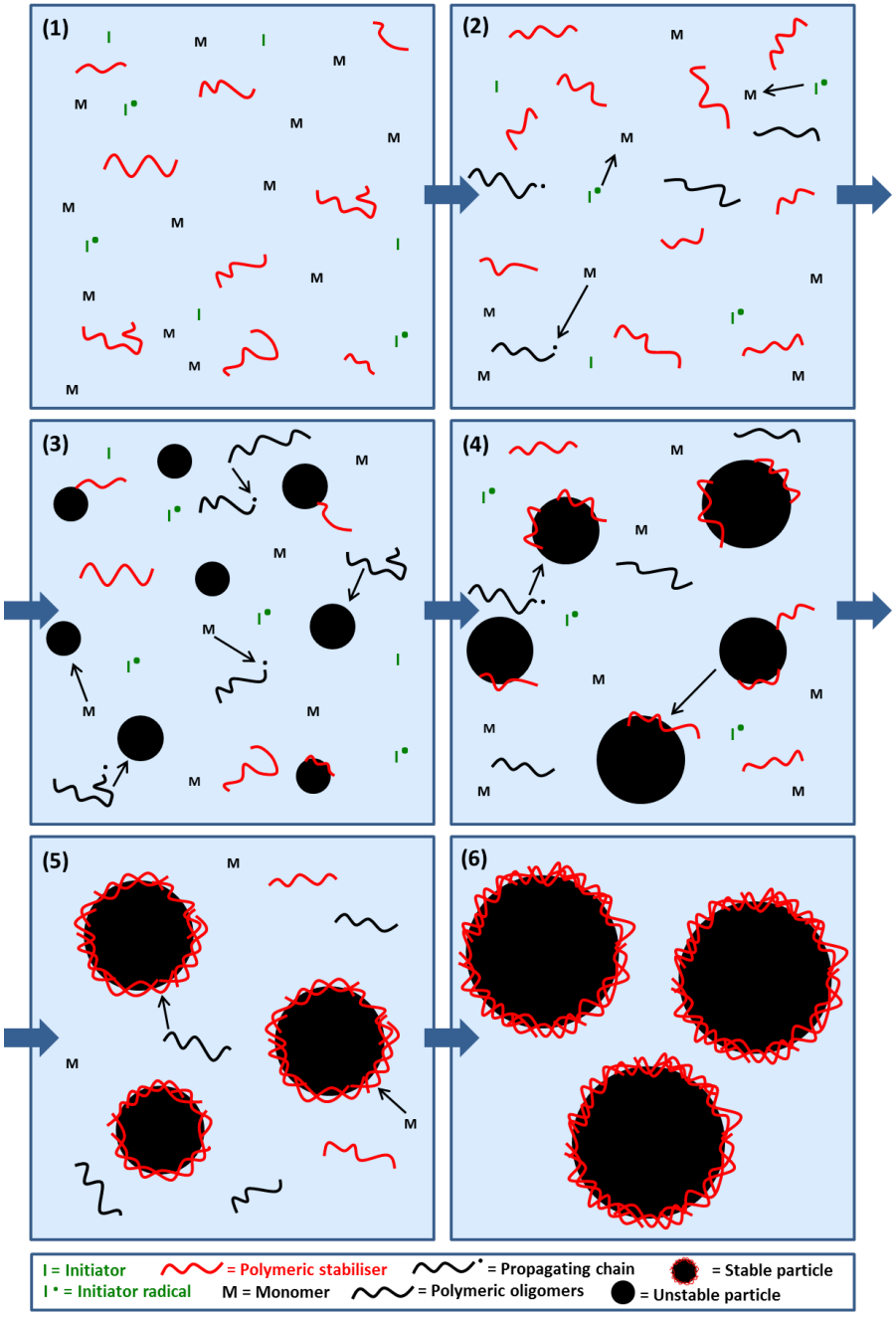

Figure 1.19 Schematic representation of the main steps involved in dispersion polymerisation.[50-52]

Although the majority of the literature involves non-polar solvents, 2-hydroxypropyl methacrylate (HPMA) is a rare example of a vinyl monomer that is water-soluble but leads to a water-insoluble polymer.[53] Ali et al. reported the synthesis of PHPMA latexes by dispersion polymerisation (Figure 1.20). These latexes were stabilised by poly(*N*-vinyl pyrrolidone) (PNVP) and were synthesised at 60 °C.[53] Control over the particle size from 0.1 – 1.0 μm was achieved by varying the choice of initiator and the stabiliser concentration.

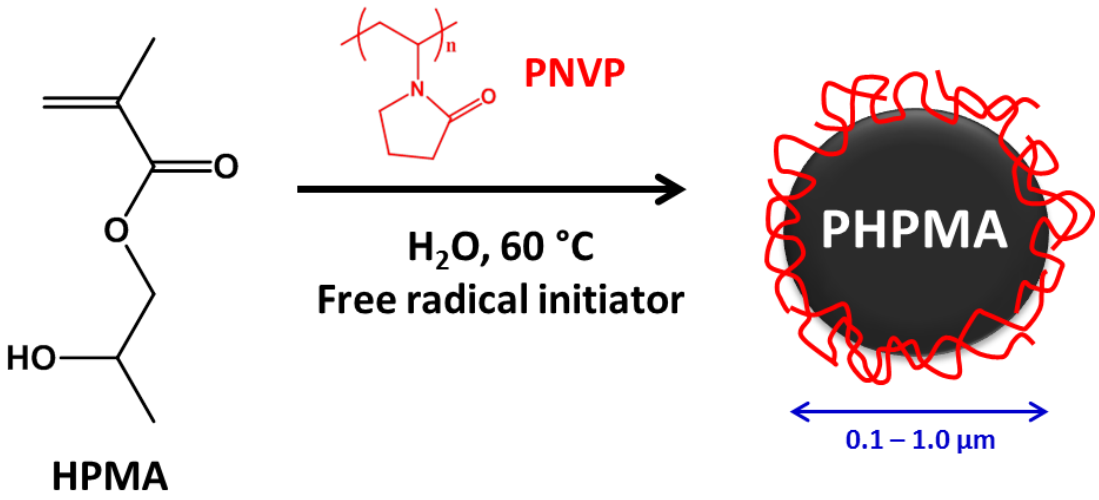

Figure 1.20 Schematic representation of the synthesis of PNVP-stabilised PHPMA latex particles via aqueous dispersion polymerisation at 60 °C.[53]

1.8 Self-Assembly

An amphiphilic molecule contains two distinctly different components connected by a chemical bond. Usually, one part of the molecule is hydrophilic and has a strong affinity to water, whereas the other part is hydrophobic and repels water molecules. The most common example of an amphiphilic molecule is a surfactant. Surfactants have long hydrocarbon tails joined to a hydrophilic head-group. Classification depends on their hydrophilic head-group which can be anionic, cationic, zwitterionic or neutral. Common examples include sodium dodecyl sulfate (SDS), cetyltriammonium bromide (CTAB), phospholipids and stearyl alcohols, respectively. The amphiphilic nature of surfactants leads to interesting behaviour in aqueous solution. The hydrophilic head-group is able to form multiple strong hydrogen bonds to water molecules, whereas the hydrophobic alkyl chains are incapable of interacting with water molecules and therefore do not undergo hydrogen bonding. The balance between these two types of interactions causes surfactants (and

amphiphilic molecules in general) to self-assemble to form aggregates or micelle in aqueous solution.[54,55]

Self-assembly occurs spontaneously and is a thermodynamically-driven process. The self-assembled structures are not held together by strong covalent or ionic bonds but by weaker van der Waals, hydrophobic interactions, hydrogen bonding and screened electrostatic interactions.[54] This results in soft, flexible materials that can respond to changes in the solution (such as pH or electrolyte concentration).

AB block copolymers can undergo microphase separation in the bulk. This occurs because the enthalpy of demixing exceeds the entropy of mixing.[56] The covalent bond between the two blocks prevents macroscopic phase separation. A range of diblock copolymer morphologies have been observed, including spheres, cylinders, bicontinuous gyroids and lamellae (Figure 1.21).[57] Three parameters influence the final copolymer morphology. Firstly, the volume fractions f_A and f_B for the A and B blocks, where the total volume fraction must be unity ($f_A + f_B = 1$). Secondly, the total degree of polymerisation, N (where $N = N_A + N_B$) and thirdly the Flory-Huggins parameter, χ_{AB} (see Equation 7), which describes the incompatibility of the two blocks.[57-59]

$$\chi_{AB} = \left(\frac{1}{k_B T}\right)\left[\varepsilon_{AB} - \frac{1}{2}(\varepsilon_{AA}+\varepsilon_{BB})\right] \quad (7)$$

Here k_B is the Boltzmann constant, T is the absolute temperature and ε_{AB}, ε_{AA} and ε_{BB} are the interaction energies for the A and B segments.[58] The Flory-Huggins parameter varies inversely with temperature and is positive when A-B interactions result in an increase in the overall energy.

Combining the Flory-Huggins parameter (χ_{AB}) with the degree of polymerisation (N) can give the degree of segregation (χN) between the two blocks. Comparing this to the block volume fraction leads to a theoretical phase diagram, as shown in Figure 1.21. This can be used to predict the various copolymer morphologies for an AB diblock. When f_A is 0.5 (i.e equal volume fractions of A and B blocks), lamellae are observed. At lower f_A values, spheres, cylinders or bicontinuous gyroids are observed. However, increasing f_A above 0.5 leads to inverted structures.

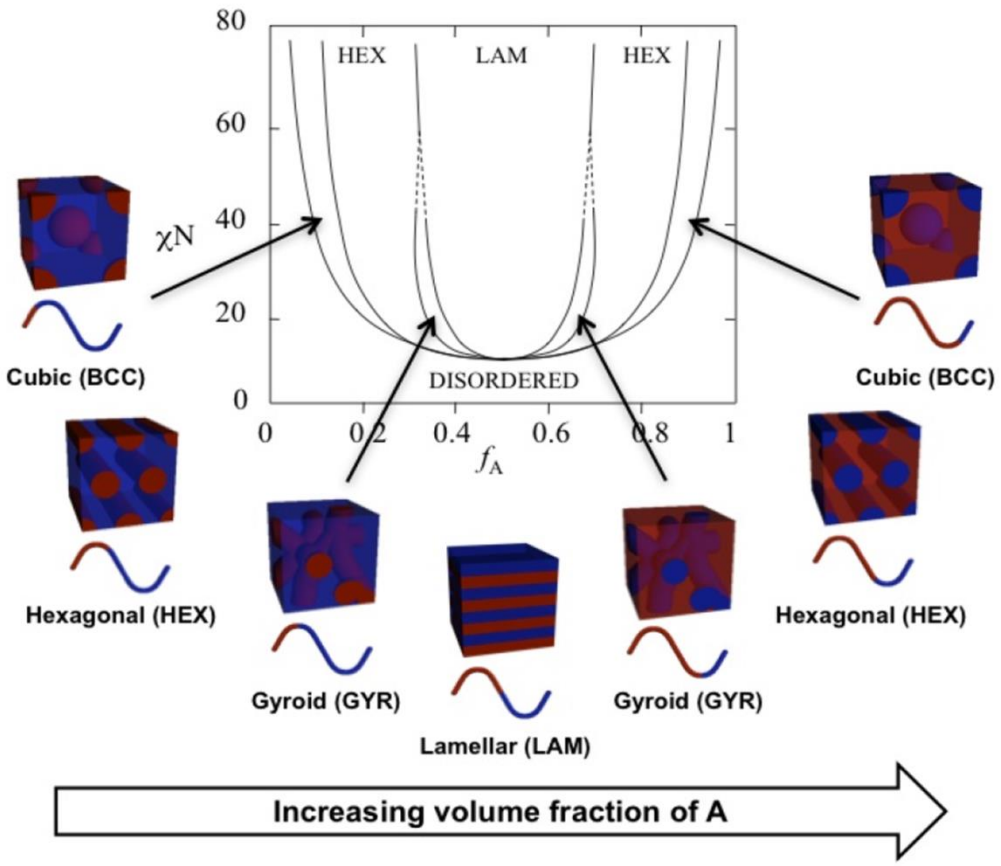

Figure 1.21 Theoretical phase diagram and corresponding solid-state morphologies for diblock copolymers. The phases are indicated as follows: body centered cubic (BCC), hexagonal cylinders (HEX), gyroid (GYR) and lamellae (LAM). f_A is the volume fraction of polymer block A, χ is the Flory-Huggins interaction parameter and *N* is the total degree of polymerisation.[56]

In solution, the composition of a block copolymer can strongly influence the final morphology. Subtle changes in the degree of polymerisation lead to a change in relative volume fractions and therefore change the copolymer morphology. This is determined by the packing parameter, P, as shown in Equation 8:

$$P = \left(\frac{V}{a_0 l_c}\right) \tag{8}$$

Here V is the volume of the hydrophobic block, a_0 is the cross-sectional area of the hydrophilic block and l_c is the length of the hydrophobic segment.[54] Figure 1.22 shows how the packing parameter influences the self-assembly of block copolymers. High curvature ($P \leq ⅓$) is observed when the hydrophobic segment is relatively small compared to the hydrophilic block; this results in a cone-like structure which self-assembles to form spherical micelles. Increasing the proportion of the hydrophobic block leads to a gradual reduction in the curvature. This can lead to worm-like

micelles, rods or cylinders when ⅓ ≤ P ≤ ½. Further increasing the hydrophobic block volume fraction can lead to very low curvature (½≤ P ≤ 1) resulting in a bilayer structure or a vesicular morphology.

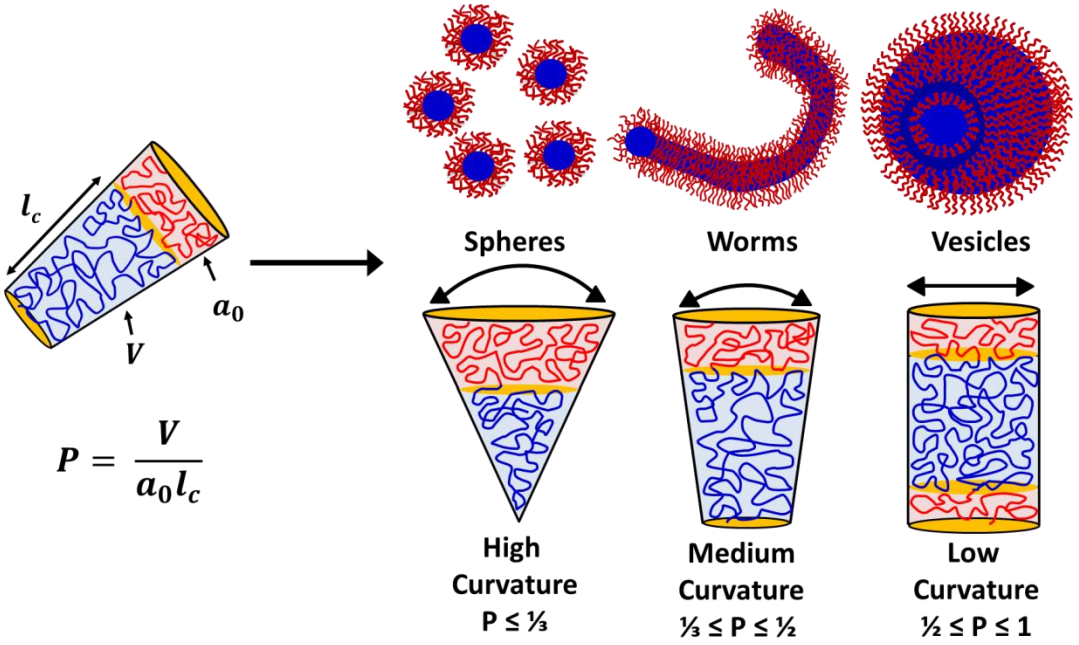

Figure 1.22 Self-assembly of block copolymers into three different morphologies (spheres, worms or vesicles) depending on the packing parameter, P.[60]

Amphiphilic block copolymers can undergo self-assembly in aqueous solution. This can be achieved in various ways including the solvent switch method[61] and thin film rehydration.[62,63] The solvent switch method involves the amphiphilic block copolymer being molecularly dissolved in a solvent which is good for both blocks. Slowly introducing a solvent that is selective (a poor solvent) for one block induces phase separation and aggregation begins to occur. For example, Eisenberg and co-workers prepared polystyrene-poly(acrylic acid) (PS-PAA) diblock copolymers by sequential anionic polymerisation.[64,65] These PS-PAA diblock copolymers were dissolved in DMF, which is a good solvent for both PS and PAA. Deionised water, which is a poor solvent for the PS block, was slowly introduced causing the diblock copolymers to self-assemble in situ. The PS-PAA system has been studied in great detail and a wide range of copolymer morphologies have been observed with varying block compositions, see Figure 1.23. Not only are spheres, worms and vesicles observed, but also bicontinuous rods, lamellae, hexagonally-packed hollow hoops (HHHs) and large compound micelles (LCMs).[57,66]

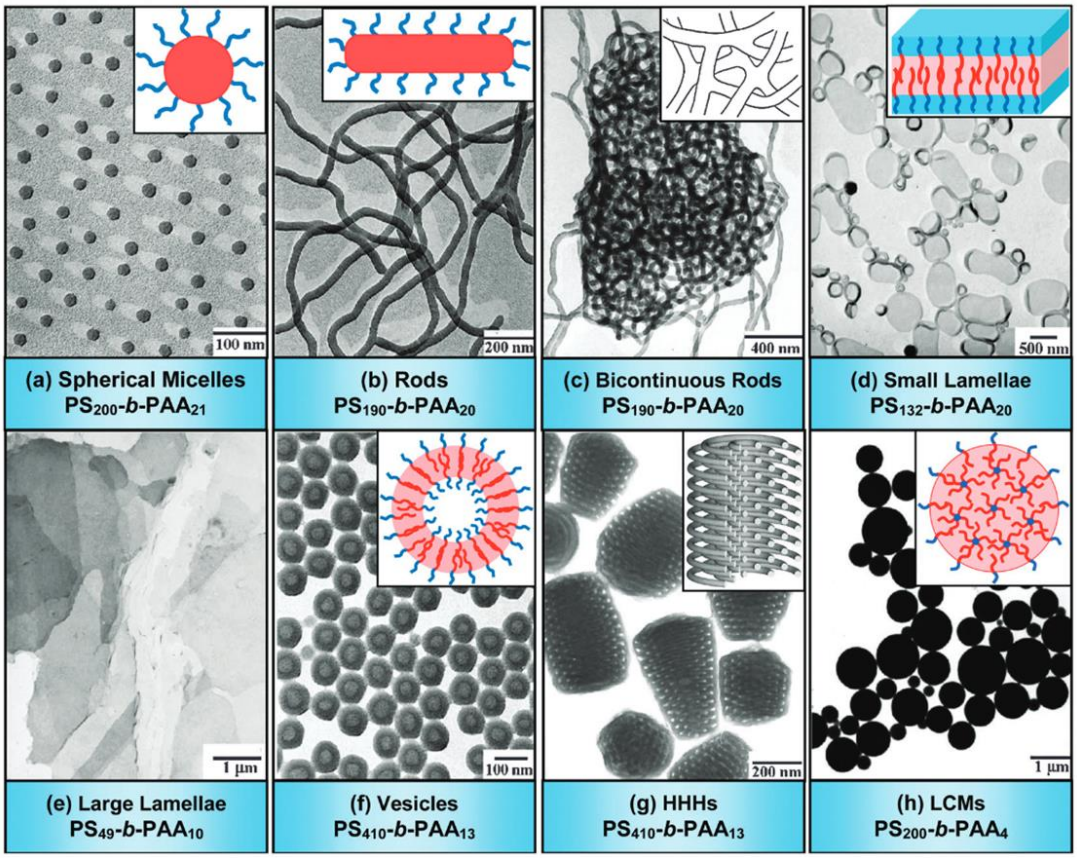

Figure 1.23 Transmission electron microscopy (TEM) images and corresponding schematic cartoons of various copolymer morphologies formed from amphiphilic PS_m-PAA_n copolymers. (hexagonally-packed hollow hoops are denoted at HHHs and large compound micelles are denoted as LCMs).[57,66]

The effect of the solvent composition for one particular block copolymer, PS_{310}-PAA_{52}, has been studied in particular detail.[67] The PS_{310}-PAA_{52} diblock copolymers were diluted in dioxane and water was slowly introduced. The system was allowed to reach equilibrium before further water addition. Figure 1.24 shows the resulting morphological behaviour of PS_{310}-PAA_{52} on addition of water. With 5 wt% water or less, this diblock copolymer remains fully soluble but for higher water contents the PS block becomes increasingly hydrophobic, resulting in the formation of spherical micelles. Further addition of water leads to an order-order morphological transition from spheres to rods to vesicles. After the initial vesicles were formed, increasing the water content led to larger vesicles but with a relatively constant wall thickness.[67,68] This morphological transition was found to be fully reversible: addition of dioxane solvates the PS block and causes the vesicles to form rods.

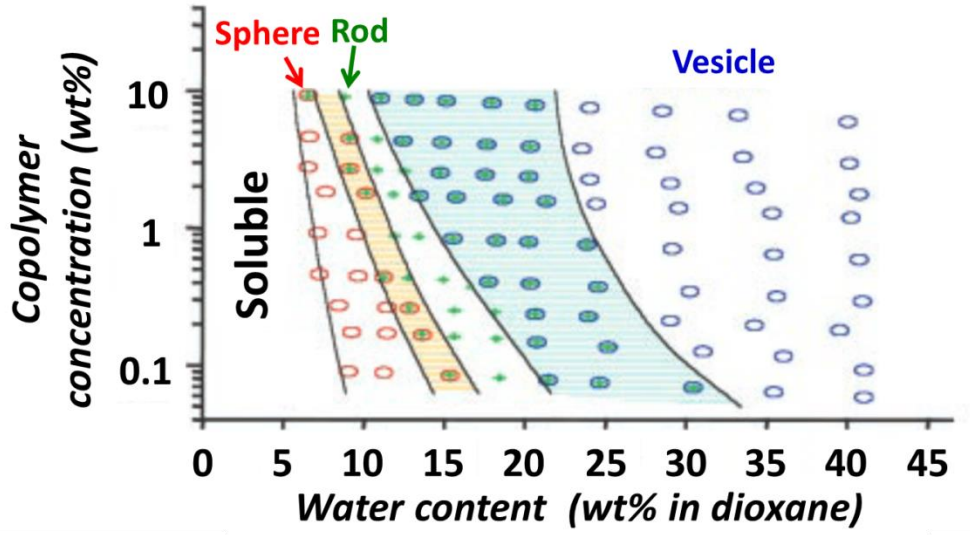

Figure 1.24 Phase diagram for a PS_{310}-PAA_{52} diblock copolymer initially dissolved in dioxane with the addition of increasing amounts of water. The morphologies and phase boundaries were determined by TEM.[67]

1.9 Polymerisation-Induced Self-Assembly (PISA)

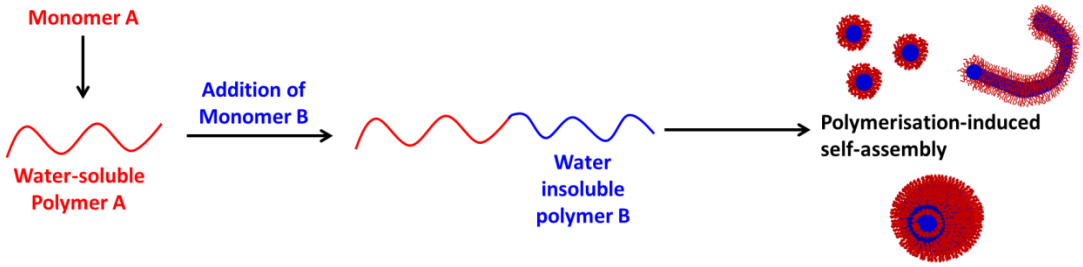

Figure 1.25 Schematic representation of polymerisation-induced self-assembly (PISA) for an amphiphilic diblock copolymer in water.

Polymerisation-induced self-assembly (PISA)[69-72] has recently become established as a powerful and versatile method for the synthesis of amphiphilic diblock copolymer nanoparticles. In essence, a soluble polymer is chain-extended using a second monomer, which is selected such that the growing polymer (or second block) becomes insoluble in the reaction medium, thus driving in situ self-assembly (Figure 1.25). Depending on the precise reaction conditions, this approach can be used to prepare a range of morphologies including spheres, worms or vesicles.[60] PISA is extremely convenient and removes the need for post-polymerisation processing to induce self-assembly. These steps are often time-consuming and have to be carried out at relatively low solids (typically < 1%) whereas PISA can be performed at relatively high solids, typically 10 – 25%. Recently, Derry et al. synthesised

poly(lauryl methacrylate)-poly(benzyl methacrylate) (PLMA-PBzMA) diblock copolymers at up to 50% w/w solids via RAFT dispersion polymerisation in mineral oil at 90 °C.[73]

The final amphiphilic diblock copolymer morphology depends on several parameters including the hydrophilic block DP, the hydrophobic core-forming block DP and the total solids content. In principle, maintaining a fixed hydrophilic block DP and systematically increasing the hydrophobic block DP leads to an evolution in morphology from spherical micelles to worms to vesicles due to a gradual reduction in the curvature resulting in an increase in the packing parameter. This approach, together with varying the solids content, can lead to the development of phase diagrams in which a specific copolymer morphology can be reproducibly targeted. Figure 1.26 shows a phase diagram for poly(glycerol monomethacrylate)$_{78}$-poly(2-hydroxypropyl methacrylate)$_x$ (PGMA$_{78}$-PHPMA$_x$) diblock copolymers synthesised via RAFT aqueous dispersion polymerisation of HPMA at 70 °C.[74] Using a PGMA$_{78}$ macro-CTA and varying both the PHPMA DP and the solids content enabled pure sphere, worm and vesicle phases to be prepared reproducibly.

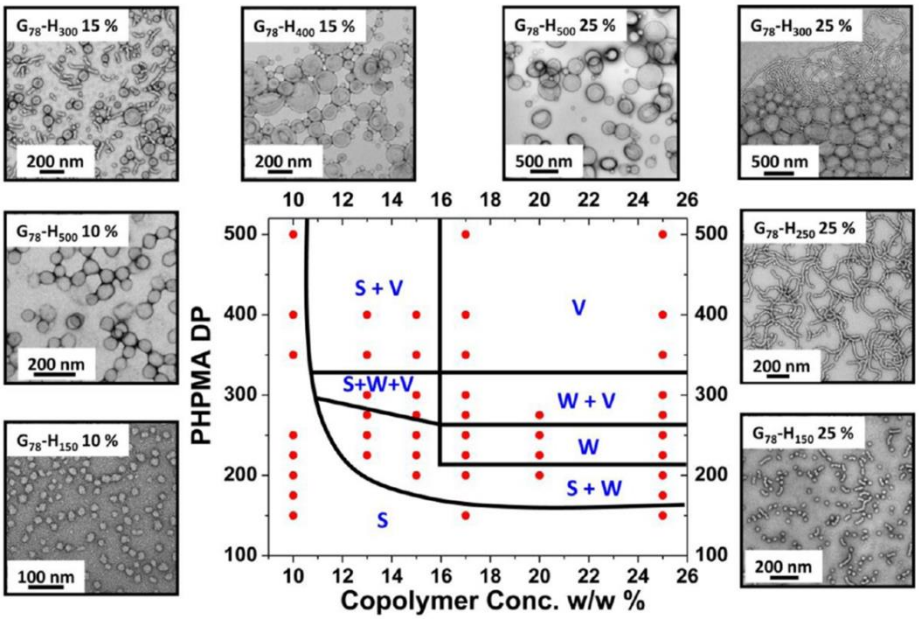

Figure 1.26 TEM images and the corresponding phase diagram for a series of PGMA$_{78}$-PHPMA$_x$ copolymers synthesised by aqueous RAFT dispersion polymerisation of HPMA at various concentrations (S = spheres, W = worms and V = vesicles).[74]

Several review articles on PISA have been published,[69-72] Charleux et al. provided a detailed overview of PISA via NMP, ATRP and RAFT polymerisation.[69] Canning et

al. focused on RAFT-mediated PISA[71] and other, more specific, reviews discuss RAFT dispersion polymerisation in either aqueous[70] or non-aqueous media.[72] Literature examples of PISA via RAFT aqueous emulsion polymerisation and RAFT dispersion polymerisation (aqueous, alcoholic and *n*-alkanes) will be discussed in the following sections.

1.9.1 PISA via RAFT Aqueous Emulsion Polymerisation

In principle, RAFT emulsion polymerisation provides a convenient surfactant-free route for the synthesis of nanolatexes. The first examples of RAFT emulsion polymerisation involved the addition of a RAFT CTA to a conventional emulsion polymerisation in the presence of surfactant. However, this led to poor control over molecular weights and dispersities, low conversions and poor colloidal stability.[75] Development of seeded RAFT emulsion polymerisation led to improved control.[76] Seeded RAFT emulsion polymerisation involves using a preformed latex, or seed, in which additional monomer can react to grow new polymer chains. However, the initial seed was not synthesised via RAFT polymerisation so the final polymers did not exhibit low dispersities. Instead, bimodal MWDs were obtained.

The first *ab initio* RAFT emulsion polymerisation was developed by Hawkett et al.[77-79] This involved the synthesis of a hydrophilic poly(acrylic acid) (PAA) macro-CTA, which acts as a steric stabiliser for chain extension of a hydrophobic monomer, *n*-butyl acrylate (*n*BA). This resulted in a stable amphiphilic PAA-P*n*BA diblock copolymer, which exhibited a linear increase in molecular weight with conversion and relatively low dispersity of 1.11, as judged by tetrahydrofuran (THF) GPC.[77] This PAA-P*n*BA diblock self-assembled to form 60 nm particles in solution. Hawkett et al. then extended this work to form triblock copolymers to demonstrate the living character of the diblock copolymer.[78] After the initial *n*BA block had been synthesised, styrene (S) was added to form a more hydrophobic block. This produced well-defined PAA-P*n*BA-PS triblocks.[78]

Since the development of *ab initio* RAFT emulsion polymerisation, Charleux and co-workers have dominated this area of research with numerous publications each year for the last decade. Several parameters have been extensively studied, including the nature of the hydrophilic stabiliser block (acrylic,[80-82] methacrylic,[83] acrylamide[84]), the hydrophobic core-forming monomer (*n*BA,[84] styrene,[83,85] methyl methacrylate

(MMA)[86] or benzyl methacrylate (BzMA)[87]), the types of RAFT agent (trithiocarbonates[80,84] or dithiobenzoates[83]) and the reaction conditions (pH[82,85] and salt concentration[81]), see Figure 1.27.

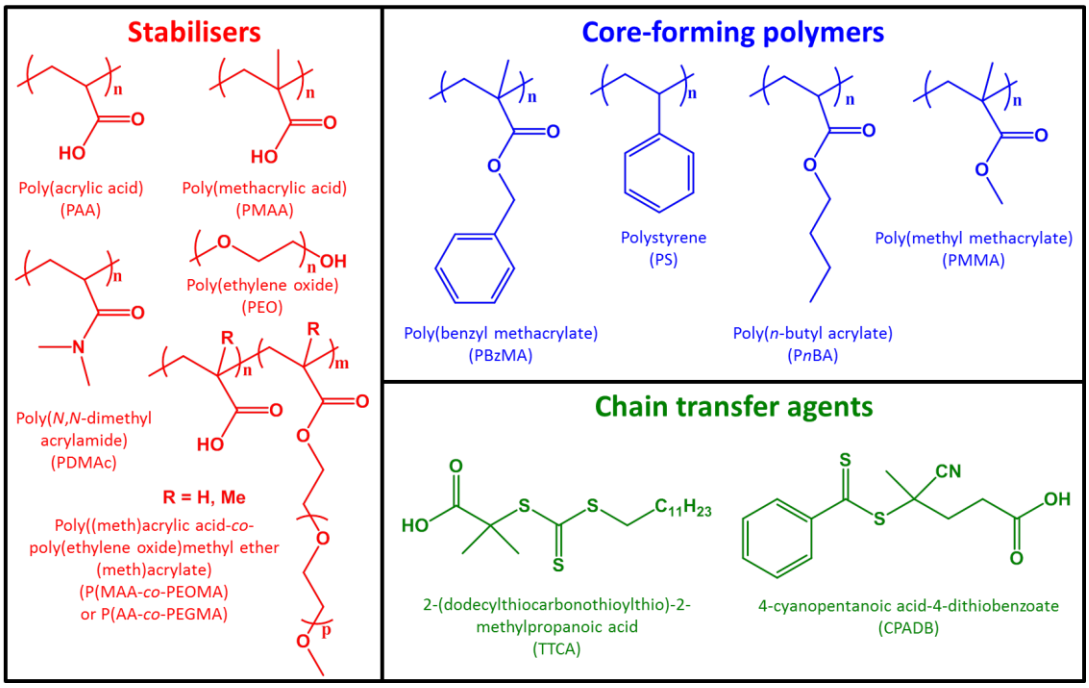

Figure 1.27 Chemical structures of various hydrophilic stabilisers, core-forming polymers and chain transfer agents used for RAFT aqueous emulsion polymerisation.[80-87]

Two common water-soluble stabilisers used are poly(*N*,*N*-dimethyl acrylamide) (PDMAc)[84] and poly(ethylene oxide) (PEO).[86,88] These have each been synthesised with a trithiocarbonate RAFT agent and extended with *n*BA. The PDMAc-P*n*BA diblock copolymers were obtained at high conversions (≥ 96%) and exhibited reasonably high blocking efficiencies by THF GPC but also relatively high dispersities, ranging from 1.32 to 1.86.[84] An initial induction period of ~35 min was typically observed, with complete conversions being achieved within a few hours. In contrast, longer induction times of around 1 h were observed for PEO-P*n*BuA diblock copolymers but high conversions were nevertheless achieved within 6 h.[88] GPC analysis indicated increasing molecular weight with conversion and relatively low dispersities were achieved (M_w/M_n < 1.26). Both the PDMAc- and PEO-based diblock copolymers self-assembled to form spherical micelles. Rieger et al. also varied the target DP of the core-forming block using a PEO_{55} macro-CTA.[88] Using styrene for the core-forming block led to long reaction times with only 67% conversion being achieved after 23 h compared to more than 95 % within 4 h using

*n*BA. Similarly, replacing the trithiocarbonate RAFT agent with a dithiobenzoate led to extremely slow polymerisations. PEO-DB chain-extended with styrene only reached 26% conversion within 23 h at 80 °C and completely inhibited the reaction with *n*BA.[88]

The effect of pH was studied by Chaduc et al. for the PISA synthesis of PAA-PS diblock copolymers.[82] Acidic conditions (pH 2.5) led to high blocking efficiencies and controlled growth of the PS block. Increasing the pH caused ionisation of the PAA stabiliser, which led to a loss of control during chain extension. It was also observed that the particle size varied with pH. At pH 2.5, 55 nm spheres were formed as judged by dynamic light scattering (DLS), whereas increasing the pH to 8.1 produced 190 nm spheres. This was also confirmed by TEM studies (Figure 1.28).[82]

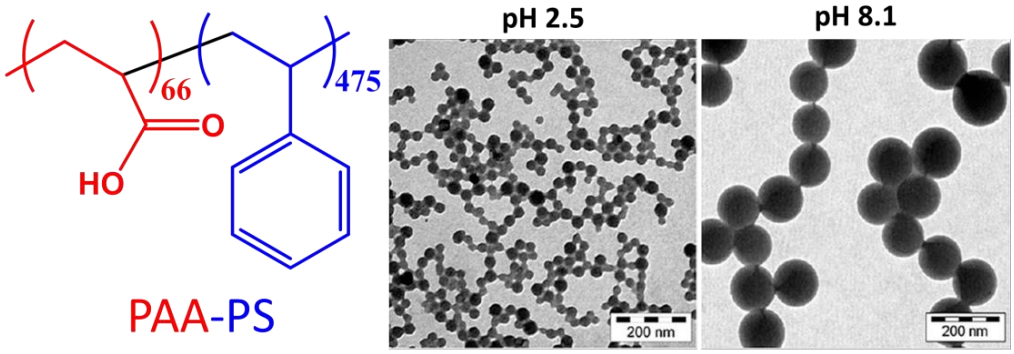

Figure 1.28 Chemical structure and TEM images obtained for the PAA_{66}-PS_{475} nanoparticles synthesised by RAFT emulsion polymerisation at either pH 2.5 or pH 8.1.[82]

In addition to the previously discussed parameters, one-pot syntheses of various diblock copolymers via RAFT emulsion polymerisation have been reported. PAA,[89] poly(methacrylic acid) (PMAA)[89,90] and poly(methacrylic acid-*co*-poly(ethylene oxide) methyl ether methacrylate) (P(MAA-*co*-PEOMA))[89,91] macro-CTAs have each been synthesised using 4-cyano-4-thiothiopropylsulfanyl pentanoic acid (CTPPA) as the RAFT CTA in water and then chain-extended with styrene in a one-pot, two-step method. Chaduc et al. studied the kinetics of the diblock copolymer synthesis using each of the above three macro-CTAs.[89] Kinetic experiments showed that syntheses using the PAA macro-CTA were significantly slower than those conducted with the other two macro-CTAs with an induction period of up to 2 h. Using either the PMAA or P(MAA-*co*-PEOMA) macro-CTA resulted in an induction period of just under an hour, with high conversions being achieved within

3 h when chain-extending with styrene. All three formulations gave a linear increase in molecular weight with conversion and relatively low dispersities ($M_w/M_n < 1.4$).[89]

Zhang et al. focused on P(MAA-*co*-PEOMA)-PS diblocks and varied both the PS DP and the PEOMA/MAA molar ratio within the stabiliser block.[91] MAA/PEOMA molar ratios of both 50/50 and 67/33 led to only spherical particles with larger particles with increasing PS DP being observed by DLS and TEM. High conversions and blocking efficiencies with low dispersities were observed for all P(MAA-*co*-PEOMA)-PS diblocks. Chaduc et al. examined the one-pot synthesis of diblock copolymers using PMAA as the stabiliser and varying the hydrophobic core-forming monomer.[90] Three hydrophobic core-forming monomers were compared: styrene, *n*BA and MMA. High conversions (≥ 99 %) were achieved within 2 h in each case and spherical micelles of ~38 nm were observed by TEM. Diblock copolymers synthesised with styrene or MMA had high blocking efficiencies and reasonably low dispersities ($M_w/M_n < 1.48$), whereas *n*BA led to relatively poor control, with high dispersities being obtained even at low conversions ($M_w/M_n = 1.52$ at 11% conversion; $M_w/M_n = 2.29$ at 98% conversion).[90] Such one-pot, two-step syntheses are highly convenient since they offer an entirely aqueous formulation, which is both environmentally friendly and inexpensive.

Several other examples of RAFT emulsion polymerisations have been reported by other research groups. For example, Bozovic-Vukic et al. used a poly(4-vinylpyridine) (P4VP) macro-CTA and extended it with styrene and acrylonitrile (AN) at low pH.[92] This formed colloidally stable spherical nanoparticles with a DLS diameter of 45 nm. Ting et al. synthesised a poly(2-(methacrylamido)-glucopyranose) (PMAG) macro-CTA using a trithiocarbonate RAFT agent, which was then chain-extended with styrene. The PMAG-PS diblocks increased in particle size with styrene conversion and formed spherical micelles of between 50 and 60 nm diameter.[93] Yeole and Hundiwale used a sodium 4-styrenesulfonate monomer with 4-cyanopentanoic acid dithiobenzoate (CPADB) to form a poly(sodium 4-styrenesulfonate)-based macro-CTA. This macro-CTA was extended with either styrene or MMA: gravimetric analysis indicated that MMA polymerised faster than styrene and the latter diblock copolymers produced spherical micelles whereas the former gave oval morphologies.[94]

A wide range of spherical nanoparticles were synthesised via RAFT emulsion polymerisation using various stabilisers and core-forming monomers. Boissé et al. reported the first example of non-spherical nano-objects synthesised by RAFT emulsion polymerisation.[80] A series of hydrophilic copolymer macro-CTAs comprising of acrylic acid (AA) and poly(ethylene glycol) methyl ether acrylate) (PEGA) was synthesised using 2-(dodecylthiocarbonothioylthio)-2-methylpropanoic acid (TTCA) as the CTA. Chain extension of these P(AA-*co*-PEGA) macro-CTAs with styrene produced amphiphilic diblock copolymers that self-assembled to form spherical micelles, worm-like micelles or vesicles. The effect of varying the macro-CTA composition (AA/PEGA molar ratio), pH and salt concentration were studied. Using either PAA or PPEGA homopolymers as the stabiliser led to only PAA-PS or PPEGA-PS spherical micelles. In contrast, worm-like micelles were observed by TEM at either acidic pH or high salt concentrations for P(AA-*co*-PEGA)-PS diblock copolymers (see Figure 1.28). Such non-spherical morphologies led to a significant increase in solution viscosity.[80] A kinetic study of one P(AA-*co*-PEGA)-PS diblock indicated an evolution in morphology from spherical micelles to worm-like micelles to vesicles was with increasing styrene conversion.

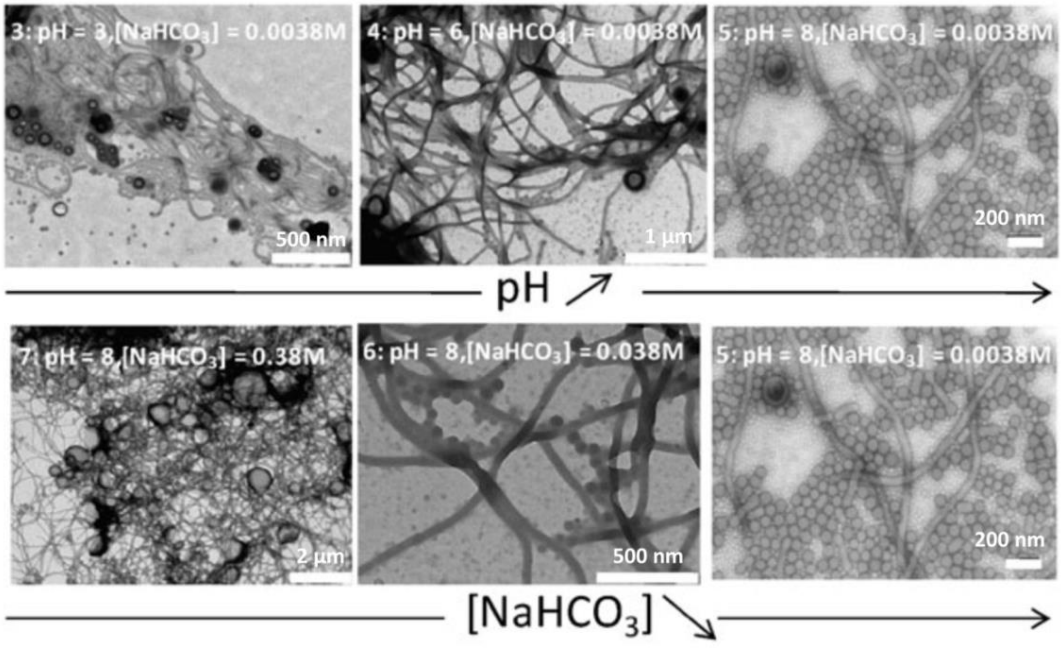

Figure 1.29 TEM images of the various copolymer morphologies obtained with P(AA-co-PEGA) (AA/PEGA = 50/50) when conducting the RAFT emulsion polymerisation of styrene at different pH and salt concentrations.[80]

A second study by Boissé et al. examined the influence of stirring speed and calcium chloride ($CaCl_2$) concentration on P(AA-*co*-PEGA)-PS nanoparticle morphologies.[81] The stirring speed was varied from 100 rpm to 750 rpm for a given P(AA-*co*-PEGA)-PS composition. Slower stirring speeds led to a reduction in the polymerisation rate, which was attributed to the rate-limiting transport of monomer from monomer droplets to the growing particles through the aqueous phase.[81] A stirring speed of 350 rpm was found to be optimum for worm-like micelle formation, with stirring speeds of 100 rpm and 750 rpm only producing spherical micelles. Secondly, the $CaCl_2$ concentration was varied from 0.004 M to 0.530 M. The molar ratio between the salt and acid units in the copolymer was also important in determining whether spherical micelles or higher order morphologies were obtained. Low salt concentrations (0.004 M, salt/acid molar ratio = 0.056) only led to spherical micelles, whereas higher salt concentrations (0.04 M, salt/acid molar ratio = 0.67) produced vesicular morphologies.[81] When a molar ratio of unity was used (and 0.072 M $CaCl_2$), a mixed phase of worm-like micelles and vesicles was observed by TEM. Similar results were obtained when the salt was replaced by sodium bicarbonate ($NaHCO_3$) targeting a molar ratio of unity. Boissé et al. concluded that the nature of the salt was not a particularly critical parameter but the molar ratio between salt and the acid groups on the hydrophilic block determined the final morphology.[81]

Given the all-acrylic P(AA-*co*-PEGA) macro-CTA employed, semi-continuous addition of styrene was required to gain control during the diblock copolymer synthesis. To improve this formulation, a further study by Zhang et al.[85] replaced the macro-CTA with P(MAA-*co*-PEOMA). Such methacrylic macro-CTAs possess higher chain transfer constants and so enable efficient chain extension to form well-defined amphiphilic block copolymers under emulsion polymerisation conditions. A series of P(MAA-*co*-PEOMA)-PS diblock copolymers were synthesised at pH 3-8 while varying the target PS DP and using various P(MAA-*co*-PEOMA) macro-CTAs.[85] The solution pH was found to be an important parameter for the synthesis of non-spherical morphologies. Zhang et al. targeted a DP of 200 for the PS block. The RAFT agent had relatively low water solubility at pH 3 and THF GPC analysis indicated poor control, with a final dispersity of 1.82 at 93% conversion. At pH 8, GPC indicated some residual macro-CTA suggesting a low blocking efficiency. An intermediate pH of between 5 and 6 was found to be optimum, with high blocking

efficiencies being achieved as judged by THF GPC and low dispersities ($M_w/M_n \leq$ 1.35). All P(MAA-*co*-PEOMA)-PS_{200} diblock copolymers synthesised at various pH only resulted in spherical micelles. At pH 5, the PS block DP was varied from 200 to 1000. Low dispersities and reasonably high conversions (typically > 90 %) were obtained. On increasing the PS DP, a change in morphology from mainly spherical micelles to vesicles was observed. Worm-like micelles were also obtained, but this was not a pure phase because a small amount of spherical micelles were also observed by TEM. A kinetic study confirmed an evolution in morphology from spherical micelles to worm-like micelles to vesicles with increasing PS DP, as previously reported by Boissé et al.[80,81] Two different P(MAA-*co*-PEOMA) macro-CTAs were also used when targeting a DP of 300 for the PS block. A longer P(MAA-*co*-PEOMA) macro-CTA with a M_n of 15 kg mol^{-1} led to mainly worm-like micelles, whereas the shorter P(MAA-*co*-PEOMA) macro-CTA (M_n = 11.8 kg mol^{-1}) led to a pure vesicle phase.

A follow-up paper focussing on the P(MAA-*co*-PEOMA)-PS formulation by Zhang et al. demonstrated that these diblock copolymer nanoparticles can be synthesised via a one-pot, two-step method (Figure 1.30). Firstly, a P(MAA-*co*-PEOMA) macro-CTA was synthesised at pH 3.5 and taken to close to 100% conversion. Then, without purification, the solution pH was adjusted to pH 5 and styrene, initiator and water were added. This approach led to the successful synthesis of P(MAA-*co*-PEOMA)-PS diblock copolymers with a high level of control. High conversions and low dispersities were reported by ^{1}H NMR and THF GPC studies, respectively.[95]

This one-pot synthesis is attractive for industry as no post-polymerisation purification step is required. Spheres, worms or vesicles were targeted and a phase diagram (Figure 1.31) indicating the copolymer morphology obtained at various PS DPs and P(MAA-*co*-PEOMA) macro-CTA molecular weights. This allowed spheres, worms or vesicles to be reproducibly targeted.

Variation in the composition of the core-forming block was also studied by (partially) replacing the PS block with PMMA.[96] All three morphologies were observed for a series of P(MAA-*co*-PEOMA)-PMMA syntheses conducted at pH 3.5, 5 and 7. However, using a mixture of styrene and MMA for the core-forming block only resulted in spherical micelles.[96]

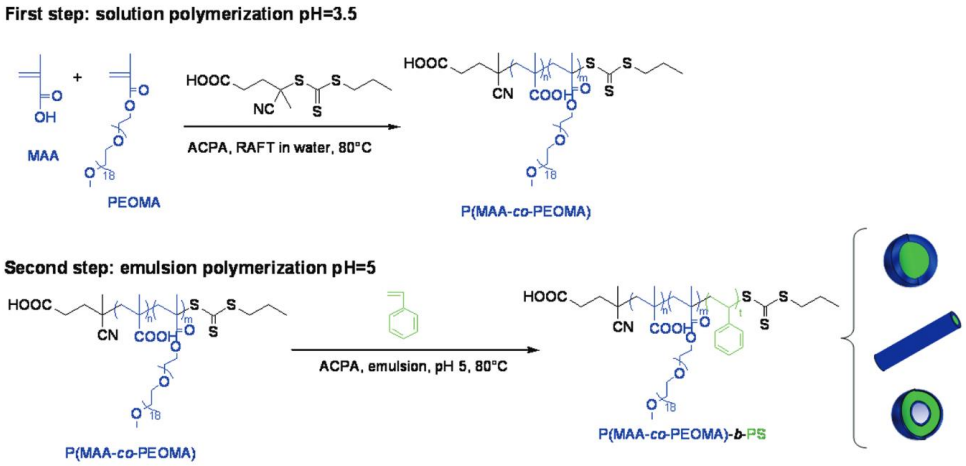

Figure 1.30 One-pot two-step synthesis of P(MAA-*co*-PEOMA)-PS diblock copolymer nano-objects via RAFT aqueous emulsion polymerisation of styrene.[95]

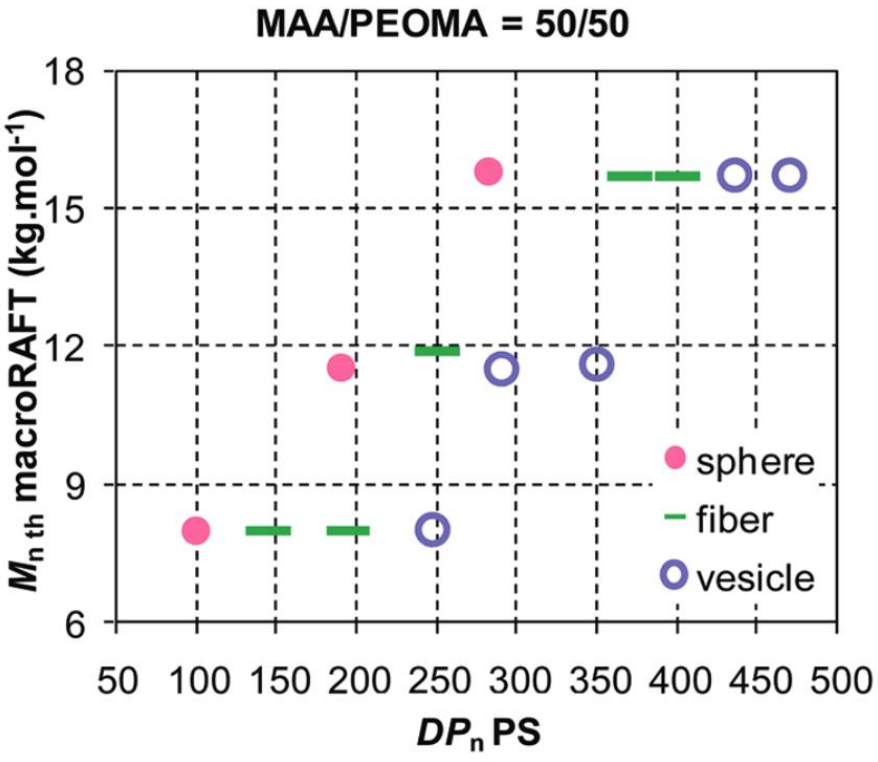

Figure 1.31 Phase diagram for P(MAA-*co*-PEOMA)-PS diblock copolymers prepared via RAFT emulsion polymerisation showing where spheres, worms (fibers) and vesicles can be obtained for various PS DP and P(MAA-*co*-PEOMA) macro-CTA molecular weights, at pH = 5.[95]

Non-spherical morphologies appear to be particularly difficult to target but with systematic variation of the reaction parameters Charleux and co-workers have shown that worm-like micelles or vesicles are attainable by RAFT aqueous emulsion polymerisation.[80,81,87,97]

1.9.2 PISA via RAFT Aqueous Dispersion Polymerisation

For a RAFT aqueous dispersion polymerisation, a water-soluble macro-CTA is chain-extended with a monomer that is water-miscible but the corresponding polymer is water-insoluble. Relatively few monomers fulfil this requirement, which led to a somewhat slower development of the field compared to RAFT aqueous emulsion polymerisation. Since the first report of RAFT aqueous dispersion polymerisation by Hawker and co-workers,[98] who described the synthesis of poly(*N*,*N*-dimethyl acrylamide)-poly(*N*-isopropylacrylamide) (PDMAc-PNIPAm) diblock copolymer nanoparticles, many stabilisers, core-forming monomers and RAFT CTAs have been employed, see Figure 1.32.

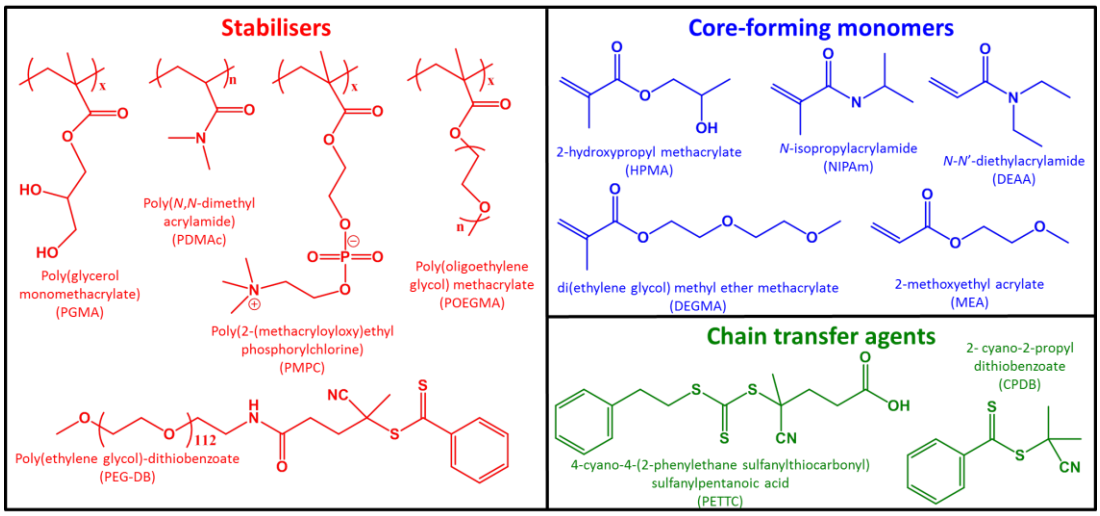

Figure 1.32 Chemical structures of hydrophilic water-soluble stabilisers, hydrophobic core-forming monomers and chain transfer agents that can be used for RAFT aqueous dispersion polymerisation.[70,71]

The most studied RAFT aqueous dispersion polymerisation formulation is for the synthesis of poly(glycerol monomethacrylate)-poly(2-hydroxypropyl methacrylate) (PGMA-PHPMA) diblock copolymers developed by Armes and co-workers.[74,99-105] The first report was by Li and Armes[99] in 2010: a dithiobenzoate-based $PGMA_{65}$ macro-CTA was chain-extended with varying amounts of HPMA. PHPMA DPs of 30 - 300 were targeted at 10% w/w solids and the resulting $PGMA_{65}$-$PHPMA_x$ diblock copolymer spheres showed an increase in particle diameter with PHPMA DP by DLS. Electron microscopy studies confirmed a well-defined spherical morphology for diblock copolymers prepared at 10% w/w. However, increasing the solids content to 20% w/w led to vesicle formation when targeting a $PGMA_{65}$-$PHPMA_{300}$ diblock copolymer.

Blanazs et al. demonstrated that this PGMA-PHPMA formulation could also yield worm-like micelles.[100] A detailed kinetic study during the synthesis of $PGMA_{47}$-$PHPMA_{200}$ provided an important insight regarding the evolution in copolymer morphology during the polymerisation. NMR was used to determine the HPMA conversion, with more than 99% being achieved within 2 h at 70 °C. DLS and TEM studies were used to monitor the self-assembly behaviour. Initially, only molecularly-dissolved copolymer chains were present, but after 65 min spherical micelles were formed that corresponded to a block composition of $PGMA_{47}$-$PHPMA_{92}$ (46% conversion). As the HPMA polymerisation progressed, these spheres begin to aggregate, forming dimers and trimers before short worm-like micelles are observed. These worms were eventually transformed into vesicles with increasing HPMA conversion. A schematic, with corresponding TEM images, shows the intermediate morphologies observed for this system, Figure 1.33.[100] The worms begin to branch and cluster before forming flat sheets with worms located on the periphery. These wrap up to form 'jellyfish', which eventually close up to form vesicles.

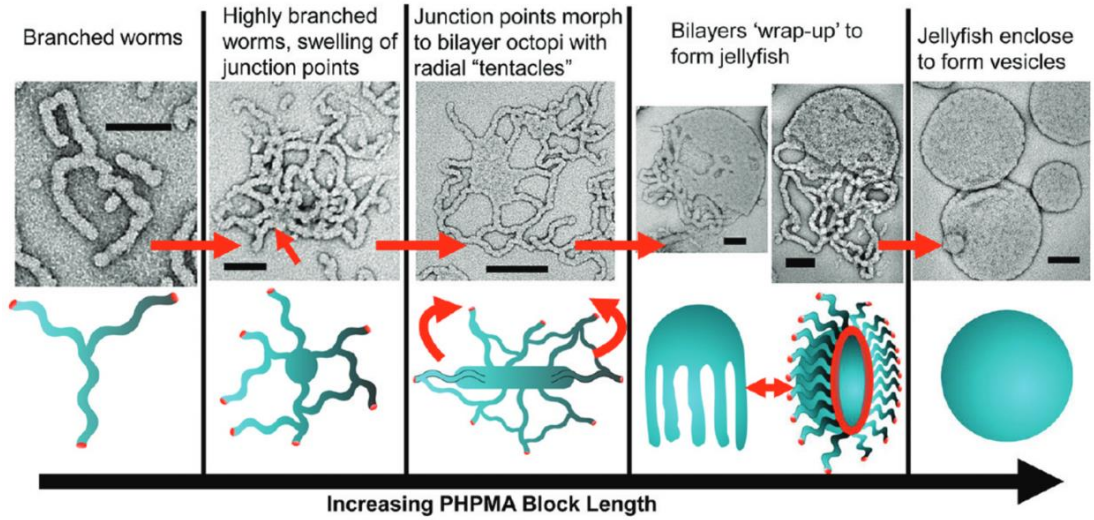

Figure 1.33 Proposed mechanism for the worm-to-vesicle transformation that occurs during the RAFT aqueous dispersion polymerisation synthesis of $PGMA_{47}$-$PHPMA_{200}$, as suggested by Blanazs et al. (scale bar = 100 nm).[100]

Phase diagrams were produced to enable spheres, worms and vesicles to be reproducibly targeted for the PGMA-PHPMA system.[74] As described earlier, the PGMA stabiliser block DP, the PHPMA core-forming block DP and the solids content each influence the final copolymer morphology. Phase diagrams require one

parameter to be fixed (usually the stabiliser block DP) in order to examine the effect of varying the other two parameters (the core-forming block DP and the solids content). Blanazs et al. constructed three phase diagrams using three different PGMA macro-CTAs (Figure 1.34).[74] Using a relatively short $PGMA_{47}$ macro-CTA enabled access to the full range of copolymer morphologies without any copolymer concentration dependence. Spheres, worms or vesicles could each be formed at either 10% w/w or 25% w/w solids. Using a slightly longer $PGMA_{78}$ macro-CTA led to exclusively spheres at 10% w/w but targeting higher solids (17% w/w or greater) enabled pure worm or vesicles phases to be produced. This strongly suggests that the spheres produced at 10% w/w solids are kinetically-trapped, rather than an equilibrium morphology. Increasing the PGMA stabiliser DP up to 112 led to almost exclusively spheres even when targeting high PHPMA DPs at high solids. This clearly shows that the copolymer morphology depends not only on the core-forming block DP and solids content but also on the DP of the stabiliser block.

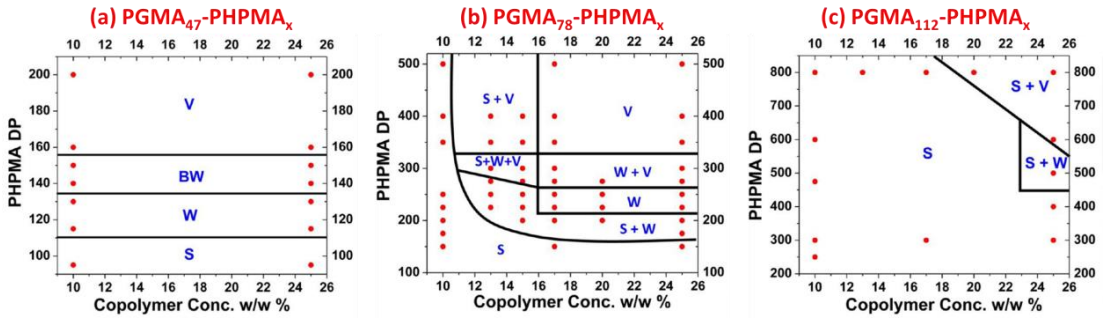

Figure 1.34 Phase diagrams determined by TEM analysis for (a) $PGMA_{47}$-$PHPMA_x$, (b) $PGMA_{78}$-$PHPMA_x$ and (c) $PGMA_{112}$-$PHPMA_x$ diblock copolymers synthesised at various concentrations between 10 and 25% w/w (S = spheres, W = worms, BW = branched worms and V = vesicles).[74]

In particular, the development of PGMA-PHPMA phase diagrams has enabled pure worm-like micelles to be reproducibly targeted. These PGMA-PHPMA worms form gels as a result of multiple inter-worm contacts. Cooling these gels causes degelation due to a worm-to-sphere transition (Figure 1.35).[101] This order-order transition is fully reversible: regelation occurs on heating. This thermal transition occurs due to surface plastication of the PHPMA core-forming block. This leads to a subtle lowering of the packing parameter. Rheology studies of these worm gels has enabled the critical gelation temperature (CGT) to be tuned, with lower PHPMA DPs having a higher CGT.[103] Statistical copolymerisation of a more hydrophilic monomer di(ethylene glycol) methyl ether methacrylate (DEGMA) with HPMA can also

increase the CGT.[106] This reversible (de)gelation behaviour has several potential applications in biomedical science.[101,107] Cold ultrafiltration of the biocompatible PGMA-PHPMA diblock copolymer in its low-viscosity spherical form effectively removes bacteria[101] and such sterile gels have been found to induce stasis in human pluripotent stem cells.[107]

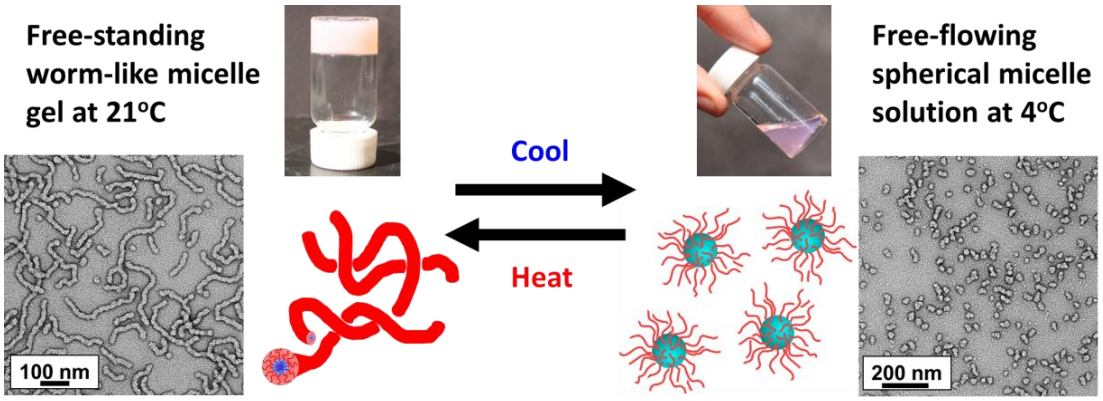

Figure 1.35 Thermoresponsive behaviour for $PGMA_{54}$-$PHPMA_{140}$ particles at 10% w/w. A gel is formed at 21 °C, which on cooling becomes a free-flowing liquid. TEM shows this coincides with a reversible worm-to-sphere transition.[101]

The vesicular morphology has also been extensively studied.[102,108-110] Warren et al. examined how the vesicles grow during PISA once they were formed.[108] It was found that the vesicles remained approximately constant in overall size but grew inwards as the membrane thickened, creating a smaller lumen. Mable et al. showed that the thermoresponsive behaviour of the PGMA-PHPMA system could be used to induce a thermally-triggered release of silica nanoparticles encapsulated during the PISA synthesis.[109] Cooling to 0 °C caused the vesicles to dissociate releasing the silica payload via a vesicle-to-sphere transition. Finally, PGMA-PHPMA-PBzMA triblock copolymers have been synthesised by addition of BzMA after the PGMA-PHPMA seed vesicles were prepared.[102,110] The hydrophobic nature of the PBzMA caused phase separation within the vesicle membranes leading to well-defined framboidal vesicles.

Polymerisation of HPMA using a water-soluble poly(2-(methacryloyloxy)ethyl phosophorylcholine) (PMPC) macro-CTA at 70 °C also enabled the PISA synthesis of a range of spheres, worms and vesicles.[111] Conversions of more than 99% were achieved within 2 h at 70 °C. For a $PMPC_{25}$ macro-CTA, the PHPMA DP was varied along with the solids content to enable the construction of a phase diagram. At 10%

w/w copolymer, only spherical micelles were obtained (similar to the $PGMA_{78}$-$PHPMA_x$ system) with an increase in particle size being observed with increasing PHPMA DP. Increasing the solids content and targeting PHPMA DPs greater than 200 enabled pure worms and vesicles to be prepared. Addition of small amounts of ethylene glycol dimethacrylate (EGDMA) to form cross-linked cores enabled an unusual 'lumpy rod' particle morphology to be observed.[112]

Warren et al. synthesised a poly(ethylene glycol) (PEG) dithiobenzoate macro-CTA for the RAFT aqueous dispersion polymerisation of HPMA.[113] Commercially available mono-hydroxy capped PEG_{113} was converted into mono-aminated PEG ($PEG\text{-}NH_2$) via a PEG-mesylate intermediate. This $PEG\text{-}NH_2$ was reacted with a succinimide-modified cyanopentanoate dithiobenzoate (SCPDB) to form the final PEG-dithiobenzoate macro-CTA (Figure 1.36a). A series of PEG_{113}-$PHPMA_x$ diblock copolymer nanoparticles were prepared in water at 50 °C. This formulation resulted in low-dispersity PEG_{113}-$PHPMA_x$ diblock copolymers even at high conversions. The PEG_{113}-$PHPMA_x$ diblock copolymers self-assembled to form a range of nano-objects. Spheres, worms and vesicles were observed, but lamellae stacks, jellyfish and oligolamellae vesicles were also observed (Figure 1.36c). The solids content was systematically varied from 5 – 20% w/w and PHPMA DPs of 100 to 400 were targeted to construct a phase diagram. A solids content of 20% w/w was required to form oligolamellar vesicles and small angle X-ray scattering (SAXS) indicated an average of three membranes per vesicle. Like the PGMA-PHPMA vesicles, the PEG-PHPMA vesicles underwent a reversible vesicle-to-sphere transition on cooling. This gave smaller lower polydispersity vesicles (compared to the original vesicles) on returning to 50 °C. This reversible change in morphology was used to encapsulate fluorescently-labelled PMPC homopolymer chains within the PEG_{113}-$PHPMA_x$ vesicles.

Although the majority of the RAFT aqueous dispersion polymerisation literature utilises HPMA as the core-forming monomer, other groups have utilised alternative monomers that become water-insoluble polymers. An and co-workers polymerised 2-methoxyethyl acrylate (MEA) using a poly(poly(ethylene glycol) methyl ether methacrylate) (PPEGMA) trithiocarbonate macro-CTA at either 30 or 40 °C using a redox initiator.[114] At least 90% conversion was achieved for a series of PPEGMA-PMEA diblock copolymers. DMF GPC analysis showed an increase in number-

average molecular weight with both conversion and PMEA DP, with relatively low final dispersities (M_w/M_n < 1.26). DLS confirmed the presence of 40 to 60 nm particles with low polydispersities. In a second study, An and co-workers used either a PEG or PPEGMA macro-CTA for the dispersion homopolymerisation of either DEGMA or the statistical copolymerisation of DEGMA with PEGMA.[115] High conversions were again achieved and the resulting nanogels had particle diameters between 52 and 154 nm with low polydispersities.

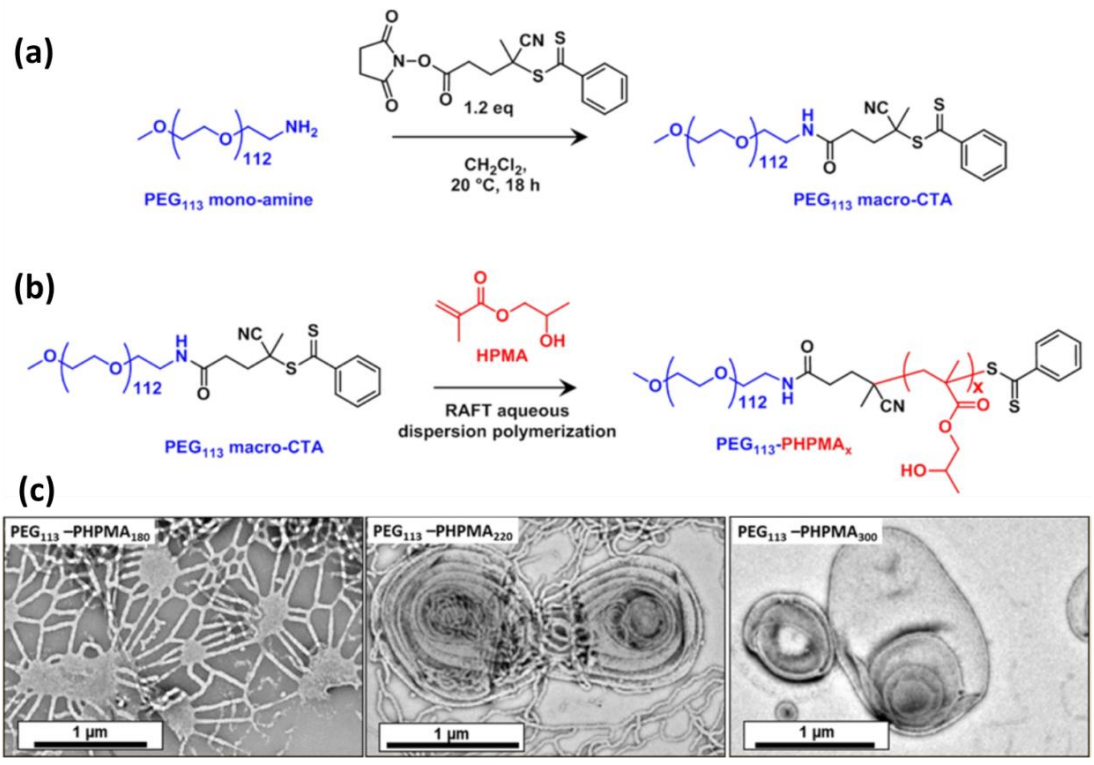

Figure 1.36 (a) Synthesis of a PEG-dithiobenzoate macro-CTA followed by (b) polymerisation of HPMA to form PEG_{113}-$PHPMA_x$ diblock copolymer nano-objects. (c) Representative TEM images for PEG_{113}-$PHPMA_{180}$, PEG_{113}-$PHPMA_{220}$ and PEG_{113}-$PHPMA_{300}$.[113]

1.9.3 PISA via RAFT Dispersion Polymerisation in non-aqueous solvents

RAFT dispersion polymerisation has been conducted in a wide range of non-aqueous solvents. These examples have been separated into three categories; dispersion polymerisation in lower alcohols (methanol, ethanol or iso-propanol), non-polar media (*n*-alkanes) and alternative media.

Lower alcohols

Pan and co-workers have synthesised several types of diblock copolymer nanoparticles utilising polystyrene as the core-forming block in methanol at 80 °C.[116-121] Typically their approach has focused on the chain extension of a poly(4-vinylpyridine) macro-CTA (P4VP) which was prepared using a trithiocarbonate RAFT agent, Figure 1.37.[116-118,122] The resulting P4VP-PS diblock copolymers self-assemble into an array of complex morphologies including nanotubes, 'yolk/shells' and large compound vesicles, as well as the more common sphere, worm and vesicle morphologies. Good control over molecular weight can be achieved, but relatively low styrene conversions are usually obtained (typically less than 70% in 24 h at 80 °C). This unreacted styrene monomer solvates the polystyrene core and therefore may influence the final copolymer morphology.

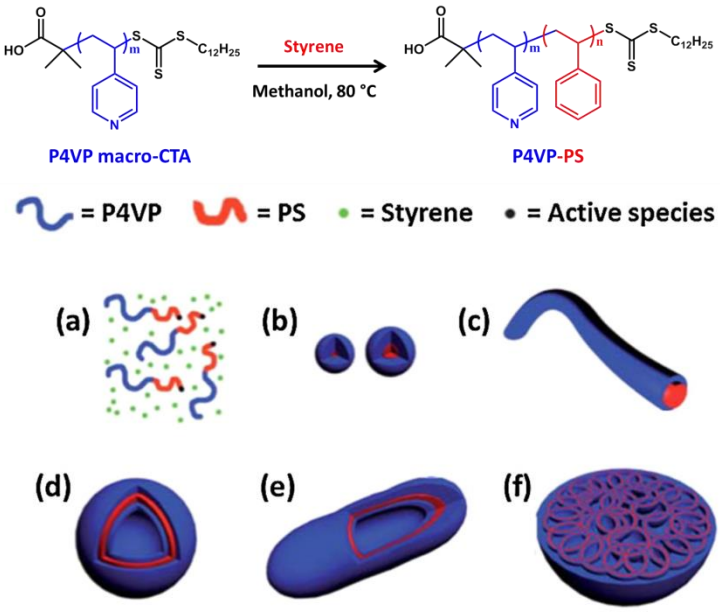

Figure 1.37 Schematic representation of the synthesis of poly(4-vinylpyridine)-polystyrene (P4VP-PS) diblock copolymers in methanol. The various morphologies into which these P4VP-PS diblocks self-assemble include (a) soluble chains, (b) spheres, (c) worms, (d) vesicles, (e) nanotubes and (f) large compound vesicles.[116,117]

In addition to utilising P4VP as an effective steric stabiliser for the polymerisation of styrene, PAA,[119] PEO[120] and poly(2-dimethylamino)ethyl methacrylate) (PDMA)[123] have also been utilised as macro-CTAs. Like the P4VP-PS diblock copolymers, spheres, worms and vesicles were observed with either a PEO or PAA macro-CTA given appropriate tuning of the block compositions. In contrast to the trithiocarbonate chemistry utilised in the P4VP, PAA and PEO macro-CTA

synthesis, the PDMA macro-CTA was synthesised using a dithiobenzoate RAFT agent (CPDB). A range of PDMA-PS diblock copolymers were synthesised in methanol at 80 °C. However, this seems unlikely as the boiling point of methanol is only 65 °C. TEM studies of the diblock copolymers indicated a range of morphologies, with spheres, worms, vesicles, nanotubes and large compound micelles all being observed (Figure 1.38). A further study in ethanol showed the formation of hexagonally-packed hollow hoops as an additional morphology.[124] Nevertheless, the high styrene monomer feed led to extremely low conversions (less than 25%).

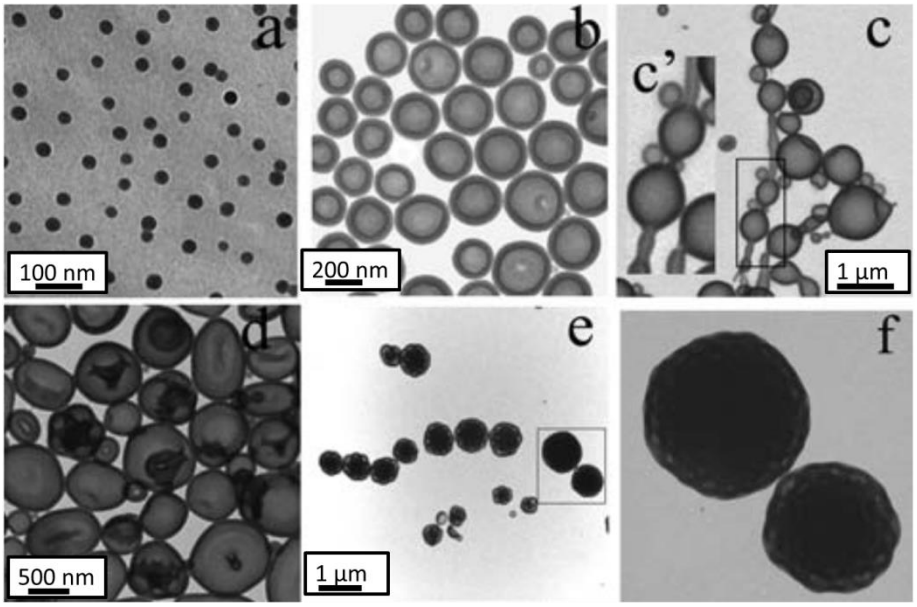

Figure 1.38 TEM images of the morphologies observed for PDMA-PS diblock copolymers prepared in methanol at 80 °C with various PS DPs.[123]

Higher conversions for styrene-based syntheses have been achieved by both Yang et al.[125] and Huo et al.[126] The former, used an alternating copolymerisation of styrene and *N*-phenylmaleimide (NMI). A PMAA macro-CTA was employed in a 50:50 w/w ethanol/1,4-dioxane mixture. This resulted in conversions of more than 90% within 10 h. These PMAA-(PS-*alt*-PNMI) diblock copolymers were unable to form vesicular morphologies because the high glass transition temperature (T_g) of the core-forming block prevented wrap-up. Instead, an evolution in morphology from spheres to worms to lamellae (or platelets) was observed.[125] Huo et al. used a solvent mixture of 95/5% ethanol/water in order to obtain high styrene conversions with a poly(*N*-(4-vinylbenzyl)-(*N*,*N*-diethylamine) trithiocarbonate macro-CTA. This formulation resulted in 90% conversion within 20 h.[126]

To eliminate the problem of incomplete styrene conversions, both Charleux's group[87] and Armes and co-workers[127-132] replaced styrene with benzyl methacrylate. For example, Semsarilar et al. synthesised four alcohol-soluble macro-CTAs using a trithiocarbonate RAFT agent: PDMA, PMAA, PGMA and PMPC (Figure 1.39). Chain extension of each precursor block with benzyl methacrylate in either ethanol or methanol led to high conversions (> 92 %) in each case and systematic variation of the target PBzMA DP produced a range of copolymer morphologies as judged by TEM.[127] With a particular focus on $PMAA_{71}$-$PBzMA_x$ a phase diagram was constructed to identify the precise copolymer compositions required for pure spheres, worms and vesicles.

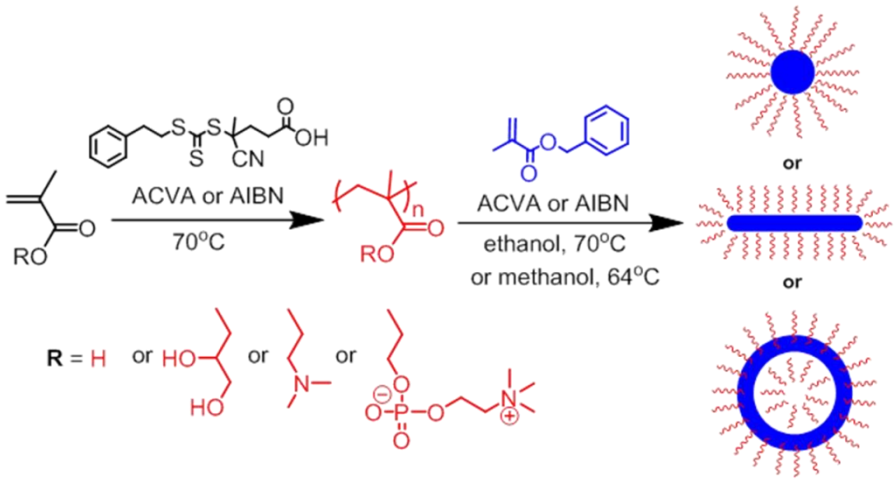

Figure 1.39 RAFT alcoholic dispersion polymerisation of benzyl methacrylate using four different macro-CTAs to form diblock copolymers that undergo polymerisation-induced self-assembly.[127]

Cross-linking of PMAA-PBzMA nanoparticles with EGDMA enabled Semsarilar et al. to transfer these ethanolic dispersions into alkaline solution without dissolution to give a mixed phase of worms and spheres.[128] Triblock copolymers were also prepared where 2,2,2-trifluoroethylmethacrylate (TFEMA) was added as a third block after the PMAA-PBzMA diblock copolymer synthesis. This enabled the synthesis of semi-fluorinated triblocks. These undergo self-assembly into a range of complex morphologies with incompatibility between the PBzMA and PTFEMA core-forming blocks driving phase separation on the nanometre length scale.[128]

A binary mixture of PMAA macro-CTAs enabled the synthesis of low-polydispersity PMAA-PBzMA block copolymer vesicles.[129] This method involves using both a relatively short vesicle-forming $PMAA_x$ macro-CTA together with a longer $PMAA_y$

macro-CTA (where y > x) which favours the formation of spherical micelles. For example, combining a $PMAA_{62}$ and $PMAA_{171}$ macro-CTA in the dispersion polymerisation of BzMA in ethanol leads to relatively small vesicles. Low polydispersity is achieved because the shorter $PMAA_{62}$-PBzMA chains are preferentially expressed at the inner surface of the vesicles while the longer $PMAA_{171}$-PBzMA chains are located at the outer surface.

Jones et al. focused on the synthesis of PDMA-PBzMA diblock copolymers.[130] High conversions were observed and using a relatively short $PDMA_{31}$ macro-CTA enabled the construction of a phase diagram for access to pure sphere, worm and vesicle phases. However, utilising a longer $PDMA_{74}$ macro-CTA only enabled the synthesis of kinetically-trapped spherical micelles even when targeting highly asymmetric $PDMA_{74}$-$PBzMA_{1000}$ diblock copolymers. This is similar to the situation for the RAFT aqueous dispersion polymerisation of HPMA when using a relatively long $PGMA_{112}$ macro-CTA. In a separate study, Jones et al. synthesised a series of $PDMA_{94}$-$PBzMA_x$ diblock copolymers to explore how spherical micelles grow during a RAFT PISA synthesis.[131] SAXS studies confirmed an increase in number of copolymer chains per micelle (N_{agg}) with increasing PBzMA DP. Two possible mechanisms for this increase in N_{agg} with particle size were proposed (Figure 1.40).[131] Firstly, exchange of individual copolymer chains with micelles after nucleation, Figure 1.40a. The second mechanism invokes sphere-sphere fusion to explain the formation of larger spherical nanoparticles, Figure 1.40b. It was concluded that both mechanisms may contribute to the observed increase in nanoparticle dimensions with the use of a relatively long $PDMA_{94}$ macro-CTA ensuring that sphere-sphere fusion merely resulted in larger spherical nanoparticle, as opposed to worm-like micelles or vesicles.

RAFT dispersion polymerisations conducted in alcohol tend to be particularly slow compared to aqueous dispersion polymerisation, with conversions of greater than 90% requiring typically 24 h, rather than 2-3 h. To increase the rate of BzMA polymerisation in the synthesis of PDMA-PBzMA diblock copolymers, Jones et al. examined the effect of adding water as a co-solvent to the ethanolic dispersion polymerisation.[132] Varying amounts of water (5 - 20%) were added to anhydrous ethanol. As expected, faster rates of polymerisation with increasing water content were observed. However, this change in solvent composition also affected the final

block copolymer morphology: only kinetically-trapped spheres were observed when an 80/20 ethanol/water mixture was employed for the synthesis of $PDMA_{43}$-$PBzMA_{200}$ diblock copolymers. In contrast, such copolymers formed vesicles when prepared in pure ethanol.

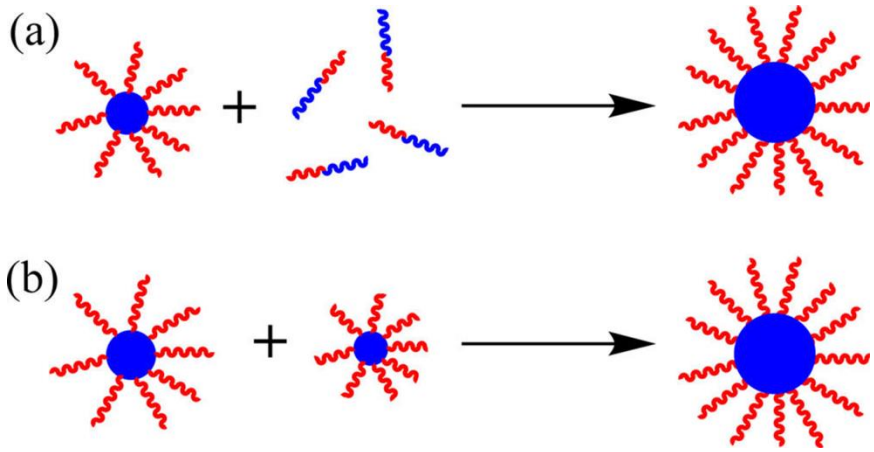

Figure 1.40 Two mechanisms suggested by Jones et al. for the growth of spheres during RAFT dispersion polymerisation, (a) exchange of individual copolymer chains between micelles following nucleation and (b) isotropic sphere-sphere fusion.[131]

Alternative core-forming monomers to styrene and BzMA have been evaluated for RAFT alcoholic dispersion polymerisation. For example, Semsarilar et al. reported the synthesis of poly(2-dimethylaminoethyl methacrylate)-poly(stearyl methacrylate) (PDMA-PSMA) in ethanol at 70 °C using PETTC as the RAFT CTA.[133] This resulted in diblock copolymer spheres, worms and vesicles with a semi-crystalline core-forming block. Lowe and co-workers synthesised several PDMA-stabilised diblock copolymers in ethanol at 70 °C.[134-136] Core-forming monomers utilised here include; 2-phenylethyl methacrylate (PEMA),[134] 3-phenylpropyl methacrylate (PPMA),[135] 2-(naphthalene-2-yloxy)ethyl methacylate (NOEMA)[136] and 2-phenoxyethyl methacrylate (POEMA).[136] PDMA-PPEMA diblock copolymers generally attained high conversions. A range of parameters were studied, including the stabiliser block DP, the core-forming block DP and the solids content. Spheres, worms and vesicles were produced and PISA syntheses at up to 40% w/w solids was achieved.[134] PDMA-PPPMA diblock copolymers also enabled spheres, worms and vesicles to be produced with conversions of at least 92%. It was found that $PDMA_{20}$-$PPPMA_{47}$ self-assembled to form thermoresponsive worms, which underwent a reversible worm-to-sphere transition when heated to 70 °C.[135] This also resulted in degelation similar to the thermoresponsive aqueous PGMA-PHPMA worm gels

reported by Blanazs et al. Unlike the well-controlled PDMA-PPEMA and PDMA-PPPMA formulations, the synthesis of PDMA-PNOEMA and PDMA-PPOEMA only led to bimodal GPC chromatograms and relatively high dispersities (M_w/M_n up to 1.83). However, spheres, worms and vesicles were observed for the PDMA-PNOEMA diblock copolymers, whereas only spherical micelles with increasing particle size were obtained for the PDMA-PPOEMA diblock copolymers.[136]

In non-polar media

The first example of RAFT dispersion polymerisation in non-polar media came from Houillot et al. for the synthesis of poly(2-ethylhexylacrylate)-poly(methyl acrylate) (PEHA-PMA) diblock copolymers in isodecane at 80 °C.[137,138] Two PEHA macro-CTAs were synthesised using either a dithiobenzoate or trithiocarbonate RAFT CTA. These precursors were then chain-extended with methyl acrylate to form diblock copolymers. Utilising a PEHA-DB macro-CTA led to a strong rate retardation and extremely poor control (M_w/M_n = 18) with residual macro-CTA identified in the THF GPC chromatograms. In contrast, faster rates of polymerisation and better control were achieved for PEHA-PMA diblock copolymers prepared using the PEHA-TTC macro-CTA, although relatively high dispersities were still observed (M_w/M_n up to 2.7).[137] PEHA-PMA diblock copolymers synthesised with the trithiocarbonate gave near monodisperse micelles of approximately 50 nm by DLS.

Fielding et al. synthesised a series of PLMA macro-CTAs via RAFT solution polymerisation in toluene at 70 °C using various RAFT CTAs.[139] In particular, a relatively short $PLMA_{17}$ and a longer $PLMA_{37}$ macro-CTA prepared using cumyl dithiobenzoate (CDB) were compared. Both were chain-extended with benzyl methacrylate via RAFT dispersion polymerisation in *n*-heptane at 90 °C (Figure 1.41a) to afford a series of $PLMA_x$-$PBzMA_y$ diblock copolymers. Utilising the longer $PLMA_{37}$ macro-CTA the PBzMA DP was varied from 100 to 900 at a solids content of 15% w/w. THF GPC analysis indicated relatively high dispersities of between 1.34 and 1.69. This is substantially lower than that reported by Houillot et al. but still compares unfavourably to other RAFT polymerisations conducted in aqueous or alcoholic media. DLS and TEM studies of these $PLMA_{37}$-$PBzMA_x$ diblock copolymers indicated only spherical micelles over a wide range of target PBzMA DP (Figure 1.41b). However, utilising the $PLMA_{17}$ macro-CTA resulted in the formation of spheres, worms and vesicles (Figure 1.41c). The PBzMA DP was

varied from 25 to 300 and the solids content was varied from 12.5% w/w to 25% w/w in order to construct a $PLMA_{17}$-$PBzMA_y$ phase diagram (Figure 1.41d). The $PLMA_{17}$-$PBzMA_y$ diblock copolymers all proceeded to at least 91% conversion and THF GPC analysis resulted in relatively low M_w/M_n values. The morphology of each diblock copolymer was assigned by TEM and enabled the phase boundaries to be defined. Like the aqueous and alcoholic RAFT dispersion polymerisations, the pure worm phase occupied very narrow phase space. Unlike some other phase diagrams, the $PLMA_{17}$-$PBzMA_y$ diblock copolymers exhibited relatively little dependence on copolymer concentration with spheres, mixed phases and vesicles being observed at all concentrations studied.[139]

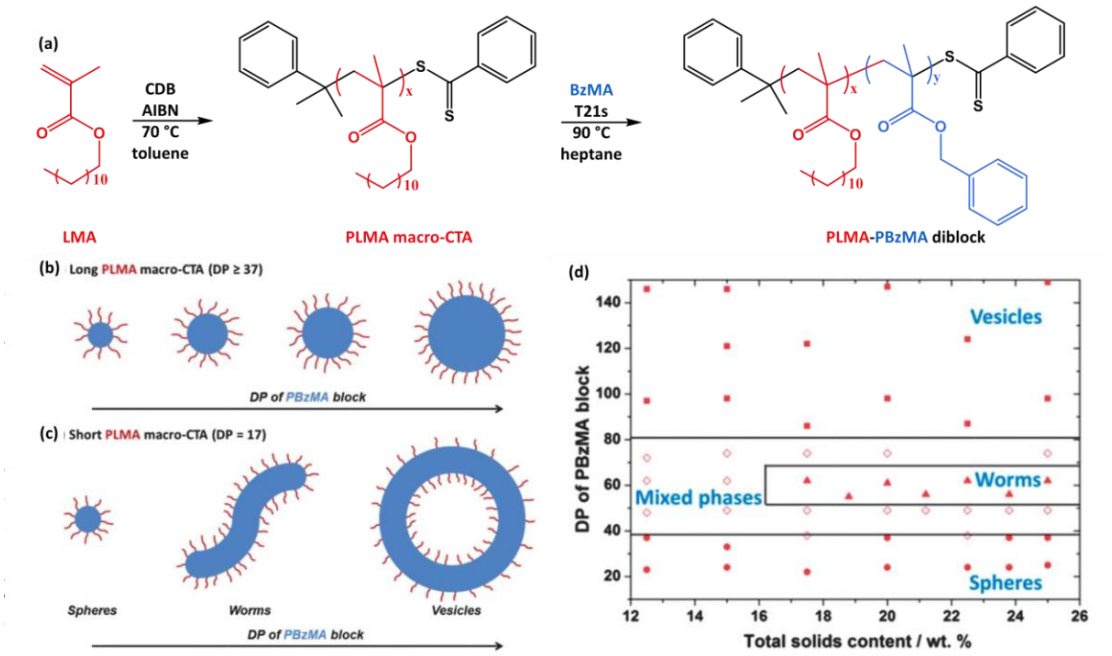

Figure 1.41 (a) RAFT synthesis of poly(lauryl methacrylate) (PLMA) macro-CTA via solution polymerisation in toluene at 70 °C, followed by the RAFT dispersion polymerisation of benzyl methacrylate (BzMA) in *n*-heptane at 90 °C. (b) Schematic representation of the change in particle size when using a long PLMA macro-CTA (DP ≥ 37). (c) Schematic representation of the change in morphology that occurs when using a short PLMA macro-CTA (DP = 17). (d) Phase diagram constructed for the $PLMA_{17}$-$PBzMA_y$ diblock copolymer nanoparticles.

These PLMA-PBzMA diblock copolymer formulations were later extended by Fielding et al. by replacing the relatively volatile *n*-heptane with *n*-dodecane. This enabled a detailed study of the thermoresponsive worm-like micelles without solvent evaporation problems.[140] A $PLMA_{16}$-$PBzMA_{37}$ worm dispersion was studied in particular detail. Like other worm-like dispersions multiple inter-worm interactions led to a soft free-standing gel. In contrast to the PGMA-PHPMA worm gels prepared

in water, *heating* the $PLMA_{16}$-$PBzMA_{37}$ worm gel resulted in degelation via a worm-to-sphere transition. This transition was more or less reversible at high copolymer concentrations, with worm reformation occurring on cooling to 20 °C (Figure 1.42). This worm-to-sphere transition was supported by rheological studies, which showed degelation on heating above 50 °C and regelation on cooling below 50 °C. Variable temperature ^{1}H NMR studies in d_{26}-dodecane indicated that heating the $PLMA_{16}$-$PBzMA_{37}$ worms caused partial solvation of the PBzMA chains. This solvation led to an increase in the effective stabiliser block volume (because the BzMA units nearest to the PLMA chains become solvated) and reduction in the effective core-forming block volume fraction leads to greater curvature, which causes a worm-to-sphere transition. Two possible mechanisms for this thermal transition were discussed. In mechanism A, worm-like micelles undergo sequential budding to form spheres, whereas mechanism B involves random worm cleavage, see Figure 1.42. SAXS studies suggest sequential budding is the more likely mechanism because of the relatively low population of spherical micelles.

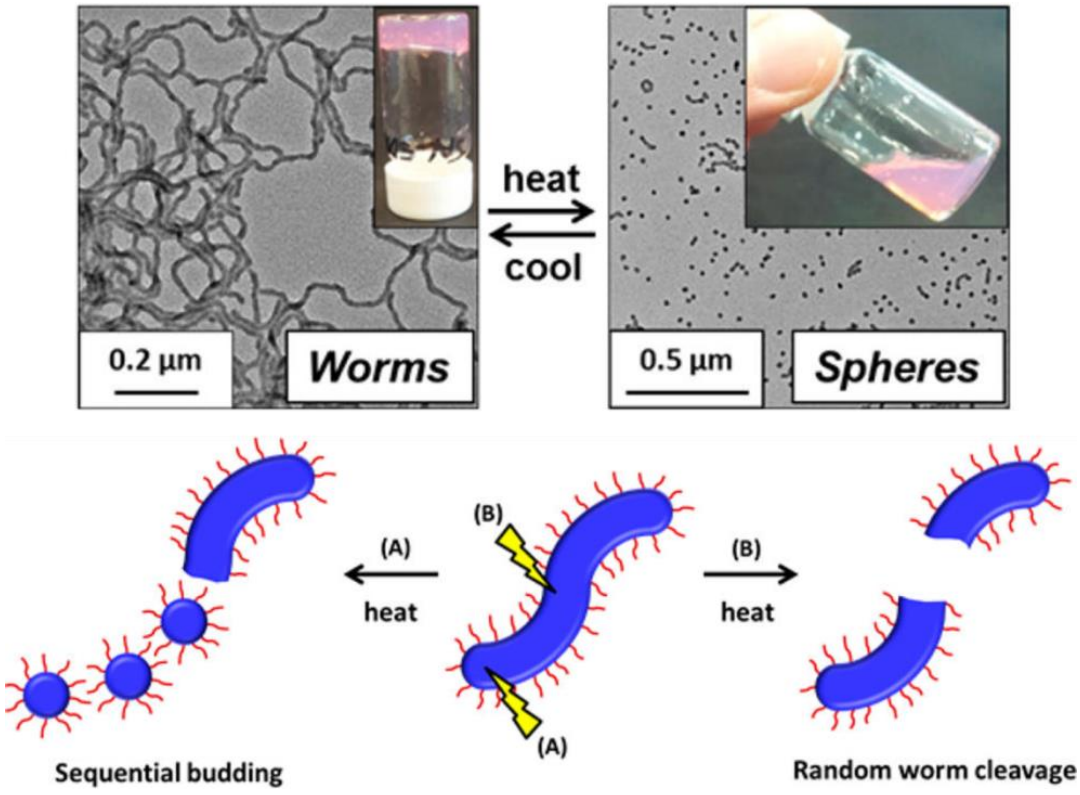

Figure 1.42 TEM images and digital photographs for the reversible worm-to-sphere transitions when heating/cooling a dispersion of $PLMA_{16}$-$PBzMA_{37}$ in *n*-dodecane. Two possible mechanisms for this are shown: (A) sequential budding and (B) random worm cleavage. The former mechanism is considered more likely.[140]

The PISA synthesis of PLMA-PBzMA was also conducted in either mineral oil or poly(α-olefin) by Derry et al.[73] The effect of solvent type was studied on the self-assembly behaviour and a phase diagram was constructed for each solvent. Pure sphere, worm and vesicle phases were observed for both mineral oil and poly(α-olefin). These phase diagrams indicated narrow worm space, as expected based on previous work by Fielding et al.[139,140] The effect of varying the total solids content for $PLMA_{47}$-$PBzMA_{96}$ and $PLMA_{47}$-$PBzMA_{495}$ was studied. PISA enabled syntheses to be conducted at up to 50% w/w solids. An increase in viscosity was observed for the $PLMA_{47}$-$PBzMA_{96}$ spheres at higher concentrations (40% or 50%). Targeting a PBzMA DP of 495 resulted in a gel-like paste, but on dilution TEM studies showed only spherical micelles. A one-pot protocol was developed for the synthesis of $PLMA_{50}$-$PBzMA_{100}$ diblock copolymer spheres. A $PLMA_{50}$ macro-CTA was synthesised in mineral oil at 70 °C by RAFT solution polymerisation. The subsequent RAFT dispersion polymerisation of BzMA was conducted at 30% w/w solids. Around 98% conversion was achieved for the final $PLMA_{50}$-$PBzMA_{100}$ diblock copolymer with a M_n of 24.4 kg mol^{-1} and a narrow dispersity of 1.18 indicating remarkably good control for this one-pot synthesis.

More recently, Lopez-Oliva converted a commercially-available monocarbinol-functionalised polydimethylsiloxane (PDMS) into a RAFT macro-CTA by esterification with PETTC.[141] The advantage of using such a commercially available precursor is the ability to have a fixed DP for the macro-CTA, which aids reproducible syntheses. This $PDMS_{66}$ macro-CTA was then employed for the synthesis of $PDMS_{66}$-$PBzMA_x$ diblock copolymers in *n*-heptane at 70 °C (Figure 1.43).[141] The PBzMA DP was varied from 50 to 300 and conversions of at least 90% were achieved. THF GPC indicated high blocking efficiencies for the $PDMS_{66}$-$PBzMA_x$ diblock copolymers relative to the macro-CTA. An increase in M_n with PBzMA DP was observed with $M_w/M_n \leq 1.34$. Synthesis of $PDMS_{66}$-$PBzMA_x$ diblock copolymers at 10 or 15% w/w solids only resulted in spherical micelles but increasing to 20% w/w (or higher) resulted in mixed phases, with pure vesicles being observed for a PBzMA DP of 200 or greater. A phase diagram indicated an extremely narrow worm phase with just two pure worm samples being identified for $PDMS_{66}$-$PBzMA_{80}$ at 25% and 30% w/w solids.

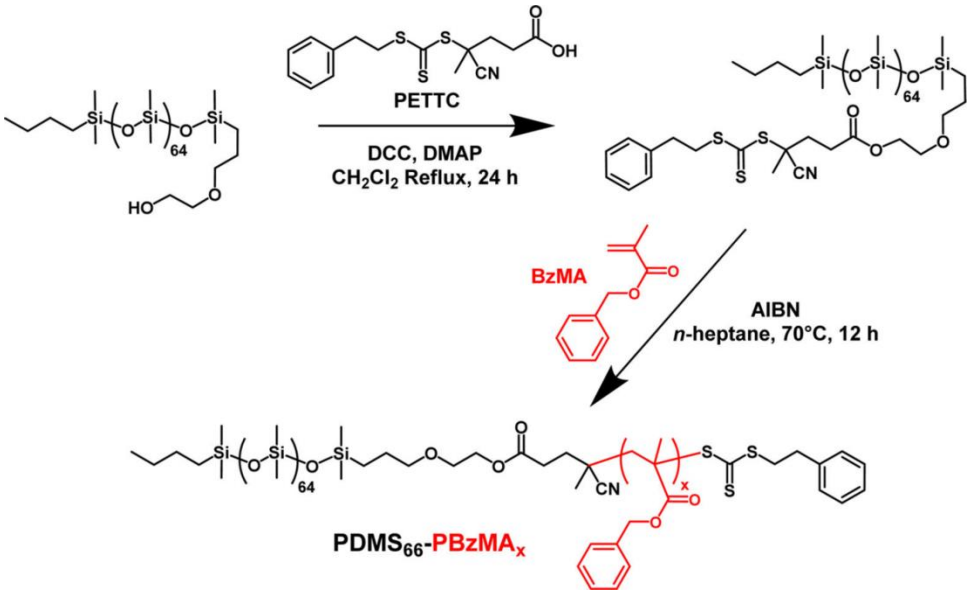

Figure 1.43 Synthesis of $PDMS_{66}$ macro-CTA via DCC/DMAP-catalysed esterification of monocarbinol-terminated PDMS using a carboxylic acid-functionalised RAFT agent (PETTC), followed by the synthesis of $PDMS_{66}$-$PBzMA_x$ nano-objects via RAFT dispersion polymerisation of BzMA in *n*-heptane at 70 °C.[141]

Alternative media

RAFT solution polymerisation was first conducted in ionic liquids in 2002 by Perrier et al.[35] for the synthesis of PMMA and PMA using a CPDB RAFT agent. The solvent was 1-alkyl-3-methylimidazoliumhexaflurophosphate ($[C_x][PF_6]$, where x = 4, 6 or 8). These solvents did not appear to work for styrene, but MMA and MA gave conversions of 70 to 91% and relatively low dispersities of less than 1.26. The first report of RAFT PISA in ionic liquids was by Zhang and Zhu.[142] A trithiocarbonate-terminated PEG macro-CTA was chain-extended with either styrene, *n*-butyl methacrylate (*n*BMA) or 2-hydroxyethyl methacrylate (HEMA) in 1-butyl-3-methylimidazolium hexafluorophosphate ($[bmim][PF_6]$) at 80 °C.[142] Diblock copolymers synthesised with either *n*BMA or HEMA were obtained at high conversion (≥ 93%), whereas styrene polymerisations resulted in generally lower conversions (79 - 94%). All diblock copolymers self-assembled to form vesicles. In a similar study, Zhou et al. examined the kinetics of styrene polymerisation for the synthesis of PEG-PS diblock copolymers in $[bmim][PF_6]$ and compared this rate to that obtained in methanol or a 80/20 methanol/water mixture.[143] Using ionic liquid led to faster reactions than in methanol, with 94% conversion achieved in 12 h. The styrene polymerisation was also slightly faster than that in the 80/20 methanol/water

mixture. A vesicular morphology was observed by TEM (after dialysis into an 80/20 methanol/water mixture).

There are several examples of RAFT dispersion polymerisation in supercritical CO_2 in the literature.[36,144-146] The dispersion polymerisation of MMA using a fluorinated macro-CTA was reported by Howdle and co-workers (Figure 1.44).[146] A 1*H*,1*H*,2*H*,2*H*-per-fluorooctyl methacrylate (FOMA) macro-CTA was synthesised in the bulk using CPDB at 60 °C. Without purification, this PFOMA macro-CTA was chain-extended with MMA in supercritical CO_2 to form a free-flowing copolymer powder. This diblock copolymer synthesis proceeded to 99% conversion after 20 h and THF GPC indicated a final M_w/M_n of 1.22. SEM studies of the resulting copolymer powder revealed polydisperse spherical particles, Figure 1.44.

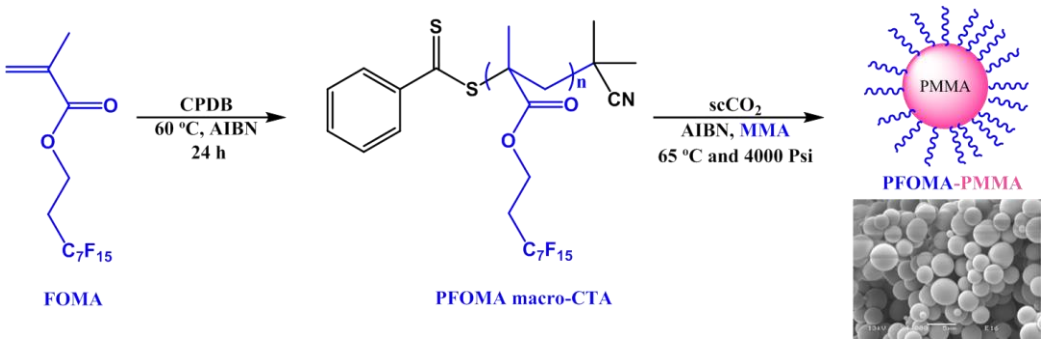

Figure 1.44 Schematic representation of the synthesis of PFOMA-PMMA diblocks via RAFT dispersion polymerisation in supercritical CO_2 ($scCO_2$) and an SEM image of the resulting spherical copolymer particles.[146]

1.10 Pickering emulsions

A Pickering emulsion is an emulsion stabilised by solid particles. They were first discovered by Ramsden[147] in 1903 although they are named based on the later work of Pickering[148] in 1907. For solid particles at an oil/water interface, the emulsion type is dictated by the particle wettability at the three-phase contact angle, θ (Figure 1.45). For hydrophilic particles, this angle will be less than 90° resulting in the particles being located predominately in the aqueous phase. In this case an oil-in-water emulsion is formed. Alternatively, for hydrophobic particles, the contact angle is greater than 90°, resulting in a water-in-oil emulsion. Using an equal volume of water and oil is a good method to determine the preferred type of emulsion for a given particle. However, variation of the droplet volume fraction has been shown to lead to phase inversion.[149]

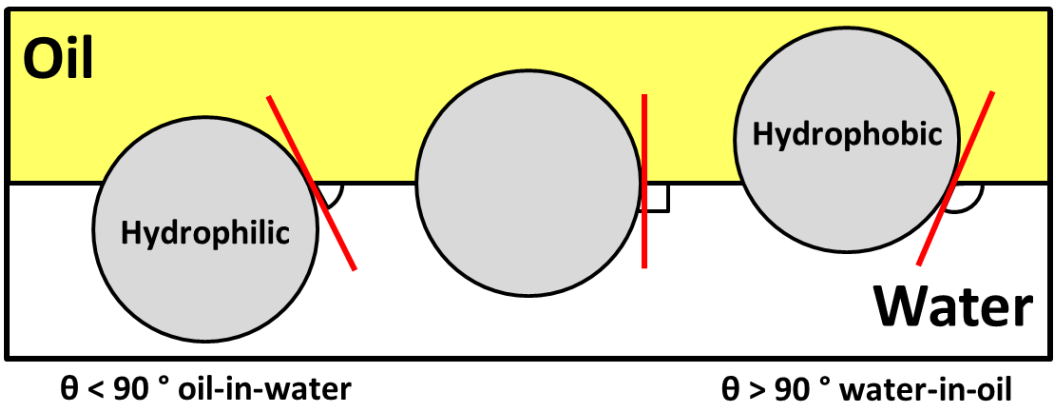

Figure 1.45 Particles adsorbed at the oil/water interface for three different contact angles. If the Pickering emulsifier has a contact angle below 90°, then an oil-in-water emulsion will be formed. If the contact angle is greater than 90°, then a water-in-oil emulsion will be formed.[150]

Once attached to the oil/water interface, the energy required to detach the particles is given by Equation 9:[150]

$$E = \pi r^2 \gamma_{ow} (1 \pm \cos\theta)^2 \qquad (9)$$

Here r is the particle radius, Υ_{ow} is the surface tension at the oil/water interface and θ is the particle contact angle. The sign in the brackets is negative for the removal of the particle into the aqueous phase and positive for the removal of the particle into the oil phase. Therefore less energy is required for the particle to detach into the water phase if θ < 90° or detach into the oil phase if θ > 90°.[150] Equation 9 shows that the energy for detachment depends on the three-phase contact angle of the particle. This is depicted in Figure 1.46. A contact angle close to 90° has the highest energy of detachment and will result in small, stable emulsion droplets. The energy of detachment rapidly decreases as the contact angle moves further away from 90° leading to larger, less stable emulsions. A contact angle of less than 20° or greater than 160° leads to a detachment energy of less than 10 kT; in this case the particles are too hydrophilic or hydrophobic to stabilise a Pickering emulsion.[150] The particle radius plays an important factor in determining the detachment energy and therefore emulsion stability (see Equation 9). The energy of detachment is proportional to the square of the particle radius as shown in Figure 1.47 for a contact angle of 90°. Very small particles have a relatively small detachment energy and therefore are able to adsorb to or desorb from an oil/water interface on a relatively fast time scale.[150] In

contrast, larger particles have a relatively large energy of detachment compared to their thermal energy (kT) and so are more likely to be permanently adsorbed to the surface. Therefore Pickering emulsions are usually far more stable than surfactant-stabilised emulsions.

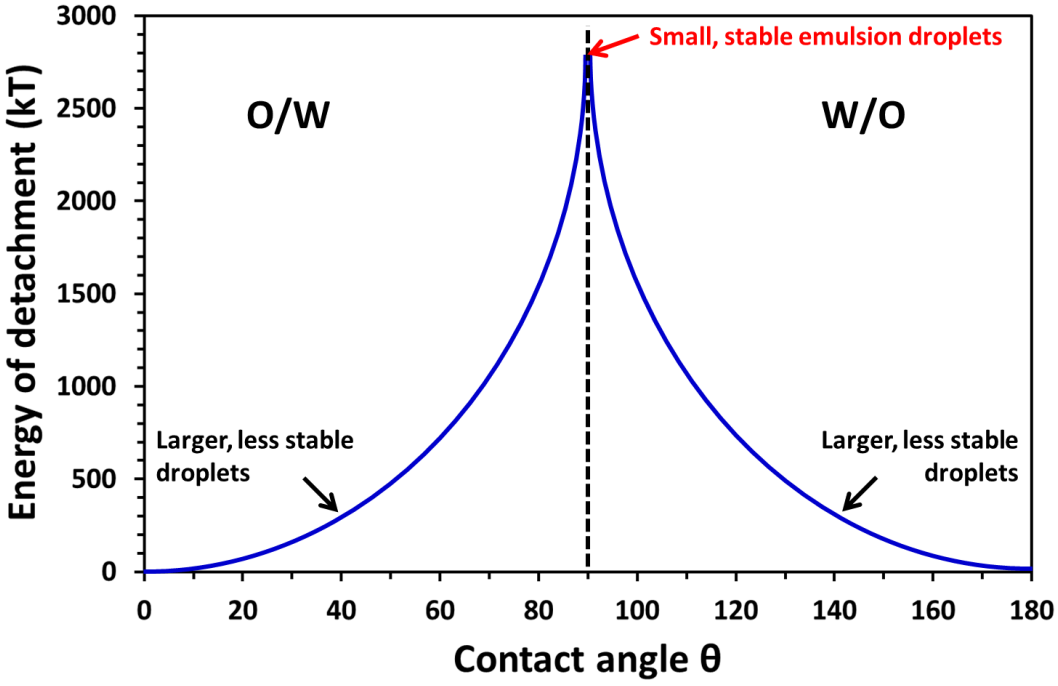

Figure 1.46 Energy of detachment versus contact angle (θ) for a nanoparticle with a radius of 10 nm at a toluene/water interface (Υ_{ow} = 0.036 Nm^{-1}).[151]

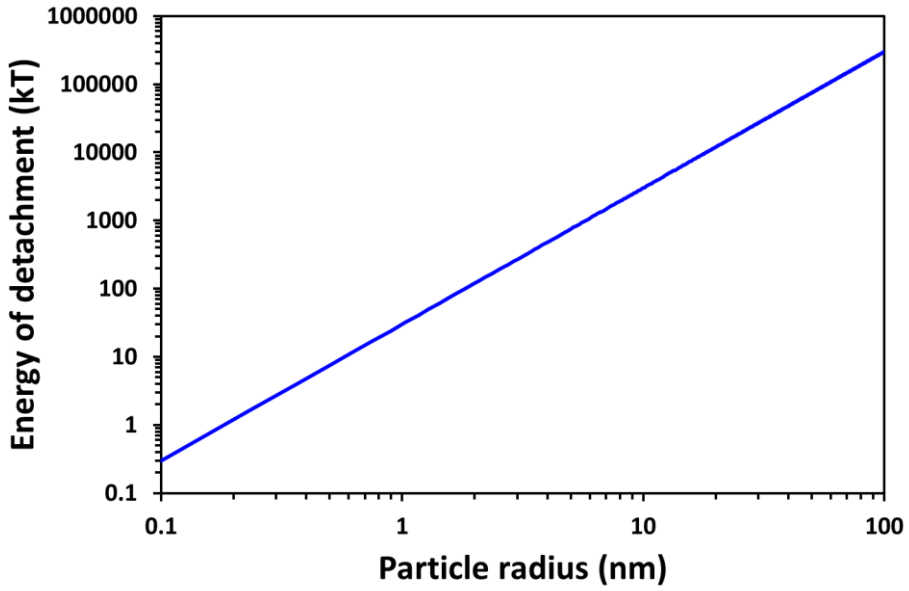

Figure 1.47 Variation of the theoretical energy of detachment (expressed in kT units) required to detach a single spherical particle from an oil/water interface (Υ_{ow} = 0.05 N m^{-1}) with particle radius. Assuming a particle contact angle of 90° at 298 K.[150]

Initially, inorganic particles such as silica,[152,153] barium sulfate[154] and calcium carbonate[155] were used to form stable Pickering emulsions. Velev and co-workers reported the first example of organic (polymer latex) particles being used to stabilise an emulsion.[156] In this case, charge stabilised polystyrene particles stabilised 1-octanol droplets. Similar latexes have since been used to stabilise a range of Pickering emulsions.[157-159] Spherical nanoparticles prepared via RAFT aqueous dispersion polymerisation can form stable Pickering emulsions.[160] For example, cross-linked PGMA-PHPMA spheres were homogenised with *n*-dodecane to form a series of oil-in-water emulsions. Without the presence of EGDMA as a cross-linker these PGMA-PHPMA spheres dissociate during the high shear homogenisation process required for emulsification. In this latter case the PGMA-PHPMA chains merely act as polymeric surfactants. Figure 1.48 provides evidence for these two types of behaviour. Cross-linked PGMA-PHPMA spheres exhibit a concentration dependence with emulsion droplet diameter, i.e. larger droplets are formed at lower copolymer concentrations, whereas using the linear (non cross-linked) spheres lead to no change in emulsion size when varying the copolymer concentration. The former copolymer concentration size dependence is characteristic of Pickering emulsions.[161]

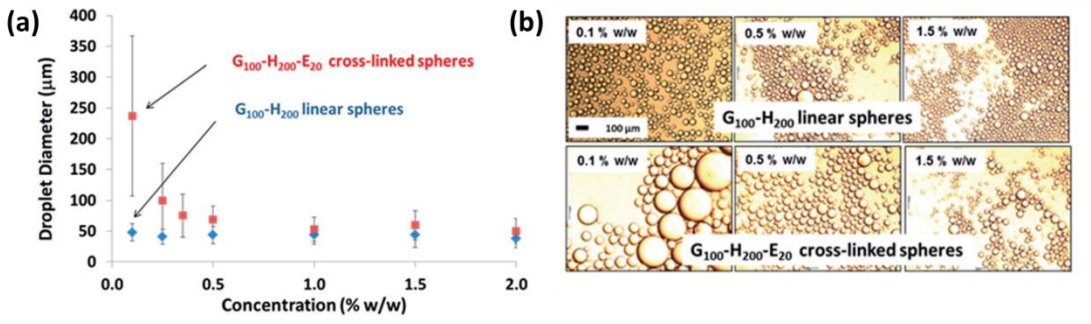

Figure 1.48 (a) Mean laser diffraction droplet diameter versus copolymer concentration for both linear $PGMA_{100}$-$PHPMA_{200}$ spheres and cross-linked $PGMA_{100}$-$PHPMA_{200}$-$PEGDMA_{20}$ spheres, (b) optical microscopy images recorded for selected emulsions corresponding to the data points shown in (a). The 100 µm scale bar applies to all images. [160]

More recently, anisotropic block copolymer nanoparticles have been evaluated as effective Pickering emulsifiers.[160,162-164] Thompson et al. used PLMA-PBzMA worm-like micelles in *n*-dodecane to prepare stable water-in-oil emulsions.[163] The mean droplet diameters could be tuned from 8 µm to 117 µm by varying the worm copolymer concentration. Similar PLMA-PBzMA worms were also used in a related

study to make isorefractive ethylene glycol-in-*n*-alkane Pickering emulsions.[164] *n*-Tetradecane was selected as the immiscible *n*-alkane because it has the closest refractive index to ethylene glycol. Such contrast matching resulted in transparent emulsions which exhibited transmittance of up to 81% at low worm copolymer concentrations.[164] PDMA-PBzMA worm-like micelles prepared in methanol have also been employed as Pickering emulsifiers by Rizzelli et al.[162] These anisotropic nanoparticles formed stable sunflower oil-in-methanol emulsions. Mable et al. synthesised a series of framboidal PGMA-PHPMA-PBzMA triblock copolymer vesicles via RAFT polymerisation.[110] These nanoparticles were used to prepare stable oil-in-water emulsions and, unlike smooth PGMA-PHPMA diblock copolymer vesicles, they do not require crosslinking.[110,165] Increasing the PBzMA DP led to greater vesicle surface roughness as judged by TEM and SAXS. This resulted in higher Pickering efficiencies as determined by turbidimetry.

1.11 Thesis Outline

The present work focuses on the synthesis of diblock copolymers via RAFT polymerisation. These diblock copolymers have been selected so that one block is solvophilic and the other solvophobic. During polymerisation of the second solvophobic block, these diblock copolymers undergo PISA. In Chapter 2, the RAFT emulsion polymerisation of BzMA from a water-soluble PGMA macro-CTA is explored in detail. A series of $PGMA_x$-$PBzMA_y$ diblock copolymers are synthesised and analysed by a wide range of techniques, including GPC, TEM, NMR and DLS. The PGMA-PBzMA nanoparticles are selectively adsorbed onto phenylboronic acid functionalised surfaces and also assessed as Pickering emulsifiers. Chapter 3 covers the synthesis of poly(stearyl methacrylate)-poly(*N*-2-(methacryloyloxy)ethyl pyrrolidone) (PSMA-PNMEP) diblock copolymers via RAFT dispersion polymerisation in *n*-dodecane. The PNMEP DP and solids content is varied to construct a phase diagram in which pure spheres, worms and vesicles are obtained. These PSMA-PNMEP diblock copolymers are also analysed as potential Pickering emulsifiers. In Chapter 4, detailed polymerisation kinetics for a series of PNMEP homopolymers synthesised via RAFT solution polymerisation are presented. A PNMEP macro-CTA is synthesised and chain-extended with BzMA via RAFT alcoholic dispersion polymerisation. These diblock copolymers form a range of copolymer morphologies and a robust one-pot protocol is developed. Finally,

Chapter 5 examines the RAFT aqueous dispersion polymerisation of NMEP using a relatively short PGMA macro-CTA. Very high PNMEP DPs are targeted which enables the synthesis of high molecular weight PNMEP in a convenient low-viscosity form.

1.12 References

(1) Staudinger, H. *Berichte der Deutschen Chemischen Gesellschaft (A and B Series)* **1920**, *53*, 1073.
(2) Flory, P. J. *Principles of Polymer Chemistry* Cornell University Press: New York, 1953.
(3) Ebewele, R. O. *Polymer Science and Technology*; CRC press: Florida, 2000.
(4) Odian, G. *Principles of Polymerization*; 4th edition ed.; John Wiley & Sons: New Jersey, 2004.
(5) Kamigaito, M.; Ando, T.; Sawamoto, M. *Chemical Reviews* **2001**, *101*, 3689.
(6) Moad, G.; Rizzardo, E.; Thang, S. H. *Accounts of Chemical Research* **2008**, *41*, 1133.
(7) Webster, O. W. *Science* **1991**, *251*, 887.
(8) Moad, G.; Rizzardo, E.; Thang, S. H. *Australian Journal of Chemistry* **2005**, *58*, 379.
(9) Szwarc, M.; Levy, M.; Milkovich, R. *Journal of the American Chemical Society* **1956**, *78*, 2656.
(10) Hirao, A.; Loykulnant, S.; Ishizone, T. *Progress in Polymer Science* **2002**, *27*, 1399.
(11) Ishizone, T.; Goseki, R. In *Encyclopedia of Polymeric Nanomaterials*; Kobayashi, S., Müllen, K., Eds.; Springer: Berlin, 2014.
(12) Matyjaszewski, K.; Davis, T. P. *Handbook of Radical Polymerization*; Wiley, 2002; Vol. 5.
(13) Zetterlund, P. B.; Kagawa, Y.; Okubo, M. *Chemical Reviews* **2008**, *108*, 3747.
(14) Bates, F. S.; Fredrickson, G. H. *Annual Review of Physical Chemistry* **1990**, *41*, 525.
(15) Hamley, I. *Nanotechnology* **2003**, *14*, R39.
(16) Hadjichristidis, N.; Pispas, S.; Floudas, G. *Block Copolymers: Synthetic Strategies, Physical Properties, and Applications*; John Wiley & Sons: New Jersey, 2003.
(17) Braunecker, W. A.; Matyjaszewski, K. *Progress in Polymer Science* **2007**, *32*, 93.
(18) Nicolas, J.; Guillaneuf, Y.; Lefay, C.; Bertin, D.; Gigmes, D.; Charleux, B. *Progress in Polymer Science* **2013**, *38*, 63.
(19) Hawker, C. J. *Journal of the American Chemical Society* **1994**, *116*, 11185.
(20) Hawker, C. J.; Barclay, G. G.; Orellana, A.; Dao, J.; Devonport, W. *Macromolecules* **1996**, *29*, 5245.
(21) *Macromolecular Engineering* Matyjaszewski, K.; Gnanou, Y.; Leibler, L., Eds.; Wiley-VCH: Weinheim, 2007; Vol. 1.
(22) Kato, M.; Kamigaito, M.; Sawamoto, M.; Higashimura, T. *Macromolecules* **1995**, *28*, 1721.

(23) Wang, J.-S.; Matyjaszewski, K. *Journal of the American Chemical Society* **1995**, *117*, 5614.
(24) Matyjaszewski, K. *Macromolecules* **2012**, *45*, 4015.
(25) Chiefari, J.; Chong, Y. K.; Ercole, F.; Krstina, J.; Jeffery, J.; Le, T. P. T.; Mayadunne, R. T. A.; Meijs, G. F.; Moad, C. L.; Moad, G.; Rizzardo, E.; Thang, S. H. *Macromolecules* **1998**, *31*, 5559.
(26) Moad, G.; Rizzardo, E.; Thang, S. H. *Australian Journal of Chemistry* **2006**, *59*, 669.
(27) Moad, G.; Rizzardo, E.; Thang, S. H. *Australian Journal of Chemistry* **2009**, *62*, 1402.
(28) Moad, G.; Rizzardo, E.; Thang, S. H. *Australian Journal of Chemistry* **2012**, *65*, 985.
(29) Chong, Y. K.; Le, T. P. T.; Moad, G.; Rizzardo, E.; Thang, S. H. *Macromolecules* **1999**, *32*, 2071.
(30) Lu, L.; Zhang, H.; Yang, N.; Cai, Y. *Macromolecules* **2006**, *39*, 3770.
(31) Hong, C. Y.; You, Y. Z.; Bai, R. K.; Pan, C. Y.; Borjihan, G. *Journal of Polymer Science Part A: Polymer Chemistry* **2001**, *39*, 3934.
(32) Barner-Kowollik, C. *Handbook of RAFT Polymerization*; John Wiley & Sons: Weinheim, 2008.
(33) He, T.; Zou, Y.-F.; Pan, C.-Y. *Polymer Journal* **2002**, *34*, 138.
(34) McCormick, C. L.; Lowe, A. B. *Accounts of Chemical Research* **2004**, *37*, 312.
(35) Perrier, S.; Davis, T. P.; Carmichael, A. J.; Haddleton, D. M. *Chemical Communications* **2002**, 2226.
(36) Gregory, A. M.; Thurecht, K. J.; Howdle, S. M. *Macromolecules* **2008**, *41*, 1215.
(37) Willcock, H.; O'Reilly, R. K. *Polymer Chemistry* **2010**, *1*, 149.
(38) Benaglia, M.; Chiefari, J.; Chong, Y. K.; Moad, G.; Rizzardo, E.; Thang, S. H. *Journal of the American Chemical Society* **2009**, *131*, 6914.
(39) Barner-Kowollik, C.; Perrier, S. *Journal of Polymer Science Part A: Polymer Chemistry* **2008**, *46*, 5715.
(40) Chong, Y. K.; Moad, G.; Rizzardo, E.; Thang, S. H. *Macromolecules* **2007**, *40*, 4446.
(41) Moad, G.; Chong, Y.; Postma, A.; Rizzardo, E.; Thang, S. H. *Polymer* **2005**, *46*, 8458.
(42) Wang, Z.; He, J.; Tao, Y.; Yang, L.; Jiang, H.; Yang, Y. *Macromolecules* **2003**, *36*, 7446.
(43) Liu, Y.; He, J.; Xu, J.; Fan, D.; Tang, W.; Yang, Y. *Macromolecules* **2005**, *38*, 10332.
(44) Inglis, A. J.; Sinnwell, S.; Davis, T. P.; Barner-Kowollik, C.; Stenzel, M. H. *Macromolecules* **2008**, *41*, 4120.
(45) Lovell, P. A.; El-Aasser, M. S. *Emulsion Polymerization and Emulsion Polymers*; Wiley: Chichester, 1997.
(46) Chern, C. S. *Progress in Polymer Science* **2006**, *31*, 443.
(47) Harkins, W. D. *Journal of the American Chemical Society* **1947**, *69*, 1428.
(48) Gilbert, R. G. *Emulsion Polymerization: A Mechanistic Approach*; Academic Press: London, 1995.
(49) Thickett, S. C.; Gilbert, R. G. *Polymer* **2007**, *48*, 6965.
(50) Richez, A. P.; Yow, H. N.; Biggs, S.; Cayre, O. J. *Progress in Polymer Science* **2013**, *38*, 897.

(51) Kawaguchi, S.; Ito, K. In *Polymer Particles*; Okubo, M., Ed.; Springer: Berlin, 2005, p 299.
(52) Shen, S.; Sudol, E. D.; El-Aasser, M. S. *Journal of Polymer Science Part A: Polymer Chemistry* **1994**, *32*, 1087.
(53) Ali, A. M. I.; Pareek, P.; Sewell, L.; Schmid, A.; Fujii, S.; Armes, S. P.; Shirley, I. M. *Soft Matter* **2007**, *3*, 1003.
(54) Israelachvili, J. *Intermolecular & Surface Forces*; 2nd ed.; Academic Press: London, 1991.
(55) Alexandridis, P.; Lindman, B. *Amphiphilic Block Copolymers: Self-assembly and Applications*; Elsevier: Amsterdam, 2000.
(56) Swann, J. M.; Topham, P. D. *Polymers* **2010**, *2*, 454.
(57) Mai, Y.; Eisenberg, A. *Chemical Society Reviews* **2012**, *41*, 5969.
(58) Bates, F. S. *Science* **1991**, *251*, 898.
(59) Bates, F. S.; Fredrickson, G. *Physics Today* **1999**, *52*, 32.
(60) Blanazs, A.; Armes, S. P.; Ryan, A. J. *Macromolecular Rapid Communications* **2009**, *30*, 267.
(61) Zhang, L.; Eisenberg, A. *Polymers for Advanced Technologies* **1998**, *9*, 677.
(62) Discher, D. E.; Ahmed, F. In *Annual Review of Biomedical Engineering*; Annual Reviews: Palo Alto, 2006; Vol. 8, p 323.
(63) LoPresti, C.; Lomas, H.; Massignani, M.; Smart, T.; Battaglia, G. *Journal of Materials Chemistry* **2009**, *19*, 3576.
(64) Clarke, C. J.; Zhang, L.; Zhu, J.; Yu, K.; Bruce Lennox, R.; Eisenberg, A. *Macromolecular Symposia* **1997**, *118*, 647.
(65) Zhang, L.; Eisenberg, A. *Journal of the American Chemical Society* **1996**, *118*, 3168.
(66) Cameron, N. S.; Corbierre, M. K.; Eisenberg, A. *Canadian Journal of Chemistry* **1999**, *77*, 1311.
(67) Shen, H.; Eisenberg, A. *The Journal of Physical Chemistry B* **1999**, *103*, 9473.
(68) Discher, D. E.; Eisenberg, A. *Science* **2002**, *297*, 967.
(69) Charleux, B.; Delaittre, G.; Rieger, J.; D'Agosto, F. *Macromolecules* **2012**, *45*, 6753.
(70) Warren, N. J.; Armes, S. P. *Journal of the American Chemical Society* **2014**, *136*, 10174.
(71) Canning, S. L.; Smith, G. N.; Armes, S. P. *Macromolecules* **2016**, *49*, 1985.
(72) Derry, M. J.; Fielding, L. A.; Armes, S. P. *Progress in Polymer Science* **2016**, *52*, 1.
(73) Derry, M. J.; Fielding, L. A.; Armes, S. P. *Polymer Chemistry* **2015**, *6*, 3054.
(74) Blanazs, A.; Ryan, A. J.; Armes, S. P. *Macromolecules* **2012**, *45*, 5099.
(75) Cunningham, M. F. *Progress in Polymer Science* **2008**, *33*, 365.
(76) Prescott, S. W.; Ballard, M. J.; Rizzardo, E.; Gilbert, R. G. *Macromolecules* **2002**, *35*, 5417.
(77) Ferguson, C. J.; Hughes, R. J.; Pham, B. T. T.; Hawkett, B. S.; Gilbert, R. G.; Serelis, A. K.; Such, C. H. *Macromolecules* **2002**, *35*, 9243.
(78) Ferguson, C. J.; Hughes, R. J.; Nguyen, D.; Pham, B. T. T.; Gilbert, R. G.; Serelis, A. K.; Such, C. H.; Hawkett, B. S. *Macromolecules* **2005**, *38*, 2191.
(79) Sprong, E.; Leswin, J. S. K.; Lamb, D. J.; Ferguson, C. J.; Hawkett, B. S.; Pham, B. T. T.; Nguyen, D.; Such, C. H.; Serelis, A. K.; Gilbert, R. G. *Macromolecular Symposia* **2006**, *231*, 84.
(80) Boissé, S.; Rieger, J.; Belal, K.; Di-Cicco, A.; Beaunier, P.; Li, M.-H.; Charleux, B. *Chemical Communications* **2010**, *46*, 1950.

(81) Boissé, S.; Rieger, J.; Pembouong, G.; Beaunier, P.; Charleux, B. *Journal of Polymer Science Part A: Polymer Chemistry* **2011**, *49*, 3346.
(82) Chaduc, I.; Crepet, A.; Boyron, O.; Charleux, B.; D'Agosto, F.; Lansalot, M. *Macromolecules* **2013**, *46*, 6013.
(83) Manguian, M.; Save, M.; Charleux, B. *Macromolecular Rapid Communications* **2006**, *27*, 399.
(84) Rieger, J.; Zhang, W.; Stoffelbach, F.; Charleux, B. *Macromolecules* **2010**, *43*, 6302.
(85) Zhang, X.; Boissé, S.; Zhang, W.; Beaunier, P.; D'Agosto, F.; Rieger, J.; Charleux, B. *Macromolecules* **2011**, *44*, 4149.
(86) Rieger, J.; Osterwinter, G.; Bui, C.; Stoffelbach, F.; Charleux, B. *Macromolecules* **2009**, *42*, 5518.
(87) Zhang, X.; Rieger, J.; Charleux, B. *Polymer Chemistry* **2012**, *3*, 1502.
(88) Rieger, J.; Stoffelbach, F.; Bui, C.; Alaimo, D.; Jérôme, C.; Charleux, B. *Macromolecules* **2008**, *41*, 4065.
(89) Chaduc, I.; Zhang, W.; Rieger, J.; Lansalot, M.; D'Agosto, F.; Charleux, B. *Macromolecular Rapid Communications* **2011**, *32*, 1270.
(90) Chaduc, I.; Girod, M.; Antoine, R.; Charleux, B.; D'Agosto, F.; Lansalot, M. *Macromolecules* **2012**, *45*, 5881.
(91) Zhang, W.; D'Agosto, F.; Boyron, O.; Rieger, J.; Charleux, B. *Macromolecules* **2011**, *44*, 7584.
(92) Božović-Vukić, J.; Mañon, H. T.; Meuldijk, J.; Koning, C.; Klumperman, B. *Macromolecules* **2007**, *40*, 7132.
(93) Ting, S. R. S.; Min, E. H.; Zetterlund, P. B.; Stenzel, M. H. *Macromolecules* **2010**, *43*, 5211.
(94) Yeole, N.; Hundiwale, D. *RSC Advances* **2013**, *3*, 22213.
(95) Zhang, W.; D'Agosto, F.; Boyron, O.; Rieger, J.; Charleux, B. *Macromolecules* **2012**, *45*, 4075.
(96) Zhang, W.; D'Agosto, F.; Dugas, P.-Y.; Rieger, J.; Charleux, B. *Polymer* **2013**, *54*, 2011.
(97) Lesage de la Haye, J.; Zhang, X.; Chaduc, I.; Brunel, F.; Lansalot, M.; D'Agosto, F. *Angewandte Chemie* **2016**, *128*, 3803.
(98) An, Z.; Shi, Q.; Tang, W.; Tsung, C.-K.; Hawker, C. J.; Stucky, G. D. *Journal of the American Chemical Society* **2007**, *129*, 14493.
(99) Li, Y.; Armes, S. P. *Angewandte Chemie International Edition* **2010**, *49*, 4042.
(100) Blanazs, A.; Madsen, J.; Battaglia, G.; Ryan, A. J.; Armes, S. P. *Journal of the American Chemical Society* **2011**, *133*, 16581.
(101) Blanazs, A.; Verber, R.; Mykhaylyk, O. O.; Ryan, A. J.; Heath, J. Z.; Douglas, C. W. I.; Armes, S. P. *Journal of the American Chemical Society* **2012**, *134*, 9741.
(102) Chambon, P.; Blanazs, A.; Battaglia, G.; Armes, S. P. *Macromolecules* **2012**, *45*, 5081.
(103) Verber, R.; Blanazs, A.; Armes, S. *Soft Matter* **2012**, *8*, 9915.
(104) Ratcliffe, L. P. D.; Ryan, A. J.; Armes, S. P. *Macromolecules* **2013**, *46*, 769.
(105) Lovett, J. R.; Warren, N. J.; Armes, S. P.; Smallridge, M. J.; Cracknell, R. B. *Macromolecules* **2016**, *49*, 1016.
(106) Cunningham, V. J.; Ratcliffe, L. P. D.; Blanazs, A.; Warren, N. J.; Smith, A. J.; Mykhaylyk, O. O.; Armes, S. P. *Polymer Chemistry* **2014**, *5*, 6307.
(107) Canton, I.; Warren, N. J.; Chahal, A.; Amps, K.; Wood, A.; Weightman, R.; Wang, E.; Moore, H.; Armes, S. P. *ACS Central Science* **2016**, *2*, 65.

(108) Warren, N. J.; Mykhaylyk, O. O.; Ryan, A. J.; Williams, M.; Doussineau, T.; Dugourd, P.; Antoine, R.; Portale, G.; Armes, S. P. *Journal of the American Chemical Society* **2015**, *137*, 1929.
(109) Mable, C. J.; Gibson, R. R.; Prevost, S.; McKenzie, B. E.; Mykhaylyk, O. O.; Armes, S. P. *Journal of the American Chemical Society* **2015**, *137*, 16098.
(110) Mable, C. J.; Warren, N. J.; Thompson, K. L.; Mykhaylyk, O. O.; Armes, S. P. *Chemical Science* **2015**, *6*, 6179.
(111) Sugihara, S.; Blanazs, A.; Armes, S. P.; Ryan, A. J.; Lewis, A. L. *Journal of the American Chemical Society* **2011**, *133*, 15707.
(112) Sugihara, S.; Armes, S. P.; Blanazs, A.; Lewis, A. L. *Soft Matter* **2011**, *7*, 10787.
(113) Warren, N. J.; Mykhaylyk, O. O.; Mahmood, D.; Ryan, A. J.; Armes, S. P. *Journal of the American Chemical Society* **2014**, *136*, 1023.
(114) Liu, G.; Qiu, Q.; Shen, W.; An, Z. S. *Macromolecules* **2011**, *44*, 5237.
(115) Shen, W.; Chang, Y.; Liu, G.; Wang, H.; Cao, A.; An, Z. *Macromolecules* **2011**, *44*, 2524.
(116) Wan, W. M.; Sun, X. L.; Pan, C. Y. *Macromolecular Rapid Communications* **2010**, *31*, 399.
(117) Wan, W.-M.; Pan, C.-Y. *Polymer Chemistry* **2010**, *1*, 1475.
(118) Wan, W.-M.; Pan, C.-Y. *Macromolecules* **2010**, *43*, 2672.
(119) He, W.-D.; Sun, X.-L.; Wan, W.-M.; Pan, C.-Y. *Macromolecules* **2011**, *44*, 3358.
(120) Huang, C.-Q.; Pan, C.-Y. *Polymer* **2010**, *51*, 5115.
(121) Sun, J.-T.; Hong, C.-Y.; Pan, C.-Y. *Polymer Chemistry* **2013**, *4*, 873.
(122) Wan, W.-M.; Hong, C.-Y.; Pan, C.-Y. *Chemical Communications* **2009**, *1*, 5883.
(123) Cai, W.; Wan, W.; Hong, C.; Huang, C.; Pan, C.-Y. *Soft Matter* **2010**, *6*, 5554.
(124) Zhang, W. J.; Hong, C. Y.; Pan, C. Y. *Macromolecular Rapid Communications* **2015**, *36*, 1428.
(125) Yang, P.; Ratcliffe, L. P. D.; Armes, S. P. *Macromolecules* **2013**, *46*, 8545.
(126) Huo, F.; Li, S.; He, X.; Shah, S. A.; Li, Q.; Zhang, W. *Macromolecules* **2014**, *47*, 8262.
(127) Semsarilar, M.; Jones, E. R.; Blanazs, A.; Armes, S. P. *Advanced Materials* **2012**, *24*, 3378.
(128) Semsarilar, M.; Ladmiral, V.; Blanazs, A.; Armes, S. P. *Polymer Chemistry* **2014**, *5*, 3466.
(129) Gonzato, C.; Semsarilar, M.; Jones, E. R.; Li, F.; Krooshof, G. J. P.; Wyman, P.; Mykhaylyk, O. O.; Tuinier, R.; Armes, S. P. *Journal of the American Chemical Society* **2014**, *136*, 11100.
(130) Jones, E. R.; Semsarilar, M.; Blanazs, A.; Armes, S. P. *Macromolecules* **2012**, *45*, 5091.
(131) Jones, E. R.; Mykhaylyk, O. O.; Semsarilar, M.; Boerakker, M.; Wyman, P.; Armes, S. P. *Macromolecules* **2015**, *49*, 172.
(132) Jones, E. R.; Semsarilar, M.; Wyman, P.; Boerakker, M.; Armes, S. P. *Polymer Chemistry* **2016**, *7*, 851.
(133) Semsarilar, M.; Penfold, N. J.; Jones, E. R.; Armes, S. P. *Polymer Chemistry* **2015**, *6*, 1751.
(134) Pei, Y.; Lowe, A. B. *Polymer Chemistry* **2014**, *5*, 2342.
(135) Pei, Y.; Dharsana, N. C.; van Hensbergen, J. A.; Burford, R. P.; Roth, P. J.; Lowe, A. B. *Soft Matter* **2014**, *10*, 5787.

(136) Pei, Y.; Dharsana, N. C.; Lowe, A. B. *Australian Journal of Chemistry* **2015**, *68*, 939.
(137) Houillot, L.; Bui, C.; Save, M.; Charleux, B.; Farcet, C.; Moire, C.; Raust, J.-A.; Rodriguez, I. *Macromolecules* **2007**, *40*, 6500.
(138) Houillot, L.; Bui, C.; Farcet, C.; Moire, C.; Raust, J.-A.; Pasch, H.; Save, M.; Charleux, B. *Acs Applied Materials & Interfaces* **2010**, *2*, 434.
(139) Fielding, L. A.; Derry, M. J.; Ladmiral, V.; Rosselgong, J.; Rodrigues, A. M.; Ratcliffe, L. P.; Sugihara, S.; Armes, S. P. *Chemical Science* **2013**, *4*, 2081.
(140) Fielding, L. A.; Lane, J. A.; Derry, M. J.; Mykhaylyk, O. O.; Armes, S. P. *Journal of the American Chemical Society* **2014**, *136*, 5790.
(141) Lopez-Oliva, A. P.; Warren, N. J.; Rajkumar, A.; Mykhaylyk, O. O.; Derry, M. J.; Doncom, K. E.; Rymaruk, M. J.; Armes, S. P. *Macromolecules* **2015**, *48*, 3547.
(142) Zhang, Q.; Zhu, S. *ACS Macro Letters* **2015**, *4*, 755.
(143) Zhou, H.; Liu, C.; Gao, C.; Qu, Y.; Shi, K.; Zhang, W. *Journal of Polymer Science Part A: Polymer Chemistry* **2016**, *54*, 1517.
(144) Hasell, T.; Thurecht, K. J.; Jones, R. D. W.; Brown, P. D.; Howdle, S. M. *Chemical Communications* **2007**, 3933.
(145) Lee, H.; Terry, E.; Zong, M.; Arrowsmith, N.; Perrier, S.; Thurecht, K. J.; Howdle, S. M. *Journal of the American Chemical Society* **2008**, *130*, 12242.
(146) Zong, M.; Thurecht, K. J.; Howdle, S. M. *Chemical Communications* **2008**, 5942.
(147) Ramsden, W. *Proceedings of the royal Society of London* **1903**, *72*, 156.
(148) Pickering, S. U. *Journal of the Chemical Society, Transactions* **1907**, *91*, 2001.
(149) Aveyard, R.; Binks, B. P.; Clint, J. H. *Advances in Colloid and Interface Science* **2003**, *100*, 503.
(150) Binks, B. P. *Current Opinion in Colloid & Interface Science* **2002**, *7*, 21.
(151) Binks, B. P.; Lumsdon, S. O. *Langmuir* **2000**, *16*, 8622.
(152) Binks, B. P.; Lumsdon, S. O. *Langmuir* **2000**, *16*, 2539.
(153) Binks, B. P.; Lumsdon, S. O. *Physical Chemistry Chemical Physics* **2000**, *2*, 2959.
(154) Schulman, J. H.; Leja, J. *Transactions of the Faraday Society* **1954**, *50*, 598.
(155) Aveyard, R.; Binks, B. P.; Fletcher, P. D. I.; Rutherford, C. E. *Colloids and Surfaces A: Physicochemical and Engineering Aspects* **1994**, *83*, 89.
(156) Velev, O. D.; Furusawa, K.; Nagayama, K. *Langmuir* **1996**, *12*, 2374.
(157) Strohm, H.; Löbmann, P. *Journal of Materials Chemistry* **2004**, *14*, 2667.
(158) Binks, B. P.; Lumsdon, S. O. *Langmuir* **2001**, *17*, 4540.
(159) Giermanska-Kahn, J.; Schmitt, V.; Binks, B. P.; Leal-Calderon, F. *Langmuir* **2002**, *18*, 2515.
(160) Thompson, K.; Mable, C.; Cockram, A.; Warren, N.; Cunningham, V.; Jones, E.; Verber, R.; Armes, S. *Soft Matter* **2014**, *10*, 8615.
(161) Thompson, K. L.; Armes, S. P.; Howse, J. R.; Ebbens, S.; Ahmad, I.; Zaidi, J. H.; York, D. W.; Burdis, J. A. *Macromolecules* **2010**, *43*, 10466.
(162) Rizzelli, S. L.; Jones, E. R.; Thompson, K. L.; Armes, S. P. *Colloid and Polymer Science* **2015**, *294*, 1.
(163) Thompson, K.; Fielding, L.; Mykhaylyk, O.; Lane, J.; Derry, M.; Armes, S. *Chemical Science* **2015**, *6*, 4207.
(164) Thompson, K. L.; Lane, J. A.; Derry, M. J.; Armes, S. P. *Langmuir* **2015**, *31*, 4373.
(165) Thompson, K. L.; Chambon, P.; Verber, R.; Armes, S. P. *Journal of the American Chemical Society* **2012**, *134*, 12450.

Chapter 2

Poly(glycerol monomethacrylate)-poly(benzyl methacrylate) diblock copolymer nanoparticles via RAFT emulsion polymerisation

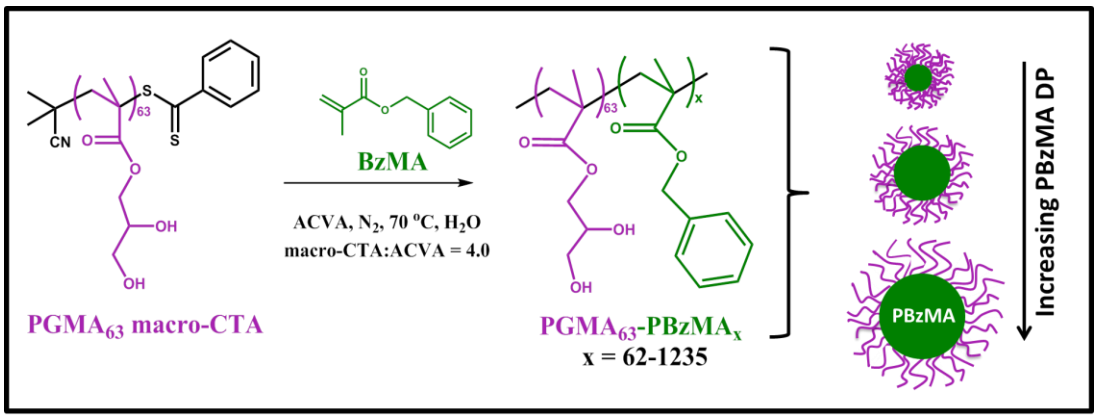

Reproduced in part with permission from:

[Cunningham, V. J.; Alswieleh, A. M.; Thompson, K. L.; Williams, M.; Leggett, G. J.; Armes, S. P.; Musa, O. M. *Macromolecules*, **2014**, *47*, 5613.] Copyright [2014] American Chemical Society.

2.1 Introduction

Glycerol monomethacrylate (GMA) is a relatively expensive specialty monomer. It is used in the synthesis of soft contact lenses and is usually formed via a multistep process leading to a mixture of 1,3- and 2,3-hydroxy isomers.[1,2] Recently, Ratcliffe et al. reported its cost-effective synthesis from an aqueous emulsion of glycidyl methacrylate (GlyMA).[3] This ring-opening reaction in water at 80 °C resulted in an aqueous solution of GMA within 9 h. NMR spectroscopy studies confirmed no hydrolysis of the methacrylic ester and negligible polymerisation occurred during the ring opening reaction. This GMA monomer was then used in the one-pot synthesis of PGMA-PHPMA diblock copolymer nano-objects (Figure 2.1). The first step involved the synthesis of a PGMA macro-CTA via RAFT solution polymerisation in water. This was followed by the addition of HPMA in a RAFT aqueous dispersion polymerisation. Sampling during the reaction showed an evolution in morphology from spheres to worms to vesicles with 99% conversion being achieved after 90 min.[3]

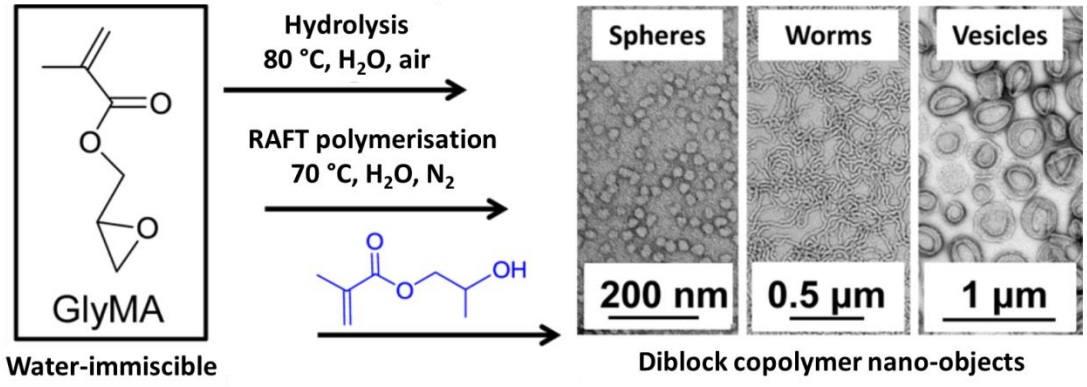

Figure 2.1 One-pot synthesis of PGMA-PHPMA diblock copolymer nano-objects. Glycidyl methacrylate (GlyMA) is converted to glycerol monomethacrylate (GMA) in water at 80 °C, followed by the preparation of a PGMA macro-CTA. Chain extension of the PGMA macro-CTA with 2-hydroxypropyl methacrylate (HPMA) produced well-defined PGMA-PHPMA diblock copolymer nano-objects.[3]

The cis-diol functionality of PGMA has also been utilised for pH-dependent complexation with phenylboronic acid.[4-6] It is well documented that such boronic acid species can react with dialcohols.[7-9] For example, poly(vinyl alcohol) can be mixed with borax to form 'polymer slime'.[10] Several other applications, particularly in the biomedical field, include lipase inhibition,[11] drug delivery[12] and controlled release. [13] Cambre and Sumerlin published a comprehensive review of the

biomedical applications of boronic acid-based polymers in 2011.[9] The important feature which enables these applications is the ability of boronic acid species to covalently bind with cis-diols to form cyclic esters in alkaline aqueous solution.

Thompson et al. reported the synthesis of PGMA-stabilised polystyrene (PGMA-PS) latexes by conventional aqueous emulsion polymerisation.[14] Pelton et al. examined the pH-dependent adsorption of these PGMA-PS latexes onto functionalised regenerated cellulose films (Figure 2.2).[4] At pH 10.5 the cis-diol and boronic acid react to form a boronate ester. This complexation occurs due to the pH being above the pK_a of the phenylboronic acid (pK_a ~ 9).[15] In contrast, reducing the pH to 4 led to desorption of the PGMA-PS latex from the cellulose surface. This reversible transition was confirmed by confocal microscopy using Alizarin Red S dye which only fluoresces when present as a boronate complex.[16] This work was extended to look at the interaction of the PGMA-PS latexes with phenylboronic acid functionalised silica surfaces.[6] This showed similar results, with adsorption occurring at high pH but no adsorption observed at pH 4.

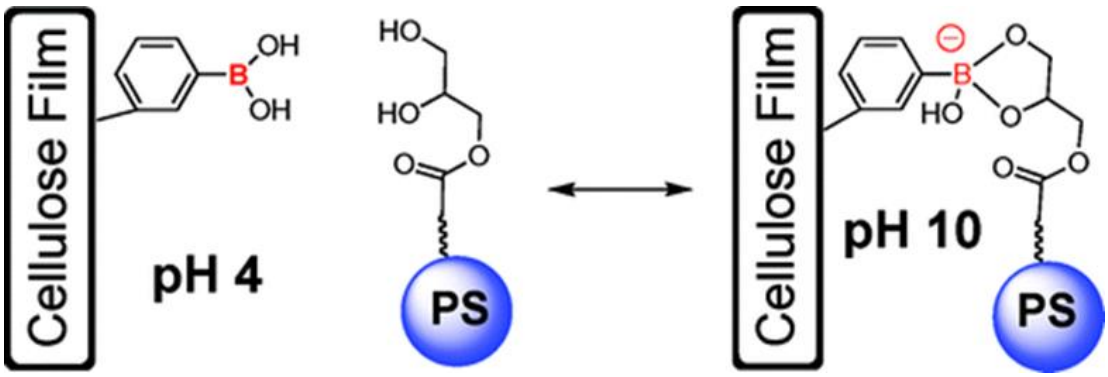

Figure 2.2 Schematic representation of the pH-dependent adsorption of PGMA-PS latexes to phenylboronic acid-functionalised regenerated cellulose films.[4]

This Chapter describes a relatively rare example of a RAFT aqueous emulsion polymerisation formulation based on a *non-ionic* steric stabiliser block, poly(glycerol monomethacrylate) (PGMA). Two PGMA macro-CTAs have been chain-extended using a water-immiscible monomer, benzyl methacrylate (BzMA), via RAFT aqueous emulsion polymerisation. The effect of varying the target degree of polymerisation of the core-forming PBzMA block and the overall copolymer concentration on the particle size, blocking efficiency and conversion has been systematically investigated. These $PGMA_{63}$-$PBzMA_x$ nanoparticles are also assessed as Pickering emulsifiers for four model oils, namely sunflower oil, *n*-hexane, *n*-

dodecane and isopropyl myristate. Finally, the dihydroxy functionality of the PGMA stabiliser chains has been used to control the surface adsorption of $PGMA_{63}$-$PBzMA_{124}$ nanoparticles on a micro-patterned planar substrate via phenylboronic acid chemistry. The work presented herein has already formed the basis of a publication in Macromolecules.[17] Since the publication of this manuscript, further analysis of the PGMA macro-CTA revealed an actual DP of 63 (rather than DP 51).

2.2 Experimental Details

2.2.1 Materials

Glycerol monomethacrylate (GMA) was donated by GEO Specialty Chemicals (Hythe, UK). Benzyl methacrylate (BzMA), 4,4'-azobis(4-cyanopentanoic acid) (ACVA; 99 %), *n*-dodecane, isopropyl myristate, sunflower oil and 3-formylphenylboronic acid were purchased from Sigma-Aldrich UK. 2-Cyano-2-propyl dithiobenzoate (CPDB) was purchased from STREM Chemicals Ltd. (Cambridge, UK). 2,2'-Azobis[2-(2-imidazolin-2-yl)propane]dihydrochloride (AIPD) was purchased from Wako Pure Chemicals, Ltd (Osaka, Japan). All chemicals were used as received. d_6-Dimethyl sulfoxide, d_7-dimethyl formamide and d_4-methanol were purchased from Goss Scientific Instruments Ltd., (Cheshire, UK). All other solvents were purchased from Fisher Scientific (Loughborough, UK) and used as received. De-ionised water was used for all experiments.

2.2.2 Preparation of $PGMA_{63}$ macro-CTA

CPDB RAFT agent (1.650 g, 7.454 mmol), GMA (78.144 g, 488 mmol) and ACVA (0.3790 g, 1.352 mmol; CPDB/ACVA molar ratio = 5.0) were weighed into a 500 ml round-bottom flask and degassed with nitrogen for 15 min. Ethanol (148 ml) was deoxygenated separately with nitrogen for 30 min prior to addition to the other reagents. The reaction solution was stirred and degassed in an ice bath for a further 30 min before placing in an oil bath at 70 °C. The polymerisation was allowed to proceed for 150 min, resulting in a monomer conversion of 68 % as judged by ^{1}H NMR (comparing the integrated vinyl signals at 5.6 and 6.0 ppm to the two oxymethylene protons at 3.7 - 4.3 ppm). The crude homopolymer was purified by precipitating into a ten-fold excess of dichloromethane. This purification process was repeated twice to give a pure PGMA macro-CTA (53.14 g, < 1 % monomer

remaining). ^{1}H NMR indicated a mean degree of polymerisation of 63 via end-group analysis (by comparing the aromatic RAFT signals 7.3 – 8.0 ppm to the two oxymethylene protons at 3.7 - 4.3 ppm). DMF GPC analysis indicated a M_n of 15,000 g mol^{-1} and an M_w/M_n of 1.19 (vs. a series of near-monodisperse PMMA calibration standards). The same method was used for the synthesis of a $PGMA_{18}$ macro-CTA by simply varying the CPDB/GMA molar ratio.

2.2.3 RAFT aqueous emulsion polymerisation of benzyl methacrylate

A typical protocol for the synthesis of $PGMA_{63}$-$PBzMA_{371}$ diblock copolymer was as follows: $PGMA_{63}$ macro-CTA (0.0696 g), BzMA (0.4414 g, 2.505 mmol), ACVA (0.600 mg, 2.141 μmol; CTA/ACVA molar ratio = 4.0) and water (4.58 g, 10% w/w) were weighed into a 25 ml round-bottom flask and purged with nitrogen for 30 min, prior to immersion in an oil bath set at 70 °C for 6 h. The resulting copolymer was analysed by DMF GPC (M_n = 62,100 g mol^{-1}, M_w/M_n = 1.18 vs. PMMA standards). ^{1}H NMR spectroscopy analysis in d_7-DMF indicated less than 1% residual BzMA monomer (comparing the vinyl signals at 5.8 and 6.3 ppm to the five aromatic protons at 7 - 7.8 ppm). DLS studies of a 0.20% w/w copolymer dispersion indicated an intensity-average particle diameter of 91 nm (DLS polydispersity, PDI = 0.05).

2.2.4 Synthesis of fluorescently-labelled $PGMA_{63}$-$PBzMA_{124}$ nanoparticles

An excess of methylamine solution (33 wt.% in absolute ethanol) was added to $PGMA_{63}$-$PBzMA_{124}$ (1.50 g) synthesised via RAFT aqueous emulsion polymerisation. After 10 min, this aqueous copolymer dispersion was reacted with rhodamine B isothiocyanate (3.10 mg, 5.78 μmol) for 40 h at 20 °C with continuous magnetic stirring. The resulting fluorescently-labelled nanoparticles were purified by dialysis for eight days with 2-5 water changes per day. DLS studies of a 0.20% w/w copolymer dispersion indicated an intensity-average particle diameter of 46 nm (PDI = 0.15). The resulting copolymer was analysed by DMF GPC (M_n = 29,200 g mol^{-1}, M_w/M_n = 1.10 vs. PMMA standards).

2.2.5 RAFT aqueous emulsion polymerisation of PEG_{113}-$PBzMA_{200}$

The PEG_{113}-$PBzMA_{200}$ nanoparticles were prepared by Dr. Kate Thompson. AIPD azo initiator (6.10 mg, 0.0189 mmol), PEG_{113}-dithiobenzoate macro-CTA (0.2996 g, 0.0568 mmol; [CTA]/[AIPD] molar ratio = 3.0) and BzMA monomer (2.00 g, 11.4 mmol, target DP = 200) were weighed into a round-bottomed flask containing a magnetic stir bar. These reagents were dissolved in previously deoxygenated water (9.20 mL, 10% w/w solids) and purged with nitrogen for 30 min at 20 °C. The flask was sealed and immersed in an oil bath at 50 °C for 24 h, after which the reaction was quenched by exposure to air and cooling to 20 °C. (N.B. Synthesis and characterisation of the PEG_{113}-DB macro-CTA was by Dr Nick Warren has been reported elsewhere).[18]

2.2.6 Preparation of Pickering emulsions using PGMA-PBzMA latex particles

Either sunflower oil, *n*-hexane, *n*-dodecane or isopropyl myristate (2.0 ml) was homogenised with 2.0 ml of a 0.0675 – 2.50% w/w aqueous $PGMA_{63}$-$PBzMA_x$ copolymer dispersion for 2 min using a IKA Ultra-Turrax T-18 homogeniser equipped with a 10 mm dispersing tool operating at 12,000 rpm.

2.2.7 Preparation of surface-aminated silicon wafers using (*N*-[2-(2-nitrophenyl)propan-1-oxycarbonyl]-3-aminopropyl)

All glassware and substrates were cleaned by immersing them in 'piranha' solution (a 3:7 mixture of hydrogen peroxide and concentrated sulfuric acid) for 2 h. The glassware and the substrates were washed with deionised water several times then sonicated for 10 min and rinsed with deionised water. Glassware and substrates were dried in a 120 °C oven for 1 h. The silicon wafers were submerged in a 1:1:5 solution of ammonium hydroxide, 30% hydrogen peroxide and deionised water (The Radio Cooperative America). The solution was heated to 85 °C for 30 min and allowed to cool. The samples were rinsed with deionised water, sonicated and dried in an oven before use.

Silicon wafers were immersed into a 1 mM solution of (*N*-[2-(2-nitrophenyl)propan-1-oxycarbonyl]-3-aminopropyl)triethoxysilane (NPPOC-silane) in toluene for 48 h at

20 °C. The coated wafers were rinsed with toluene, followed by ethanol, and dried under a stream of nitrogen gas.

2.2.8 Photopatterning of NPPOC functionalised surfaces

A He-Cd laser (Kimmon IK3202R-D) with an UV emission wavelength of 325 nm was used to irradiate samples. The area illuminated by the laser beam was 0.20 cm^2 and the laser power was 11 mW. Micropatterns were obtained by irradiation of NPPOC-coated silicon wafers using an electron microscopy copper grid (Agar, Cambridge, UK) as a convenient mask.

2.2.9 Selective adsorption of $PGMA_{63}$-$PBzMA_{124}$ nanoparticles onto patterned NPPOC-functionalised silicon wafers

Patterned NPPOC-functionalised silicon wafers were immersed in a 20 mM ethanolic solution of 3-formylphenylboronic acid for 2 h at 20 °C. The wafers were rinsed with ethanol and dried using a nitrogen gas stream. The phenylboronic acid functionalised wafers were then immersed in a 0.01% w/w aqueous dispersion of fluorescently-labelled $PGMA_{63}$-$PBzMA_{124}$ nanoparticles at either pH 4 or pH 10 for 2 h at 20 °C. Finally, each wafer was rinsed with water several times and dried gently under a nitrogen gas stream.

2.2.10 Copolymer characterisation

^{1}H NMR Spectroscopy

All ^{1}H NMR spectra were recorded using a 400 MHz Bruker Avance-400 spectrometer using d_4-methanol, d_7-dimethylformamide or d_6-dimethyl sulfoxide.

Gel Permeation Chromatography (GPC)

The molecular weights and dispersities of the PGMA macro-CTA and PGMA-PBzMA diblock copolymers were determined by DMF GPC at 60 °C. The GPC set-up consisted of two Polymer Laboratories PL gel 5 μm Mixed C columns connected in series to a Varian 390 LC multi-detector suite (refractive index detector) and a Varian 290 LC pump injection module. The mobile phase was HPLC grade DMF containing 10 mmol LiBr with a flow rate of 1.0 ml min^{-1}. Copolymer solutions (1.0% w/v) were prepared in DMF using DMSO as the flow rate marker. Ten near-monodisperse poly(methyl methacrylate) standards (PMMA; M_n = 625 – 618,000 g

mol^{-1}) were used for calibration. Data were analysed using Varian Cirrus GPC software (version 3.3).

Dynamic Light Scattering (DLS)

The intensity-average hydrodynamic diameter of each batch of spherical diblock copolymer nanoparticles was determined using a Malvern Zetasizer NanoZS instrument. Aqueous dispersions (0.20% w/w) were analysed using disposable plastic cuvettes and data were averaged over three consecutive runs.

Transmission Electron Microscopy (TEM)

Copper/palladium TEM grids (Agar Scientific) were coated in-house to yield a thin film of amorphous carbon. The grids were then subjected to a glow discharge for 30 seconds to create a hydrophilic surface. Individual samples (0.20% w/w aqueous dispersion, 10.0 µL) were adsorbed onto the freshly treated grids for one minute and then blotted with filter paper to remove excess solution. To stain the nanoparticles, uranyl formate (9.0 µL of a 0.75% w/w solution) was absorbed onto the sample-loaded grid for 20 seconds and then carefully blotted to remove excess stain. The grids were then dried using a vacuum hose. Imaging was performed using a Philips CM100 instrument operating at 100 kV and equipped with a Gatan 1 k CCD camera.

Optical Microscopy

Optical microscopy images were recorded using a Motic DMBA300 digital biological microscope equipped with a built-in camera and Motic Images Plus 2.0 ML software.

Laser Diffraction

A Malvern Mastersizer 2000 instrument equipped with a small volume Hydro 2000SM sample dispersion unit (ca. 50 ml), a HeNe laser operating at 633 nm, and a solid-state blue laser operating at 466 nm was used to size each emulsion. The stirring rate was adjusted to 1,000 rpm in order to avoid creaming of the emulsion during analysis. After each measurement, the cell was rinsed once with ethanol, followed by two rinses with distilled water; the glass walls of the cell were carefully wiped with tissue to avoid cross-contamination and the laser was aligned centrally to the detector prior to data acquisition.

Fluorescence Microscopy

A single droplet of a Pickering emulsion was placed on a microscope slide and viewed using an Olympus Upright Epifluorescence microscope equipped with a Hamamatsu ORCA-ER monochrome camera and Volocity software.

Atomic Force Microscopy (AFM)

AFM studies were carried out using a Nanoscope IV Multimode Atomic Force Microscope (Veeco, Santa Barbara, USA) with a 'J' scanner (0 - 125 µm). Silicon probes (Bucker, Germany) with average spring constants between 20 and 80 Nm^{-1} were used for tapping mode studies. Mean heights were determined for micro-patterned particles.

2.3 Results and Discussion

2.3.1 Synthesis of $PGMA_{63}$ macromolecular chain transfer agent via RAFT solution polymerisation

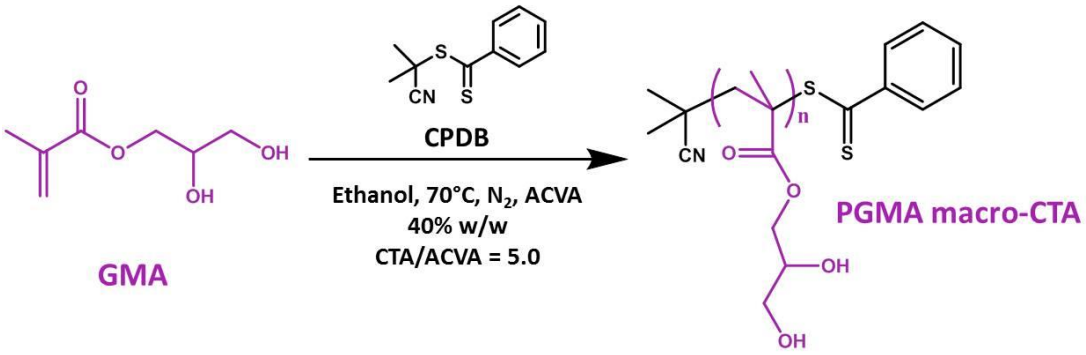

Scheme 2.1 Synthesis of poly(glycerol monomethacrylate) (PGMA) macro-CTA using CPDB as the RAFT chain transfer agent.

Reaction kinetics for the synthesis of a PGMA macro-CTA in ethanol at 70 °C and 40% w/w solids (Scheme 2.1) have previously been published by Blanazs et al.[19] Utilising this data, a DP of 70 was targeted. The reaction proceeded for 150 minutes, resulting in a GMA conversion of 68%. For the synthesis of a macro-CTA it is desirable to terminate the polymerisation prior to reaching full conversion to ensure RAFT chain-end fidelity. This is essential to ensure high blocking efficiencies when making block copolymers via chain extension. The PGMA macro-CTA was purified by repeated precipitation into excess dichloromethane. The resulting polymer was

dissolved in water and freeze dried to give a pure PGMA macro-CTA (< 1% residual monomer remaining). ^{1}H NMR analysis of the dried polymer indicated a mean DP of 63. DMF GPC analysis of the $PGMA_{63}$ macro-CTA indicated a M_n of 15,000 g mol^{-1} with a low dispersity (M_w/M_n) of 1.19 (Figure 2.3).

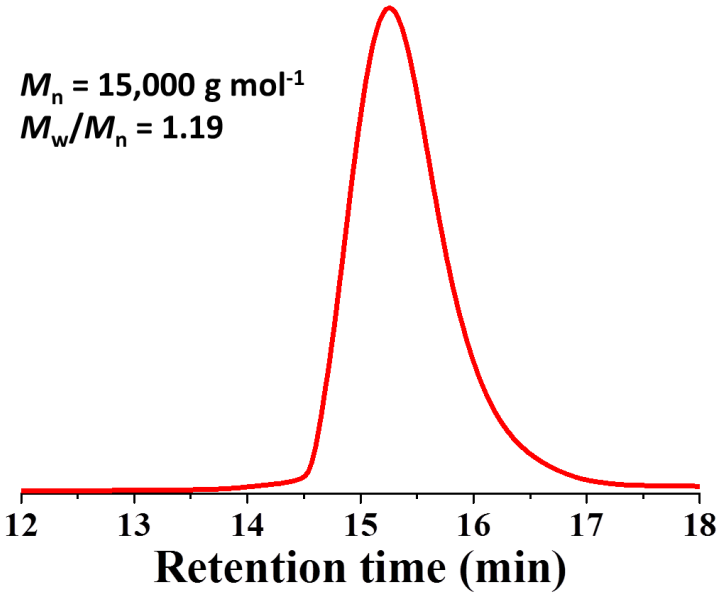

Figure 2.3 DMF GPC chromatogram of the $PGMA_{63}$ macro-CTA (vs. PMMA calibration standards).

2.3.2 Kinetics of $PGMA_{63}$-$PBzMA_{309}$ via RAFT emulsion polymerisation

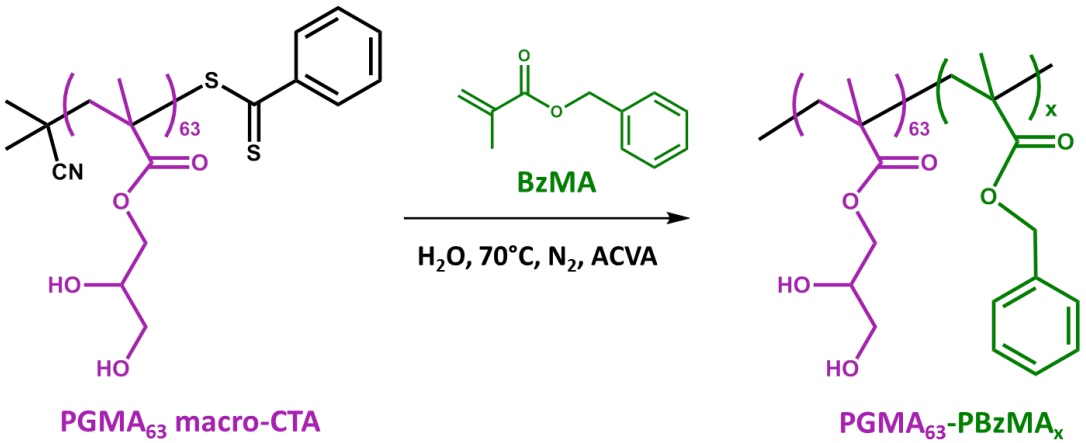

Scheme 2.2 Diblock synthesis of poly(glycerol monomethacrylate)$_{63}$-poly(benzyl methacrylate)$_x$ ($PGMA_{63}$-$PBzMA_x$) at 70 °C.

The $PGMA_{63}$ macro-CTA synthesised was then chain-extended with BzMA via RAFT aqueous emulsion polymerisation (Scheme 2.2). The kinetics for a block composition of $PGMA_{63}$-$PBzMA_{309}$ was studied at 10% w/w solids and 70 °C. The

$PGMA_{63}$ macro-CTA/ACVA molar ratio was varied from 3.0 to 10.0 to see how this affected the polymerisation rate and dispersity of the $PGMA_{63}$-$PBzMA_{309}$ diblock copolymer. The reaction was sampled every 15 minutes and each sample was analysed by ^{1}H NMR spectroscopy in d_7-DMF, which is a good solvent for both the PGMA and PBzMA.

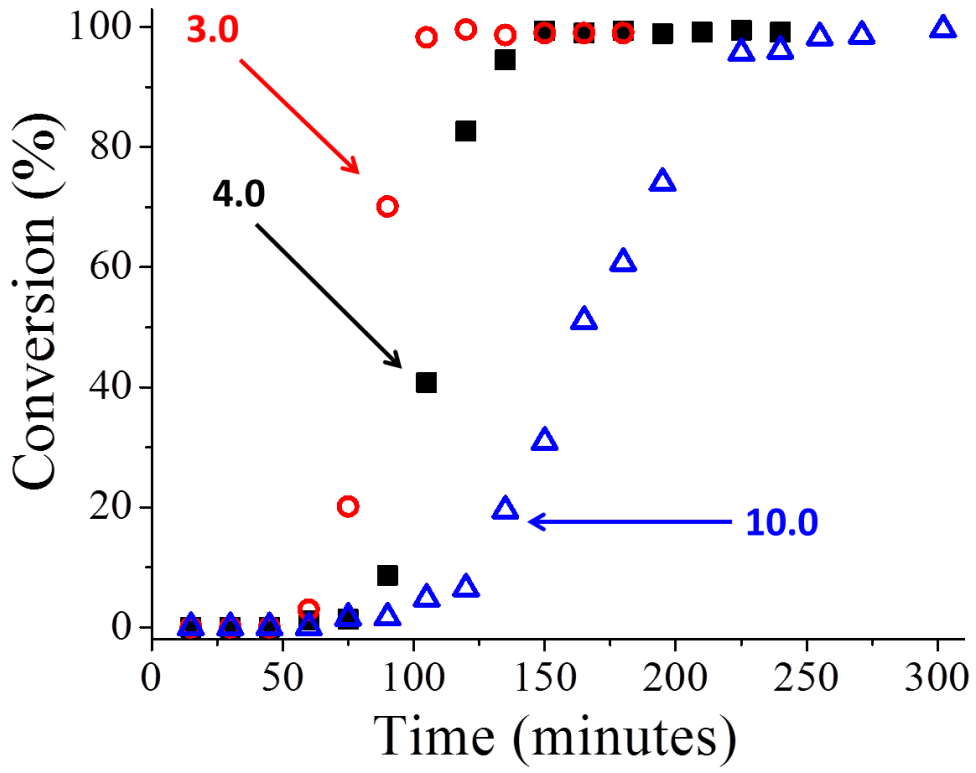

Figure 2.4 Kinetics of polymerisation of BzMA at 70 °C prepared at 10% w/w solids with varying $PGMA_{63}$ macro-CTA/ACVA molar ratios of 3.0 (circle), 4.0 (square) and 10.0 (triangle). The target diblock copolymer composition in each case was $PGMA_{63}$-$PBzMA_{309}$.

As can be seen in Figure 2.4 all three $PGMA_{63}$ macro-CTA/ACVA molar ratios led to very high conversion (≥ 99%) within 6 h. As expected, the highest macro-CTA/ACVA molar ratio (10.0) led to the slowest polymerisation with 99% conversion achieved within 6 h. In comparison, utilising a macro-CTA/ACVA ratio of 4.0 or 3.0 led to significantly faster reactions with 99% conversion reached in 2.5 h and 2 h respectively. Low macro-CTA/ACVA molar ratios such as 3.0 can often hinder the RAFT living character resulting in high dispersities (typically greater than 1.30). Therefore, higher molar ratios are used in order to reduce termination and maintain living character. In this particular case, this did not seem to be a problem as

all three reactions when analysed by DMF GPC showed high blocking efficiencies relative to the $PGMA_{63}$ macro-CTA as well as having low dispersities of less than 1.20 (Figure 2.5).

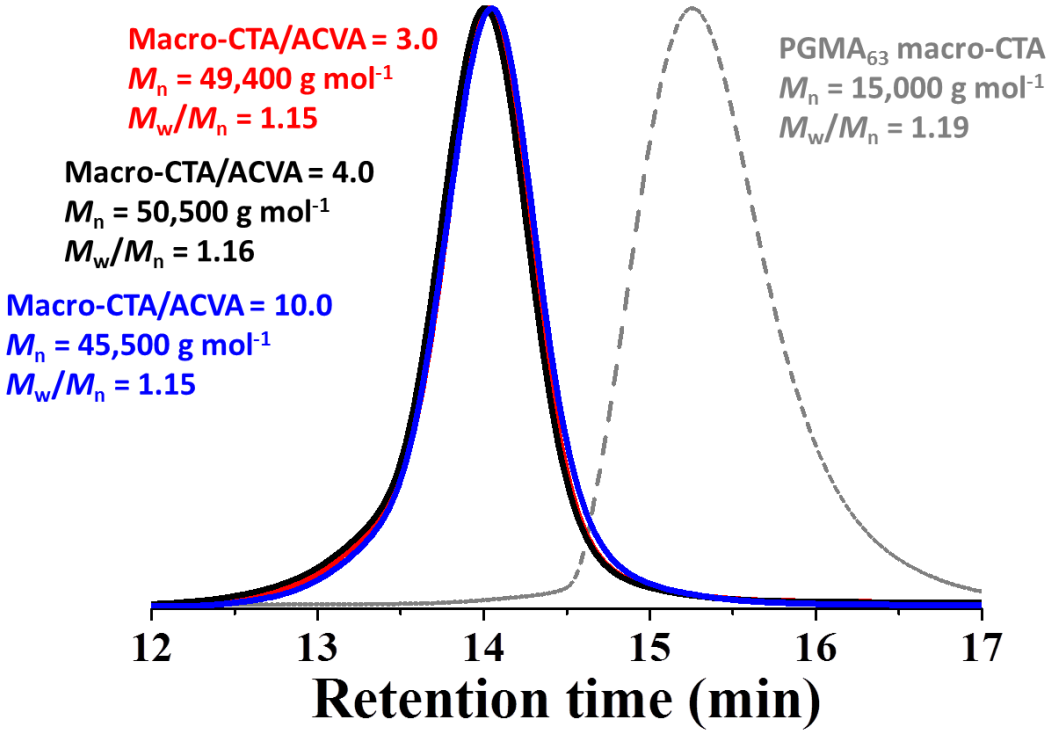

Figure 2.5 DMF GPC chromatograms of the $PGMA_{63}$ macro-CTA and the resulting $PGMA_{63}$-$PBzMA_{309}$ diblock copolymers after 99% BzMA conversion had been attained for the kinetics with varying the macro-CTA/ACVA molar ratio from 3.0 to 10.0.

2.3.3 Synthesis of $PGMA_{63}$-$PBzMA_x$ diblock copolymers via RAFT emulsion polymerisation at 10% w/w solids

A series of $PGMA_{63}$-$PBzMA_x$ diblock copolymers have been prepared via RAFT emulsion polymerisation at 70 °C. The target PBzMA DP was varied from 62-1235. A macro-CTA/ACVA molar ratio of 4.0 and solids content of 10% w/w was selected for all polymerisations. All diblock copolymers were analysed by ^{1}H NMR spectroscopy, DMF GPC, DLS and TEM. The results are summarised in Table 2.1.

Very high conversions of at least 98%, as judged by ^{1}H NMR spectroscopy were achieved for the polymerisation of BzMA in the synthesis of $PGMA_{63}$-$PBzMA_x$ diblock copolymers. DMF GPC analysis shows an increase in M_n with increasing PBzMA DP. The dispersities of the $PGMA_{63}$-$PBzMA_x$ diblock copolymers remain low (M_w/M_n < 1.30) even for highly asymmetric diblocks such as $PGMA_{63}$-$PBzMA_{1235}$. Figure 2.6 shows representative DMF GPC chromatograms for six of the $PGMA_{63}$-$PBzMA_x$ diblock copolymers. These all show high blocking relative to

the $PGMA_{63}$ macro-CTA chromatogram with little evidence of contamination from the macro-CTA in the diblock copolymer curves.

Table 2.1 Solids contents, conversions, number-average molecular weights (M_n), dispersities (M_w/M_n) and mean DLS and TEM diameters obtained for $PGMA_{63}$-$PBzMA_x$ (G_{63}-B_x) diblock copolymer nanoparticles and the corresponding $PGMA_{63}$ macro-CTA. The numbers in brackets refer to the polydispersity (PDI) of the sample.

	Target composition	Solids content (% w/w)	Conversion[a] (%)	GPC		Particle diameter	
				M_n[b] (g mol^{-1})	M_w/M_n[b]	DLS (nm)	TEM (nm)
1	G_{63}	40	67	15,000	1.19	-	-
2	G_{63}-B_{62}	10	>99	19,700	1.19	28 (0.10)	20
3	G_{63}-B_{93}	10	>99	20,900	1.23	30 (0.13)	23
4	G_{63}-B_{124}	10	>99	26,900	1.22	41 (0.15)	27
5	G_{63}-B_{154}	10	>99	30,400	1.21	53 (0.25)	35
6	G_{63}-B_{185}	10	>99	34,600	1.26	55 (0.12)	36
7	G_{63}-B_{216}	10	>99	39,800	1.23	58 (0.06)	43
8	G_{63}-B_{247}	10	98	45,600	1.26	64 (0.07)	44
9	G_{63}-B_{309}	10	>99	51,100	1.19	81 (0.10)	55
10	G_{63}-B_{371}	10	>99	62,100	1.18	91 (0.05)	73
11	G_{63}-B_{494}	10	>99	77,100	1.21	113 (0.04)	82
12	G_{63}-B_{618}	10	>99	83,400	1.24	137 (0.02)	105
13	G_{63}-B_{1235}	10	>99	116,800	1.26	230 (0.02)	193

a. Monomer conversion determined by ^{1}H NMR spectroscopy
b. Determined by DMF GPC using a series of near-monodisperse PMMA calibration standards

Each of the $PGMA_{63}$-$PBzMA_x$ diblock copolymers were analysed by DLS and TEM. Dilute copolymer dispersions (0.20% w/w) were used for both techniques to analyse the nanoparticles formed during the polymerisation. The amphiphilic nature of the $PGMA_{63}$-$PBzMA_x$ diblock copolymers leads to polymerisation-induced self-assembly (PISA). Figure 2.7a shows the intensity-average diameters as measured by DLS. As the core-forming PBzMA DP increases from 62 to 1235 an increase in diameter was observed by DLS. All data show unimodal peaks with low PDIs. The TEM images in Figure 2.7b indicate the formation of spherical nanoparticles for each diblock copolymer targeted. A plot of mean particle diameter as measured by TEM and DLS against PBzMA DP was shown in Figure 2.7c. A linear increase in particle diameter with PBzMA DP is observed. This provides a convenient route to the synthesis of spherical nanoparticles, with a particular diameter between 28 nm and 230 nm, simply by varying the PBzMA DP.

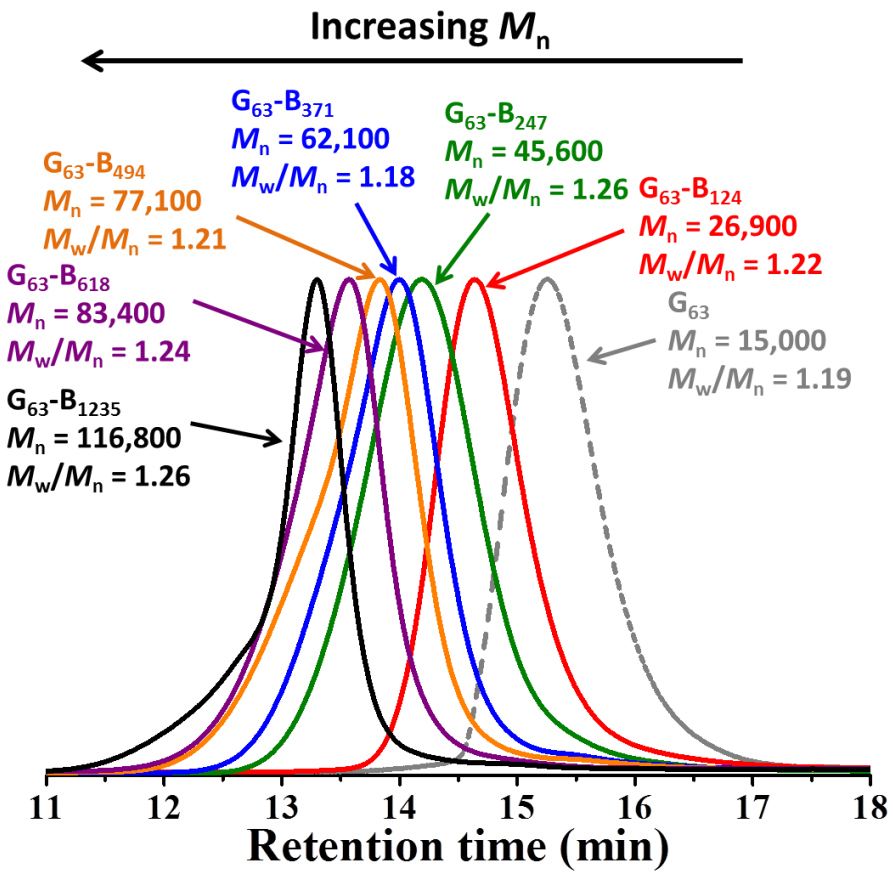

Figure 2.6 DMF GPC chromatograms for $PGMA_{63}$-$PBzMA_x$ diblock copolymers prepared at 10% w/w solids, where x = 124, 247, 371, 494, 618 or 1235. Molecular weight data are expressed in units of g mol^{-1} (G = PGMA and B = PBzMA).

The colloidal stability of three $PGMA_{63}$-$PBzMA_x$ nanoparticles (x = 124, 216 and 309) was assessed (Table 2.2). Firstly, a freeze-thaw cycle was conducted. Nanoparticle dispersions were placed at -21 °C overnight and then allowed to heat back to 20 °C. Secondly, the stability after the addition of salt (0.25 M $MgSO_4$) was studied. The stability was measured by DLS as this technique is very sensitive to small increases in particle size. All three diblock copolymers showed a small increase in particle diameter (< 10 nm) after these tests compared to previously. This confirms strong steric stabilisation from the hydrophilic PGMA stabiliser.

These $PGMA_{63}$-$PBzMA_x$ spheres synthesised at 10% solids offer excellent size control and compared with other PGMA-stabilised systems such as PGMA-PHPMA spheres they appear very well-defined when imaged by TEM.[20-22] Unlike the PGMA-PHPMA system, the PGMA-PBzMA diblocks only appear to form spherical micelles at 10% w/w. This will be studied further in section 2.3.4 and 2.3.5.

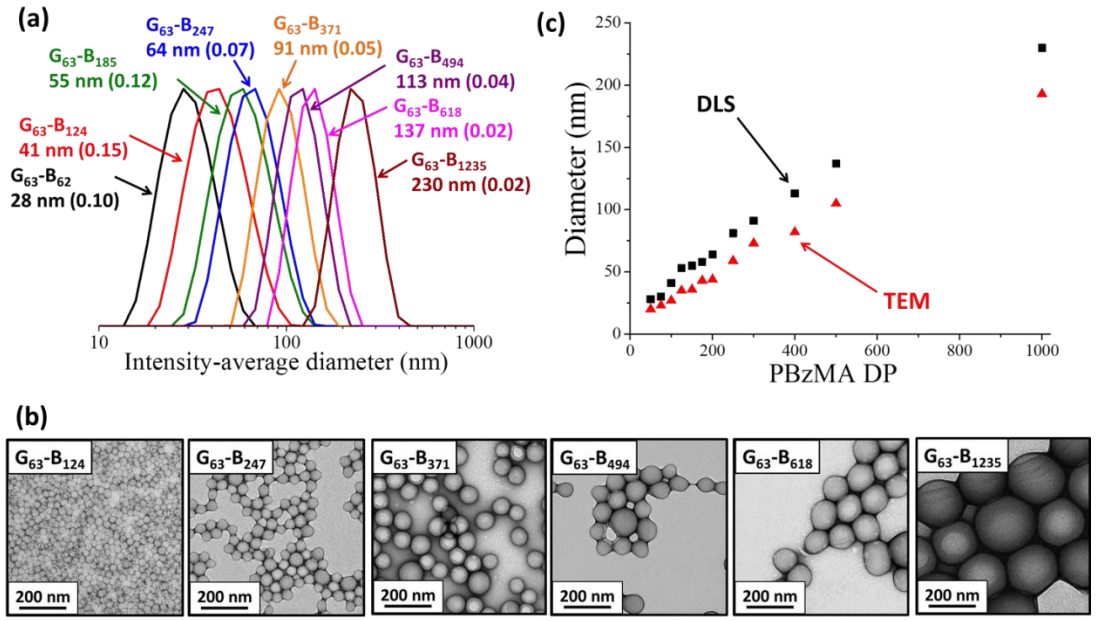

Figure 2.7 $PGMA_{63}$-$PBzMA_x$ diblock copolymers prepared at 10% w/w solids: (a) DLS intensity-average size distributions, (b) TEM images and (c) a plot of mean particle diameter versus mean degree of polymerisation of the PBzMA core-forming block (G = PGMA and B = PBzMA).

Table 2.2 DLS particle diameter (nm) determined before and after either the addition of 0.25 M $MgSO_4$ or a single freeze-thaw cycle (at -21 °C). The numbers in brackets refer to the polydispersity of the sample (N.B. 'G' denotes PGMA and 'B' denotes PBzMA).

Target composition	Initial particle diameter	Following addition of 0.25 M $MgSO_4$	Following one freeze-thaw cycle
G_{63}-B_{124}	41 (0.15)	48 (0.14)	44 (0.17)
G_{63}-B_{216}	58 (0.06)	67 (0.05)	60 (0.13)
G_{63}-B_{309}	81 (0.10)	89 (0.13)	83 (0.14)

2.3.4 Synthesis of $PGMA_{63}$-$PBzMA_x$ diblock copolymers via RAFT emulsion polymerisation at 10-50% w/w solids

The solids content of a PISA synthesis can play a crucial part in determining the final copolymer morphology. For example, Blanazs et al. showed that a series of $PGMA_{78}$-$PHPMA_x$ diblock copolymers synthesised at 10% w/w solids by RAFT aqueous dispersion polymerisation only formed spherical micelles.[20] On increasing the solids content to 13% w/w, mixed phases of spherical micelles, worm-like micelles and vesicles were formed. Pure worm and vesicle phases were formed above 17% w/w solids. It was suggested that the spherical micelles can become kinetically-trapped at 10% w/w and are therefore not necessarily the equilibrium

morphology, particularly when targeting higher degrees of polymerisation for the core-forming PHPMA block (DP > 200).[20] This highlights the importance of examining higher solids syntheses to see whether the spherical $PGMA_{63}$-$PBzMA_x$ diblock copolymers prepared at 10% w/w solids are merely kinetically-trapped.

A series of $PGMA_{63}$-$PBzMA_{309}$ diblock copolymers were prepared at 10, 20, 30, 40 and 50% w/w solids. A PBzMA DP of 309 was selected. Previous RAFT dispersion polymerisations with PBzMA in ethanol (PMAA-PBzMA[23] and PDMA-PBzMA[24]) and *n*-alkanes (PLMA-PBzMA[25]) suggest that a DP greater than 200 forms worm-like micelles or vesicles. The five $PGMA_{63}$-$PBzMA_{309}$ diblocks all proceeded to more than 99% conversions, as judged by ^{1}H NMR spectroscopy (Table 2.3).

Table 2.3 Solids contents, conversions, number-average molecular weights (M_n), dispersities (M_w/M_n) and mean DLS and TEM diameters obtained for $PGMA_{63}$-$PBzMA_{309}$. The numbers in brackets refer to the polydispersity of the sample. (N.B. 'G' denotes PGMA and 'B' denotes PBzMA).

	Target composition	Solids content (% w/w)	Conversion[a] (%)	GPC		Particle diameter	
				M_n[b] (g mol^{-1})	M_w/M_n[b]	DLS (nm)	TEM (nm)
1	G_{63}-B_{309}	10	>99	51,100	1.19	81 (0.10)	55
2	G_{63}-B_{309}	20	>99	52,900	1.16	78 (0.12)	55
3	G_{63}-B_{309}	30	>99	52,700	1.13	76 (0.09)	47
4	G_{63}-B_{309}	40	>99	52,700	1.13	86 (0.04)	55
5	G_{63}-B_{309}	50	>99	52,600	1.16	97 (0.10)	57

a. Monomer conversion determined by ^{1}H NMR spectroscopy
b. Determined by DMF GPC using a series of near-monodisperse PMMA calibration standards

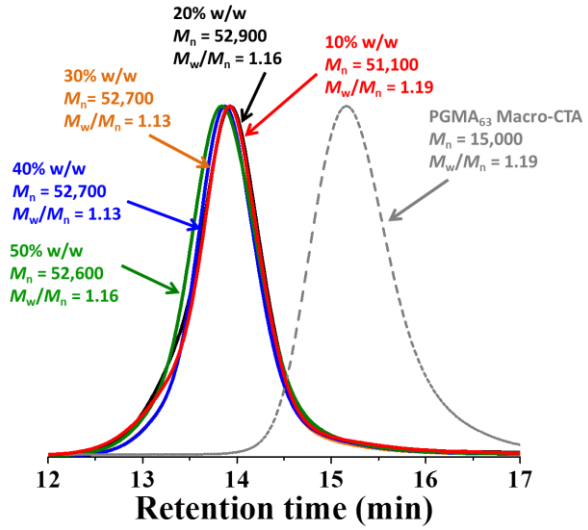

Figure 2.8 GPC chromatograms of $PGMA_{63}$-$PBzMA_{309}$ prepared at 10-50% w/w and the corresponding $PGMA_{63}$ macro-CTA. Molecular weights are expressed in units of g mol^{-1}.

Each of the $PGMA_{63}$-$PBzMA_{309}$ diblock copolymers were analysed by DMF GPC analysis (Figure 2.8). All exhibit molecular weights of approximately 52,000 g mol^{-1}, as expected for the same target block composition, and relatively low dispersities (M_w/M_n < 1.20). High blocking efficiencies with minimal residual $PGMA_{63}$ macro-CTA were observed for all diblock copolymers.

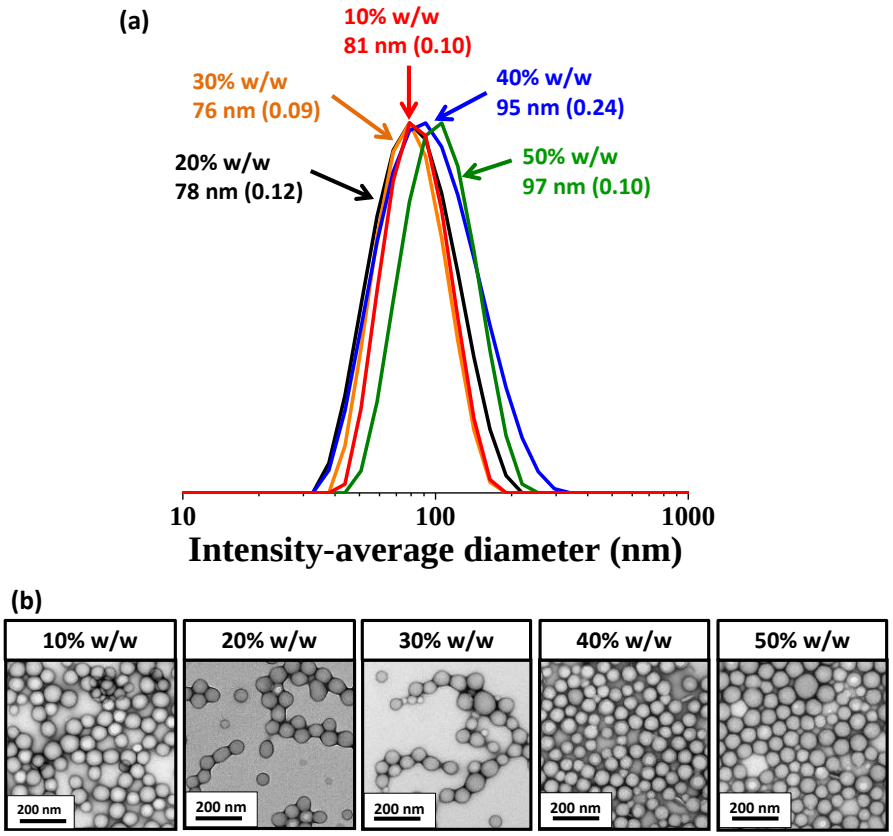

Figure 2.9 $PGMA_{63}$-$PBzMA_{309}$ spherical nanoparticles prepared at 10, 20, 30, 40 and 50% w/w solids: (a) DLS intensity-average size distributions and polydispersities, (b) representative TEM images.

DLS of the five $PGMA_{63}$-$PBzMA_{309}$ diblock copolymers show unimodal peaks with low PDIs. A slight increase in diameter with solids content is observed (Figure 2.9). TEM shows well-defined spherical micelles for all solids content. Unlike the previous work on PGMA-PHPMA, the PGMA-PBzMA diblocks do not appear to form higher order morphologies. This is perhaps unusual as other RAFT emulsion polymerisations by Charleux and co-workers have resulted in the formation of these higher order morphologies.[26,27] The mean number-average diameters determined from TEM images (with at least 100 particles being counted in each case) suggest very little variation in particle size with copolymer concentration (Table 2.3). The number-average diameter for $PGMA_{63}$-$PBzMA_{309}$ diblock copolymers prepared at

10% w/w and 50% w/w were 55 ± 8 nm and 57 ± 16 nm respectively. Thus, there is very little difference in size when conducting such syntheses at high solids.

One apparent difference in the five syntheses of $PGMA_{63}$-$PBzMA_{309}$ diblocks was the paste-like consistency observed at 50% w/w solids (see Figure 2.10). This was only observed at 50% w/w and all other concentrations resulted in a free-flowing liquid (10% - 40% w/w). As the particle size has been shown to be very similar for both 10% w/w and 50% w/w solids in dilute solutions (0.20% w/w) this change in viscosity could be due to weak attractive interparticle interactions which at lower concentrations the $PGMA_{63}$ stabiliser is able to counterbalance.

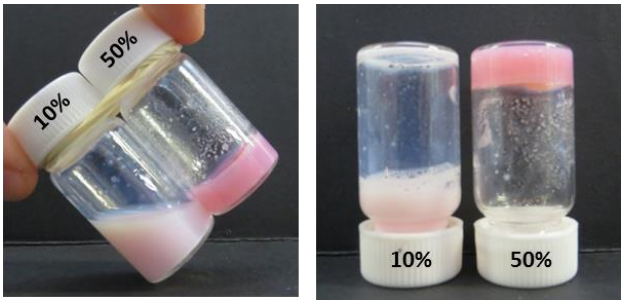

Figure 2.10 Digital photographs of $PGMA_{63}$-$PBzMA_{309}$ prepared at 10 and 50% w/w.

2.3.5 Synthesis of $PGMA_{18}$-$PBzMA_x$ (using a shorter macro-CTA)

Varying both the core-forming block DP and solids content have resulted in only spherical nanoparticle formation. One final important parameter is the PGMA macro-CTA stabiliser block length. A shorter $PGMA_{18}$ macro-CTA was synthesised by the same method as the $PGMA_{63}$ macro-CTA. This $PGMA_{18}$ macro-CTA was chain-extended with 50, 100 and 150 units of PBzMA at 20% w/w solids (see Table 2.4).

Table 2.4 Solids contents, conversions, number-average molecular weights (M_n), dispersities (M_w/M_n) and mean DLS and TEM diameters obtained for $PGMA_{18}$-$PBzMA_x$ diblock copolymer nanoparticles and the $PGMA_{18}$ macro-CTA. The numbers in brackets refer to the polydispersity of the sample. (N.B. G = PGMA and B = PBzMA).

	Target composition	Solids content (% w/w)	Conversion[a] (%)	GPC		Particle diameter	
				M_n[b] (g mol^{-1})	M_w/M_n[b]	DLS (nm)	TEM (nm)
1	G_{18}	40	68	6,500	1.12	-	-
2	G_{18}-B_{50}	20	>99	10,700	1.10	38 (0.16)	29
3	G_{18}-B_{100}	20	>99	16,800	1.10	97 (0.21)	78
4	G_{18}-B_{150}	20	>99	21,600	1.14	215 (0.04)	215

a. Monomer conversion determined by ^{1}H NMR spectroscopy
b. Determined by DMF GPC using a series of near-monodisperse PMMA calibration standards

All three $PGMA_{18}$-$PBzMA_x$ diblock polymerisation went to high conversions (> 99%). DMF GPC analysis of both the $PGMA_{18}$ macro-CTA and the three diblock copolymers show low dispersities (Figure 2.11). An increase in molecular weight and corresponding shift towards lower retention time is seen as the PBzMA DP is increased from 50 to 150. All three diblock copolymers show high blocking relative to the $PGMA_{18}$ macro-CTA.

DLS shows an increase in particle size with PBzMA DP, as expected (Table 2.4). However, TEM images confirm only spherical particles (see Figure 2.12). PBzMA has previous been used in several RAFT dispersion polymerisation conducted in both alcohol[23,24] and *n*-alkanes.[25,28] Both resulted in a full range of morphologies including spheres, worms and vesicles. Therefore the limitation to spherical micelles in this $PGMA_x$-$PBzMA_y$ formulation does not appear to be an intrinsic problem associated with using PBzMA as the core-forming block.

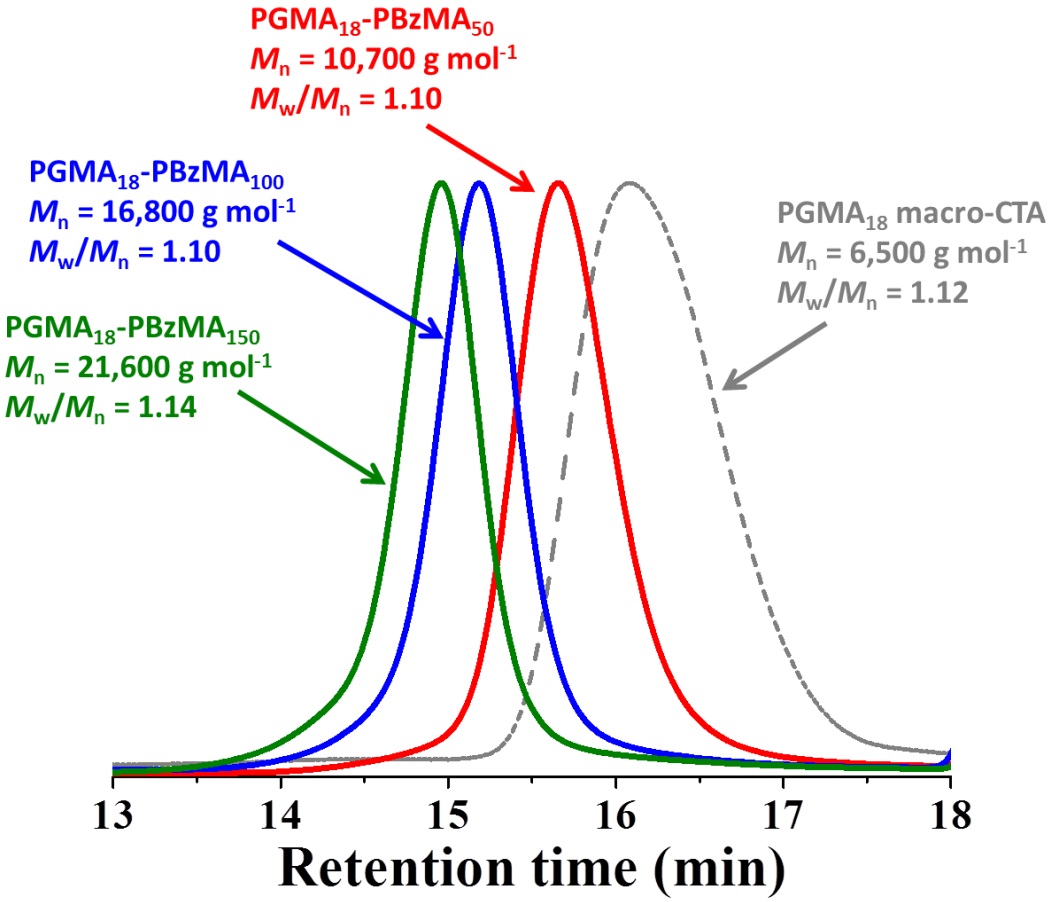

Figure 2.11 DMF GPC chromatograms of $PGMA_{18}$-$PBzMA_x$ diblock copolymers and the corresponding $PGMA_{18}$ macro-CTA.

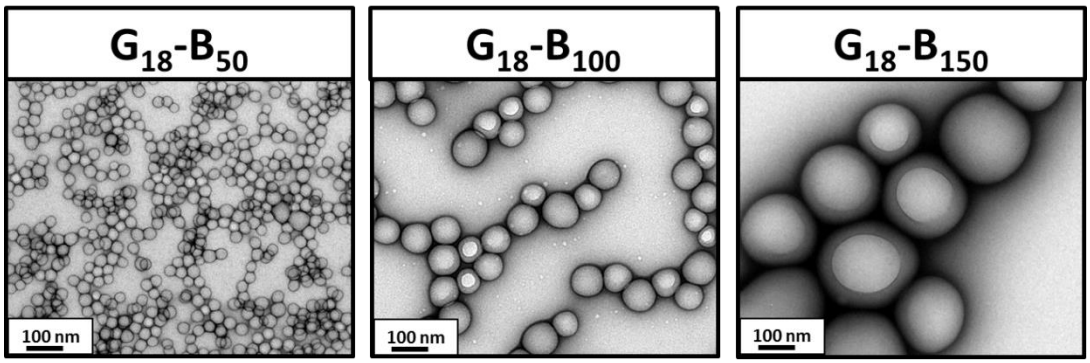

Figure 2.12 TEM images of $PGMA_{18}$-$PBzMA_x$ diblock copolymers prepared at 20% w/w.

2.3.6 $PGMA_{63}$-$PBzMA_x$ spherical nanoparticles as Pickering emulsifiers

Three $PGMA_{63}$-$PBzMA_x$ (x = 124, 216 or 309) syntheses were scaled up for use as potential Pickering emulsifiers. Initially, using only the $PGMA_{63}$-$PBzMA_{309}$ spherical micelles, four oils were evaluated for homogenisation with the aqueous diblock copolymer dispersion. Isopropyl myristate, sunflower oil, *n*-dodecane and *n*-hexane were selected as potential oils. 1.00% w/w dispersions of $PGMA_{63}$-$PBzMA_{309}$ spherical micelles were homogenised with an equal volume fraction of the four different oils for 2 minutes at 12,000 rpm (see Figure 2.13). All four oils resulted in stable oil-in-water emulsions as can be seen in Figure 2.14.

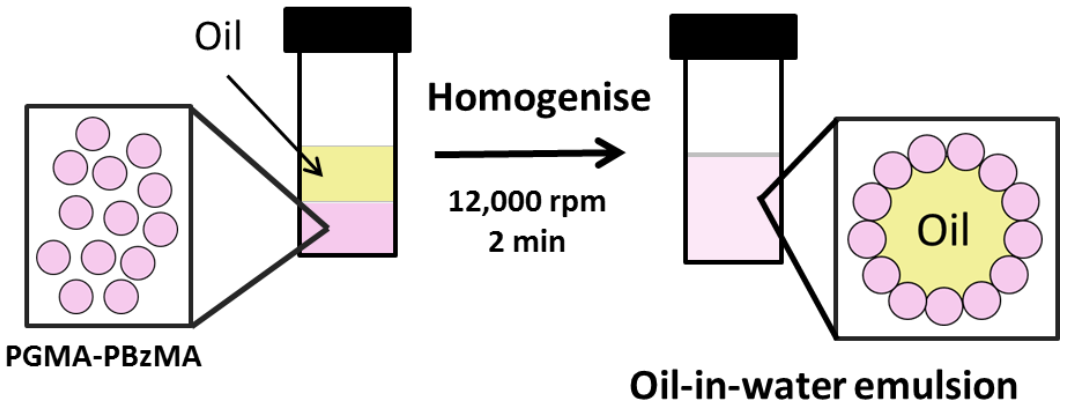

Figure 2.13 Schematic of the homogenisation of $PGMA_{63}$-$PBzMA_x$ spherical micelles in water with oil at 12,000 rpm and 20 °C for 2 minutes to produce stable oil-in-water Pickering emulsions.

Although all four oils resulted in the formation of stable oil-in-water emulsions, sunflower oil was focused on for the remainder of the study. The concentration of solid particles present during the homogenisation is known to affect the droplet size

in a Pickering emulsion.[29,30] This is due to an increased amount of particles being able to coat a larger surface area at the oil-water interface, resulting in the stability of smaller droplets. This relationship has been seen previously for the adsorption of spherical particles at the oil-water interface.[31-33]

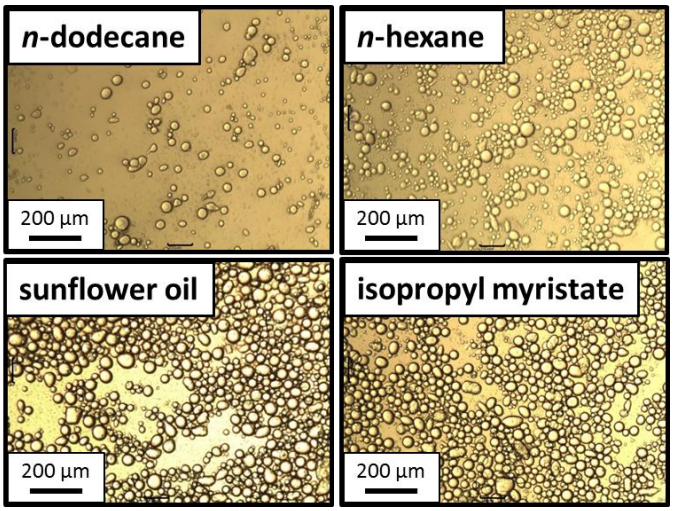

Figure 2.14 Optical microscopy images for oil-in-water Pickering emulsions prepared using $PGMA_{63}$-$PBzMA_{309}$ nanoparticles as the sole emulsifier at 1.00% w/w using either *n*-dodecane, *n*-hexane, sunflower oil or isopropyl myristate as the oil phase.

Aqueous dispersions of $PGMA_{63}$-$PBzMA_{309}$ spheres were prepared at concentrations between 0.0675% w/w and 2.50% w/w. Each aqueous copolymer dispersion was homogenised with an equal volume of sunflower oil at 12,000 rpm for 2 min. Optical microscopy was used to study the resulting emulsions (Figure 2.15). A reduction in droplet diameter with increasing copolymer concentration was observed. Images recorded at 0.250% w/w and 0.50% w/w suggest that some non-spherical droplets are observed. This has been attributed to a combination of mechanical agitation on spreading the emulsion onto the microscope slide and a drying artefact caused by the relatively hot light source. Non-spherical emulsion droplets were not expected, although there are some examples of non-spherical emulsions in the literature.[34,35]

Laser diffraction measurements were used to size the emulsion droplets. Figure 2.16 shows how the size of the emulsion droplets varies with the concentration of 81 nm $PGMA_{63}$-$PBzMA_{309}$ spheres. Similarly to the optical microscopy studies, a decrease in droplet size with increasing copolymer concentration can be seen. To see the effect of particle size on droplet diameter a series of Pickering emulsions were prepared with both $PGMA_{63}$-$PBzMA_{124}$ (41 nm) and $PGMA_{63}$-$PBzMA_{216}$ (58 nm).

The size of the droplets at varying concentrations were measured by laser diffraction and can also be seen in Figure 2.16, the results of which are comparable to the 81 nm $PGMA_{63}$-$PBzMA_{309}$ Pickering emulsions, with a reduction in droplet size with increased copolymer concentration. The smaller 41 nm spheres appear to stabilise slightly larger droplets. Binks has previously shown that the energy of detachment of a particle at the oil-water interface increases with particle size.[36] Therefore, smaller particles require significantly less energy to be desorbed from the oil/water interface, which results in larger, less stable Pickering emulsions being obtained at lower copolymer concentrations.

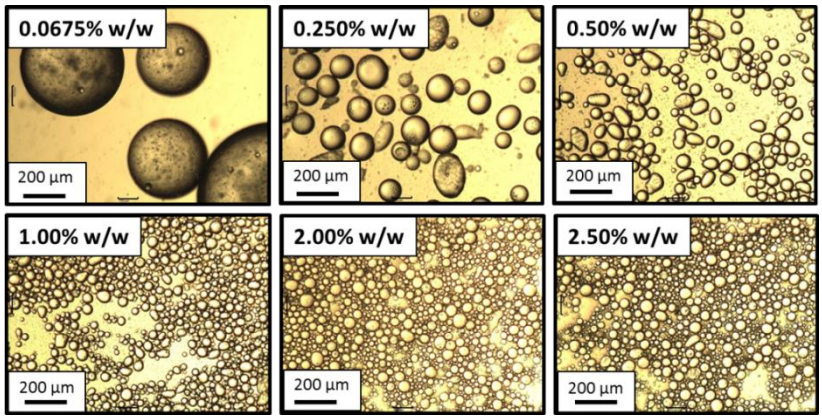

Figure 2.15 Optical microscopy images obtained for sunflower oil-in-water Pickering emulsions prepared using $PGMA_{63}$-$PBzMA_{309}$ nanoparticles at 0.0675, 0.250, 0.50, 1.00, 2.00 or 2.50% w/w.

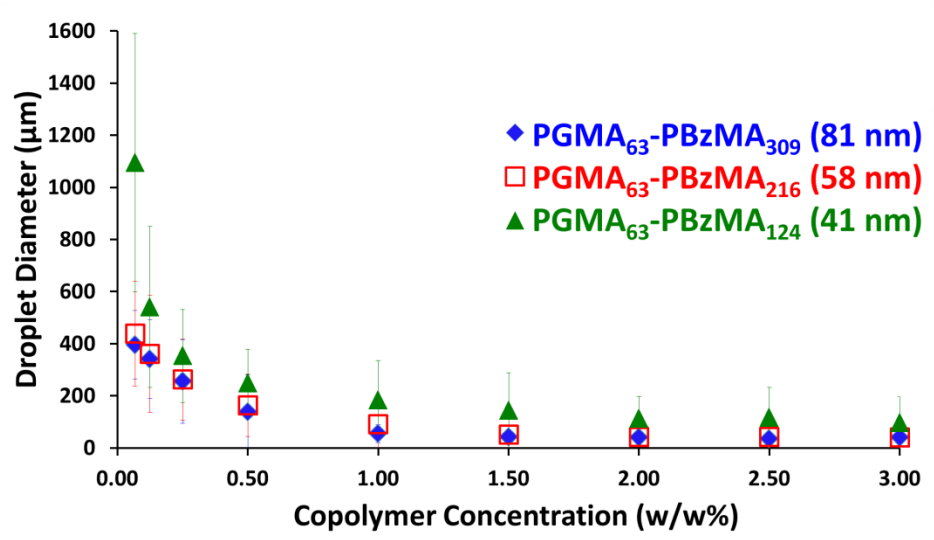

Figure 2.16 Concentration dependence of mean diameter of sunflower oil droplets (as determined by laser diffraction) prepared using $PGMA_{63}$-$PBzMA_x$ nanoparticles as the sole emulsifier, where x = 124, 216 or 309. Error bars represent the standard deviation of the volume-average droplet diameters, rather than the experimental uncertainty.

Creaming of the oil droplets occurred when they were left overnight at 20 °C. The underlying aqueous phase was weakly turbid rather than transparent, which suggested that not all of the nanoparticles are adsorbed onto the oil droplets. Similar observations have been reported for other latex-based Pickering emulsifiers.[37-41] In contrast, Thompson et al. reported that PGMA-stabilised polystyrene latexes (prepared by conducting the aqueous emulsion polymerisation of styrene in the presence of well-defined $PGMA_{50}$ macromonomers) adsorbed very efficiently onto various types of oil droplets.[31] Given that the surface of the block copolymer nanoparticles utilised in the present work is also PGMA-rich, this discrepancy is perhaps surprising. One explanation may be that the PGMA-PBzMA nanoparticles used in the present work are significantly smaller than the ~ 90 nm diameter latexes utilised by Thompson et al.[14] As discussed earlier, smaller particles are much less strongly adsorbed than larger particles when deployed as Pickering emulsifiers.[36] Moreover, given that the blocking efficiency of the $PGMA_{63}$ macro-CTA in the synthesis of the $PGMA_{63}$-$PBzMA_{309}$ nanoparticles is relatively high (> 90 %), then the surface concentration of the highly hydrophilic PGMA chains is likely to be significantly higher than that of the PGMA-stabilised polystyrene latexes previously reported by Thompson et al.[31] ^{1}H NMR analysis of the dried nanoparticles allowed the PGMA content of the particles to be calculated (13.5 - 21.2% w/w). Assuming that all the PGMA chains are located at the surface of the nanoparticles, this corresponds to an absorbed amount, Γ, of 2.0-2.5 mg m^{-2}. This is a little higher than the 1.8 mg m^{-2} reported by Thompson et al. for a $PGMA_{50}$ macromonomer,[14] which probably reflects the greater blocking efficiency of the $PGMA_{63}$ macro-CTA compared to the macromonomer grafting efficiency.

This higher surface concentration of PGMA chains is expected to lower the particle contact angle (or particle wettability), which in turn should lead to weaker interfacial adsorption. Furthermore, DLS characterisation of the non-adsorbed $PGMA_{63}$-$PBzMA_{309}$ nanoparticles remaining in the underlying aqueous phase indicated that significant flocculation had occurred during high-shear homogenisation. This problem has not been previously reported for latex-based Pickering emulsifiers.[37-41] Unfortunately, this particle aggregation also prevented the adsorption efficiency of the nanoparticles being determined by turbidimetry, as previously reported by Thompson et al. in the context of cross-linked vesicle-based Pickering emulsifiers.[41]

An alternative approach was employed whereby, after the emulsion droplets had creamed, a known amount of the underlying aqueous phase was dried at 70 °C for two days. The dry residues were then redissolved in a fixed known volume of DMF, which is a good solvent for both the PGMA and the PBzMA blocks. Molecular dissolution of the diblock copolymer in this solvent eliminated the flocculation problem and allowed the adsorption efficiency to be calculated via UV spectroscopy.

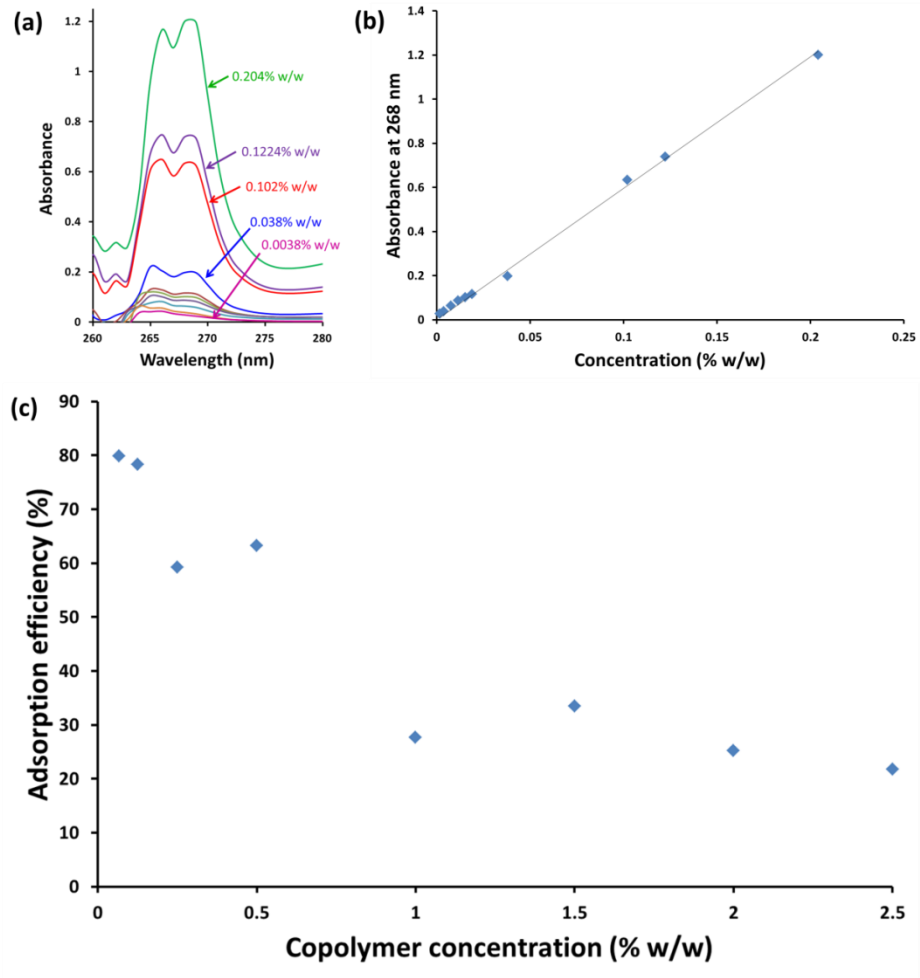

Figure 2.17 (a) UV absorption spectra recorded for various concentrations of $PGMA_{63}$-$PBzMA_{309}$ diblock copolymer dissolved in DMF. The chromophore at 268 nm is the aromatic benzyl group on the PBzMA block. (b) Beer-Lambert plot obtained for $PGMA_{63}$-$PBzMA_{309}$ diblock copolymer dissolved in DMF. (c) Adsorption efficiency vs. nanoparticle concentration for $PGMA_{63}$-$PBzMA_{309}$ nanoparticles when used as the sole Pickering emulsifier for sunflower oil, as determined using a supernatant depletion assay. This UV spectroscopy-based assay involves nanoparticle dissolution in DMF to avoid UV scattering problems at shorter wavelengths.

A linear calibration plot at 268 nm (corresponding to the aromatic benzyl chromophore in the PBzMA block) was constructed to determine the amount of non-adsorbed particles remaining in the aqueous phase (see Figure 2.17a and b). This

supernatant depletion assay was used to assess the nanoparticle adsorption efficiency for Pickering emulsions prepared using $PGMA_{63}$-$PBzMA_{309}$ particles. A maximum adsorption efficiency of 80 % was calculated when emulsification was performed using a copolymer concentration of 0.0675% w/w. A gradual reduction in adsorption efficiency was observed with increasing nanoparticle concentration, with only 22% efficiency being obtained for the highest nanoparticle concentration investigated in this work (2.50% w/w, see Figure 2.17c).

Fluorescence microscopy of a Pickering emulsion prepared using 0.50% w/w $PGMA_{63}$-$PBzMA_{124}$ tagged with rhodamine B isothiocyanate confirmed that these fluorescently-labelled nanoparticles were located at the oil droplet surface, as expected (see Figure 2.18).

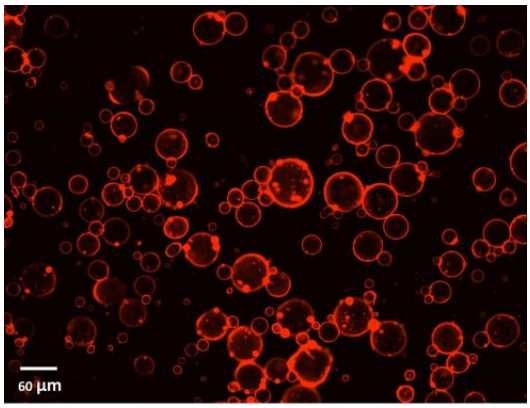

Figure 2.18 Fluorescence microscopy image of sunflower oil-in-water Pickering emulsion droplets prepared using 0.50% w/w $PGMA_{63}$-$PBzMA_{124}$ nanoparticles labelled with rhodamine B isothiocyanate.

2.3.7 pH-selective attachment of $PGMA_{63}$-$PBzMA_{124}$ to phenylboronic acid functionalised surfaces

This final section was conducted in collaboration with Dr Abdullah Alswieleh and Prof. Graham Leggett within the Department of Chemistry at the University of Sheffield.

As mentioned earlier, phenylboronic acid derivatives have been reported to form a 1:1 cyclic boronate ester complex with PGMA in aqueous alkaline solution.[4,5] More specifically, this chemistry was used to achieve pH-modulated binding of PGMA-stabilised polystyrene latexes onto cellulose films.[4] Latex adsorption was observed at pH 10.5, with substantial desorption occurring on washing with dilute acid (at pH 4).

The selective binding of $PGMA_{63}$-$PBzMA_{124}$ nanoparticles onto a micro-patterned planar silicon wafer functionalised with phenylboronic acid groups was examined (see Figure 2.19). The surface was prepared by exposing selected areas of 2-nitrophenylpropyloxycarbonyl (NPPOC) treated silicon wafers to UV irradiation at 325 nm using a patterned photomask, this method has been previously described by Leggett and co-workers.[42] Exposed primary amine surface groups were then reacted with excess 3-formylphenylboronic acid to form imine linkages via Schiff base chemistry.[43,44]

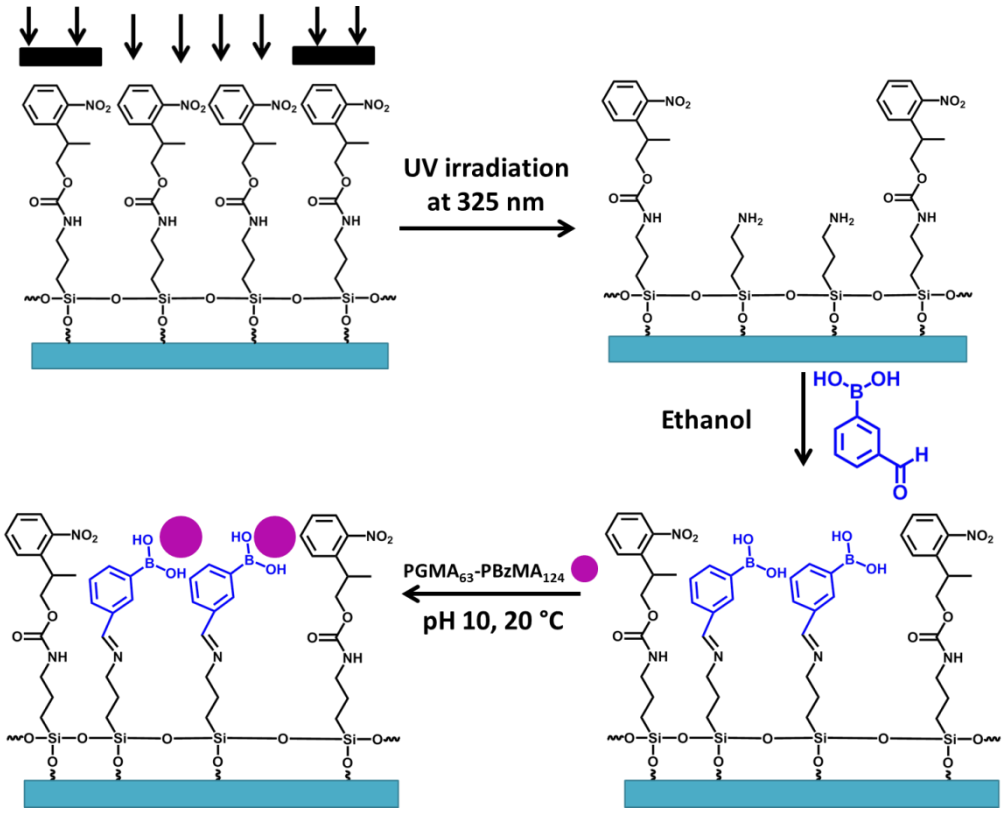

Figure 2.19 Schematic of a micropatterned NPPOC-functionalised planar silicon wafer prepared via UV irradiation (λ = 325 nm) using a photomask. Reacting the surface amine groups with excess 3-formylphenylboronic acid enables the pH-modulated selective binding of $PGMA_{63}$-$PBzMA_{124}$ nanoparticles to the planar silicon wafer.

These phenylboronic acid-functionalised planar silicon wafers were then immersed in a 0.01% w/w aqueous dispersion of $PGMA_{63}$-$PBzMA_{124}$ nanoparticles for 2 h at 20 ^{o}C. A pH of either 4 or 10 was selected and each wafer was imaged using atomic force microscopy (AFM). Figure 2.20a shows a friction force image recorded for the micro-patterned phenylboronic acid-functionalised planar silicon wafer prior to exposure to $PGMA_{63}$-$PBzMA_{124}$ nanoparticles. Adsorption of the $PGMA_{63}$-$PBzMA_{124}$ nanoparticles to the micro-patterned silicon wafer at pH 4 (below the pK_a

of approximately 8 for phenylboronic acid) showed minimal nanoparticle adsorption (Figure 2.20b). In contrast, selective nanoparticle adsorption occurs at pH 10 (above the pKa of phenylboronic acid), see Figure 2.20c. This occurs due to the complexation between the cis-diol groups on the PGMA stabiliser chains with the phenylboronic acid groups on the wafer surface. Extensive washing of this nanoparticle-coated surface with a mildly acidic solution (pH 4) only led to partial nanoparticle desorption, whereas Pelton and co-workers reported efficient desorption of PGMA-stabilised latexes from cellulose fibres using the same phenylboronic acid chemistry.[4]

Finally, to examine whether the surface binding was the result of the cis-diol from the PGMA stabiliser chains, a control experiment was conducted using poly(ethylene glycol)$_{113}$-PBzMA$_{200}$ (PEG$_{113}$-PBzMA$_{200}$) spherical nanoparticles of 122 nm diameter prepared via RAFT emulsion polymerisation. These PEG$_{113}$-PBzMA$_{200}$ nanoparticles have no cis-diol functionality and hence were unable to bind selectively to the micro-patterned surface at pH 10, see Figure 2.20d.

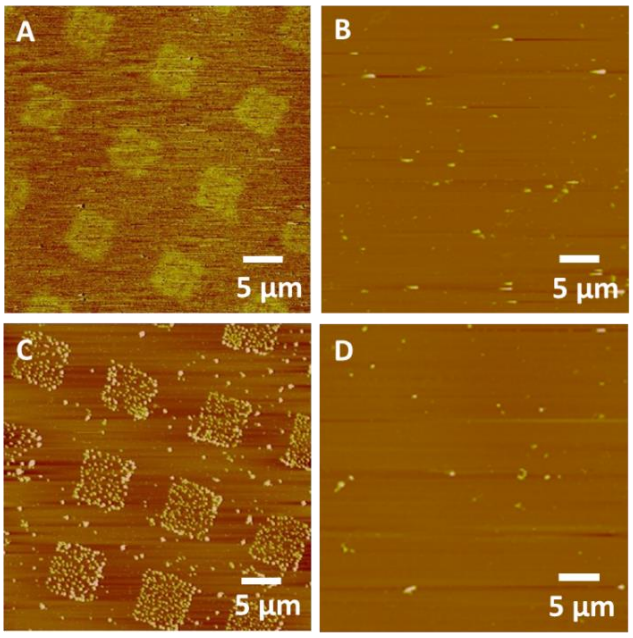

Figure 2.20 AFM images obtained for 46 nm PGMA$_{63}$-PBzMA$_{124}$ nanoparticles adsorbed from aqueous solution at 20 °C onto a micropatterned phenylboronic acid-functionalised planar silicon wafer. (a) Friction force image recorded for the patterned NPPOC silicon wafer prior to exposure to any nanoparticles, (b) height image recorded for PGMA$_{63}$-PBzMA$_{124}$ nanoparticles at pH 4, (c) height image recorded for PGMA$_{63}$-PBzMA$_{124}$ nanoparticles at pH 10, showing selective nanoparticle adsorption, (d) height image recorded for the attempted selective adsorption of 122 nm diameter PEG$_{113}$-PBzMA$_{200}$ nanoparticles at pH 10 onto the same micropatterned planar silicon wafer.

2.4 Conclusions

A series of $PGMA_{63}$-$PBzMA_x$ spherical diblock copolymer nanoparticles have been synthesised via RAFT emulsion polymerisation. The DP of the core-forming PBzMA block has been systematically varied from 62 to 1235. High conversions (≥ 98 %) were achieved within 6 h. DMF GPC analysis indicated high blocking efficiencies and low dispersities in all cases. A monotonic increase in particle size with PBzMA DP is observed by both DLS and TEM. Despite exploring a wide range of formulations and conditions, only kinetically-trapped spheres were obtained. Well-defined $PGMA_{63}$-$PBzMA_{309}$ nanoparticles have been prepared at up to 50% w/w solids with minimal difference in mean particle diameter, molecular weight and blocking efficiency. These nanoparticles are stable to both freeze-thaw cycles and the presence of added salt (up to 0.25 M $MgSO_4$) which suggests steric stabilisation. $PGMA_{63}$-$PBzMA_x$ diblock copolymers were used to prepare stable Pickering emulsions with sunflower oil, isopropyl myristate, *n*-dodecane or *n*-hexane and utilising three different particle sizes. A reduction in droplet diameter with increasing nanoparticle concentration (0.0675% - 2.50% w/w) was observed by both optical microscopy and laser diffraction. The cis-diol functionality on the PGMA stabiliser chain was used to demonstrate pH-selective binding of $PGMA_{63}$-$PBzMA_{124}$ spherical nanoparticles onto a phenylboronic acid-functionalised surface. Strong selective adsorption of the nanoparticles occurred at pH 10, as judged by AFM, whereas rather little binding was observed at pH 4. Replacement of the $PGMA_{63}$ stabiliser with a PEG_{113} stabiliser resulted in essentially no adsorption to the phenylboronic acid-functionalised surface, confirming that pH-modulated binding occurred via the cis-diol groups on the PGMA stabiliser.

2.5 References

(1) Save, M.; Weaver, J. V. M.; Armes, S. P.; McKenna, P. *Macromolecules* **2002**, *35*, 1152.
(2) Iyer, R.; McKenna, P.; Smallridge, M.; Matthews, M.; Natesh, A.; Baker, J. *Monomers and macromers for forming hydrogels*, WO2010102747: 2010.
(3) Ratcliffe, L. P. D.; Ryan, A. J.; Armes, S. P. *Macromolecules* **2013**, *46*, 769.
(4) Zhang, D.; Thompson, K. L.; Pelton, R.; Armes, S. P. *Langmuir* **2010**, *26*, 17237.
(5) Pelton, R.; Zhang, D.; Thompson, K. L.; Armes, S. P. *Langmuir* **2011**, *27*, 2118.
(6) Pelton, R.; Cui, Y.; Zhang, D.; Chen, Y.; Thompson, K. L.; Armes, S. P.; Brook, M. A. *Langmuir* **2013**, *29*, 594.
(7) Ochiai, H.; Fujino, Y.; Tadokoro, Y.; Murakami, I. *Polymer* **1980**, *21*, 485.

(8) Petasis, N. A. *Australian Journal of Chemistry* **2007**, *60*, 795.
(9) Cambre, J. N.; Sumerlin, B. S. *Polymer* **2011**, *52*, 4631.
(10) Casassa, E. Z.; Sarquis, A. M.; Van Dyke, C. H. *Journal of Chemical Education* **1986**, *63*, 57.
(11) Vainio, P.; Virtanen, J. A.; Kinnunen, P. K. *Biochimica et Biophysica Acta (BBA)-Lipids and Lipid Metabolism* **1982**, *711*, 386.
(12) Ellis, G. A.; Palte, M. J.; Raines, R. T. *Journal of the American Chemical Society* **2012**, *134*, 3631.
(13) Kim, H.; Kang, Y. J.; Kang, S.; Kim, K. T. *Journal of the American Chemical Society* **2012**, *134*, 4030.
(14) Thompson, K. L.; Armes, S. P.; York, D. W.; Burdis, J. A. *Macromolecules* **2010**, *43*, 2169.
(15) Yan, J.; Springsteen, G.; Deeter, S.; Wang, B. *Tetrahedron* **2004**, *60*, 11205.
(16) Springsteen, G.; Wang, B. *Tetrahedron* **2002**, *58*, 5291.
(17) Cunningham, V. J.; Alswieleh, A. M.; Thompson, K. L.; Williams, M.; Leggett, G. J.; Armes, S. P.; Musa, O. M. *Macromolecules* **2014**, *47*, 5613.
(18) Warren, N. J.; Mykhaylyk, O. O.; Mahmood, D.; Ryan, A. J.; Armes, S. P. *Journal of the American Chemical Society* **2014**, *136*, 1023.
(19) Blanazs, A.; Madsen, J.; Battaglia, G.; Ryan, A. J.; Armes, S. P. *Journal of the American Chemical Society* **2011**, *133*, 16581.
(20) Blanazs, A.; Ryan, A. J.; Armes, S. P. *Macromolecules* **2012**, *45*, 5099.
(21) Blanazs, A.; Verber, R.; Mykhaylyk, O. O.; Ryan, A. J.; Heath, J. Z.; Douglas, C. W. I.; Armes, S. P. *Journal of the American Chemical Society* **2012**, *134*, 9741.
(22) Li, Y.; Armes, S. P. *Angewandte Chemie International Edition* **2010**, *49*, 4042.
(23) Semsarilar, M.; Jones, E. R.; Blanazs, A.; Armes, S. P. *Advanced Materials* **2012**, *24*, 3378.
(24) Jones, E. R.; Semsarilar, M.; Blanazs, A.; Armes, S. P. *Macromolecules* **2012**, *45*, 5091.
(25) Fielding, L. A.; Derry, M. J.; Ladmiral, V.; Rosselgong, J.; Rodrigues, A. M.; Ratcliffe, L. P.; Sugihara, S.; Armes, S. P. *Chemical Science* **2013**, *4*, 2081.
(26) Zhang, W.; D'Agosto, F.; Boyron, O.; Rieger, J.; Charleux, B. *Macromolecules* **2012**, *45*, 4075.
(27) Zhang, X.; Boissé, S.; Zhang, W.; Beaunier, P.; D'Agosto, F.; Rieger, J.; Charleux, B. *Macromolecules* **2011**, *44*, 4149.
(28) Derry, M. J.; Fielding, L. A.; Armes, S. P. *Polymer Chemistry* **2015**, *6*, 3054.
(29) Tambe, D. E.; Sharma, M. M. *Advances in Colloid and Interface Science* **1994**, *52*, 1.
(30) Aveyard, R.; Binks, B. P.; Clint, J. H. *Advances in Colloid and Interface Science* **2003**, *100*, 503.
(31) Thompson, K. L.; Armes, S. P.; Howse, J. R.; Ebbens, S.; Ahmad, I.; Zaidi, J. H.; York, D. W.; Burdis, J. A. *Macromolecules* **2010**, *43*, 10466.
(32) Thompson, K.; Mable, C.; Cockram, A.; Warren, N.; Cunningham, V.; Jones, E.; Verber, R.; Armes, S. *Soft Matter* **2014**, *10*, 8615.
(33) Binks, B. P.; Whitby, C. P. *Langmuir* **2004**, *20*, 1130.
(34) Bon, S. A. F.; Mookhoek, S. D.; Colver, P. J.; Fischer, H. R.; van der Zwaag, S. *European Polymer Journal* **2007**, *43*, 4839.
(35) Schmitt, M.; Limage, S.; Grigoriev, D. O.; Krägel, J.; Dutschk, V.; Vincent-Bonnieu, S.; Miller, R.; Antoni, M. *Langmuir* **2014**, *30*, 4599.
(36) Binks, B. P. *Current Opinion in Colloid & Interface Science* **2002**, *7*, 21.

(37) Walsh, A.; Thompson, K. L.; Armes, S. P.; York, D. W. *Langmuir* **2010**, *26*, 18039.
(38) Williams, M.; Armes, S. P.; York, D. W. *Langmuir* **2011**, *28*, 1142.
(39) Morse, A. J.; Armes, S. P.; Thompson, K. L.; Dupin, D.; Fielding, L. A.; Mills, P.; Swart, R. *Langmuir* **2013**, *29*, 5466.
(40) Morse, A. J.; Dupin, D.; Thompson, K. L.; Armes, S. P.; Ouzineb, K.; Mills, P.; Swart, R. *Langmuir* **2012**, *28*, 11742.
(41) Thompson, K. L.; Chambon, P.; Verber, R.; Armes, S. P. *Journal of the American Chemical Society* **2012**, *134*, 12450.
(42) Ahmad, S. A.; Wong, L. S.; Hobbs, J.; Leggett, G.; Micklefield, J. *Journal of the American Chemical Society* **2009**, *131*, 1513.
(43) DiFlavio, J.-L.; Pelton, R.; Leduc, M.; Champ, S.; Essig, M.; Frechen, T. *Cellulose* **2007**, *14*, 257.
(44) Issa, R. M.; Khedr, A. M.; Rizk, H. *Journal of the Chinese Chemical Society* **2008**, *55*, 875.

Chapter 3

Poly(stearyl methacrylate)-poly(*N*-2-(methacryloyloxy)ethyl pyrrolidone) diblock copolymer nano-objects via RAFT dispersion polymerisation in *n*-dodecane

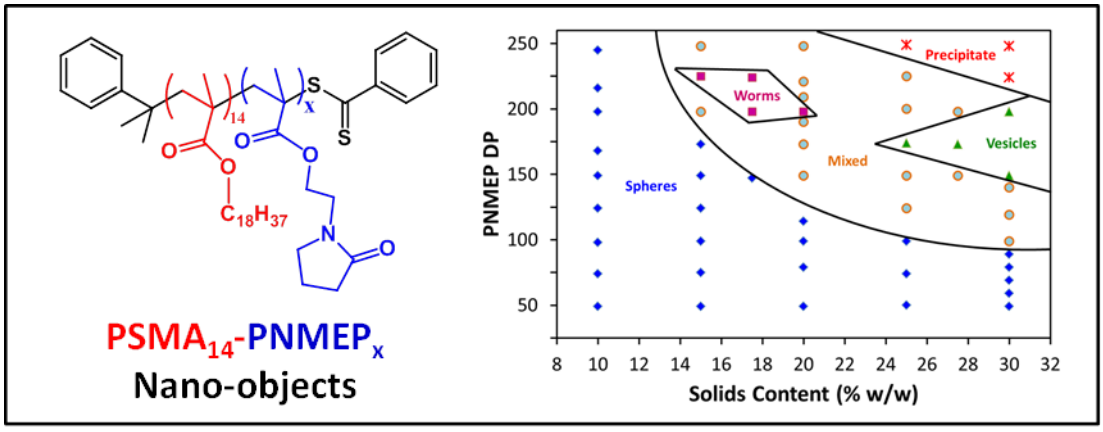

Reproduced in part with permission from:

[Cunningham, V. J.; Armes, S. P.; Musa, O. M. *Polymer Chemistry*, **2016**, *7*, 1882] Copyright [2016] Royal Society of Chemistry.

3.1 Introduction

The first example of RAFT dispersion polymerisation in *n*-alkanes was less than a decade ago by Houillot et al.[1] and although still relatively uncommon, there is increasing interest in such PISA formulations. Three stabilisers previously used for RAFT dispersion polymerisations in *n*-alkanes were discussed in Chapter 1: poly(lauryl methacrylate) (PLMA),[2-4] poly(2-ethylhexyl acrylate) (PEHA)[1,5,6] and polydimethylsiloxane (PDMS).[7] In addition, a poly(stearyl methacrylate) (PSMA) macro-CTA has been utilised for several RAFT dispersion polymerisation formulations.[8-11]

For example, Lowe and co-workers reported the synthesis of poly(stearyl methacrylate)-poly(3-phenylpropyl methacrylate) (PSMA-PPPMA) diblock copolymers in *n*-tetradecane[8] and *n*-octane.[9] Up to 92% conversion was achieved for syntheses performed in the former solvent, whereas lower conversions (73%) were observed in *n*-octane. GPC analysis indicated higher molecular weights for PSMA-PPPMA diblock copolymers when targeting higher PPMA DPs and low dispersities (below 1.23) were observed. These PSMA-PPPMA diblock copolymers self-assembled to form spheres, worms or vesicles depending on the PPPMA DP. This PSMA-PPPMA system was later extended by Pei et al., who prepared a poly(stearyl methacrylate-*stat*-pentafluorophenyl methacrylate) (P(SMA-*stat*-PFPMA)) macro-CTA.[10] This was chain-extended with PPPMA in both *n*-octane and *n*-tetradecane and post-polymerisation modification of the resulting spherical nanoparticles was demonstrated via nucleophilic acyl substitution.

Derry et al. synthesised three PSMA macro-CTAs via RAFT solution polymerisation in toluene at 70 °C and 40% w/w solids.[11] Figure 3.1 shows the kinetics of polymerisation for the synthesis of a $PSMA_{30}$ macro-CTA using cumyl dithiobenzoate (CDB) as the RAFT CTA. A short induction period was observed followed by an increase in conversion with time up to approximately 70% conversion after 10 h. SMA polymerisations were terminated at conversions between 72 – 76% to ensure high blocking efficiencies for the subsequent chain extension of these macro-CTAs.

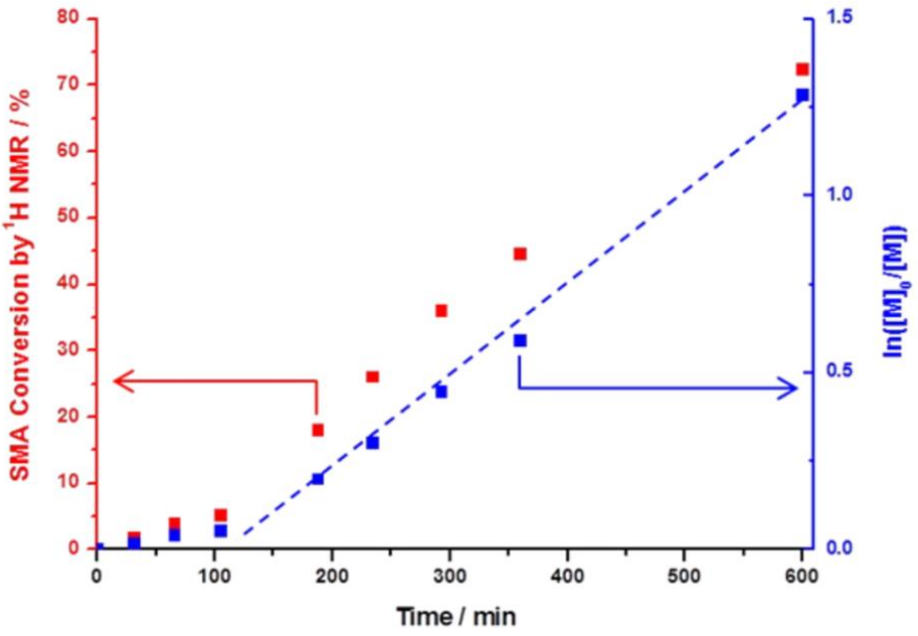

Figure 3.1 Conversion versus time curve and corresponding semi-logarithmic plot for the RAFT solution polymerisation of SMA in toluene at 70 °C using AIBN initiator and CDB CTA targeting a DP of 30.[11]

All three macro-CTAs were chain-extended with benzyl methacrylate. High conversions (≥ 97%) were achieved. The two longest PSMA macro-CTAs (DP = 18 or 31) only produced spherical micelles. In contrast, utilising the shorter $PSMA_{13}$ macro-CTA enabled spheres, worms or vesicles to be prepared even at relatively low (5% w/w) solids. Synthesis of a range of diblock copolymers at various copolymer concentrations targeting PBzMA DPs of 20-150 enabled Derry et al. to construct a detailed $PSMA_{13}$-$PBzMA_x$ phase diagram (Figure 3.2).[11] This PSMA-PBzMA system was also studied by in situ small angle X-ray scattering to monitor the change in copolymer morphology during the BzMA polymerisation.[11]

In this Chapter, a range of new poly(stearyl methacrylate)-poly(*N*-2-(methacryloyloxy)ethyl pyrrolidone) (PSMA-PNMEP) diblock copolymer nano-objects are synthesised via RAFT dispersion polymerisation of NMEP in *n*-dodecane. The diblock copolymer chains are characterised by ^{1}H NMR and GPC, while DLS and TEM have been used to assess the particle size and copolymer morphology. A phase diagram is constructed to enable pure spherical micelles, worm-like micelles or vesicles to be reproducibly targeted. In addition, $PSMA_{14}$-$PNMEP_{49}$ spherical nanoparticles are examined as potential Pickering emulsifiers. The work presented herein has already formed the basis of a publication in Polymer Chemistry.[12]

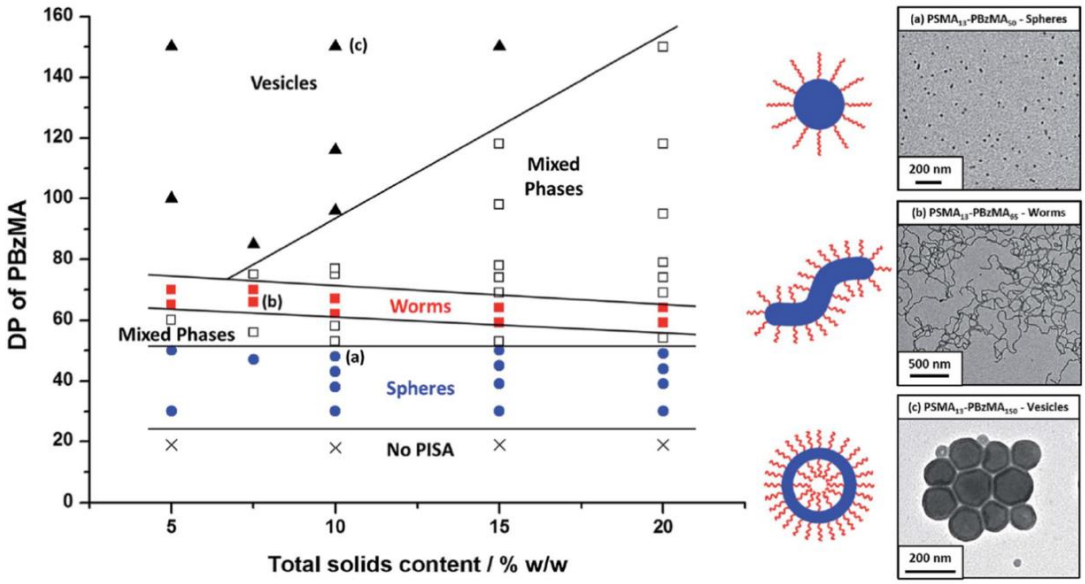

Figure 3.2 Phase diagram constructed for $PSMA_{13}$-$PBzMA_x$ diblock copolymer nanoparticles prepared by RAFT dispersion polymerisation of BzMA in mineral oil using a $PSMA_{13}$ macro-CTA and T21s initiator at 90 °C ([$PSMA_{13}$]/[T21s] molar ratio = 5.0). Diblock copolymer morphologies were obtained by TEM and images a, b and c are representative of the pure sphere, worm and vesicle phases.[11]

3.2 Experimental Details

3.2.1 Materials

Stearyl methacrylate (SMA), cumyl dithiobenzoate (CDB) and *n*-dodecane were purchased from Sigma-Aldrich (UK). *N*-2-(Methacryloyloxy)ethyl pyrrolidone (NMEP, 96% purity) was donated by Ashland Specialty Ingredients (USA). Azoisobutyronitrile (AIBN) was purchased from Molekula (Dorset, UK). *tert*-Butyl peroxy-2-ethylhexanoate (T21s) was purchased from AkzoNobel (The Netherlands). CD_2Cl_2 was purchased from Goss Scientific Ltd., (UK) and $CDCl_3$ was purchased from VWR chemicals (UK). All other solvents were purchased from Fisher Scientific (Loughborough, UK). All chemicals and solvents were used as received.

3.2.2 Preparation of $PSMA_{14}$ macro-CTA

SMA (33.4765 g, 0.099 mol), CDB RAFT agent (5.1690 g, 19 mmol; target degree of polymerisation, DP = 5) and AIBN (0.6233 g, 3.8 mmol; CTA/initiator molar ratio = 5.0) were weighed into a 250 ml round-bottomed flask. Toluene (58 ml) was deoxygenated separately with nitrogen for 30 min prior to addition to the other reagents. The reaction solution was stirred and degassed in an ice bath for a further 30 min, before placing in an oil bath at 70 °C. The polymerisation was allowed to

proceed for 10 h, resulting in a final monomer conversion of 80 % as judged by ^{1}H NMR. The crude homopolymer was purified by precipitating into a ten-fold excess of ethanol. This purification step was repeated twice. The purified polymer was dissolved in *n*-hexane and dried to give a pure PSMA macro-CTA (21.6 g, < 1 % monomer remaining). The mean DP was calculated to be 14, as judged by ^{1}H NMR spectroscopy by comparing the integrated aromatic CDB proton signal at 7.0 - 8.0 ppm with that assigned to the two oxymethylene PSMA protons at 3.6 - 4.2 ppm. GPC analysis using a 3:1 v/v chloroform/methanol mixed eluent indicated an M_n of 7,500 g mol^{-1} and an M_w/M_n of 1.12 (vs. a series of near-monodisperse PMMA calibration standards).

3.2.3 Synthesis of $PSMA_{14}$-$PNMEP_x$ via RAFT dispersion polymerisation of NMEP

A typical protocol for the synthesis of $PSMA_{14}$-$PNMEP_{98}$ diblock copolymer nanoparticles was as follows: $PSMA_{14}$ macro-CTA (0.0706 g), NMEP (0.2787 g, 1.413 mmol; target DP = 100), T21s (0.755 mg, 3.49 μmol; dissolved at 10% v/v in *n*-dodecane; CTA/T21s molar ratio = 4.0) were dissolved in *n*-dodecane (4.1 ml, 10% w/w) in a 14 ml vial. The reaction mixture was sealed and purged with nitrogen for 30 min, prior to immersion in an oil bath set at 90 °C for 2 h. The resulting copolymer was analysed by GPC using a 3:1 chloroform/methanol mixed eluent (M_n = 49,600 g mol^{-1}, M_w/M_n = 1.19 vs. PMMA standards). ^{1}H NMR spectroscopy analysis of the final reaction solution diluted approximately ten-fold in $CDCl_3$ indicated 98% NMEP conversion by comparing the integrated vinyl proton signals at 5.5 – 6.5 ppm to that of the methylene carbonyl proton signal at 2.5 ppm. DLS studies conducted on a 0.20% w/w copolymer dispersion indicated an intensity-average particle diameter of 36 nm (DLS polydispersity, PDI = 0.01). Other diblock copolymer compositions were targeted by adjusting the NMEP/$PSMA_{14}$ macro-CTA molar ratio and/or by varying the volume of solvent in the PISA formulation.

3.2.4 Preparation of Pickering emulsions using $PSMA_{14}$-$PNMEP_{49}$ spherical nanoparticles

Water (2.0 ml) was homogenised with 2.0 ml of a 0.0675 – 2.50% w/w $PSMA_{14}$-$PNMEP_{49}$ diblock copolymer dispersion in *n*-dodecane for 2 min at 20 °C using an

IKA Ultra-Turrax T-18 homogeniser equipped with a 10 mm dispersing tool. The shear rate was systematically varied between 3,500 rpm and 24,000 rpm.

3.2.5 Copolymer characterisation

^{1}H NMR Spectroscopy

All ^{1}H NMR spectra were recorded at 20 °C in either CD_2Cl_2 or $CDCl_3$ using a 400 MHz Bruker Avance-400 spectrometer with 64 scans being averaged per spectrum.

Gel Permeation Chromatography (GPC)

The molecular weights and dispersities of the $PSMA_{14}$ macro-CTA and $PSMA_{14}$-$PNMEP_x$ diblock copolymers were obtained using a GPC set-up comprising of a Hewlett Packard HP1090 liquid chromatograph pump unit and two Polymer Laboratories PL gel 5 μm 'Mixed C' columns connected in series with a guard column at 40 °C connected to a Gilson Model 131 refractive index detector. The eluent was a 3:1 v/v chloroform/methanol mixture containing 2 mM LiBr at a flow rate of 1.0 ml min^{-1}. A series of near-monodisperse poly(methyl methacrylate) (PMMA) standards were used for calibration. Data analysis was carried out using Cirrus GPC software supplied by Agilent.

Dynamic Light Scattering (DLS)

The intensity-average hydrodynamic diameter of each batch of nanoparticles was determined at 25 °C using a Malvern Zetasizer NanoZS instrument at a scattering angle of 173°. Dilute dispersions (0.20% w/w) in *n*-heptane were analysed using quartz cuvettes and data were averaged over three consecutive runs.

Transmission Electron Microscopy (TEM)

Copper/palladium TEM grids (Agar Scientific, UK) were coated in-house to yield a thin film of amorphous carbon. Dilute dispersions (0.20% w/w in *n*-heptane, 10.0 μL) were placed on the carbon-coated grids and left for 30 min to allow solvent evaporation. The grids were exposed to ruthenium (VIII) oxide vapour for 7 min at 20 °C prior to analysis. Imaging was performed using a Philips CM100 instrument operating at 100 kV and equipped with a Gatan 1 k CCD camera.

The ruthenium (VIII) oxide was prepared as follows: ruthenium (IV) oxide (0.30 g) was added to water (50 g) to form a black slurry; addition of sodium periodate (2.0 g) with stirring produced a yellow solution of ruthenium (VIII) oxide within 1 min.[13]

Optical Microscopy

See Chapter 2, Section 2.2.10 for details.

Laser Diffraction

See Chapter 2, Section 2.2.10 for details.

3.3 Results and Discussion

3.3.1 Synthesis of $PSMA_{14}$ macromolecular chain transfer agent via RAFT solution polymerisation

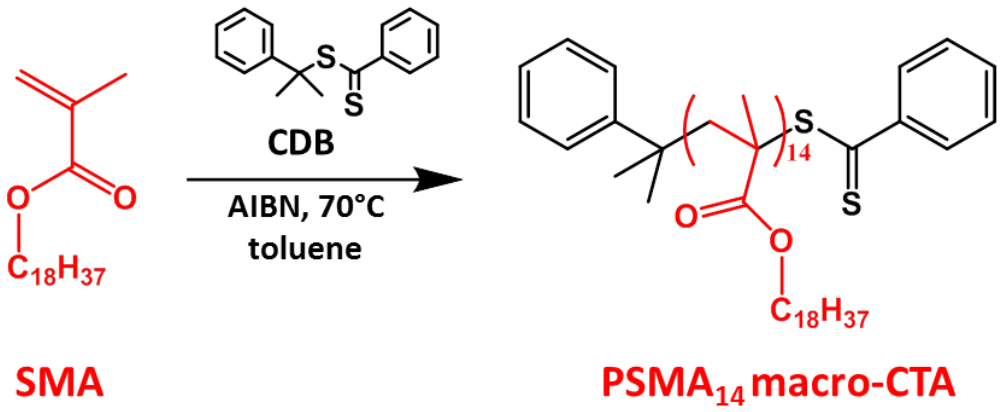

Scheme 3.1 Synthesis of a poly(stearyl methacrylate)$_{14}$ macro-CTA by RAFT solution polymerisation

A PSMA macro-CTA was synthesised via RAFT solution polymerisation at 70 °C using CDB as a chain transfer agent (Scheme 3.1). Following the kinetics by Derry et al.[11] the reaction was quenched after 10 h. ^{1}H NMR spectroscopy confirmed a conversion of 80%. After purification by repeated precipitation into ethanol a DP of 14 was calculated. GPC analysis of the purified PSMA macro-CTA using a 3:1 v/v chloroform/methanol mixed eluent indicated a M_n of 7,500 g mol^{-1} with a dispersity of 1.12, which suggested good control for this pseudo-living polymerisation. This $PSMA_{14}$ macro-CTA was chain extended with an additional 100 units of SMA in a self-blocking experiment in *n*-dodecane at 90 °C. A conversion of 87% resulted in a $PSMA_{14}$-$PSMA_{87}$ diblock copolymer. GPC analysis of the self-blocking experiment showed good chain extension relative to the $PSMA_{14}$ macro-CTA with a low final dispersity of 1.13, see Figure 3.3. This indicates high chain-end fidelity for the $PSMA_{14}$ macro-CTA.

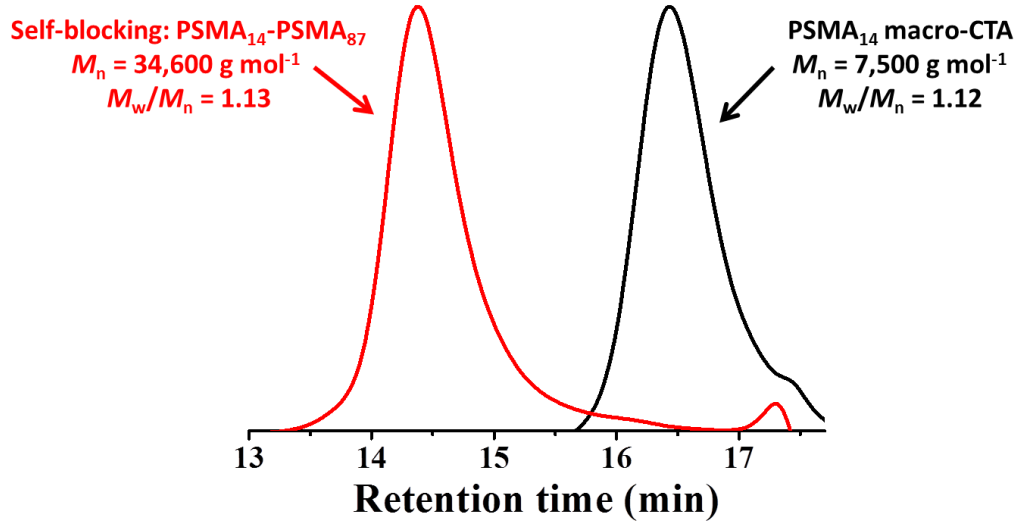

Figure 3.3 Chloroform/methanol (3:1) GPC curves obtained for the initial $PSMA_{14}$ macro-CTA and the corresponding $PSMA_{14}$-$PSMA_{87}$ after a 'self-blocking' chain extension experiment at 90 °C.

3.3.2 Kinetics of the RAFT dispersion polymerisation of NMEP targeting $PSMA_{14}$-$PNMEP_{100}$ at 20% w/w

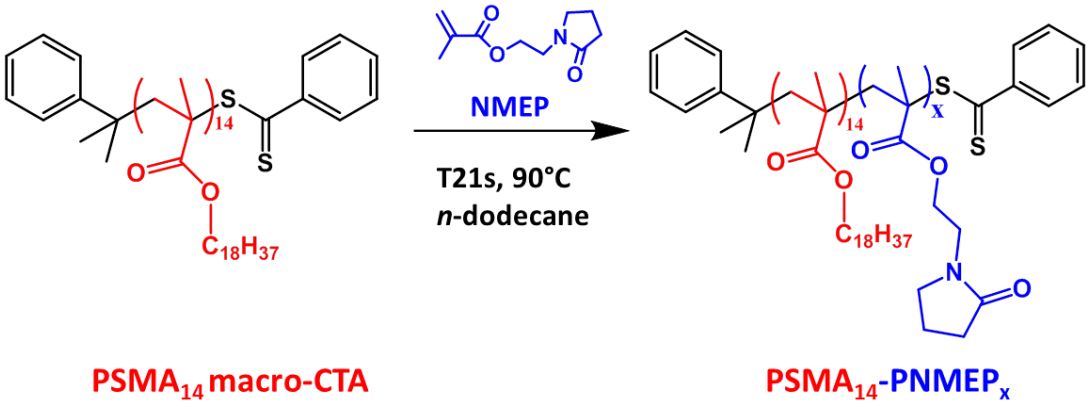

Scheme 3.2 Synthesis of $PSMA_{14}$-$PNMEP_x$ diblock copolymers via RAFT dispersion polymerisation of NMEP at 90 °C in *n*-dodecane.

Targeting a block composition of $PSMA_{14}$-$PNMEP_{100}$, a kinetic study for the chain extension of the $PSMA_{14}$ macro-CTA via RAFT dispersion polymerisation of NMEP in *n*-dodecane was conducted (Figure 3.4). A solids content of 20% w/w was selected using a macro-CTA/initiator molar ratio of 4.0 at 90 °C. The reaction solution was sampled every 5 minutes for 50 minutes and ^{1}H NMR spectroscopy was used to monitor the polymerisation. Figure 3.4 shows a plot of conversion against time. The reaction proceeds very rapidly, with conversions above 90% within 20 minutes and above 99% conversion is achieved within 30 minutes. This kinetics is significantly

faster than other RAFT dispersion polymerisations conducted in *n*-alkanes.[2-4,9,11] For example, Fielding et al. reported that the polymerisation of benzyl methacrylate at 90 °C in *n*-heptane using a PLMA macro-CTA at 15% solids took 5 h to reach 95% conversion.[2] Moreover, these PLMA-PBzMA diblock copolymers were prepared using a lower macro-CTA/initiator molar ratio of 2.0 compared to the PSMA-PNMEP diblock copolymer synthesis reported in the present study. To make a direct comparison the kinetics of a $PSMA_{14}$-$PBzMA_{100}$ diblock copolymer was monitored under exactly the same conditions as the $PSMA_{14}$-$PNMEP_{100}$ (90 °C, 20% w/w solids, macro-CTA/initiator molar ratio = 4.0). The conversion versus time data for the $PSMA_{14}$-$PBzMA_{100}$ kinetics is also shown in Figure 3.4. This shows a very slow reaction with only 19% BzMA conversion within 30 minutes in comparison to 99% for the corresponding $PSMA_{14}$-$PNMEP_{100}$ diblock copolymer. After 6 h the $PSMA_{14}$-$PBzMA_{100}$ diblock does eventually reach 95% conversion but this indicates a much slower rate of polymerisation.

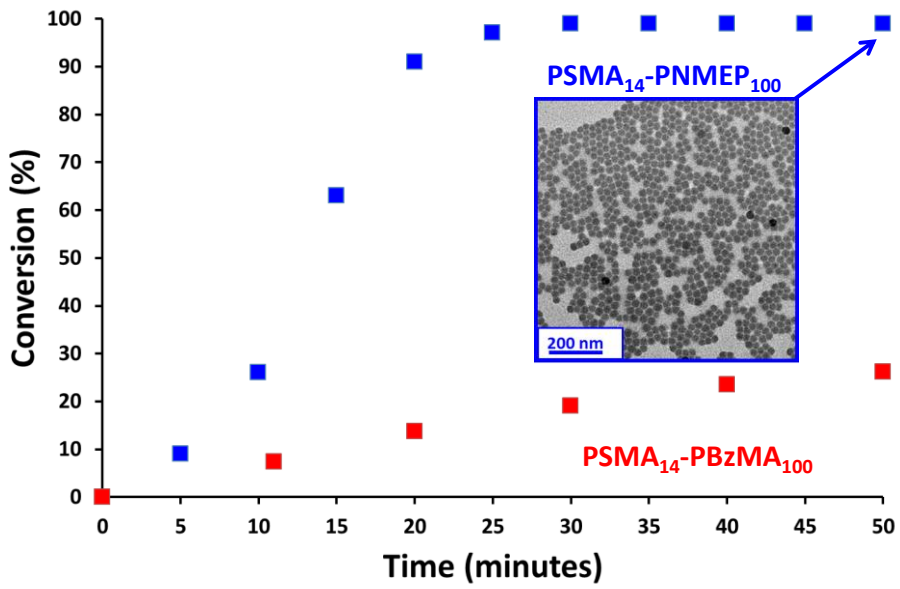

Figure 3.4 Kinetics of the polymerisation of NMEP and BzMA when targeting $PSMA_{14}$-$PNMEP_{100}$ (blue) and $PSMA_{14}$-$PBzMA_{100}$ (red) at 90 °C and 20% w/w solids. Inset: TEM image obtained after 50 min for $PSMA_{14}$-$PNMEP_{100}$ showing spherical nanoparticles with a mean diameter of 27 nm.

Figure 3.5 shows the semi-logarithmic plots for the two diblocks. A short induction period is observed for the $PSMA_{14}$-$PNMEP_{100}$ formulation, but then the rate of this NMEP polymerisation proceeds with an apparent pseudo-first order rate constant that is 38 times greater than that of the BzMA polymerisation when targeting $PSMA_{14}$-

$PBzMA_{100}$. This rate enhancement is attributed to the highly polar NMEP monomer. Similar polarity effects have been observed in literature for monomers and solvents.[14-16]

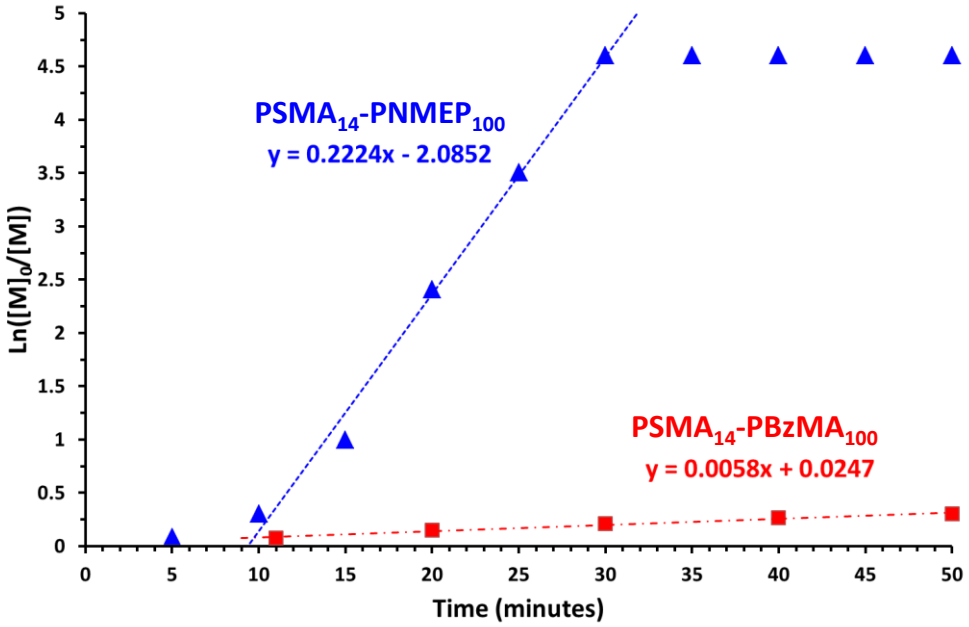

Figure 3.5 A plot of $Ln([M]_0/[M])$ against time for the kinetics of RAFT dispersion polymerisation of either NMEP or BzMA at 90 °C when targeting either $PSMA_{14}$-$PNMEP_{100}$ (blue) or $PSMA_{14}$-$PBzMA_{100}$ (red), respectively.

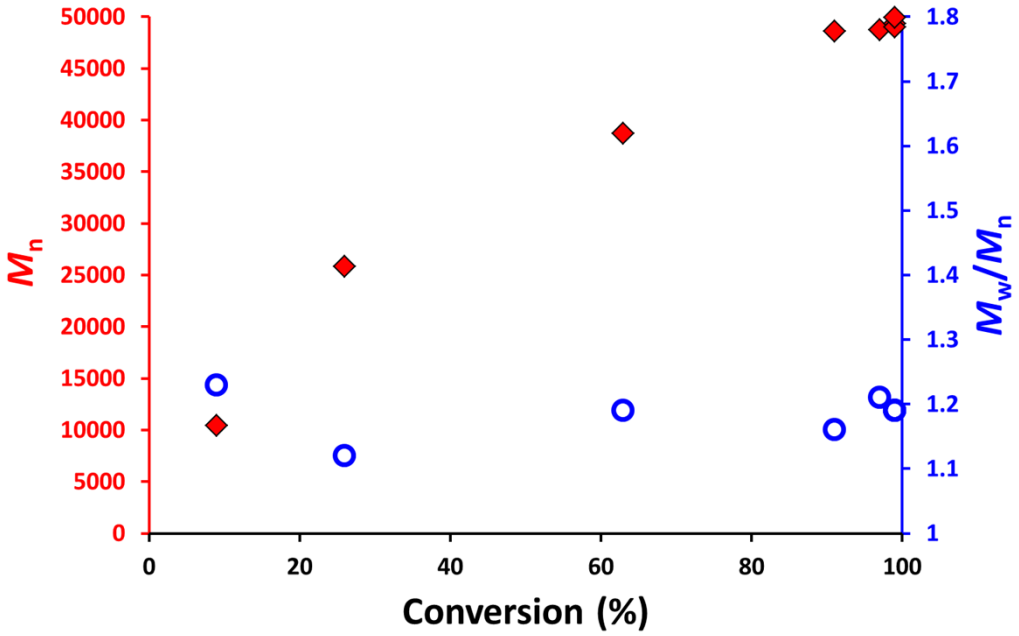

Figure 3.6 Chloroform/methanol (3:1) GPC data obtained for the kinetics of polymerisation of NMEP when targeting $PSMA_{14}$-$PNMEP_{100}$ (vs. a series of PMMA standards).

Each sample for the $PSMA_{14}$-$PNMEP_{100}$ kinetics was analysed by 3:1 chloroform/methanol GPC. A linear increase in number average molecular weight with conversion is observed with low dispersities throughout (see Figure 3.6). After 50 minutes a final M_n of 49,900 g mol^{-1} and a low dispersity of 1.19 is obtained. TEM analysis of the $PSMA_{14}$-$PNMEP_{100}$ sample after 50 minutes indicted spherical micelles with a mean diameter of 27 ± 3 nm (Figure 3.4, inset).

3.3.3 Synthesis of $PSMA_{14}$-$PNMEP_x$ diblock copolymer spheres via RAFT dispersion polymerisation

A series of $PSMA_{14}$-$PNMEP_x$ diblock copolymers were prepared at 10% w/w solids. The target PNMEP DP was systematically varied from 50 to 1000 (Table 3.1). All diblock copolymers went to at least 96% conversion as judged by ^{1}H NMR spectroscopy. Diblock copolymers with a PNMEP DP of 245 or less were analysed by GPC. GPC chromatograms for the $PSMA_{14}$-$PNMEP_x$ diblock copolymers and the corresponding $PSMA_{14}$ macro-CTA chromatogram are shown in Figure 3.7a. All diblock copolymers show high blocking efficiencies with very little $PSMA_{14}$ macro-CTA contamination. A linear increase in molecular weight with PNMEP DP was observed as shown in Figure 3.7b, this is characteristic of a pseudo living polymerisation. Unfortunately, an increase in dispersity with PNMEP DP was also observed. This appears as a high molecular weight shoulder in the chromatogram which became more prominent as the PNMEP DP increased. This high molecular weight shoulder could be a result of either a dimethacrylate impurity in the NMEP monomer (only 96% pure) or a result of chain transfer to polymer, with the two methylene carbonyl protons on the pyrrolidone ring being particularly prone to abstraction.[17] $PSMA_{14}$-$PNMEP_x$ diblock copolymers with a target PNMEP DP of greater than 250 were unable to be analysed by GPC as they became insoluble in the 3:1 chloroform/methanol eluent. This suggests some cross-linking leading to a small (micro)gel fraction. Although these high DP (> 250) $PSMA_{14}$-$PNMEP_x$ diblock copolymers were not analysed by GPC they are expected to continue to have even higher disperities than the 2.85 obtained for $PSMA_{14}$-$PNMEP_{245}$.

Other diblock copolymers prepared by RAFT dispersion polymerisation in *n*-alkanes have shown higher dispersities than that typically expected for RAFT polymerisations (M_w/M_n < 1.30). Fielding et al. reported dispersities as high as 1.76

for a $PLMA_{47}$-$PBzMA_{900}$ diblock copolymer prepared in *n*-heptane.[2] Whereas, PSMA-PPPMA diblock copolymers prepared in *n*-tetradecane by Pei and co-workers resulted in low dispersities ($M_w/M_n \leq 1.17$).[8] Although the PSMA-PPPMA diblock copolymers targeted had a fixed PSMA DP of 19, which is very similar to the $PSMA_{14}$ macro-CTA utilised here, only relatively low PPPMA DPs of 165 or less were targeted. In the present study, dispersities only begin to increase significantly for $PSMA_{14}$-$PNMEP_x$ copolymers when targeting DPs of 150 or greater.

Table 3.1 Conversions, molecular weights (M_n), dispersities (M_w/M_n), mean DLS and TEM diameters obtained for $PSMA_{14}$-$PNMEP_x$ (S_{14}-N_x) diblock copolymer nanoparticles at 10% w/w solids and the corresponding $PSMA_{14}$ macro-CTA.

	Diblock composition	Conversion[a] (%)	Solids content (% w/w)	GPC[b]		DLS particle diameter[c] (nm)
				M_n (kg mol^{-1})	M_w/M_n	
1	S_{14}	80	40	7.5	1.12	-
2	S_{14}-N_{49}	98	10	30.1	1.15	23 (0.21)
3	S_{14}-N_{74}	99	10	40.5	1.14	30 (0.03)
4	S_{14}-N_{98}	98	10	49.6	1.19	36 (0.04)
5	S_{14}-N_{124}	99	10	60.1	1.19	42 (0.03)
6	S_{14}-N_{149}	99	10	72.5	1.36	47 (0.05)
7	S_{14}-N_{168}	96	10	83.8	1.63	56 (0.01)
8	S_{14}-N_{198}	99	10	95.0	1.64	62 (0.02)
9	S_{14}-N_{216}	96	10	107.0	1.92	76 (0.03)
10	S_{14}-N_{245}	98	10	109.8	2.85	95 (0.01)
11	S_{14}-N_{270}	98	10	-	-	153 (0.01)
12	S_{14}-N_{291}	97	10	-	-	173 (0.01)
13	S_{14}-N_{392}	98	10	-	-	274 (0.03)
14	S_{14}-N_{485}	97	10	-	-	340 (0.04)
15	S_{14}-N_{960}	96	10	-	-	462 (0.01)

a. Monomer conversion determined by ^{1}H NMR spectroscopy in $CDCl_3$.
b. Determined by 3:1 v/v chloroform/methanol GPC against PMMA calibration standards using a refractive index detector.
c. The number in brackets refers to the DLS polydispersity.

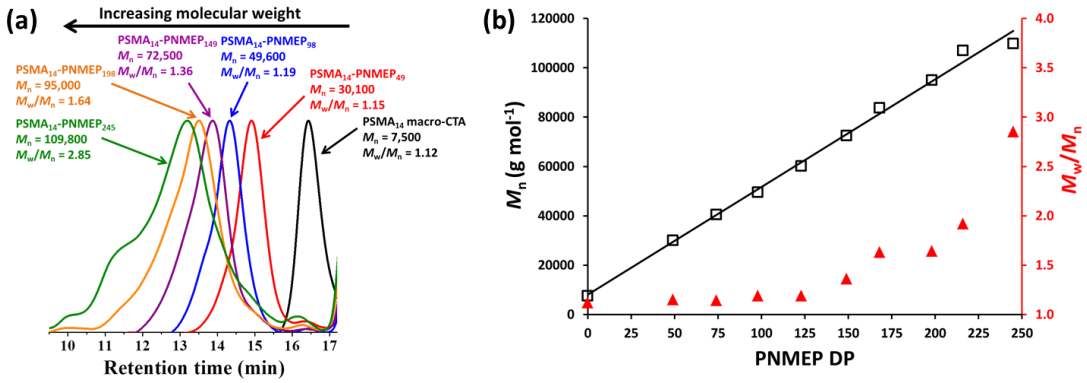

Figure 3.7 (a) 3:1 Chloroform/methanol GPC curves obtained for $PSMA_{14}$-$PNMEP_x$ diblock copolymer nanoparticles prepared at 10% w/w solids via RAFT dispersion polymerisation of NMEP at 90 °C, (b) a plot of PNMEP DP against M_n (black axis) and M_w/M_n (red axis) for the same series of $PSMA_{14}$-$PNMEP_x$ diblock copolymer nanoparticles.

DLS shows an increase in particle diameter with increasing PNMEP DP (Figure 3.8). All diblock copolymers show narrow size distributions, typically below 0.05 (except for $PSMA_{14}$-$PNMEP_{49}$ which has a polydispersity of 0.21). The smallest $PSMA_{14}$-$PNMEP_{49}$ diblock copolymer forms small 23 nm particles whereas the largest $PSMA_{14}$-$PNMEP_{960}$ forms 462 nm particles. TEM analysis of the $PSMA_{14}$-$PNMEP_x$ diblock copolymers prepared at 10% w/w confirms only a spherical morphology, despite the extremely large size of the $PSMA_{14}$-$PNMEP_{960}$ diblock copolymer, Figure 3.9. These appear to be the largest spheres prepared by RAFT PISA.[18] Figure 3.8b shows the relationship between the core-forming PNMEP DP and the diameter from DLS. An initial linear increase in particle size with PNMEP DP is observed up to a PNMEP DP of approximately 200. After this there is an increase in particle size. This complex behaviour is not currently understood as this increase does not coincide with a change in morphology by TEM. Although as discussed earlier GPC provides some evidence of potential cross-linking for these higher targeted PNMEP DPs.

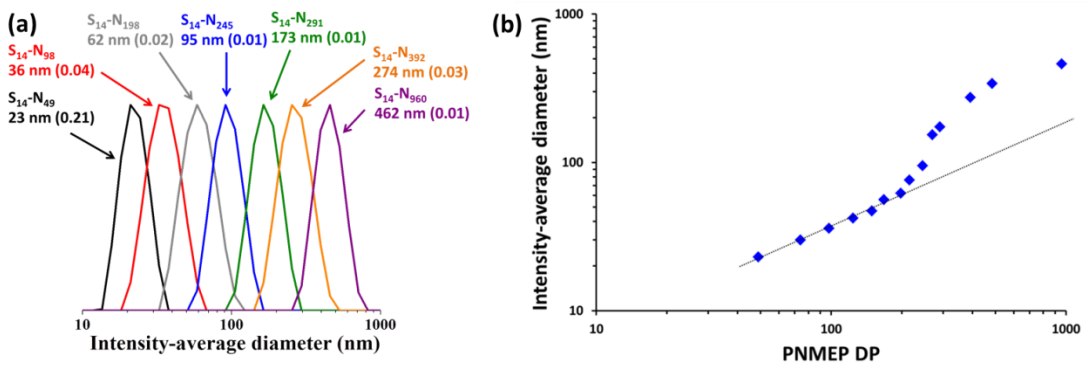

Figure 3.8 (a) DLS intensity-average size distributions for $PSMA_{14}$-$PNMEP_x$ diblock copolymer nanoparticles prepared via RAFT dispersion polymerisation of NMEP at 10% w/w solids in *n*-dodecane at 90 °C, (b) a plot of intensity-average diameter vs. mean degree of polymerisation of the PNMEP core-forming block.

TEM confirmed an exclusive sphere forming series for the $PSMA_{14}$-$PNMEP_x$ diblock copolymers prepared at 10% w/w solids. No evidence of higher order morphologies such as worm-like micelles or vesicles was observed. This limitation to spherical micelles at lower concentrations has previously been seen in other RAFT dispersion polymerisations and will be discussed further in Section 3.3.4.[2,19-21]

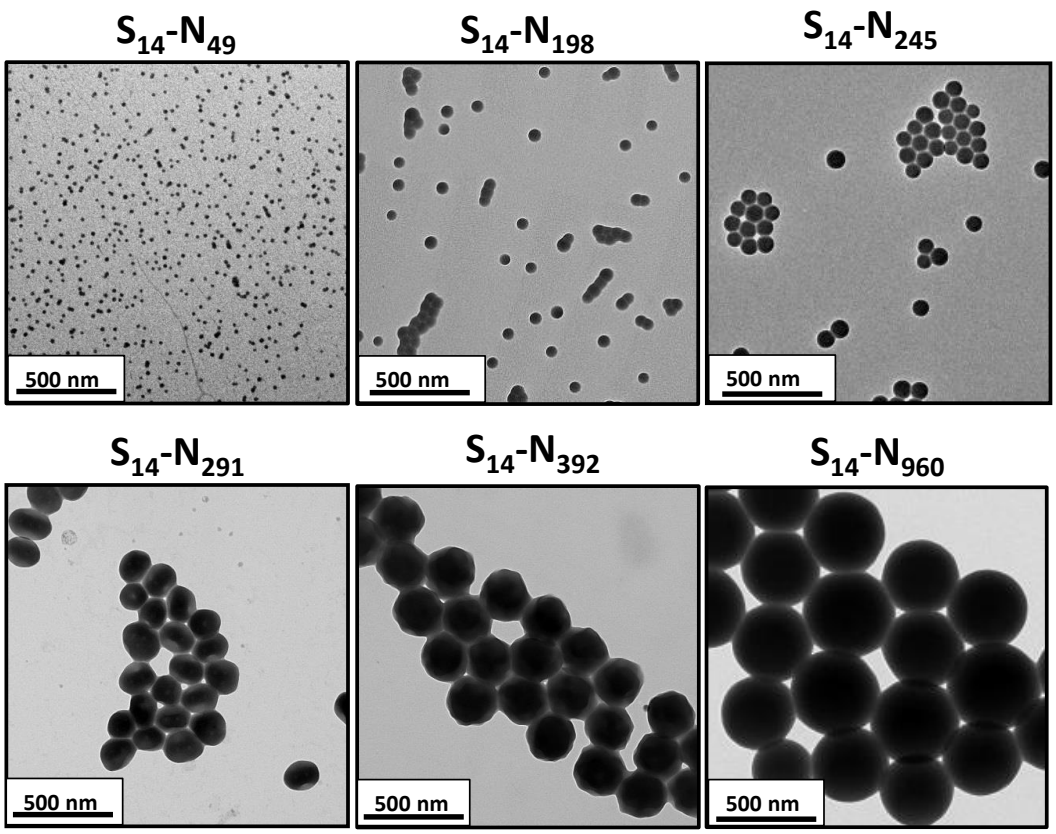

Figure 3.9 TEM images obtained for $PSMA_{14}$-$PNMEP_x$ diblock copolymer nanoparticles prepared at 10% w/w solids in *n*-dodecane showing well-defined spherical nanoparticles (N.B. 'S' denotes PSMA and 'N' denotes PNMEP).

3.3.4 Construction of a $PSMA_{14}$-$PNMEP_x$ diblock copolymer phase diagram

For post-polymerisation processing of PS-PAA diblock copolymers in dilute solution using a solvent switch, Eisenberg and co-workers have reported that, spherical nanoparticles can become kinetically-trapped and hence no longer represent the equilibrium morphology.[22,23] Derry et al. have shown that the DP of the PSMA macro-CTA is critical for the formation of higher order structures.[11] A PSMA macro-CTA with a DP of 18 or 31 only formed spherical micelles when extended with BzMA, whereas a DP of 13 enabled the formation of spheres, worms and vesicles. The $PSMA_{14}$ macro-CTA synthesised herein is therefore expected to allow access to higher order morphologies. Bearing this in mind, a series of $PSMA_{14}$-$PNMEP_x$ diblock copolymers were prepared at 20% w/w solids (Table 3.2). The target PNMEP DP was varied from 50 to 250. Each diblock copolymer synthesis proceeded to at least 95% conversion.

Table 3.2 Conversions, molecular weights (M_n), dispersities (M_w/M_n), DLS and TEM diameters obtained for $PSMA_{14}$-$PNMEP_x$ (S_{14}-N_x) diblock copolymer nanoparticles prepared at 20% w/w solids and the corresponding $PSMA_{14}$ macro-CTA prepared at 40% w/w solids.

	Diblock Composition	Conversion[a] (%)	Solids content (% w/w)	GPC[b]		DLS particle diameter[c] (nm)	Particle morphology[d]
				M_n [b] (kg mol^{-1})	M_w/M_n [b]		
1	S_{14}	80	40	7.5	1.12	-	-
2	S_{14}-N_{49}	99	20	29.7	1.15	26 (0.05)	Spheres
3	S_{14}-N_{79}	99	20	44.5	1.22	36 (0.06)	Spheres
4	S_{14}-N_{99}	99	20	52.7	1.27	39 (0.05)	Spheres
5	S_{14}-N_{114}	95	20	63.3	1.34	48 (0.05)	Spheres
6	S_{14}-N_{149}	99	20	84.3	1.59	151 (0.09)	Mixed
7	S_{14}-N_{173}	99	20	85.0	1.48	1174 (0.32)	Mixed
8	S_{14}-N_{190}	>99	20	89.8	1.75	824 (0.31)	Mixed
9	S_{14}-N_{198}	99	20	99.4	2.01	722 (0.35)	Worms
10	S_{14}-N_{209}	99	20	105.8	1.79	729 (0.46)	Mixed
11	S_{14}-N_{221}	98	20	111.5	1.94	1370 (0.30)	Mixed
12	S_{14}-N_{248}	99	20	121.9	2.04	1169 (0.12)	Mixed

a. Monomer conversion determined by ^{1}H NMR spectroscopy in $CDCl_3$.
b. Determined by 3:1 v/v chloroform/methanol GPC against PMMA calibration standards using a refractive index detector.
c. The number in brackets refers to the DLS polydispersity.
d. Determined by TEM

Each $PSMA_{14}$-$PNMEP_x$ diblock copolymer prepared at 20% w/w was analysed by 3:1 chloroform/methanol GPC (Figure 3.10). High blocking efficiencies were achieved for all diblock copolymers relative to the $PSMA_{14}$ macro-CTA. A linear increase in M_n with PNMEP DP is observed (Figure 3.10b). Similarly to the series prepared at 10% w/w, dispersity increases gradually with increasing PNMEP DP, with a final dispersity of 2.04 for $PSMA_{14}$-$PNMEP_{248}$.

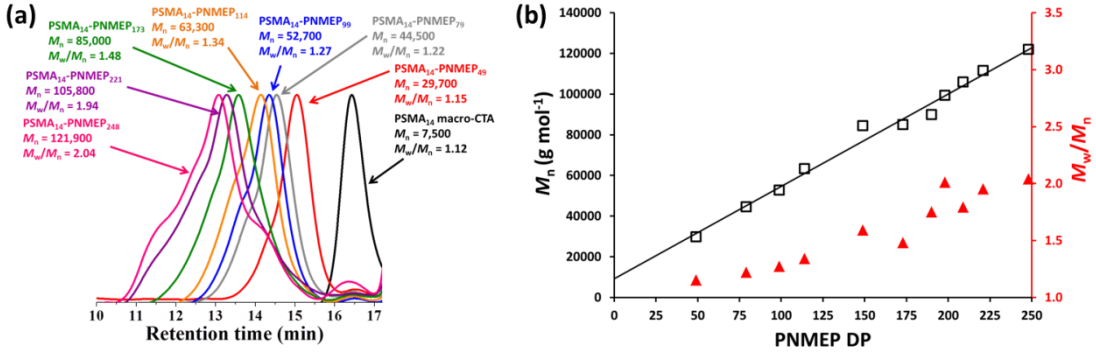

Figure 3.10 (a) 3:1 Chloroform/methanol GPC curves obtained for a selection of $PSMA_{14}$-$PNMEP_x$ diblock copolymer nanoparticles prepared at 20% w/w solids via RAFT dispersion polymerisation of NMEP at 90 °C, (b) a plot of M_n (black axis) and M_w/M_n (red axis) against PNMEP DP for the same series of $PSMA_{14}$-$PNMEP_x$ diblock copolymer nanoparticles.

TEM reveals a range of morphologies for the series prepared at 20% w/w (Figure 3.11). For a PNMEP DP of 114 or less spherical micelles are observed. An increase in sphere size with PNMEP DP is observed by TEM and supported by DLS (Table

3.2). DLS shows low polydispersities for the $PSMA_{14}$-$PNMEP_x$ diblock copolymers which form spherical micelles. Increasing the PNMEP DP above 114 led to mixed phases with worm-like micelles present in the TEM. This change in morphology coincides with an increase in polydispersity by DLS (Table 3.2). One pure worm sample was obtained for a block composition of $PSMA_{14}$-$PNMEP_{198}$. These worms appear to be extremely long, with lengths in the region of 10 μm being measured. When spheres and worms coexist, the width of the worms corresponds well to the sphere diameter ($PSMA_{14}$-$PNMEP_{149}$). This provides evidence of the sphere-sphere fusion which must occur to form worm-like micelles.[2,24] Increasing the PNMEP DP further led to mixed phases of vesicles with worms. Targeting a PNMEP DP greater than 250 at 20% w/w led to macroscopic precipitation and therefore a pure vesicles phase was not observed at 20% w/w solids.

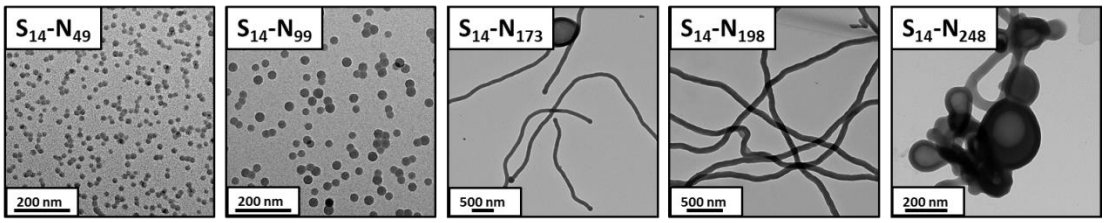

Figure 3.11 Representative TEM images obtained for $PSMA_{14}$-$PNMEP_x$ diblock copolymer nano-objects prepared via RAFT dispersion polymerisation of NMEP at 20% w/w solids.

A detailed phase diagram was constructed to aid the reproducible targeting of $PSMA_{14}$-$PNMEP_x$ copolymer morphologies (Figure 3.12). Further experiments were set up between 10 and 30% w/w solids with target PNMEP DPs between 50 and 250. All diblock copolymers went to > 90% conversion and each was analysed by TEM to determine the final morphology. Spherical micelles take up a predominate amount of the phase diagram, with them being the sole morphology at both 10% w/w solids and when a PNMEP DP of 90 or less is targeted. The upper limit PNMEP DP for spheres decreases with increasing copolymer concentrations, with $PSMA_{14}$-$PNMEP_{90}$ being the last sphere only composition at 30% w/w solids. This supports the hypothesis that spheres produces at lower concentrations become kinetically trapped and do not represent the equilibrium morphology, particularly when targeting higher PNMEP DPs.

A small phase space represents 'pure' worm-like micelles. This is defined as more than 95% of nano-objects analysed by TEM being classified as worms. The narrow

phase space for the worm-like micelles is consistent with the observations made by Fielding et al. for other RAFT dispersion polymerisation in *n*-alkanes.[2,4] A large proportion of the phase diagram represents mixed phases where two or more morphologies co-exist.

Vesicles are often formed at high core-forming block DP (~ 200) and high solids content (20% w/w).[19,21] However, in this case only a few examples of vesicles were observed. These were at high concentrations of 27.5% w/w and 30% w/w solids but were at PNMEP DPs between 150 and 200. Targeting a PNMEP DP above 200 at 30% w/w solids resulted in a colloidally unstable macroscopic precipitate. Similar observations were observed by Warren et al. for a phase diagram constructed for a series of PEG-PHPMA diblock copolymers prepared via PISA.[25] TEM of $PSMA_{14}$-$PNMEP_{250}$ diblock copolymers prepared above 25% w/w solids confirmed the presence of large vesicular aggregates (see Figure 3.13).

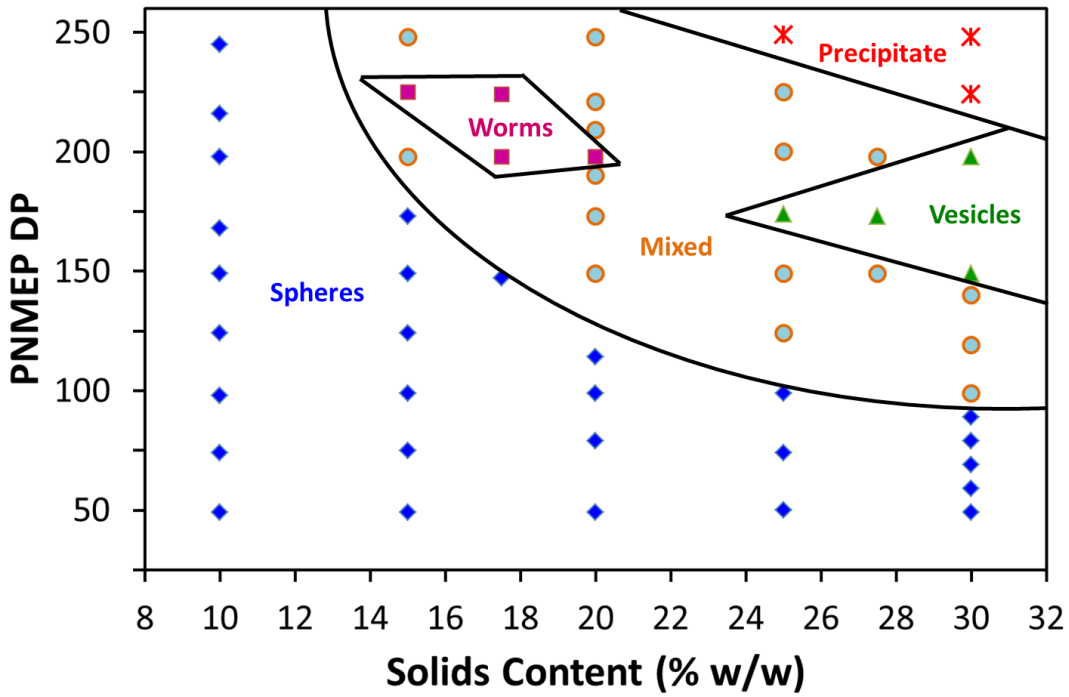

Figure 3.12 Phase diagram for a series of $PSMA_{14}$-$PNMEP_x$ diblock copolymers synthesised by RAFT dispersion polymerisation in *n*-dodecane at various concentrations ranging between 10 and 30% w/w. Post-polymerisation analysis of the diblock copolymer dispersions by TEM determined the phase boundaries.

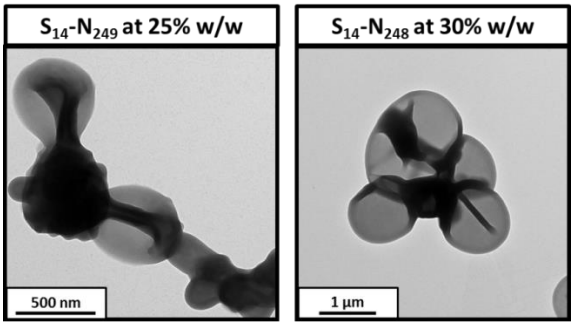

Figure 3.13 Representative TEM images recorded for the unstable precipitate phase obtained for $PSMA_{14}$-$PNMEP_x$ syntheses conducted at either 25% or 30% solids when targeting a PNMEP DP of 250.

The $PSMA_{14}$-$PNMEP_{198}$ composition is particularly interesting, since varying the copolymer concentration yields the full range of morphologies (spheres, worms and vesicles). A near-monodisperse spherical morphology is observed at 10% w/w solids, whereas worms are produced at 20% w/w solids and a vesicle phase comprising mainly oligolamellar vesicles[25] is formed at 30% w/w solids (Figure 3.14). This example nicely illustrates the concentration-dependent morphologies that can be obtained via such PISA syntheses.

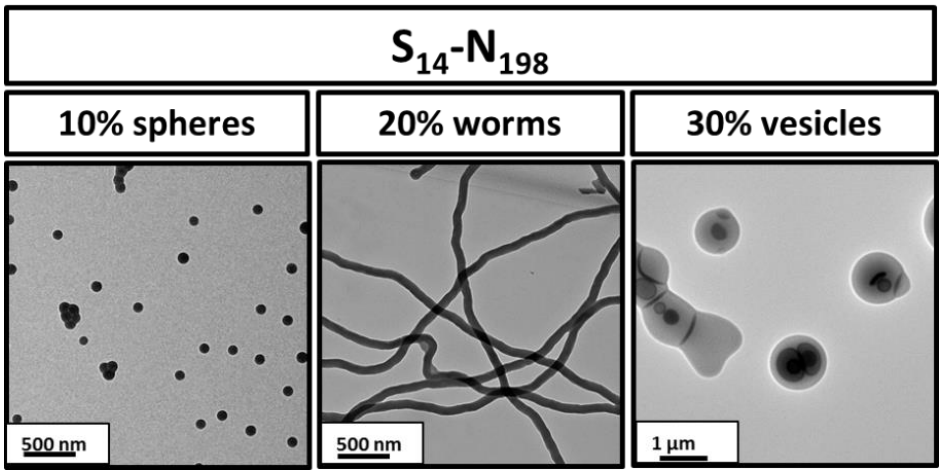

Figure 3.14 TEM images obtained for $PSMA_{14}$-$PNMEP_{198}$ diblock copolymer nano-objects prepared at 10, 20 or 30% w/w solids confirming the formation of well-defined spheres, highly anisotropic worms and polydisperse oligolamellar vesicles, respectively.

3.3.5 Pickering emulsifier studies using $PSMA_{14}$-$PNMEP_{49}$ spheres

The $PSMA_{14}$-$PNMEP_{49}$ diblock copolymer synthesis was scaled up to form a 10 g batch of nanoparticles at 10% w/w solids. These 25 nm spheres were analysed as potential Pickering emulsifiers. Homogenisation of the $PSMA_{14}$-$PNMEP_{49}$ diblock copolymer in *n*-dodecane with water could lead to four potential outcomes, see Scheme 3.3.

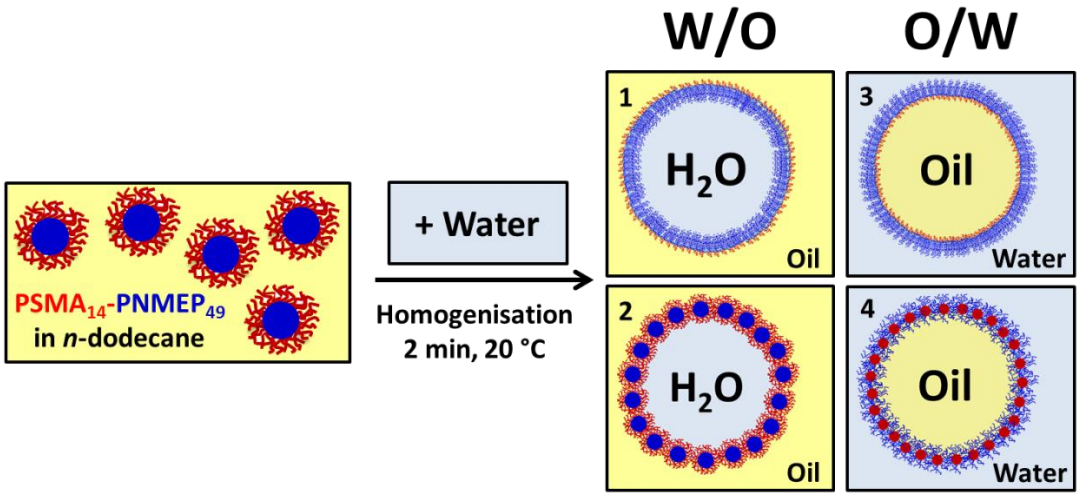

Scheme 3.3 Schematic representation of the 4 possible types of emulsions which could form as a result of homogenising the $PSMA_{14}$-$PNMEP_{49}$ nanoparticles prepared in *n*-dodecane with water. In scenarios 1 and 3, the nanoparticles dissociate to produce amphiphilic diblock copolymer chains that act as a polymeric surfactant stabiliser, producing either water-in-oil or oil-in-water emulsions, respectively. In scenario 2, the hydrophobic nanoparticles are retained intact and adsorb at the oil/water interface to form water-in-oil Pickering emulsions. In scenario 4, morphological inversion to form hydrophilic nanoparticles that stabilise oil-in-water Pickering emulsions.

Homogenisation could be detrimental to the stability of the particles leading to molecularly dissolved chains that act as a polymeric surfactant. These could stabilise either a water-in-oil emulsion (scenario 1) or an oil-in-water emulsion (scenario 3) depending on whether the PSMA or the PNMEP block act as the stabiliser. This disassembly of diblock copolymer nanoparticles under high shear has recently been reported by Thompson et al. for PGMA-PHPMA spheres prepared in water.[26] However, based on further studies by Thompson and co-workers using PLMA-PBzMA worms or spheres prepared in *n*-dodecane,[27] the $PSMA_{14}$-$PNMEP_{49}$ spheres may simply remain intact and stabilise a water-in-oil Pickering emulsion (scenario 2). Due to the hydrophobic nature of the $PSMA_{14}$-$PNMEP_{49}$ diblock copolymer nanoparticles this is perhaps the most likely outcome. Scheme 3.3, scenario 4 depicts the possible inversion of the hydrophobic $PSMA_{14}$-$PNMEP_{49}$ spheres to form hydrophilic $PNMEP_{49}$-$PSMA_{14}$ spheres. In this case, the hydrophilic particles could stabilise an oil-in-water Pickering emulsion.

Initially, a fixed concentration of 1.0% w/w $PSMA_{14}$-$PNMEP_{49}$ nanoparticles was used to study the effect of shear rate on emulsion formation. A fixed volume ratio of 50:50 water/*n*-dodecane was used to homogenise the particles for 2 minutes. The

shear rate was varied from 3,500 rpm to 24,000 rpm with one additional emulsion being prepared by hand-shaking (very low shear).

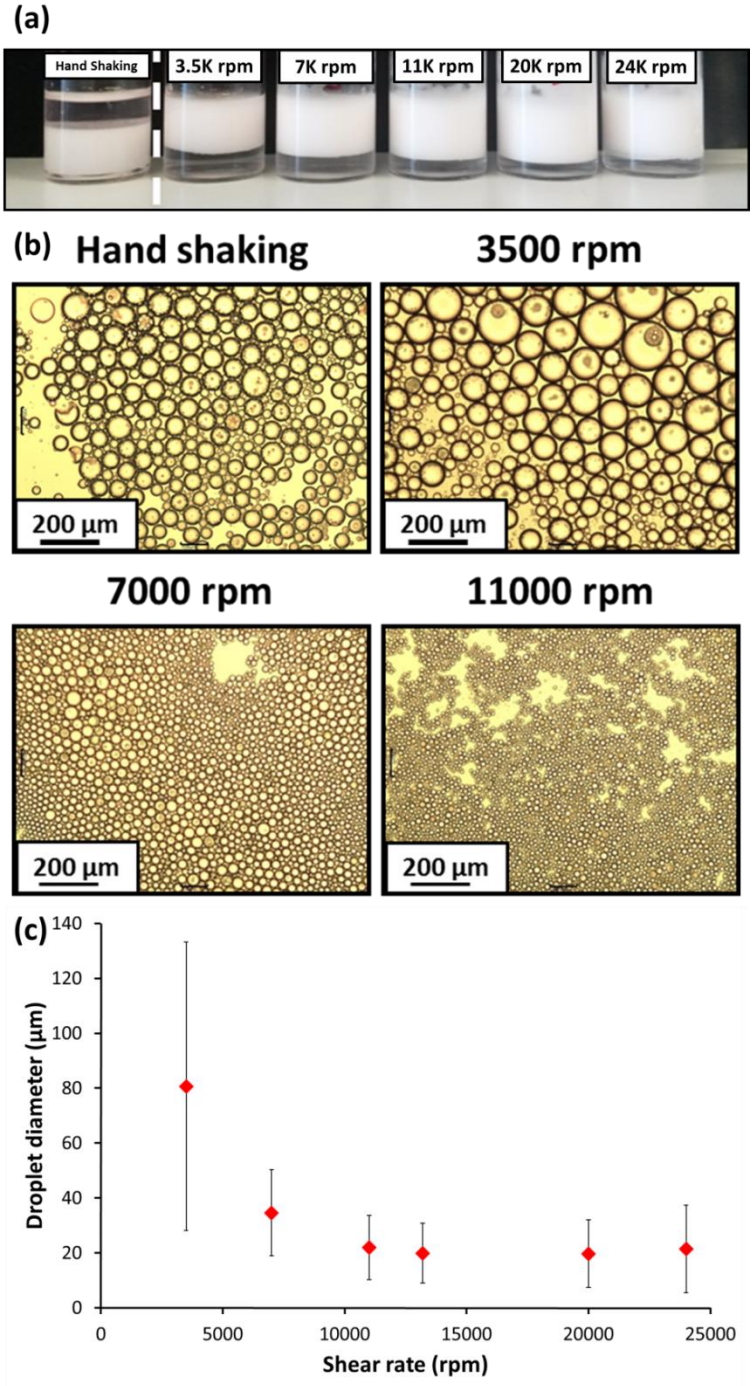

Figure 3.15 (a) Digital photographs obtained for the Pickering emulsions prepared using 1.00% w/w particles at various shear rates. Oil-in-water emulsions are formed in all cases, except when hand-shaking is used; this latter approach results in a water-in-oil emulsion instead, (b) optical microscopy images recorded for the droplets prepared via hand-shaking, or homogenisation at 3,500 rpm, 7,000 rpm or 11,000 rpm, (c) shear rate dependence for the mean droplet diameter (as determined by laser diffraction) for emulsions prepared using $PSMA_{14}$-$PNMEP_{49}$ spherical nanoparticles as the sole emulsifier.

A digital photograph of the resulting emulsions is shown in Figure 3.15a. There is a clear switch between the presence of a water-in-oil emulsion being formed via hand-shaking for 2 minutes, to oil-in-water emulsions when high speed homogenisation is used. Figure 3.15b shows the optical microscopy images for selected emulsions prepared at different shear rates. Droplet size appears to reduce with increasing shear rate. Laser diffraction was used to measure the emulsion droplet size for the oil-in-water emulsions (Figure 3.15c). A gradual reduction in droplet size from ~80 μm at a shear rate of 3,500 rpm to ~20 μm when a shear rate of 11,000 rpm or higher was used. Thompson et al. observed a similar observation for water-in-oil emulsions stabilised by PLMA-PBzMA worms in *n*-dodecane.[28]

At this point, it is unclear as to whether the $PSMA_{14}$-$PNMEP_{49}$ was stabilising the oil-in-water emulsion in the form of individual copolymer chains or as spherical nanoparticles (scenario 3 or 4). DLS studies were used to investigate whether the nanoparticles were stable to homogenisation (Figure 3.16). Prior to homogenisation a 1.0% w/w dispersion of the $PSMA_{14}$-$PNMEP_{49}$ nanoparticles form stable 25 nm spheres with a low polydispersity of 0.07. After homgenisation at 13,200 rpm (without the presence of water to form an emulsion) DLS indicated a large increase in both particle diameter and polydispersity. A reduction in the count rate by a factor of three provides evidence that the particle undergo dissociation when subjected to high shear.

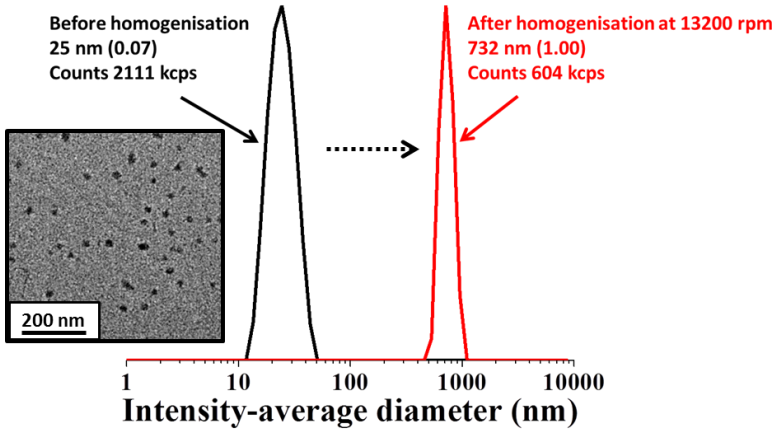

Figure 3.16 DLS particle size distributions obtained for $PSMA_{14}$-$PNMEP_{49}$ nanoparticles before (black) and after (red) homogenisation at 13,200 rpm at 20 °C. High shear homogenisation causes the initial 25 nm spherical nanoparticles to break up, resulting in a relatively low count rate and a very high polydispersity. Inset: TEM image before homgenisation.

To examine if this dissociation led to the $PSMA_{14}$-$PNMEP_{49}$ acting as a polymeric stabiliser (scenario 3, in Scheme 3.3) a series of oil-in-water emulsions were prepared in which the nanoparticle concentration was varied from 0.0675% w/w to 2.50% w/w for a fixed shear rate of 13,200 rpm. The oil-in-water emulsions were measured by laser diffraction and imaged by optical microscopy (Figure 3.17). Strong concentration dependence is observed, in which large (up to 80 μm) droplets are formed at low copolymer concentrations with much smaller droplets of ~10 μm at 2.50% w/w. This is supported by the optical microscopy images. This concentration dependence indicates that the copolymer actually adsorbs in the form of nanoparticles, rather than individual chains. This unexpected result was reinforced by TEM of an emulsion prepared at 13,200 rpm (Figure 3.18a). Spherical nanoparticles are observed on an emulsion droplet suggesting that the hydrophobic $PSMA_{14}$-$PNMEP_{49}$ diblock copolymer spheres invert under high shear to form hydrophilic $PNMEP_{49}$-$PSMA_{14}$ diblock copolymer spheres which can stabilise oil-in-water emulsions (scenario 4). TEM of the water-in-oil emulsion formed via hand-shaking also confirmed the presence of spherical micelles on the droplet surface (scenario 2).

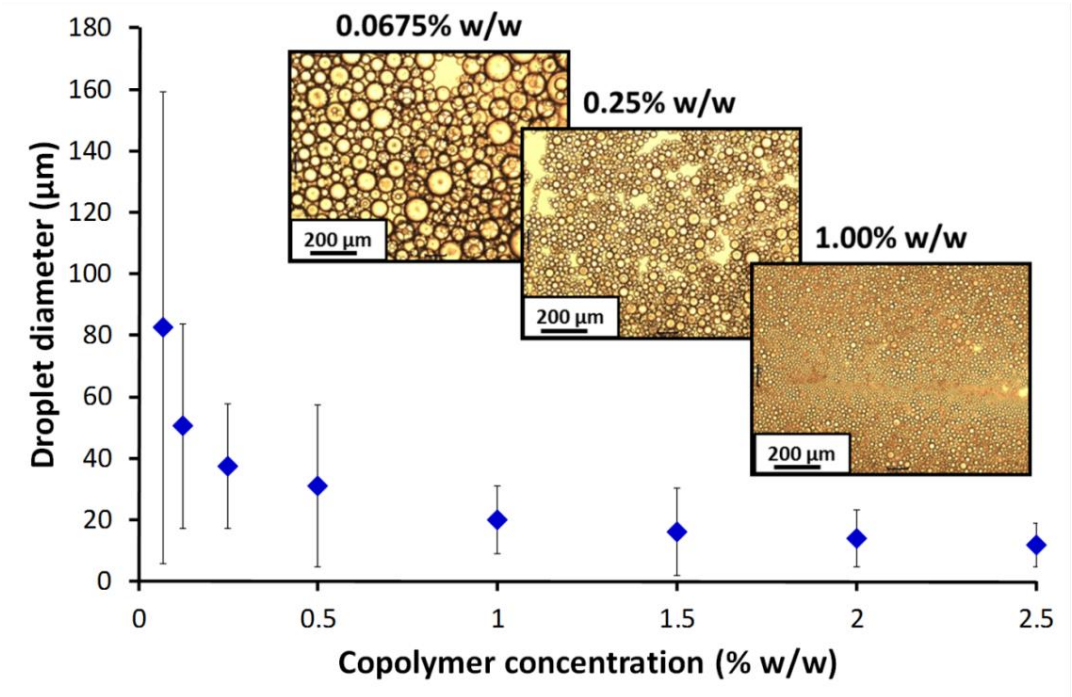

Figure 3.17 Concentration dependence of the mean volume-average droplet diameter (as determined by laser diffraction) for oil-in-water Pickering emulsions prepared at a constant shear rate of 13,200 rpm using $PSMA_{14}$-$PNMEP_{49}$ spheres. Inset: optical microscopy images of the droplets prepared at 0.0675, 0.25 and 1.00% w/w.

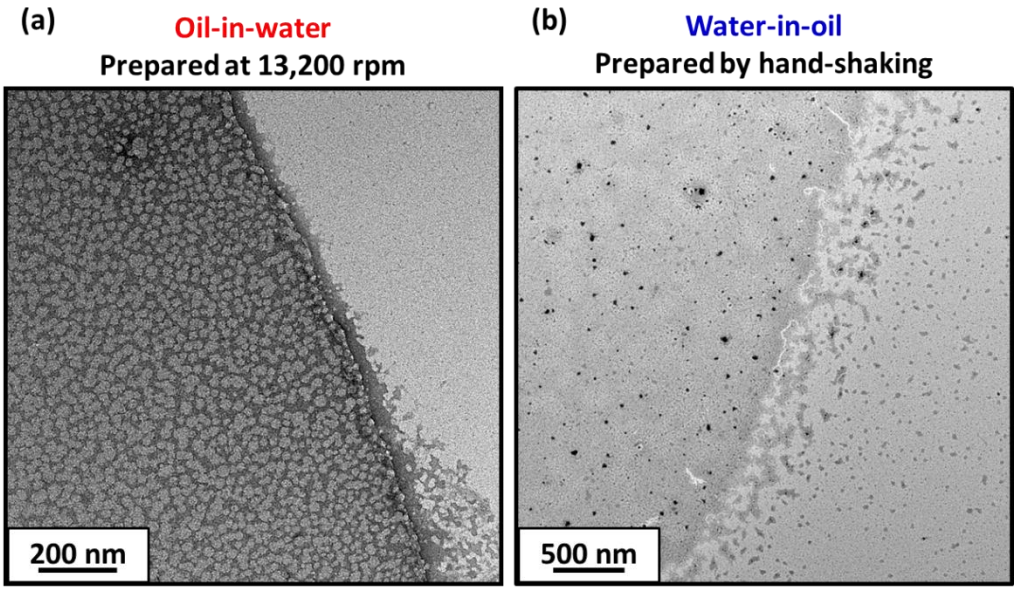

Figure 3.18 Transmission electron microscopy of Pickering emulsion droplets prepared using $PSMA_{14}$-$PNMEP_{49}$; (a) an oil-in-water droplet prepared at 13,200 rpm and stained using uranyl formate and (b) a water-in-oil droplet prepared by hand-shaking and stained using ruthenium (VIII) oxide. Both show the presence of spherical nanoparticles absorbing at the oil-water interface.

To further analyse the water-in-oil emulsions prepared via hand-shaking, a series of such emulsions were prepared. Equal volumes of water and copolymer dispersions in *n*-dodecane were used. The copolymer concentration was varied from 0.125% w/w to 1.50% w/w. Water-in-oil emulsions were formed in all cases, see Figure 3.19. The optical microscopy images suggest some concentration dependence with droplet size. Unfortunately, these water-in-oil emulsions were not stable enough to enable laser diffraction analysis. Instead, ImageJ was utilised to estimate the mean droplet diameters by sizing at least 100 droplets per emulsion (Figure 3.20). Concentration dependence is observed backing up the TEM analysis that the particles are absorbing as $PSMA_{14}$-$PNMEP_{49}$ nanoparticles rather than individual chains.

DLS studies were conducted on the supernatant of both an oil-in-water emulsion (prepared at 13,200 rpm) and a water-in-oil emulsion (prepared by hand-shaking) (Figure 3.21). The *n*-dodecane supernatant for the water-in-oil emulsion contained 28 nm particles with a narrow polydispersity of 0.03 and TEM confirms the spherical particles remain intact after hand-shaking. In contrast, the aqueous supernatant for the oil-in-water emulsion prepared at 13,200 rpm shows a very large diameter of 1688 nm and high polydispersity of 0.47. This is substantially different from the 25 nm spheres used to prepare the emulsions.

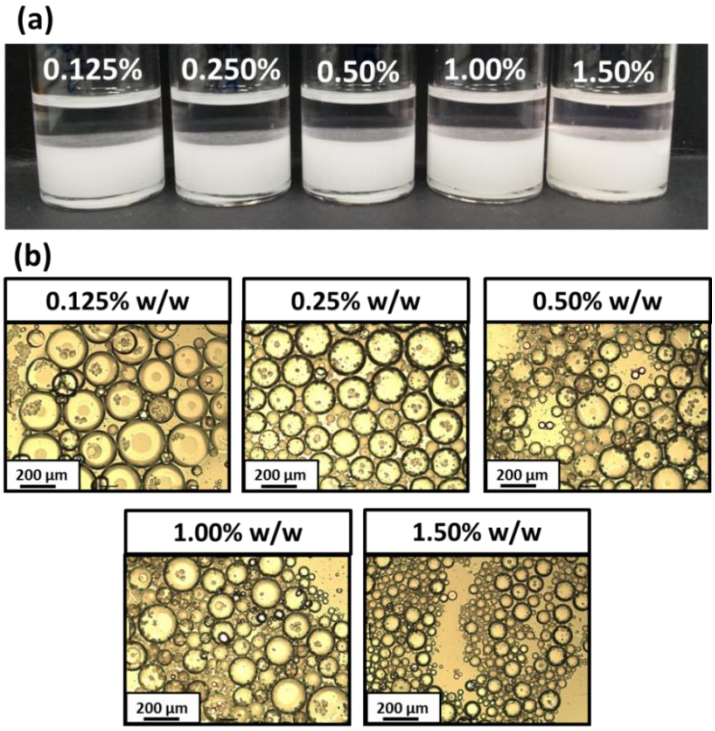

Figure 3.19 Water-in-oil emulsions prepared by hand-shaking of 50:50 v/v mixtures of *n*-dodecane and water using either 0.125, 0.25, 0.50, 1.00 or 1.50% w/w $PSMA_{14}$-$PNMEP_{49}$ nanoparticles: (a) digital photograph of the resulting five emulsions and (b) corresponding optical microscopy images.

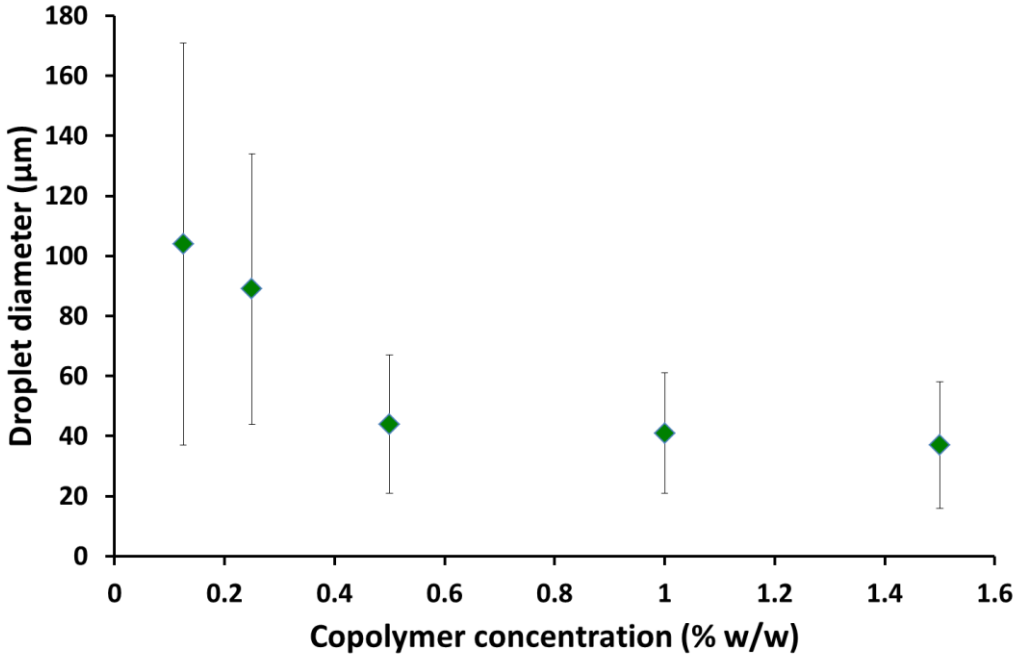

Figure 3.20 Concentration dependence of the mean aqueous droplet diameter obtained for the water-in-oil emulsions prepared by hand-shaking using either 0.125, 0.25, 0.50, 1.00 or 1.50% w/w $PSMA_{14}$-$PNMEP_{49}$ nanoparticles. Mean droplet diameters were estimated from optical microscopy images by analysing at least 100 droplets.

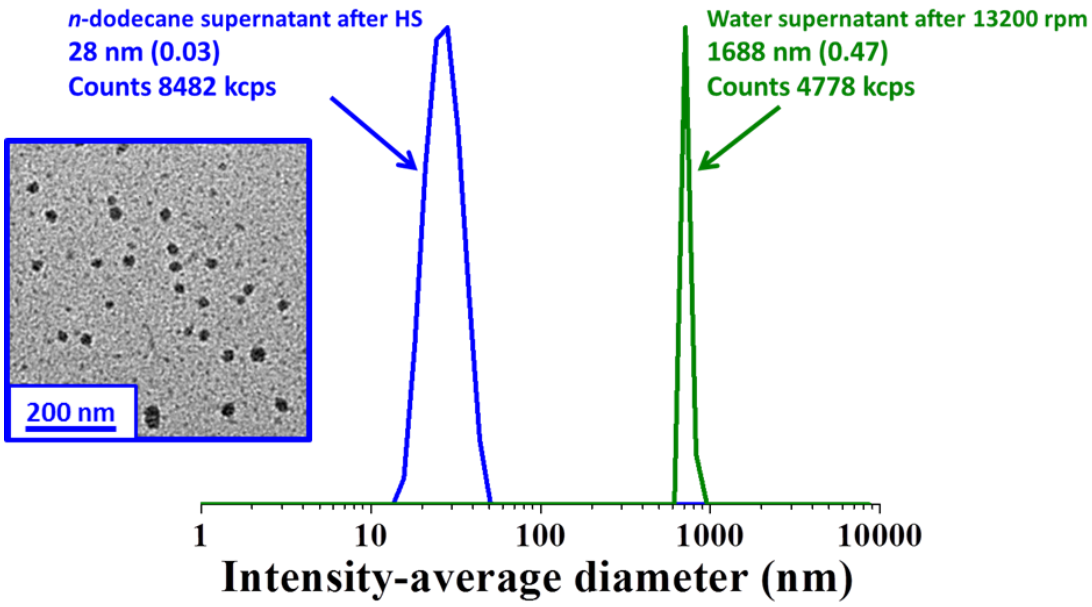

Figure 3.21 DLS particle size distributions obtained for the *supernatants* (after gravitational sedimentation on standing at 20 °C overnight) of the emulsions prepared using 1.00% w/w $PSMA_{14}$-$PNMEP_{49}$ nanoparticles. The blue trace shows the DLS size distribution (and corresponding TEM image) obtained for the *n*-dodecane *supernatant* of the water-in-oil emulsion prepared by hand-shaking, confirming that these nanoparticles are stable to homogenisation at *low* shear. The green trace shows the *aqueous* supernatant of the oil-in-water emulsion obtained after preparation via homogenisation at 13,200 rpm.

Finally, the effect of varying the volume fraction of the aqueous phase was studies. A concentration of 0.50% w/w was selected to prepare three Pickering emulsions at 13,200 rpm. Volume fractions of 25%, 50% and 75% water relative to the $PSMA_{14}$-$PNMEP_{49}$ nanoparticle dispersion in *n*-dodecane were selected. Using both 75% and 50% water resulted in oil-in-water emulsions, as had been observed previously. Interestingly, using only 25% water and 75% nanoparticles in *n*-dodecane led to a water-in-oil emulsion. A digital photograph and optical microscopy of the emulsions is shown in Figure 3.22.

This indicates that the $PSMA_{14}$-$PNMEP_{49}$ spherical nanoparticles enable the preparation of water-in-oil emulsions by two methods, either using very low shear rates (hand-shaking) or by using a 25% water/75% *n*-dodecane formulation in order to prevent nanoparticle inversion.

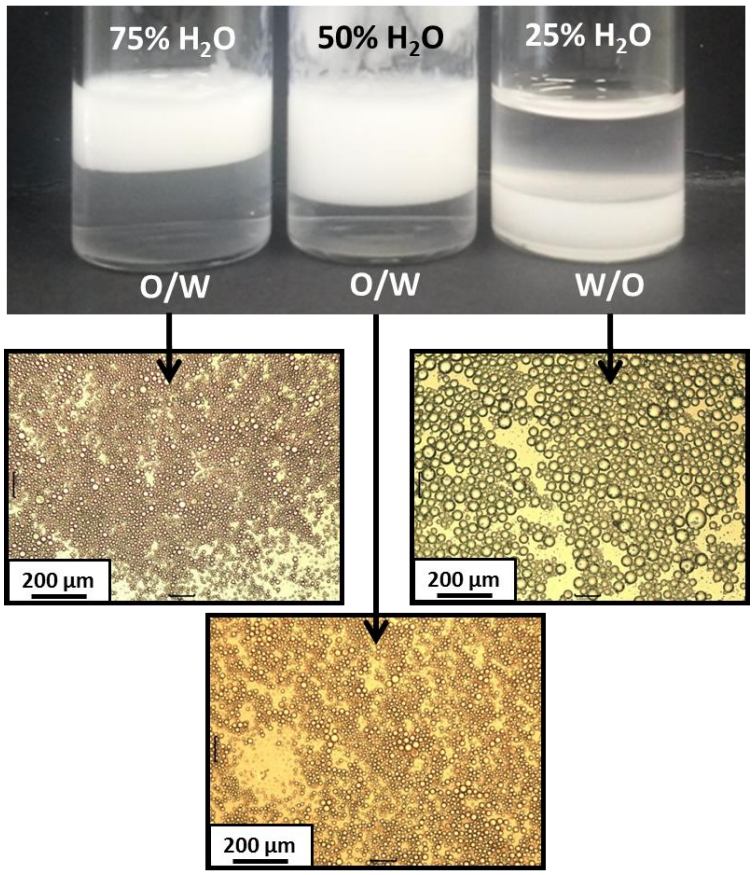

Figure 3.22 Digital photographs and corresponding optical microscopy images obtained for $PSMA_{14}$-$PNMEP_{49}$ emulsions formed using water volume fractions 0.25, 0.50 or 0.75 relative to *n*-dodecane. Emulsions were prepared using 0.50% w/w $PSMA_{14}$-$PNMEP_{49}$ nanoparticles at 13,200 rpm. The latter water volume fractions resulted in the formation of *oil-in-water* (O/W) emulsions, whereas the lowest water volume fraction produced a *water-in-oil* (W/O) emulsion.

3.4 Conclusions

A near-monodisperse PSMA macro-CTA was prepared via RAFT solution polymerisation in toluene at 70 °C. This $PSMA_{14}$ macro-CTA was then chain-extended with 100 units of NMEP in a kinetic experiment. ^{1}H NMR indicated an extremely fast reaction for this RAFT dispersion polymerisation in *n*-dodecane, with 99% conversion being achieved within 30 min at 90 °C. The reaction kinetics was compared to that of a non-polar monomer, benzyl methacrylate (BzMA). The $PSMA_{14}$-$PNMEP_{100}$ synthesis exhibited a rate enhancement of 38 compared to the $PSMA_{14}$-$PBzMA_{100}$ synthesis which took 6 h to reach 95% conversion under the same conditions. The $PSMA_{14}$ macro-CTA was used for the synthesis of a series of $PSMA_{14}$-$PNMEP_x$ diblock copolymers. High conversions (≥ 95%) were achieved for all diblock copolymers within 2 h at 90 °C. GPC analysis showed the expected

increase in molecular weight with target PNMEP DP but high dispersities were observed, particularly when targeting PNMEP DPs of 150 or greater. This loss of control was attributed to dimethacrylate impurity in the PNMEP monomer, which has a purity of only 96%. These diblock copolymers underwent polymerisation-induced self-assembly. TEM analysis of the $PSMA_{14}$-$PNMEP_x$ diblock copolymers prepared at 10% w/w indicated an exclusively spherical morphology, even when targeting highly asymmetric diblock copolymers such as $PSMA_{14}$-$PNMEP_{1000}$. Increasing the solids content to 15% w/w enabled access to higher order morphologies. A phase diagram was constructed that enabled pure spheres, worms and vesicles to be reproducibly targeted. $PSMA_{14}$-$PNMEP_{49}$ spherical nanoparticles were also evaluated as potential Pickering emulsifiers. Water-in-oil Pickering emulsions were formed when a low shear rate (hand-shaking) was employed or if a volume fraction of 75% particles in *n*-dodecane and only 25% water was used. However, oil-in-water Pickering emulsions were also formed when emulsification was conducted using a high shear rate (≥ 3,500 rpm). This unexpected result suggested that the hydrophobic $PSMA_{14}$-$PNMEP_{49}$ spherical nanoparticles invert under high shear to form hydrophilic $PNMEP_{49}$-$PSMA_{14}$ spherical nanoparticles.

3.5 References

(1) Houillot, L.; Bui, C.; Save, M.; Charleux, B.; Farcet, C.; Moire, C.; Raust, J.-A.; Rodriguez, I. *Macromolecules* **2007**, *40*, 6500.
(2) Fielding, L. A.; Derry, M. J.; Ladmiral, V.; Rosselgong, J.; Rodrigues, A. M.; Ratcliffe, L. P.; Sugihara, S.; Armes, S. P. *Chemical Science* **2013**, *4*, 2081.
(3) Fielding, L. A.; Lane, J. A.; Derry, M. J.; Mykhaylyk, O. O.; Armes, S. P. *Journal of the American Chemical Society* **2014**, *136*, 5790.
(4) Derry, M. J.; Fielding, L. A.; Armes, S. P. *Polymer Chemistry* **2015**, *6*, 3054.
(5) Houillot, L.; Bui, C.; Farcet, C.; Moire, C.; Raust, J.-A.; Pasch, H.; Save, M.; Charleux, B. *Acs Applied Materials & Interfaces* **2010**, *2*, 434.
(6) Raust, J.-A.; Houillot, L.; Save, M.; Charleux, B.; Moire, C.; Farcet, C.; Pasch, H. *Macromolecules* **2010**, *43*, 8755.
(7) Lopez-Oliva, A. P.; Warren, N. J.; Rajkumar, A.; Mykhaylyk, O. O.; Derry, M. J.; Doncom, K. E.; Rymaruk, M. J.; Armes, S. P. *Macromolecules* **2015**, *48*, 3547.
(8) Pei, Y.; Thurairajah, L.; Sugita, O. R.; Lowe, A. B. *Macromolecules* **2015**, *48*, 236.
(9) Pei, Y.; Sugita, O. R.; Thurairajah, L.; Lowe, A. B. *RSC Advances* **2015**, *5*, 17636.
(10) Pei, Y.; Noy, J.-M.; Roth, P. J.; Lowe, A. B. *Journal of Polymer Science Part A: Polymer Chemistry* **2015**, *53*, 2326.
(11) Derry, M. J.; Fielding, L. A.; Warren, N. J.; Mable, C. J.; Smith, A. J.; Mykhaylyk, O. O.; Armes, S. P. *Chemical Science* **2016**, *7*, 5078.

(12) Cunningham, V. J.; Armes, S. P.; Musa, O. M. *Polymer Chemistry* **2016**, *7*, 1882.
(13) Trent, J. S. *Macromolecules* **1984**, *17*, 2930.
(14) Brown, S. L.; Rayner, C. M.; Perrier, S. *Macromolecular Rapid Communications* **2007**, *28*, 478.
(15) Lobb, E. J.; Ma, I.; Billingham, N. C.; Armes, S. P.; Lewis, A. L. *Journal of the American Chemical Society* **2001**, *123*, 7913.
(16) Beuermann, S.; Buback, M. *Progress in Polymer Science* **2002**, *27*, 191.
(17) Haaf, F.; Sanner, A.; Straub, F. *Polymer Journal* **1985**, *17*, 143.
(18) Truong, N. P.; Dussert, M. V.; Whittaker, M. R.; Quinn, J. F.; Davis, T. P. *Polymer Chemistry* **2015**, *6*, 3865.
(19) Sugihara, S.; Blanazs, A.; Armes, S. P.; Ryan, A. J.; Lewis, A. L. *Journal of the American Chemical Society* **2011**, *133*, 15707.
(20) Semsarilar, M.; Jones, E. R.; Blanazs, A.; Armes, S. P. *Advanced Materials* **2012**, *24*, 3378.
(21) Blanazs, A.; Ryan, A. J.; Armes, S. P. *Macromolecules* **2012**, *45*, 5099.
(22) Zhang, L.; Eisenberg, A. *Polymers for Advanced Technologies* **1998**, *9*, 677.
(23) Mai, Y.; Eisenberg, A. *Chemical Society Reviews* **2012**, *41*, 5969.
(24) Blanazs, A.; Madsen, J.; Battaglia, G.; Ryan, A. J.; Armes, S. P. *Journal of the American Chemical Society* **2011**, *133*, 16581.
(25) Warren, N. J.; Mykhaylyk, O. O.; Mahmood, D.; Ryan, A. J.; Armes, S. P. *Journal of the American Chemical Society* **2014**, *136*, 1023.
(26) Thompson, K.; Mable, C.; Cockram, A.; Warren, N.; Cunningham, V.; Jones, E.; Verber, R.; Armes, S. *Soft Matter* **2014**, *10*, 8615.
(27) Thompson, K.; Fielding, L.; Mykhaylyk, O.; Lane, J.; Derry, M.; Armes, S. *Chemical Science* **2015**, *6*, 4207.
(28) Thompson, K. L.; Mable, C. J.; Lane, J. A.; Derry, M. J.; Fielding, L. A.; Armes, S. P. *Langmuir* **2015**, *31*, 4137.

Chapter 4

Poly(*N*-2-(methacryloyloxy)ethyl pyrrolidone)-poly(benzyl methacrylate) diblock copolymer nano-objects via RAFT alcoholic dispersion polymerisation

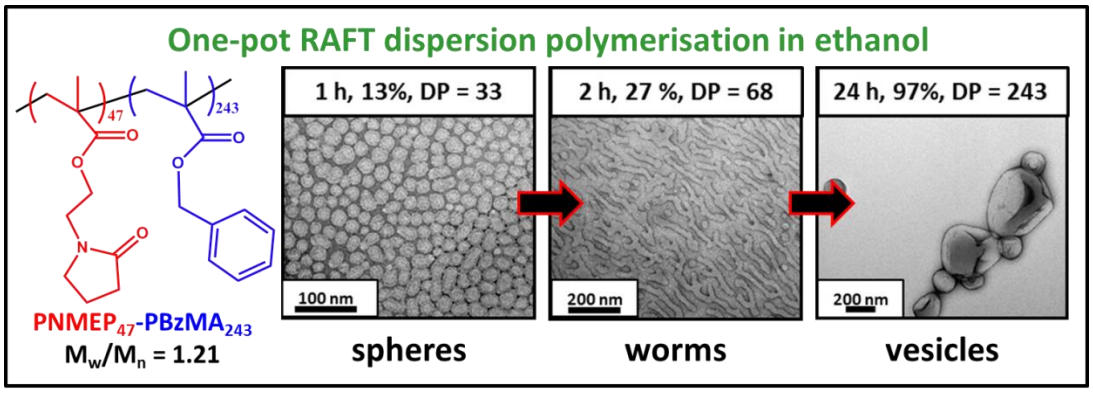

4.1 Introduction

RAFT PISA has enabled the synthesis of various nano-objects. Research groups led by Pan,[1-3] Lowe,[4-6] Zhang,[7-9] Charleux[10] and Armes[11-15] have reported papers in this field, using various lower alcohols as the continuous phase.

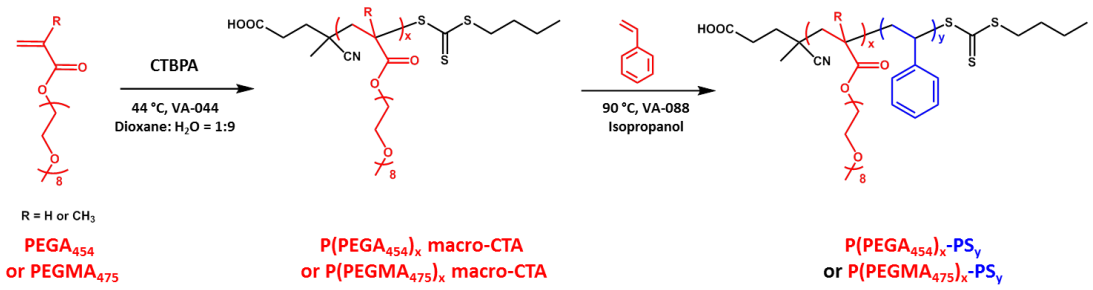

Figure 4.1 Schematic representation of the synthesis of $P(PEGA_{454})_x$-PS_y and $P(PEGMA_{475})_x$-PS_y diblock copolymers via RAFT dispersion polymerisation in isopropanol.[16]

Perrier and co-workers recently described the RAFT alcoholic dispersion polymerisation of styrene in isopropanol (see Figure 4.1).[16] Two trithiocarbonate macro-CTAs were prepared; poly(ethylene glycol) methyl ether acrylate ($P(PEGA_{454})$) and poly(ethylene glycol) methyl ether methacrylate ($P(PEGMA_{475})$). These two macro-CTAs were each chain-extended with 2000 units of styrene in isopropanol at 90 °C (although the boiling point of isopropanol is ~ 83 °C). Only relatively low final conversions of 30 to 50 % were achieved after 72 h. GPC analysis indicated increasing molecular weight with conversion, but the dispersity of the diblock copolymers increased with conversion (final $M_w/M_n > 1.50$). Despite the incomplete conversions both $P(PEGMA_{475})_{20}$-PS_x and $P(PEGA_{454})_{21}$-PS_x diblock copolymers exhibited a gradual evolution of copolymer morphology from spherical micelles to worms to vesicles (and large compound vesicles) with increasing styrene conversion. However, utilising a slightly longer $P(PEGA_{454})_{75}$ or $P(PEGMA_{475})_{75}$ macro-CTA only led to kinetically-trapped spherical micelles.

Zhang and co-workers prepared a poly(ethylene glycol) trithiocarbonate (PEG-TTC) macro-CTA by esterification of monohydroxy-PEG with the carboxylic group of DDMAT (see Figure 4.2 for structure).[9] This PEG_{45}-TTC macro-CTA was chain-extended by copolymerising 4-vinylpyridine (4VP) and styrene (S) in an 80/20 ethanol/water solvent mixture. The styrene to 4VP molar ratio was varied and this statistical copolymerisation was compared to the homopolymerisation of styrene

alone. The copolymerisation led to more than 83% comonomer conversion after 36 h at 70 °C. High blocking efficiencies and low dispersities ($M_w/M_n \leq 1.23$) were observed by GPC analysis. Increasing amounts of styrene led to higher order morphologies (see TEMs in Figure 4.2).[9] TEM analysis at various time points throughout the synthesis of PEG_{45}-P($4VP_{87}$-S_{282}) indicated a gradual evolution in morphology from spheres to worms to lamellae and finally vesicles. For a fixed core-forming DP, both homopolystyrene and a 75 mol% styrene copolymer were prepared and their morphologies compared. PEG_{45}-PS_x diblock copolymers went to at least 97% conversion in 24 h and formed vesicles when targeting $x \geq 100$, whereas an overall core-forming block DP of 369 was required for the PEG_{45}-P($4VP_x$-S_{3x}) diblock copolymers to form vesicles. These observations illustrate how subtle changes in the solvophilic/solvophobic balance within the block copolymers can have a dramatic effect on the final copolymer morphology.

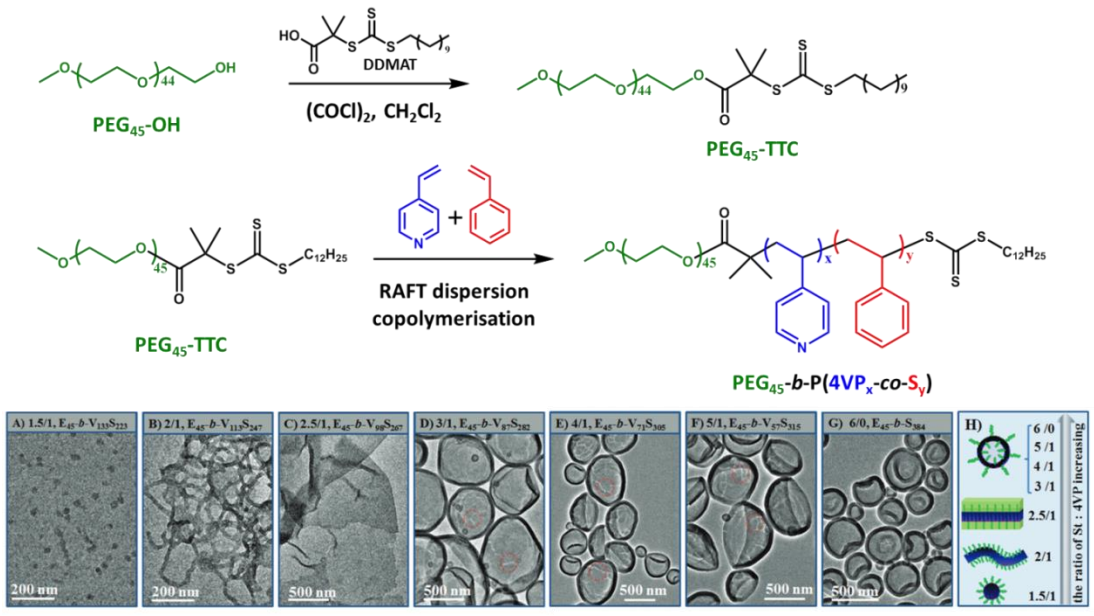

Figure 4.2 Schematic representation for the synthesis of PEG_{45}-*b*-P($4VP_x$-*co*-S_y) diblock copolymers via RAFT dispersion copolymerisation and TEM images of the various resulting morphologies reported by Zhang and co-workers.[9]

Zehm et al. examined the polymerisation of benzyl methacrylate using either a poly(2-hydroxyethyl methacrylate) (PHEMA) macro-CTA or a PHPMA macro-CTA in either methanol, ethanol or isopropanol at 65 °C.[17] Greater than 90% conversions were achieved for all diblock copolymers, typically within 24 h. GPC analysis of the $PHEMA_{62}$-$PBzMA_x$ and $PHPMA_{48}$-$PBzMA_x$ diblock copolymers confirmed high blocking efficiencies and relatively low final dispersities ($M_w/M_n \leq 1.26$). The

PHEMA-PBzMA diblock copolymers proved to be colloidally unstable when prepared in ethanol but preparation in methanol led to various morphologies. However, only mixed phases could be obtained. In contrast, using a PHPMA macro-CTA led to pure spheres, worms or vesicles using either ethanol or isopropanol as the reaction solvent. A phase diagram was constructed for $PHPMA_{48}$-$PBzMA_x$ diblock copolymers prepared in ethanol (Figure 4.3).

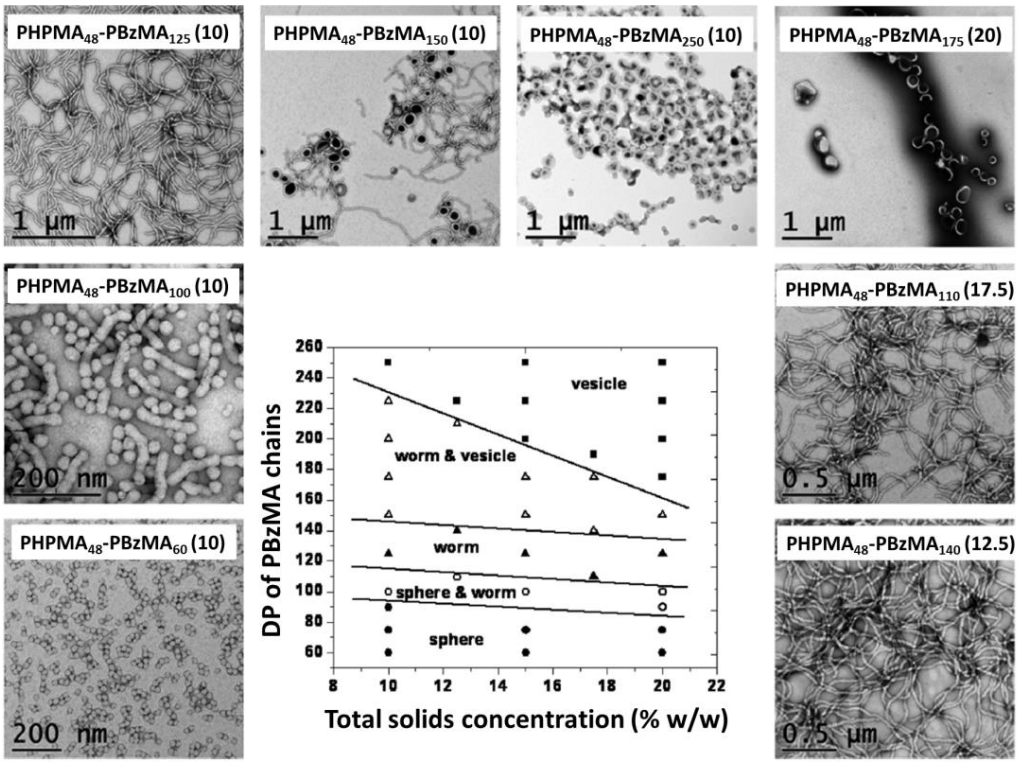

Figure 4.3 Phase diagram and corresponding TEM images for $PHPMA_{48}$-$PBzMA_x$ diblock copolymers prepared in ethanol reported by Zehm and co-workers.[17]

There are no reports of one-pot synthesis of diblock copolymers via RAFT alcoholic dispersion polymerisation. This would involve the synthesis of a solvophilic macro-CTA at close to full conversion with subsequent addition of a second monomer without purification. Zehm et al. synthesised both the PHPMA macro-CTA and PHPMA-PBzMA diblock copolymers in ethanol, so there is potential for a one-pot synthesis via RAFT alcoholic dispersion polymerisation. Several other RAFT dispersion polymerisations have been performed as one-pot syntheses. For example, Ratcliffe et al. described the synthesis of PGMA-PHPMA diblock copolymers via a one-pot aqueous PISA formulation.[18] Similarly, Derry et al. prepared PLMA-PBzMA spherical nanoparticles via a one-pot PISA synthesis in mineral oil.[19]

In this Chapter, a series of poly(*N*-(2-methacryloyloxy)ethyl pyrrolidone) (PNMEP) homopolymers are prepared via RAFT solution polymerisation in ethanol. Kinetics of the PNMEP syntheses are evaluated with respect to both the PNMEP DP and the CTA/initiator molar ratio. A $PNMEP_{50}$ macro-CTA is then prepared and chain-extended with benzyl methacrylate in ethanol via RAFT alcoholic dispersion polymerisation. The resulting PNMEP-PBzMA diblock copolymers are analysed by ^{1}H NMR, GPC and TEM. Finally, a one-pot synthesis of a PNMEP-PBzMA diblock copolymer was briefly examined.

4.2 Experimental Details

4.2.1 Materials

NMEP was kindly donated by Ashland Specialty Ingredients (New Jersey, USA). BzMA and ACVA were purchased from Sigma-Aldrich (Dorset, UK). CPDB was purchased from Strem Chemicals Ltd. (Cambridge, UK). d_4-Methanol was purchased from Goss Scientific Instruments Ltd (Cheshire, UK) and *d*-chloroform was purchased from VWR chemicals (UK). All other solvents were purchased from Fisher Scientific (Loughborough, UK). All chemicals were used as received.

4.2.2 Kinetics of the RAFT solution homopolymerisation of NMEP in ethanol

A typical protocol for the RAFT solution homopolymerisation of NMEP when targeting $PNMEP_{100}$ was conducted as follows. NMEP (4.6473 g, 23.563 mmol), CPDB RAFT agent (0.0499 g, 0.225 mmol; target DP = 100), ACVA (12.5 mg, 44.598 µmol; CPDB/ACVA molar ratio = 5.0) and ethanol (6.9540 g, 40% w/w) were weighed into a 28 ml vial. The reaction solution was stirred and degassed in an ice bath for 30 min before being placed in an oil bath at 70 °C. The polymerisation was sampled every 30 min for the first 4 h and then every 1 h for a total of 10 h. Each aliquot was analysed by ^{1}H NMR spectroscopy and DMF GPC. A range of other $PNMEP_x$ homopolymers were prepared by either varying the CPDB/ACVA molar ratio or the CPDB/NMEP molar ratio.

4.2.3 Preparation of $PNMEP_{50}$ macro-CTA

NMEP (33.4012 g, 0.17 mol), CPDB RAFT agent (1.0006 g, 4.52 mmol; target DP = 45), ACVA (337.8 mg, 1.21 mmol; CPDB/ACVA molar ratio = 3.0) and ethanol (22.2815 g, 60% w/w solids) were weighed into a 250 ml round-bottom flask. The reaction solution was stirred and degassed in an ice bath for 45 min before being placed in an oil bath at 70 °C. The polymerisation proceeded for 5.75 h, resulting in a monomer conversion of 91 % as judged by ^{1}H NMR. The crude homopolymer was purified by precipitating into a ten-fold excess of diethyl ether, redissolved in methanol, then the precipitation was repeated. The purified PNMEP macro-CTA was dissolved in the minimum volume of water and this concentrated aqueous solution was freeze-dried overnight to afford a pure PNMEP macro-CTA (< 1 % residual monomer). The mean DP was calculated to be 50 using ^{1}H NMR by comparing the integrated aromatic proton signals at 7 - 8 ppm to that of the methylene carbonyl proton signal at 2.5 ppm. DMF GPC analysis indicated a M_n of 8,000 g mol^{-1} and a M_w/M_n of 1.15 (vs. PMMA calibration standards).

4.2.4 Synthesis of $PNMEP_{50}$-$PBzMA_x$ diblock copolymers via RAFT alcoholic dispersion polymerisation of BzMA

A typical protocol for the synthesis of $PNMEP_{50}$-$PBzMA_{47}$ diblock copolymer nanoparticles was conducted as follows. $PNMEP_{50}$ macro-CTA (0.3607 g), BzMA (0.3124 g, 1.77 mmol; target DP = 50) and ACVA (2.0 mg, 7.13 μmol; macro-CTA/ACVA molar ratio = 5.0) were dissolved in ethanol (2.6948 g, 20% w/w) in a 14 ml vial. The reaction mixture was sealed and purged in an ice bath with nitrogen for 30 min, prior to immersion in an oil bath set at 70 °C for 24 h. The resulting crude copolymer was analysed by DMF GPC (M_n = 12,000 g mol^{-1}, M_w/M_n = 1.20). ^{1}H NMR spectroscopy analysis of the final reaction solution (diluted in $CDCl_3$) indicated 94 % BzMA conversion. Other diblock copolymer compositions were obtained by systematically adjusting the BzMA/$PNMEP_{50}$ molar ratio to give target PBzMA DPs ranging from 50 to 250.

4.2.5 One-pot protocol for the synthesis of $PNMEP_{47}$-$PBzMA_{243}$ diblock copolymer nano-objects

NMEP (4.6480 g, 0.024 mol), CPDB RAFT agent (0.1250 g, 0.565 mmol; target DP = 50), ACVA (42.1 mg, 0.150 mmol; CPDB/ACVA molar ratio = 3.0) and ethanol

(3.0844 g, 60% w/w solids) were weighed into a 28 ml vial. The reaction solution was stirred and degassed in an ice bath for 30 min before being placed in an oil bath at 70 °C. The polymerisation was sampled every 30 min for 4 h and sampled thereafter every 60 min up to 6 h, resulting in 97 % NMEP conversion and a DP of 47 for the PNMEP was determined by ^{1}H NMR. A portion of the crude $PNMEP_{47}$ macro-CTA solution (1.0002 g at 60% w/w solids) was diluted with a degassed mixture of BzMA (2.7832, 15.795 mmol), ACVA (0.0034 g, 0.121 mmol) and ethanol (7.5363 g, 30% w/w solids). The reaction mixture was sampled every 60 min for 10 h. Each aliquot was analysed by DMF GPC and ^{1}H NMR. A final BzMA conversion of 97% was obtained after 24 h at 70 °C.

The same protocol was followed for the synthesis of $PNMEP_{45}$-$PBzMA_{232}$ diblock copolymer nano-objects but the reaction was only sampled after 6 h, prior to the direct addition of BzMA, ACVA and ethanol (which had been degassed in ice for 30 minutes).

4.2.6 Copolymer characterisation

^{1}H NMR Spectroscopy

All ^{1}H NMR spectra were recorded using a 400 MHz Bruker Avance-400 spectrometer using either CD_3OD or $CDCl_3$.

Gel Permeation Chromatography (GPC)

The molecular weights and dispersities of the various PNMEP homopolymers and $PNMEP_{50}$-$PBzMA_x$ diblock copolymers were determined by DMF GPC at 60 °C (vs. PMMA standards). See Chapter 2, Section 2.2.10 for full details of the GPC set-up.

Transmission Electron Microscopy (TEM)

See Chapter 2, Section 2.2.10 for details.

Scanning Electron Microscopy (SEM).

SEM samples were imaged by Yin Ning. Samples were analysed using a FEI Inspect F scanning electron microscope at 10 kV. All samples were gold-coated for ~ 60 seconds using a current of 15 mA prior to imaging to prevent sample charging.

4.3 Results and Discussion

4.3.1 Kinetics of the RAFT solution homopolymerisation of NMEP

Compared to related pyrrolidone-functional monomers such as *N*-vinyl pyrrolidone,[20-25] there are rather few literature reports describing the RAFT polymerisation of NMEP.[26-28] Therefore a detailed study of the kinetics of the RAFT solution homopolymerisation of PNMEP in ethanol at 70 °C was conducted (Scheme 4.1). The NMEP concentration was fixed at 40% w/w solids in these experiments, while the RAFT CTA/initiator molar ratio and the target DP were systematically varied.

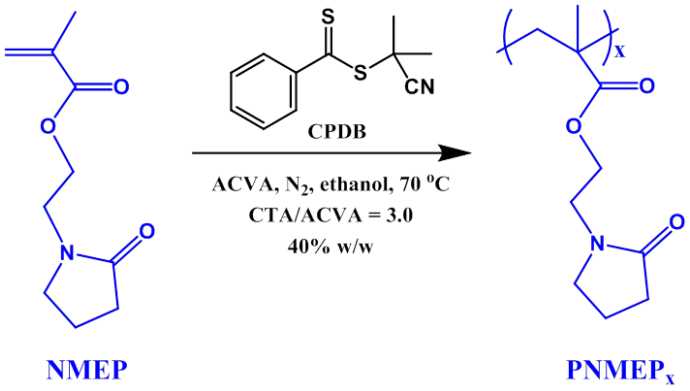

Scheme 4.1 Synthesis of a PNMEP homopolymer via RAFT solution polymerisation.

Initially, the PNMEP target DP was fixed at 100 in order to study the effect of systematically increasing the CPDB/ACVA molar ratio from 3.0 to 10.0. Each reaction was sampled every 30 min for the first 4 h and then every 60 min for 10 h. Each polymerisation was terminated after 24 h. Aliquots were analysed by ^{1}H NMR and DMF GPC. Figure 4.4a shows the monomer conversion versus time curves obtained when using four different CPDB/ACVA molar ratios. As expected, a CPDB/ACVA molar ratio of 3.0 resulted in a fast polymerisation rate, with greater than 90 % NMEP conversion observed within 8 h at 70 °C (and 98% conversion being achieved after 24 h). In contrast, a CPDB/ACVA molar ratio of 10.0 led to a much slower polymerisation: only 58% conversion was achieved after 10 h (and a final conversion of 72% after 24 h). CPDB/ACVA molar ratios of 5.0 or 7.0 gave intermediate behaviour. Figure 4.4a illustrates the longer induction times observed when employing higher CPDB/ACVA molar ratios. Figure 4.4b, shows the corresponding semi-logarithmic plots obtained for the four sets of kinetic data when

targeting $PNMEP_{100}$ with different CPDB/ACVA molar ratios. After the initial induction period, first order kinetics with respect to monomer are observed, with higher pseudo-first order rate constants being obtained for lower CPDB/ACVA molar ratios. In each case, deviations from linearity occur prior to full conversion.

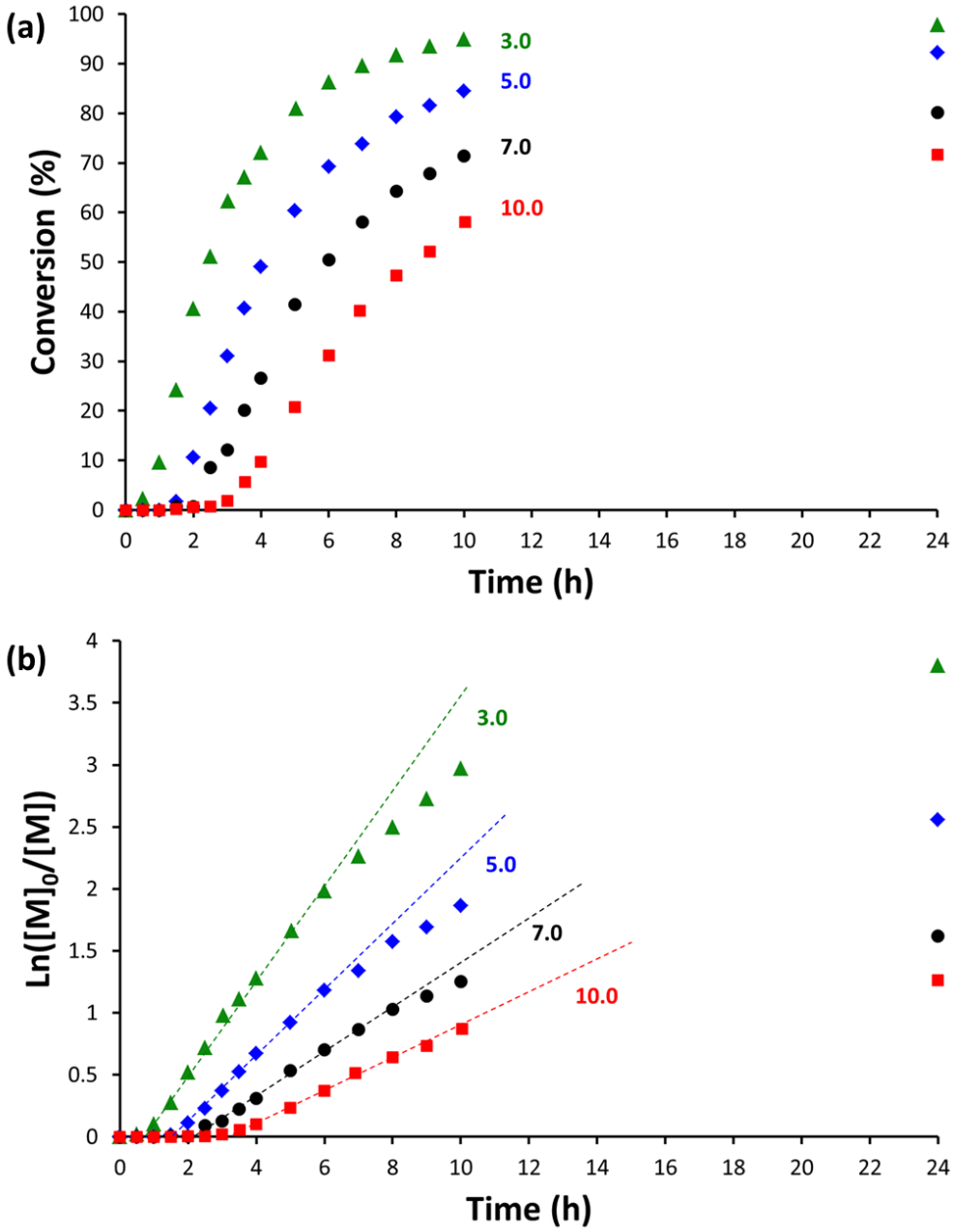

Figure 4.4 Kinetics of the RAFT solution polymerisation of NMEP in ethanol at 40% w/w solids and 70 °C. (a) Conversion vs. time curves and (b) corresponding semi-logarithmic plots obtained when targeting $PNMEP_{100}$ using CPDB/ACVA molar ratios of 3.0, 5.0, 7.0 and 10.0. Pseudo-first order rate constants calculated for the initial linear regimes are 1.08 x 10^{-4} s^{-1} (3.0), 7.42 x 10^{-5} s^{-1} (5.0), 4.94 x 10^{-5} s^{-1} (7.0) and 3.48 x 10^{-5} (10.0), where the numbers in brackets refer to the CPDB/ACVA molar ratio in each case.

Figure 4.5 shows the DMF GPC data for the same four sets of $PNMEP_{100}$ kinetic data. A linear increase in M_n with NMEP conversion is observed, as expected for a well-controlled RAFT polymerisation.[29] Relatively low dispersities are obtained throughout each polymerisation, with final dispersities of less than 1.26. This is perhaps surprising for the relatively low CPDB/ACVA molar ratio of 3.0 since it is well-known that higher initiator concentrations can often lead to a lack of control.[2,30]

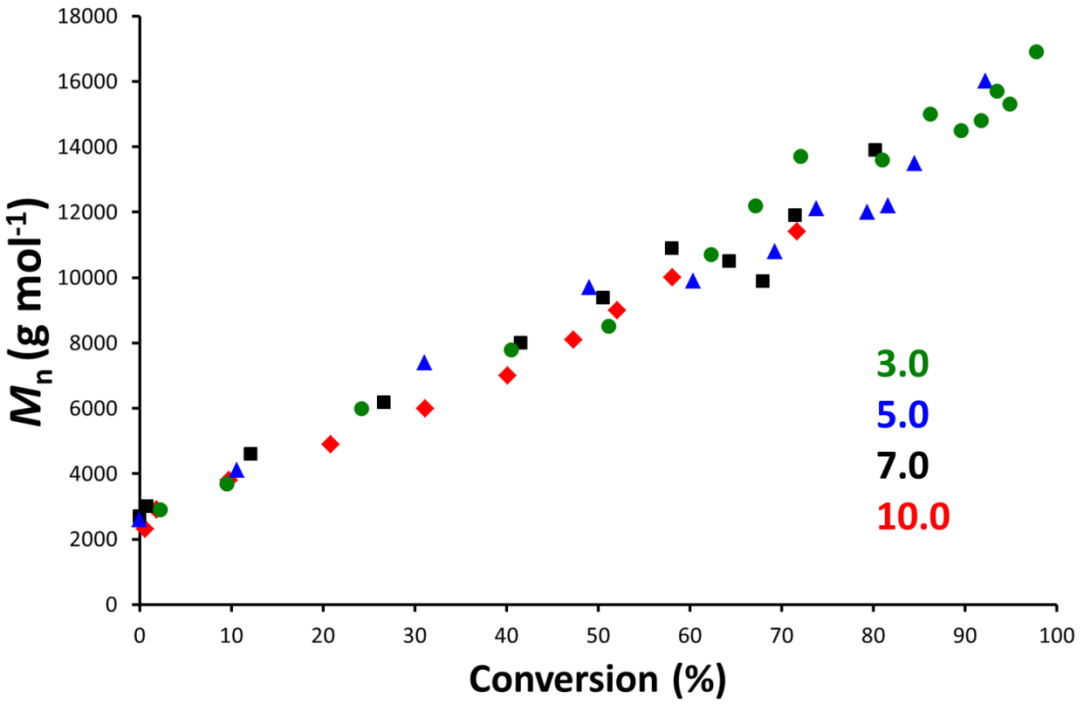

Figure 4.5 Number-average molecular weight data (M_n) obtained from DMF GPC analysis during the RAFT solution polymerisation of NMEP in ethanol at 70 °C. Conditions: NMEP concentration 40 % w/w; target DP = 100; CPDB/ACVA molar ratios = 3.0 (green), 5.0 (blue), 7.0 (black) and 10.0 (red).

The effect of varying the target PNMEP DP on the homopolymerisation kinetics in ethanol at 40% w/w solids, 70 °C and utilising a constant CPDB/ACVA molar ratio of 5.0 was studied. Four PNMEP DPs were targeted, ranging from 70 to 400. Aliquots were taken from the polymerisation solution every 30 min for the first 4 h and then every 60 min for 10 h. Figure 4.6a shows the four monomer conversion versus time curves. In each case, an induction period of approximately 1 h is observed. When targeting a PNMEP DP of 70 or 100, greater than 90% conversion was achieved after 24 h, whereas higher target PNMEP DPs led to somewhat lower conversions. DMF GPC was used to assess the evolution of molecular weight during these polymerisations, see Figure 4.6b. In each case a linear increase in molecular weight with conversion was observed. As expected, the target PNMEP DP of 400

exhibits the highest final M_n, with an appropriate reduction in M_n being observed when targeting the lower PNMEP DPs.

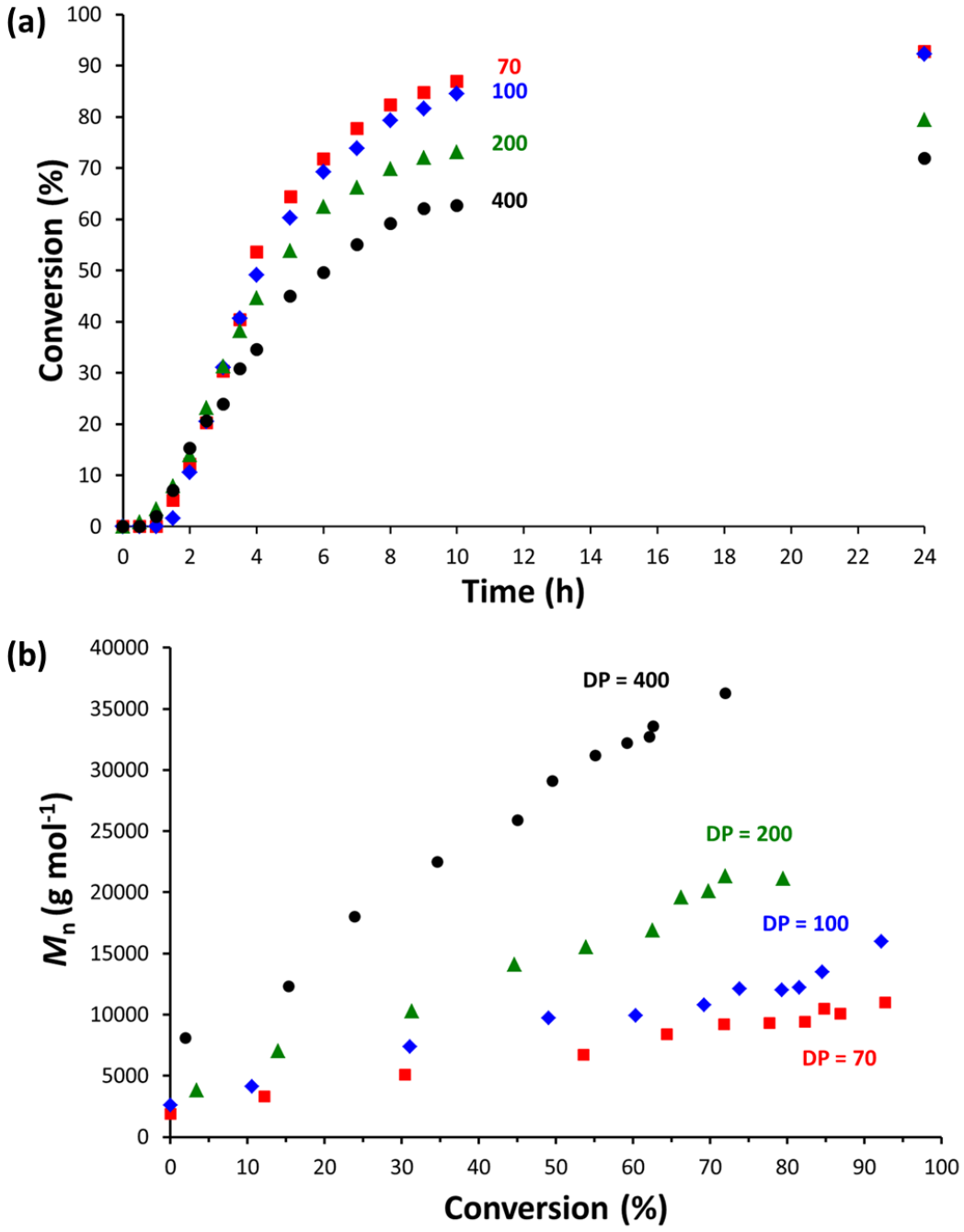

Figure 4.6 (a) Conversion versus time plot obtained for the RAFT solution polymerisation of NMEP at 70 °C for a CPDB/ACVA molar ratio of 5.0 at 40% w/w solids targeting a PNMEP DP (x) of 70, 100, 200 or 400. (b) Corresponding M_n vs. conversion plots for PNMEP$_{70}$, PNMEP$_{100}$, PNMEP$_{200}$ and PNMEP$_{400}$.

4.3.2 Synthesis of $PNMEP_{50}$-$PBzMA_x$ diblock copolymers via RAFT alcoholic dispersion polymerisation of BzMA

A PNMEP macro-CTA was synthesised by RAFT solution polymerisation targeting a DP of 45, at 60% w/w solids and using a CPDB/ACVA molar ratio of 3.0. BzMA conversion of 91% was achieved after 5h 45 min at 70 °C (as judged by ^{1}H NMR). After purification a PNMEP DP of 50 was determined by ^{1}H NMR and DMF GPC analysis indicated an M_n of 8,000 g mol^{-1} and dispersity of 1.15.

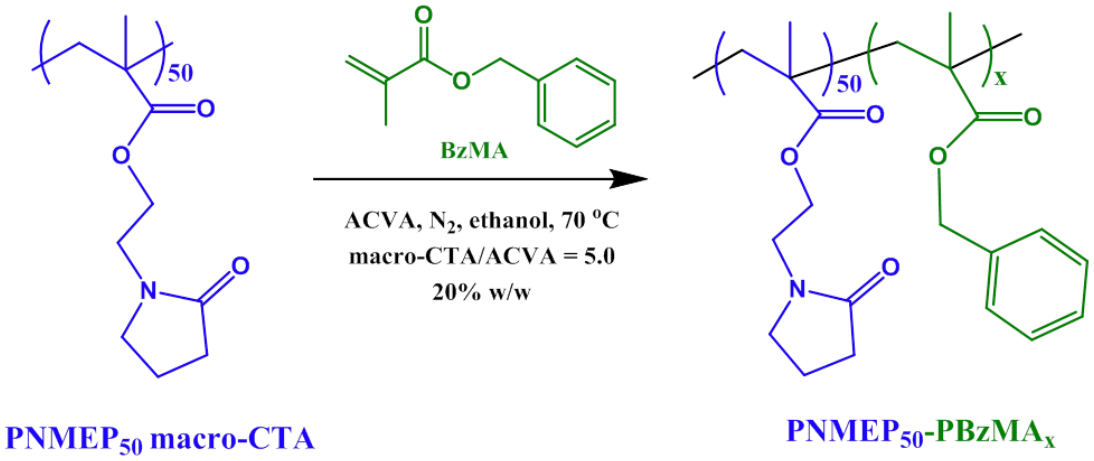

Scheme 4.2 Synthesis of $PNMEP_{50}$-$PBzMA_x$ diblock copolymers via RAFT alcoholic dispersion polymerisation in ethanol.

This $PNMEP_{50}$ macro-CTA was chain-extended with 200 units of BzMA via RAFT alcoholic dispersion polymerisation in ethanol at 70 °C, Scheme 4.2. Aliquots of the reaction mixture were taken every hour for the first 12 h and the reaction was stopped after 24 h. Each aliquot was analysed by ^{1}H NMR and GPC. Plotting BzMA conversion against time (Figure 4.7a) shows high conversions of 90% are achieved within 12 h, with a final conversion of 94% after 24 h. The semi-logarithmic plot has three distinct phases. For the first 5 h, pseudo-first order kinetics are followed, after this an increase in the rate is observed. This new polymerisation rate is followed linearly up to 10 h. A similar rate enhancement has been reported previously for the synthesis of diblock copolymers via RAFT PISA. However, this is most often associated with the nucleation of micelles. These micelles offer a locally high concentration of monomer resulting in an increase in the rate of polymerisation.[31-33] For the $PNMEP_{50}$-$PBzMA_{200}$ synthesis, the formation of nascent nanoparticles are observed at conversions of ~ 35% after just 3 h. As such the cause of the rate enhancement after 5 h is unclear. It is worth noting that a rate enhancement which

does not correspond with the onset of nucleation has also been observed by Lopez-Oliva for the synthesis of PDMS-PBzMA diblock copolymers prepared via RAFT dispersion polymerisation in *n*-heptane and by Jones et al. for the synthesis of PDMA-PBzMA diblock copolymers in ethanol.[15,34]

DMF GPC analysis of the samples taken during the polymerisation indicated a linear increase in molecular weight with conversion (Figure 4.7b), indicating a well-controlled polymerisation. The dispersity of the sample remains low throughout the BzMA polymerisation, with a final dispersity of 1.17 after 24 h (94% conversion), with no evidence of homopolymer contamination.

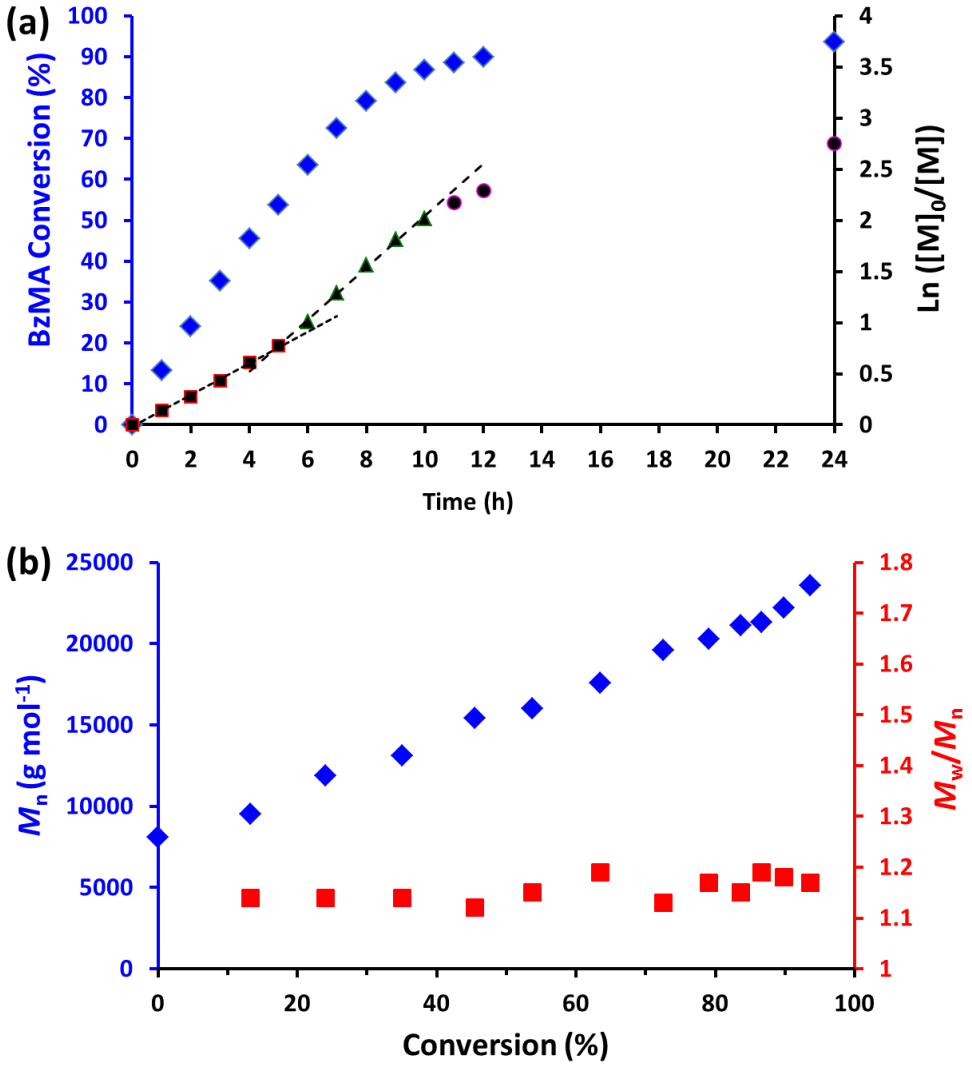

Figure 4.7 Kinetic and GPC data obtained during the RAFT alcoholic dispersion polymerisation of BzMA at 70 °C targeting PNMEP$_{50}$-PBzMA$_{200}$ at 20% w/w solids using a macro-CTA/ACVA molar ratio of 5.0: (a) conversion vs. time curve and corresponding semi-logarithmic plots as determined by ^{1}H NMR analysis in CDCl$_3$; (b) evolution of M_n (blue axis) and M_w/M_n (red axis) with conversion.

A series of $PNMEP_{50}$-$PBzMA_x$ diblock copolymers were prepared. The target PBzMA DP was varied from 50 to 250, using a fixed macro-CTA/initiator molar ratio of 5.0 and an overall solids content of 20% w/w. Reactions were allowed to proceed for 24 h at 70 °C. See Table 4.1 for details of each reaction.

Table 4.1 Conversions, solids content, molecular weights (M_n), dispersities (M_w/M_n), mean particle diameter and morphology obtained for $PNMEP_{50}$-$PBzMA_x$ (N_{50}-B_x) diblock copolymer nanoparticles and the corresponding $PNMEP_{50}$ macro-CTA.

	Block composition	Solids content (% w/w)	Conversion[a] (%)	DMF GPC		Morphology
				M_n[b] (g mol^{-1})	M_w/M_n[b]	
1	N_{50}	60	91	8,000	1.15	-
2	N_{50}-B_{47}	20	94	12,000	1.20	Spheres[c]
3	N_{50}-B_{69}	20	93	13,100	1.20	Spheres[c]
4	N_{50}-B_{93}	20	93	14,400	1.21	Spheres[c] (+ short worms)
5	N_{50}-B_{115}	20	94	16,400	1.21	Worms[d]
6	N_{50}-B_{144}	20	96	17,900	1.24	Worms[d]
7	N_{50}-B_{158}	20	90	19,700	1.20	Worms[d] (+ vesicles)
8	N_{50}-B_{188}	20	94	21,200	1.23	Vesicles[c]
9	N_{50}-B_{233}	20	93	24,100	1.25	Vesicles[c]

a. Monomer conversion determined by ^{1}H NMR spectroscopy in *d*-chloroform except for entry 1 where d_4-methanol was used
b. Determined by DMF GPC using a series of near-monodisperse PMMA calibration standards
c. Determined by TEM
d. Determined by SEM

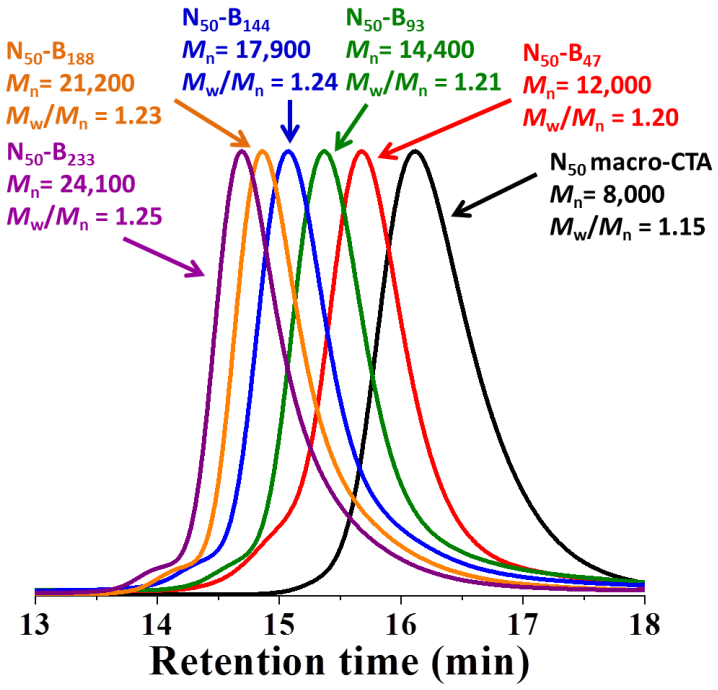

Figure 4.8 DMF GPC chromatograms for $PNMEP_{50}$-$PBzMA_x$ diblock copolymers prepared at 20% w/w solids via RAFT alcoholic dispersion polymerisation in ethanol.

All polymerisations went to high conversions of at least 90%. DMF GPC analysis shows an increase in molecular weight with PBzMA DP. Figure 4.8 shows high blocking efficiency from the $PNMEP_{50}$ macro-CTA, with no residual peak at low molecular weight. Relatively low dispersities of 1.25 or less were obtained, indicating the formation of well-defined $PNMEP_{50}$-$PBzMA_x$ diblock copolymers.

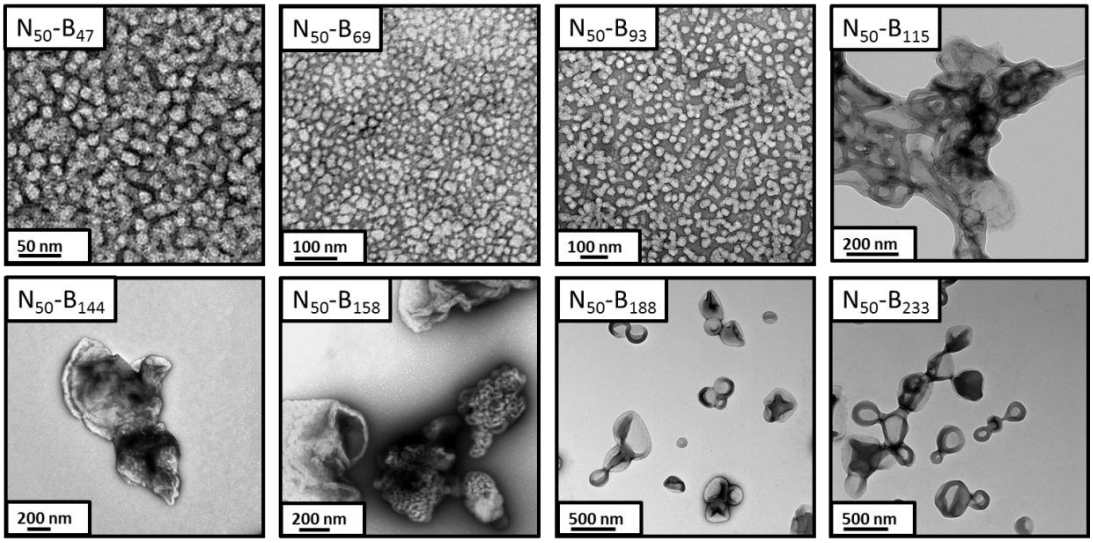

Figure 4.9 TEM images of the $PNMEP_{50}$-$PBzMA_x$ nano-objects prepared via RAFT dispersion polymerisation of BzMA at 70 °C in ethanol at 20% w/w solids (where N = PNMEP and B = PBzMA).

The $PNMEP_{50}$-$PBzMA_x$ diblock copolymers showed an increase in turbidity with target PBzMA DP at 20% w/w solids. A free-flowing liquid was obtained for the PBzMA DPs of less than 100, whereas a brittle paste was observed between DP 100 and 188. Each $PNMEP_{50}$-$PBzMA_x$ diblock copolymer was diluted to 0.20% w/w in ethanol to be analysed by TEM (Figure 4.9). Spherical micelles were observed for PNMEP DPs of less than 100. Unfortunately, the paste-like nature of many samples ($PNMEP_{50}$-$PNMEP_{115\text{-}188}$) led to aggregates which could not be completely dispersed in ethanol (even after 24 h of magnetic stirring). These proved difficult to image by TEM and large worm-like clusters were observed. As an alternative to TEM, SEM was employed to see if this could help identify the morphology of these diblock copolymers (Figure 4.10). SEM revealed highly anisotropic worms with mean worm widths of 96 nm and worm lengths ranging from 1 μm to 6 μm. However, these were extremely rigid worms and more rod-like compared to the flexible worms usually obtained by RAFT PISA.[35] This perhaps explains the brittle paste-like nature of these diblock copolymers compared to the soft worm-gels for PGMA-PHPMA diblock

copolymers. Both $PNMEP_{50}$-$PBzMA_{115}$ and $PNMEP_{50}$-$PBzMA_{144}$ resulted in a pure worm (rod) morphology, the $PNMEP_{50}$-$PBzMA_{158}$ diblock copolymer comprised of a mixed worm and vesicle phase. Similarly to when imaged by TEM a few clusters were also observed in the SEM images. For block compositions where the PBzMA DP was at least 188 or higher pure vesicles were obtained, Figure 4.9.

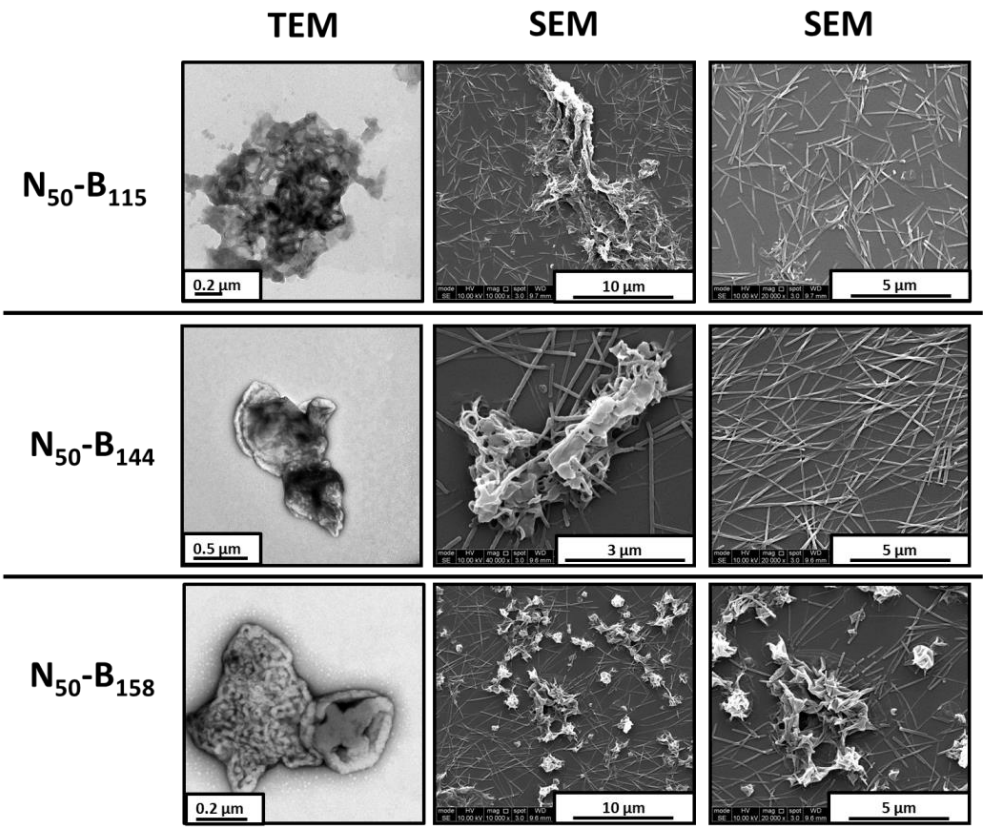

Figure 4.10 Representative TEM and SEM images obtained for $PNMEP_{50}$-$PBzMA_{115-158}$ (N_{50}-$B_{115-158}$) diblock copolymer worms.

4.3.3 Synthesis of $PNMEP_{50}$-$PBzMA_{250}$ diblock copolymer nano-objects via a one-pot protocol

Recently, several one-pot protocols have been reported for various PISA formulations.[18,19,36-38] Remarkably good results have been achieved despite adding the second monomer under monomer-starved conditions, which in principle might be expected to compromise RAFT chain-end fidelity. Therefore, the feasibility of a one-pot protocol was examined for the synthesis of PNMEP-PBzMA diblock copolymers.

Firstly, a PNMEP macro-CTA was prepared. A PNMEP DP of 50 was targeted, using a CPDB/ACVA molar ratio of 3.0 at 70 °C and 60% w/w solids. The reaction

was sampled every 30 minutes for 4 h and then every hour up to 6 h. Figure 4.11a shows both the conversion and semi-logarithmic plot versus time for this PNMEP macro-CTA synthesis. The reaction proceeds to 97% conversion within 6 h. An initial induction period of approximately 45 min is observed, after this pseudo-first order kinetics is followed up to greater than 90% conversion. ^{1}H NMR spectroscopy indicated a DP of 47 for the crude PNMEP macro-CTA. This unpurified macro-CTA was then chain-extended with 250 units of BzMA. Additional ethanol and initiator were added leading to a total solids content of 30% w/w. The reaction was sampled every hour for 10 h and then stopped after 24 h at 70 °C. Figure 4.11b shows the conversion versus time plot. A steady increase in BzMA conversion with time is obtained with a final BzMA conversion of 97% after 24 h. Each time point was also analysed by TEM (see Figure 4.11 inset). After just 1 h, spherical micelles were observed with a mean diameter of 21 ± 2 nm by TEM. This corresponds to a BzMA conversion of 13% and therefore a block composition of $PNMEP_{47}$-$PBzMA_{33}$. This indicates that a critical PBzMA DP of around 30 is required for micellar nucleation. This result is comparable to that reported by Jones et al. for the synthesis of a $PDMA_{31}$-$PBzMA_{37}$ diblock copolymer in ethanol at 70 °C.[11] After 2 h (27% conversion), a mixed phase of predominantly worm-like micelles plus a few spheres is observed. These worms have a mean thickness of 24 ± 3 nm. Taking experimental error into account, this is comparable to the mean diameter of the original spherical micelles, which suggests that worm formation involves multiple sphere-sphere fusion events. Similar observations have been reported for many other PISA formulations.[39-42] Finally, a pure vesicle phase was observed after 8 h (82% conversion), see Figure 4.11b. This corresponds to a mean PBzMA DP of 205 which is comparable to the DP of 188 required to produce vesicles when using the purified $PNMEP_{50}$ macro-CTA (see entry 8 in Table 1). The presence of residual monomer which is a good solvent for the PBzMA block could be causing this slight change in the block composition for each morphology. A pure vesicle phase was also observed after 24 h (97% conversion), when the BzMA polymerisation was terminated. This indicated a final block composition of $PNMEP_{47}$-$PBzMA_{243}$.

Both the $PNMEP_{47}$ macro-CTA synthesis and the RAFT dispersion polymerisation of BzMA were analysed by DMF GPC, see Figure 4.12. A linear increase in molecular weight with conversion is observed for both the RAFT solution

polymerisation and the RAFT dispersion polymerisation. The $PNMEP_{47}$ macro-CTA is well controlled with a final M_n of 7,700 g mol^{-1} and low dispersity of 1.15. The $PNMEP_{47}$-$PBzMA_{243}$ synthesis has a slight increase in dispersity with increasing BzMA conversion resulting in a final disperity of 1.21 and M_n of 23,600 g mol^{-1}.

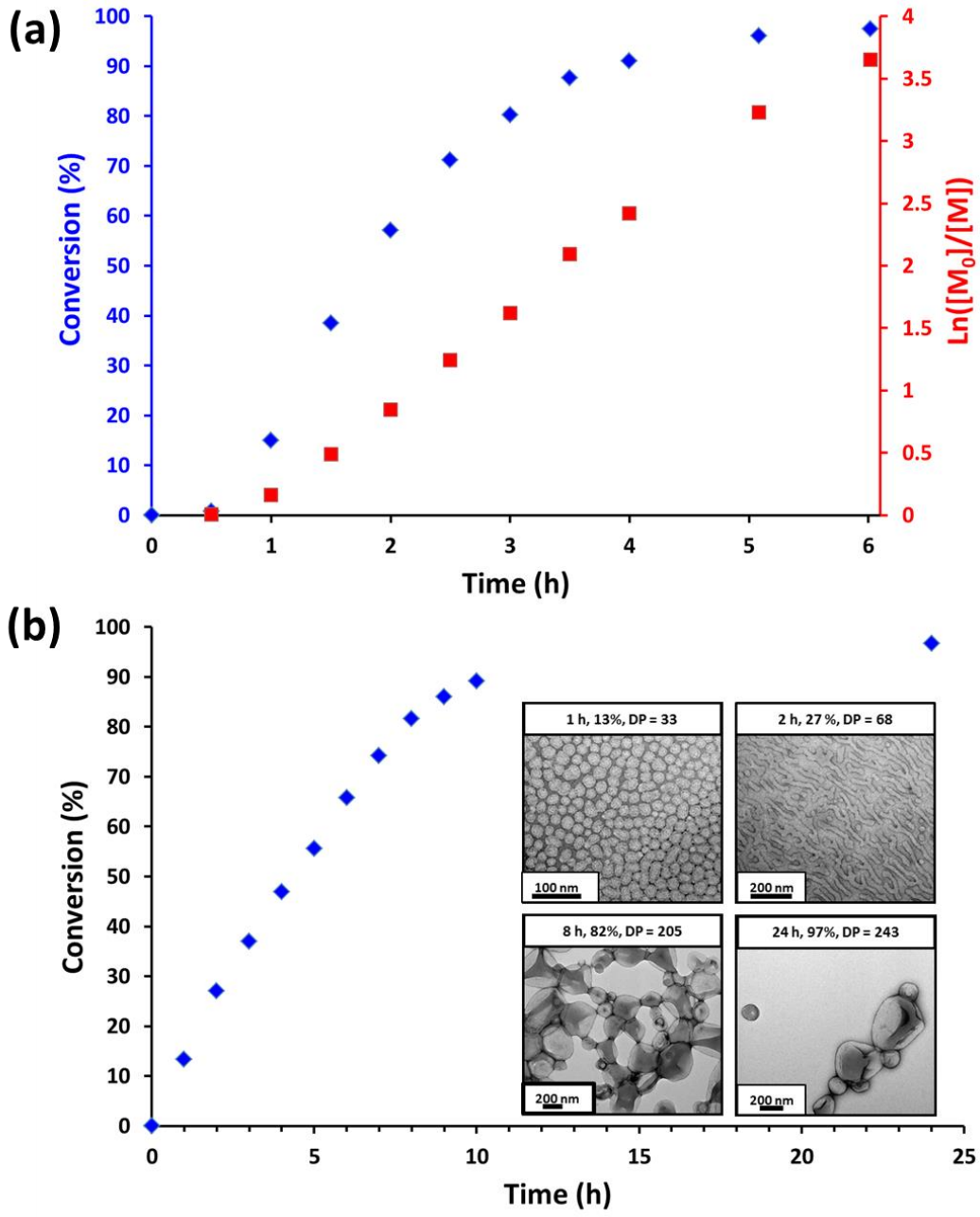

Figure 4.11 Kinetic data obtained for the one-pot two-step synthesis of $PNMEP_{47}$-$PBzMA_{243}$ diblock copolymer vesicles. (a) RAFT solution polymerisation of a $PNMEP_{47}$ macro-CTA at 60% w/w in ethanol at 70 °C, (b) RAFT alcoholic dispersion polymerisation of BzMA using this unpurified $PNMEP_{47}$ macro-CTA at 30% w/w solids and 70 °C in ethanol. Inset: representative TEM images obtained for the growing $PNMEP_{47}$-$PBzMA_{243}$ nano-objects after 1 h (13% BzMA conversion), 2 h (27% BzMA), 8 h (82% BzMA) and 24 h (97% BzMA).

Finally, to demonstrate a convenient one-pot synthesis without continuous sampling or quenching of the polymerisation, a $PNMEP_{50}$-$PBzMA_{250}$ diblock copolymer was targeted. Initially, a PNMEP macro-CTA was synthesised at 60% w/w solids at 70 °C. After 6 h, the reaction solution was sampled; ^{1}H NMR spectroscopy revealed 93% conversion and a mean PNMEP DP of 45. Then BzMA, ACVA and additional ethanol were degassed separately and added to the macro-CTA without stopping the reaction (resulting in approximately 30% w/w solids). This second-stage polymerisation was left for an additional 24 h at 70 °C. The BzMA polymerisation proceeded to high conversion (97% by ^{1}H NMR analysis), resulting in a final block composition of $PNMEP_{45}$-$PBzMA_{232}$.

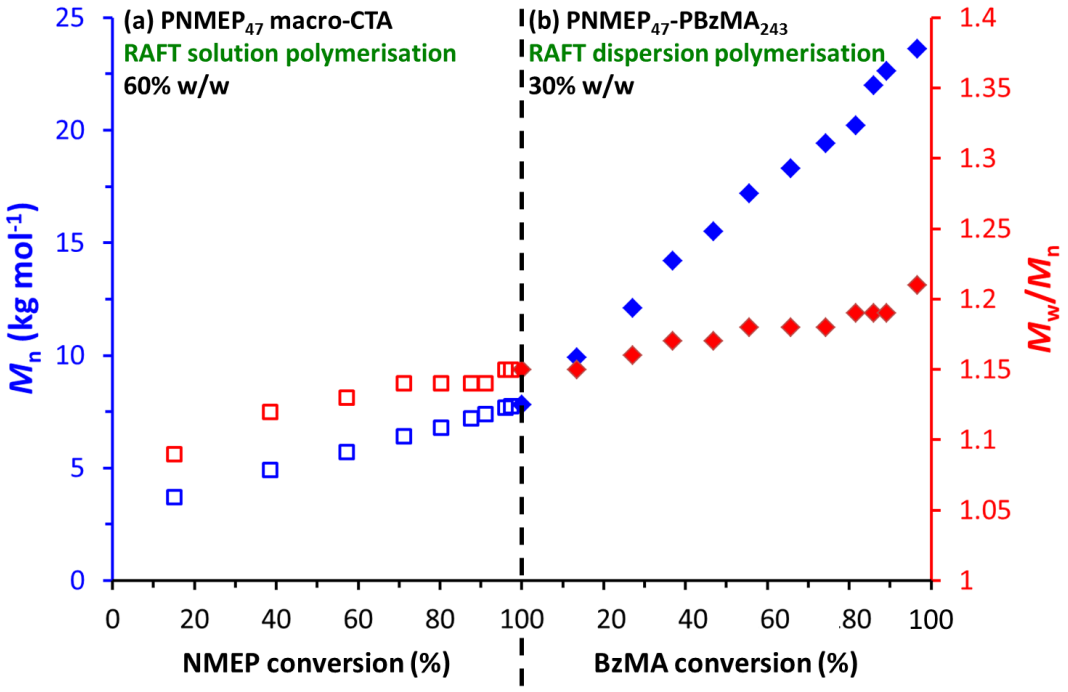

Figure 4.12 DMF GPC data obtained during the one-pot two-step synthesis of $PNMEP_{47}$-$PBzMA_{243}$ vesicles at 70 °C using a CTA/initiator molar ratio of 3.0. (a) Synthesis of $PNMEP_{47}$ macro-CTA via RAFT solution polymerisation of NMEP at 60% w/w solids, (b) synthesis of $PNMEP_{47}$-$PBzMA_{243}$ diblock copolymer vesicles via RAFT alcoholic dispersion polymerisation of BzMA at 30% w/w solids.

Both the $PNMEP_{45}$ macro-CTA and the $PNMEP_{45}$-$PBzMA_{232}$ diblock copolymer were analysed by DMF GPC (Figure 4.13). A high blocking efficiency was observed for the diblock copolymer with minimal macro-CTA contamination. This indicates high RAFT chain-end fidelity for the $PNMEP_{45}$ macro-CTA. Relatively low dispersities of 1.15 and 1.20 were achieved for the PNMEP macro-CTA and diblock copolymer, respectively. Despite a slightly different final diblock composition from

the two-step synthesis described above, very similar molecular weights were obtained by GPC analysis ($PNMEP_{45}$-$PNMEP_{232}$ M_n = 23,700 g mol^{-1} and $PNMEP_{47}$-$PNMEP_{243}$ M_n = 23,600 g mol^{-1}), indicating good reproducibility for this reaction. TEM analysis of the final $PNMEP_{45}$-$PBzMA_{232}$ diblock copolymer indicated a vesicular morphology (Figure 4.13 inset). These data indicate that well-defined PNMEP-PBzMA diblock copolymers can be synthesised via a convenient one-pot protocol.

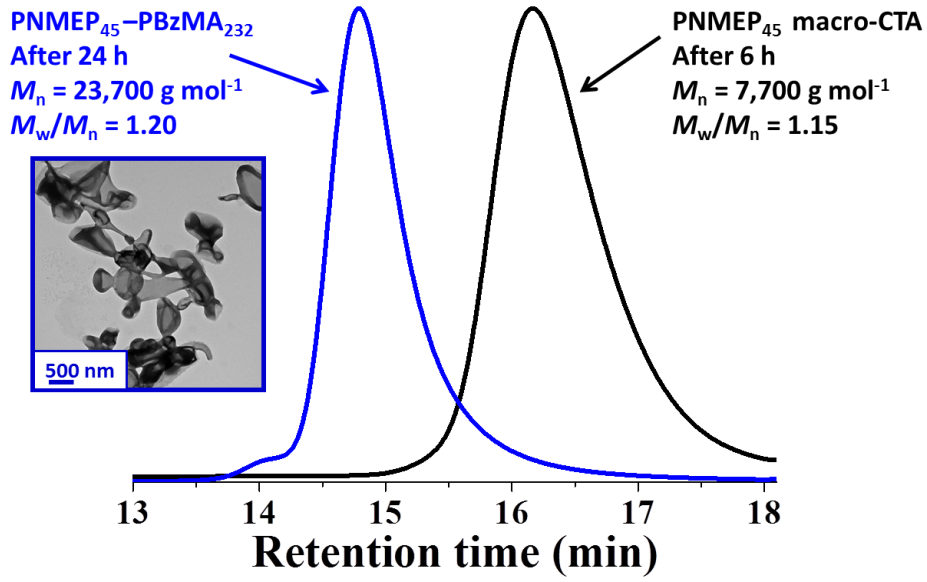

Figure 4.13 DMF GPC analysis of the one-pot synthesis of $PNMEP_{45}$-$PBzMA_{232}$ at 70 °C. The black trace shows the $PNMEP_{45}$ macro-CTA obtained after 6 h (93% conversion for an aliquot taken just before BzMA addition) synthesised using a CTA/initiator molar ratio of 3.0 at 60% w/w solids. The blue trace shows the $PNMEP_{45}$-$PBzMA_{232}$ diblock copolymer obtained after 24 h using a macro-CTA/initiator molar ratio of 5.0 at 30% w/w solids. Inset: TEM image obtained after 24 h, indicating a vesicular morphology.

4.4 Conclusions

A series of $PNMEP_x$ homopolymers were synthesised via RAFT solution polymerisation in ethanol at 70 °C. The PNMEP DP (x) and the CPDB/ACVA molar ratio was varied and the polymerisation kinetics were recorded in each case. The CPDB/ACVA molar ratio was varied from 3.0 to 10.0 and in each case a PNMEP DP of 100 was targeted. As expected, using a relatively low CPDB/ACVA molar ratio of 3.0 led to a faster rate of polymerisation than when using higher molar ratios of 5.0,

7.0 or 10.0. Despite this rather low CPDB/ACVA molar ratio, dispersities below 1.26 could be achieved. For a fixed CPDB/ACVA molar ratio of 5.0, the PNMEP DP was varied from 70 to 400. Increasing the PNMEP DPs led to reduced final conversions (from 93% to 72% after 24 h). All $PNMEP_x$ homopolymers exhibited a linear increase in molecular weight with conversion when analysed by DMF GPC. A $PNMEP_{50}$ macro-CTA was synthesised and chain-extended with BzMA via RAFT alcoholic dispersion polymerisation in ethanol at 70 °C. Kinetics of a $PNMEP_{50}$-$PBzMA_{200}$ diblock copolymer revealed that 94% monomer conversion can be achieved within 24 h at 70 °C. A series of $PNMEP_{50}$-$PBzMA_x$ diblock copolymers were prepared at 20% w/w solids and the PBzMA DP was systematically varied from 50 to 250. High BzMA conversions (at least 90%) were achieved and DMF GPC analysis of these $PNMEP_{50}$-$PBzMA_x$ diblock copolymers indicated high blocking efficiencies and increasing number-average molecular weights with target PNMEP DP. Low dispersities ($M_w/M_n \leq 1.25$) were also achieved, indicating well-defined block copolymers. Electron microscopy was used to assess the block copolymer morphology. Spheres, worms or vesicles were observed depending on the target PNMEP DP. Finally, a one-pot protocol was developed which enabled the synthesis of $PNMEP_{45}$-$PBzMA_{232}$ nanoparticles at 30% w/w solids. ^{1}H NMR analysis indicated 97% BzMA conversion for this diblock copolymer synthesis and TEM studies revealed a vesicular morphology.

4.5 References

(1) Wan, W. M.; Sun, X. L.; Pan, C. Y. *Macromolecular Rapid Communications* **2010**, *31*, 399.
(2) Wan, W.-M.; Pan, C.-Y. *Macromolecules* **2010**, *43*, 2672.
(3) He, W.-D.; Sun, X.-L.; Wan, W.-M.; Pan, C.-Y. *Macromolecules* **2011**, *44*, 3358.
(4) Pei, Y.; Dharsana, N. C.; van Hensbergen, J. A.; Burford, R. P.; Roth, P. J.; Lowe, A. B. *Soft Matter* **2014**, *10*, 5787.
(5) Pei, Y.; Lowe, A. B. *Polymer Chemistry* **2014**, *5*, 2342.
(6) Pei, Y.; Dharsana, N. C.; Lowe, A. B. *Australian Journal of Chemistry* **2015**, *68*, 939.
(7) Wang, X.; Xu, J.; Zhang, Y.; Zhang, W. *Journal of Polymer Science Part A: Polymer Chemistry* **2012**, *50*, 2452.
(8) Huo, F.; Wang, X.; Zhang, Y.; Zhang, X.; Xu, J.; Zhang, W. *Macromolecular Chemistry and Physics* **2013**, *214*, 902.
(9) Shi, P.; Zhou, H.; Gao, C.; Wang, S.; Sun, P.; Zhang, W. *Polymer Chemistry* **2015**, *6*, 4911.
(10) Zhang, X.; Rieger, J.; Charleux, B. *Polymer Chemistry* **2012**, *3*, 1502.

(11) Jones, E. R.; Semsarilar, M.; Blanazs, A.; Armes, S. P. *Macromolecules* **2012**, *45*, 5091.
(12) Semsarilar, M.; Jones, E. R.; Blanazs, A.; Armes, S. P. *Advanced Materials* **2012**, *24*, 3378.
(13) Semsarilar, M.; Ladmiral, V.; Blanazs, A.; Armes, S. P. *Polymer Chemistry* **2014**, *5*, 3466.
(14) Jones, E. R.; Mykhaylyk, O. O.; Semsarilar, M.; Boerakker, M.; Wyman, P.; Armes, S. P. *Macromolecules* **2015**, *49*, 172.
(15) Jones, E. R.; Semsarilar, M.; Wyman, P.; Boerakker, M.; Armes, S. P. *Polymer Chemistry* **2016**, *7*, 851.
(16) Zhao, W.; Gody, G.; Dong, S.; Zetterlund, P. B.; Perrier, S. *Polymer Chemistry* **2014**, *5*, 6990.
(17) Zehm, D.; Ratcliffe, L. P. D.; Armes, S. P. *Macromolecules* **2013**, *46*, 128.
(18) Ratcliffe, L. P. D.; Ryan, A. J.; Armes, S. P. *Macromolecules* **2013**, *46*, 769.
(19) Derry, M. J.; Fielding, L. A.; Armes, S. P. *Polymer Chemistry* **2015**, *6*, 3054.
(20) Pound, G.; Eksteen, Z.; Pfukwa, R.; McKenzie, J. M.; Lange, R. F.; Klumperman, B. *Journal of Polymer Science Part A: Polymer Chemistry* **2008**, *46*, 6575.
(21) Johnson, I. J., Khosravi, E., Musa, O. M., Simnett, R. E. and Eissa, A. M. *J. Polym. Sci. Part A: Polym. Chem.* **2015**, *53*, 775.
(22) Bailly, N.; Pound-Lana, G.; Klumperman, B. *Australian Journal of Chemistry* **2012**, *65*, 1124.
(23) Bailly, N.; Thomas, M.; Klumperman, B. *Biomacromolecules* **2012**, *13*, 4109.
(24) Destarac, M. *Macromolecular Reaction Engineering* **2010**, *4*, 165.
(25) Guinaudeau, A.; Coutelier, O.; Sandeau, A.; Mazières, S.; Nguyen Thi, H. D.; Le Drogo, V.; Wilson, D. J.; Destarac, M. *Macromolecules* **2013**, *47*, 41.
(26) Deng, J.; Shi, Y.; Jiang, W.; Peng, Y.; Lu, L.; Cai, Y. *Macromolecules* **2008**, *41*, 3007.
(27) Sun, J.; Peng, Y.; Chen, Y.; Liu, Y.; Deng, J.; Lu, L.; Cai, Y. *Macromolecules* **2010**, *43*, 4041.
(28) Zhang, J.; Zou, M.; Dong, J.; Li, X. *Colloid and Polymer Science* **2013**, *291*, 2653.
(29) Moad, G.; Rizzardo, E.; Thang, S. H. *Australian Journal of Chemistry* **2005**, *58*, 379.
(30) Rieger, J. *Macromolecular Rapid Communications* **2015**, *36*, 1458.
(31) Blanazs, A.; Madsen, J.; Battaglia, G.; Ryan, A. J.; Armes, S. P. *Journal of the American Chemical Society* **2011**, *133*, 16581.
(32) Semsarilar, M.; Ladmiral, V.; Blanazs, A.; Armes, S. P. *Langmuir* **2013**, *29*, 7416.
(33) Su, Y.; Xiao, X.; Li, S.; Dan, M.; Wang, X.; Zhang, W. *Polymer Chemistry* **2014**, *5*, 578.
(34) Lopez-Oliva, A. P.; Warren, N. J.; Rajkumar, A.; Mykhaylyk, O. O.; Derry, M. J.; Doncom, K. E.; Rymaruk, M. J.; Armes, S. P. *Macromolecules* **2015**, *48*, 3547.
(35) Blanazs, A.; Ryan, A. J.; Armes, S. P. *Macromolecules* **2012**, *45*, 5099.
(36) Charleux, B.; Delaittre, G.; Rieger, J.; D'Agosto, F. *Macromolecules* **2012**, *45*, 6753.
(37) Zhang, W.; D'Agosto, F.; Boyron, O.; Rieger, J.; Charleux, B. *Macromolecules* **2011**, *44*, 7584.
(38) Zhang, W.; D'Agosto, F.; Dugas, P.-Y.; Rieger, J.; Charleux, B. *Polymer* **2013**, *54*, 2011.

(39) Doncom, K. E.; Warren, N. J.; Armes, S. P. *Polymer Chemistry* **2015**, *6*, 7264.
(40) Canning, S. L.; Smith, G. N.; Armes, S. P. *Macromolecules* **2016**, *49*, 1985.
(41) Warren, N. J.; Armes, S. P. *Journal of the American Chemical Society* **2014**, *136*, 10174.
(42) Derry, M. J.; Fielding, L. A.; Armes, S. P. *Progress in Polymer Science* **2016**, *52*, 1.

Chapter 5

Poly(glycerol monomethacrylate)-poly(*N*-2-(methacryloyloxy)ethyl pyrrolidone) diblock copolymers via RAFT aqueous dispersion polymerisation

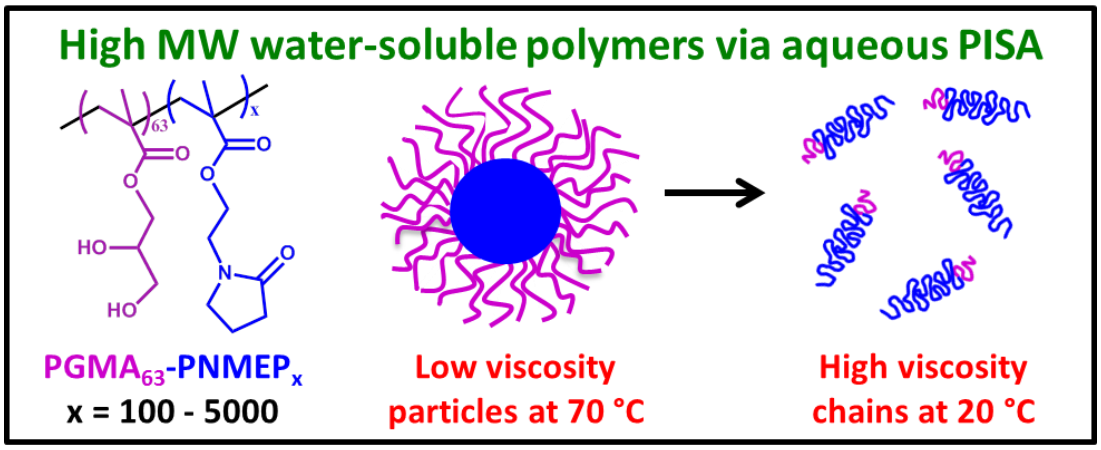

5.1 Introduction

The synthesis and polymerisation of *N*-vinylpyrrolidone (NVP) was first reported by Walter Reppe using acetylene chemistry.[1] A patent for his discovery was filed in 1939 and it has since become an extremely versatile polymer with many commercial applications.[2-5] Within the pharmaceutical industry PNVP is used as a binder in tablets and also as a disinfectant, both of which are possible due to its non-toxic nature.[6,7] PNVP is an active ingredient in personal care products such as shampoo and hairspray. It binds strongly to polyphenols, which enables its use in the clarity of beverages, such as fruit juice and beer.[2] Other applications include coatings, thickening agents and adhesives.[2] Many of these applications are due to its high solubility in water and organic solvents. NVP is a highly polar monomer which contains both hydrophilic and hydrophobic groups, enabling PNVP to be soluble in a wide range of solvents.

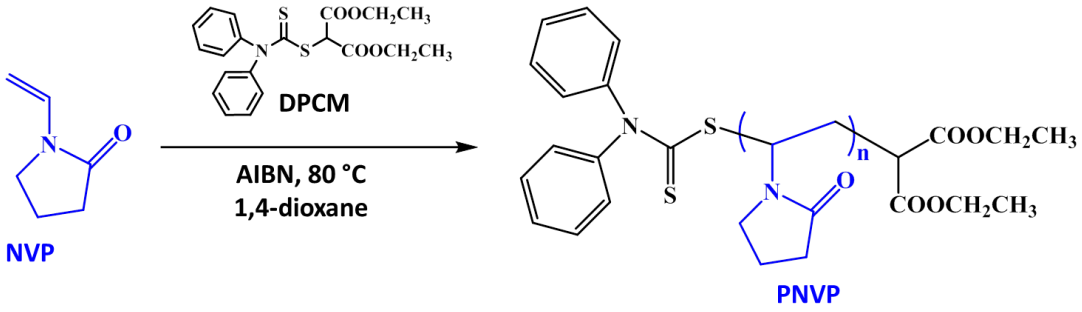

Figure 5.1 Modified reaction scheme for the RAFT polymerisation of NVP as described by Devasia et al.[8]

Typically, free radical polymerisation of NVP involves using hydrogen peroxide as an initiator in water to form PNVP.[8] Its molecular weight can be controlled by varying the initiator concentration, but better control has been achieved by using controlled radical polymerisation techniques such as RAFT polymerisation. NVP is known as a less-activated monomer (LAM) and therefore requires a RAFT agent with a relatively low transfer constant such as a xanthate or a dithiocarbamate. Devasia et al. reported the RAFT polymerisation of NVP at 80 °C using DPCM (see structure in Figure 5.1) as a RAFT CTA.[8] PNVP DPs from 50 to 500 were targeted, with conversions of between 61 and 85% being achieved within 24 to 49 h. GPC analysis of these PNVP homopolymers showed reasonably good control (M_w/M_n < 1.60). In order to determine end-group fidelity, one PNVP homopolymer was chain-

extended with styrene or *n*-butyl acrylate. However, only low blocking efficiencies were observed by GPC analysis and Devasia et al. made no mention of the conversion achieved for either styrene or *n*-butyl acrylate.

Klumperman and co-workers reported a detailed study on the side reactions that occur when polymerising NVP utilising a xanthate CTA.[9] The major side reaction was the formation of the NVP dimer (see Figure 5.2), which was obtained when using a xanthate possessing either a carboxylic acid or hydroxy functionality in the R group. This dimer was also formed when no radical initiator was added to the reaction solution. NMR and mass spectroscopy studies confirmed that other minor side reactions also occurred, including reversible hydration of NVP monomer at elevated temperatures and esterification of a carboxylic acid R group on the xanthate CTA. This study also examined xanthate end-group degradation via both elimination and hydrolysis. The former side reaction results in dead chain-ends; therefore elevated polymerisation temperatures (> 60 °C) are generally best avoided in order to minimise xanthate elimination.[9]

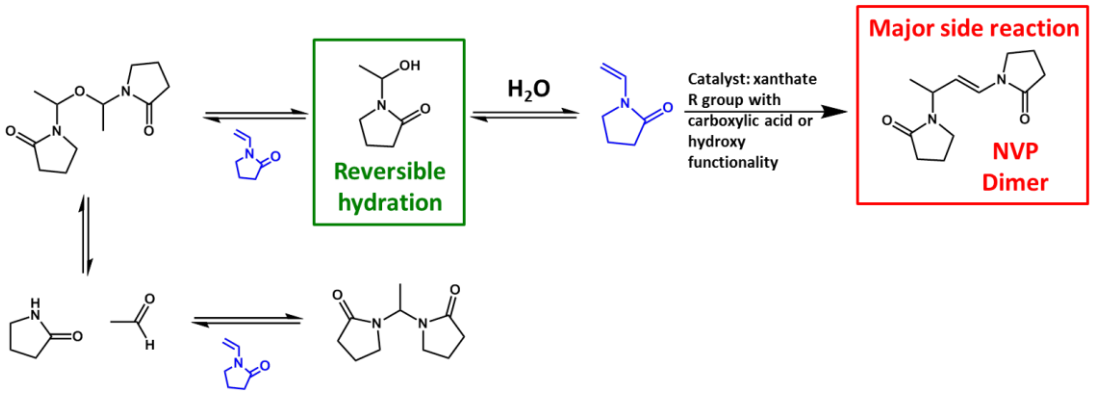

Figure 5.2 Side-reactions that can occur during the RAFT polymerisation of NVP in water using xanthates, as reported by Klumperman and co-workers.[9]

In view of the above problems, Destarac and co-workers developed an ambient temperature RAFT formulation for PNVP using a xanthate CTA.[10-12] Such mild conditions enabled greater control over the NVP polymerisation and utilising a tBuOOH/Na_2SO_3 redox initiator prevented both side reactions and xanthate degradation. A PNVP macro-CTA was successfully chain-extended with additional NVP and 85% conversion was achieved while GPC analysis indicated high blocking efficiency with minimal PNVP macro-CTA contamination. A series of double-hydrophilic diblock copolymers were subsequently prepared by polymerising NVP

using a series of hydrophilic macro-CTAs, including poly(acrylic acid), polyacrylamide, poly(3-acrylamidopropyltrimethylammonium chloride) and poly(sodium 2-acrylamido-2-methylpropanesulfonate). At least 99% conversion was achieved with dispersities of less than 1.60 being observed.[10]

More-activated monomers (MAMs) such as methacrylates are usually easier to polymerise than LAMs, with lower final dispersities typically achieved. *N*-2-(methacryloyloxy)ethyl pyrrolidone (NMEP) is a methacrylic analogue of NVP that has been successfully polymerised via RAFT solution polymersisation.[13-15] Deng et al. reported the first RAFT synthesis of NMEP in which three PNMEP homopoylmers were synthesised using a dithiobenzoate RAFT agent via visible light irradiation in methanol at 30 °C.[13] PNMEP DPs of 100, 300 or 500 were targeted and conversions of approximately 80 % were achieved within 5 h using a CTA/initiator molar ratio of 4.0. A linear increase in molecular weight with conversion and low final dispersities were indicated by GPC analysis. However, chain extension of a PNMEP macro-CTA with glycidyl methacrylate (GlyMA), 2-(dimethylamino)ethyl methacrylate (DMA) or oligoethylene glycol monomethacrylate (OEGMA) resulted in final conversions of less than 51 %. Sun et al. synthesised a series of PNMEP homopolymers by visible light activated RAFT polymerisation at 25 °C.[14] The same dithiobenzoate RAFT agent was employed and their lower critical solution temperatures (LCST) were determined. The PNMEP LCST decreased from approximately 72 to 53 °C with increasing PNMEP DP for a fixed concentration of 20.0 mg mL^{-1}.

Finally, Zhang et al. synthesised a series of poly(lauryl methacrylate)-poly(*N*-2-(methacryloyloxy)ethyl pyrrolidone) (PLMA-PNMEP) diblock copolymers by RAFT solution polymerisation in chloroform (see Figure 5.3a).[15] CPDB was used as the RAFT agent in these syntheses and the PNMEP DP was varied from 112 to 572. Conversions of between 52% and 63% were achieved after 6 h at 60 °C. An increase in molecular weight with PNMEP DP and low dispersities were observed by GPC analysis (Figure 5.3b). The PLMA-PNMEP diblock copolymers were purified by dialysis and dried to afford powders. Addition of the copolymer powder to THF caused the diblock copolymer to self-assemble to form spherical micelles as judged by DLS and TEM (Figure 5.3c).

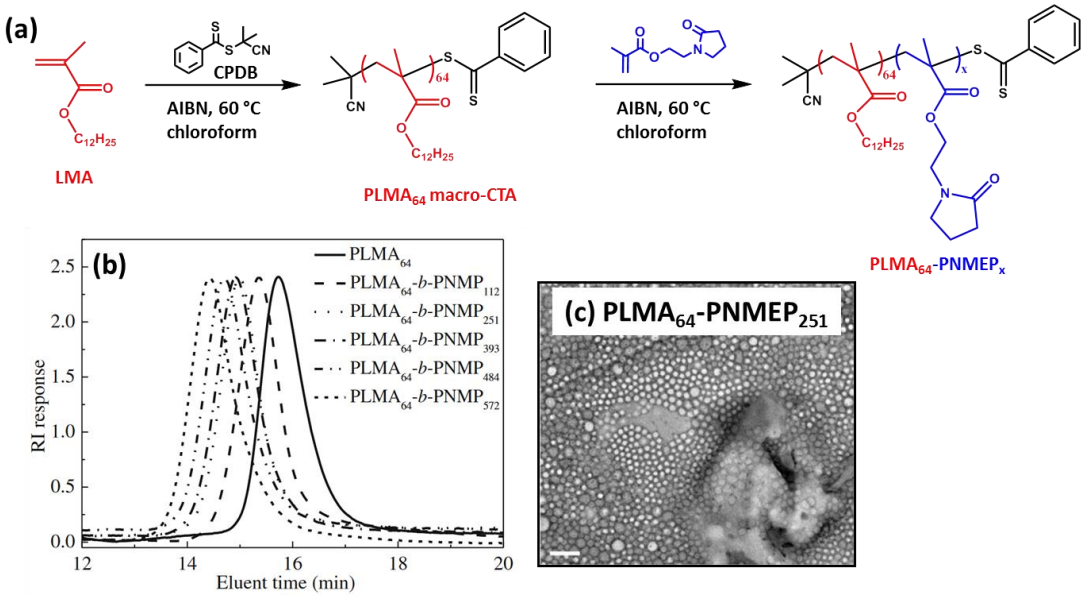

Figure 5.3 (a) Schematic representation of the RAFT solution polymerisation of $PLMA_{64}$-$PNMEP_x$ in chloroform, (b) GPC analysis of the $PLMA_{64}$ macro-CTA and $PLMA_{64}$-$PNMEP_x$ diblock copolymers and (c) TEM image of $PLMA_{64}$-$PNMEP_{251}$ after its dissolution in THF (scale bar represents 200 nm).[15]

In this Chapter, a series of PNMEP homopolymers are synthesised via RAFT solution polymerisation and the LCST was determined in each case. Poly(glycerol monomethacrylate)-poly(*N*-2-(methacryloyloxy)ethyl pyrrolidone) (PGMA-PNMEP) diblock copolymers are then prepared by RAFT aqueous dispersion polymerisation, with the target PNMEP DP systematically varied from 100 to 6000. These PGMA-PNMEP diblock copolymers are analysed by ^{1}H NMR spectroscopy and GPC. The effect of NMEP monomer purity (96% vs. 98%) is also assessed. Finally, replacing the PGMA macro-CTA with a poly(methacrylic acid) (PMAA) macro-CTA for the synthesis of PMAA-PNMEP diblock copolymers is examined. The work presented in this Chapter has been published in Macromolecules.[16]

5.2 Experimental Details

5.2.1 Materials

NMEP (either 96% or 98% purity) was provided by Ashland Specialty Ingredients (USA). GMA was kindly donated by GEO Specialty Chemicals (Hythe, UK). ACVA (99%), MAA, trimethylsilyl diazomethane solution (2.0 M in diethyl ether) and NaOH were purchased from Sigma-Aldrich UK. CPDB was purchased from Strem Chemicals Ltd. (Cambridge, UK). d_4-Methanol was purchased from Goss Scientific Instruments Ltd. (Cheshire, UK). All other solvents were purchased from Fisher

Scientific (Loughborough, UK). All chemicals and solvents were used as received. Deionised water was used for all experiments.

5.2.2 Kinetics of the RAFT solution polymerisation of NMEP

The synthesis of $PNMEP_{500}$ was conducted as follows. NMEP (4.4600 g, 22.613 mmol), CPDB RAFT agent (0.0127 g, 0.057 mmol; target DP = 500), ethanol (11.6507 g, 27.7% w/w) and ACVA (0.0031 g, 0.011 mmol; CPDB/ACVA molar ratio = 4.0) were weighed into a 28 ml vial and degassed with nitrogen in an ice bath for 30 min. This reaction solution was then placed in an oil bath set at 70 °C. The polymerisation was monitored for 24 h, resulting in a final monomer conversion of 58 % as judged by ^{1}H NMR (comparing the vinyl signals at 5.7 and 6.1 ppm to that of the methylene carbonyl proton at 2.5 ppm). DMF GPC analysis indicated a M_n of 29,000 g mol^{-1} and an M_w/M_n of 1.19. The same protocol was utilised for the synthesis of $PNMEP_{2000}$ homopolymer at 29.2% w/w solids by adjusting the NMEP/CPDB molar ratio. In each case, the solids content was selected to give the same molar concentration of NMEP as that used for the synthesis of $PGMA_{63}$-$PNMEP_x$ diblock copolymer particles (see below). This enabled a meaningful comparison of any kinetic differences between these solution and dispersion polymerisation formulations.

5.2.3 Preparation of $PGMA_{63}$ macro-CTA

The same $PGMA_{63}$ macro-CTA was used as prepared in Chapter 2, see Section 2.2.2. DMF GPC analysis indicated a M_n of 14,100 g mol^{-1} and an M_w/M_n of 1.20.

5.2.4 Synthesis of $PGMA_{63}$-$PNMEP_x$ diblock copolymers via RAFT aqueous dispersion polymerisation of NMEP

A typical protocol for the synthesis of $PGMA_{63}$-$PNMEP_{480}$ diblock copolymer nanoparticles was as follows: $PGMA_{63}$ macro-CTA (0.1008 g), NMEP (96% purity, 0.9573 g, 4.85 mmol; target DP = 500) and ACVA (0.0006 g, 2.14 μmol; macro-CTA/ACVA molar ratio = 4.0) were dissolved in deionised water (3.167 g, 25% w/w) in a 14 ml vial. The reaction mixture was sealed and purged with nitrogen for 30 min, prior to immersion in an oil bath set at 70 °C for 24 h. The resulting copolymer was analysed by DMF GPC (M_n = 70,100 g mol^{-1}, M_w/M_n = 1.24). ^{1}H NMR spectroscopy analysis of the final reaction solution in d_4-methanol indicated

96% NMEP conversion. Other diblock copolymer compositions were obtained by adjusting the NMEP/$PGMA_{63}$ macro-CTA molar ratio to give a target PNMEP DP of 100 to 6000. The same protocol was also utilised for the synthesis of $PGMA_{63}$-$PNMEP_x$ diblock copolymers prepared in ethanol instead of deionised water.

5.2.5 Synthesis of $PMAA_{85}$ macro-CTA

The $PMAA_{85}$ macro-CTA was synthesised by Dr. Lee Fielding. The RAFT synthesis of PMAA macro-CTAs has been described in detail elsewhere.[17] The $PMAA_{85}$ macro-CTA was synthesised as follows. MAA (50 g, 581 mmol), CPDB (2.0 g; assuming 80% purity gives 7.3 mmol), ACVA (407 mg, 1.5 mmol; CPDB/ACVA molar ratio = 5.0) and ethanol (98.1 ml) were weighed into a round bottom flask. The reaction was purged with nitrogen and placed in an oil bath at 70 °C for 3 h. Resulting in a MAA conversion of 84 %. The PMAA macro-CTA was purified by precipitation and dried under vacuum. ^{1}H NMR spectroscopy calculated a mean DP of 85. DMF GPC analysis of the methylated $PMAA_{85}$ macro-CTA indicated an M_n of 8,600 g mol^{-1} and an M_w/M_n of 1.21.

5.2.6 Synthesis of $PMAA_{85}$-$PNMEP_x$ diblock copolymers via RAFT aqueous dispersion polymerisation of NMEP

A typical protocol for the synthesis of $PMAA_{85}$-$PNMEP_{495}$ diblock copolymer nanoparticles was as follows: $PMAA_{85}$ macro-CTA (0.0997 g) and ACVA (0.0009 g, 3.21 μmol; macro-CTA/ACVA molar ratio = 4.0) were dissolved in deionised water (4.2321 g, 25% w/w) in a 28 ml vial. The pH was adjusted to 5.01 using 1 M NaOH. NMEP (96% purity, 1.3019 g, 6.60 mmol; target DP = 500) was added and the reaction mixture was sealed and purged with nitrogen for 30 min, prior to immersion in an oil bath set at 70 °C for 24 h. ^{1}H NMR spectroscopy of the final reaction solution in d_4-methanol indicated 99% NMEP conversion. A sample of the $PMAA_{85}$-$PNMEP_{495}$ diblock copolymer was dissolved in a mixed solvent of 3:2 toluene/methanol and methylated overnight using trimethylsilyl diazomethane solution (2.0 M in diethyl ether) prior to being analysed by DMF GPC (M_n = 73,500 g mol^{-1}, M_w/M_n = 1.35). Other diblock copolymer compositions were obtained by adjusting the NMEP/$PMAA_{85}$ macro-CTA molar ratio to give a target PNMEP DP of 300 to 4000.

5.2.7 Copolymer characterisation

^{1}H NMR Spectroscopy

^{1}H NMR spectra were recorded in d_4-methanol using a 400 MHz Bruker Advance-400 spectrometer. Variable temperature ^{1}H NMR spectra were recorded for $PGMA_{63}$-$PNMEP_{990}$ using a 500 MHz Bruker Advance-500 spectrometer in D_2O. 4,4-Dimethyl-4-silapentane-1-sulfonic acid (DSS, 0.01 mol) was added as an internal standard.

Gel Permeation Chromatography (GPC)

Molecular weights and dispersities were determined by DMF GPC at 60 °C. The same GPC set-up was used as in Chapter 2, see Section 2.2.10. The $PMAA_{85}$-$PNMEP_x$ diblock copolymers were methylated prior to GPC analysis.

Visible Absorption Spectroscopy

Spectra were recorded from 400 to 800 nm for 1.0 % w/w aqueous solutions of various PNMEP homopolymers between 40 and 80 °C in 5 °C increments using a Varian Cary 300 Bio UV-visible spectrometer. An increase in turbidity at 600 nm indicated the LCST.

5.3 Results and Discussion

5.3.1 Synthesis of $PNMEP_x$ homopolymers via RAFT solution polymerisation

A series of $PNMEP_x$ homopolymers were prepared via RAFT solution polymerisation in ethanol at 70 °C. The homopolymers were purified by precipitation and ^{1}H NMR confirmed DPs between 31 and 467. DMF GPC analysis of each copolymer confirmed an increase in molecular weight with PNMEP DP and low dispersities of less than 1.23. The LCST of 1% w/w aqueous solutions of $PNMEP_x$ were measured by UV-vis at 600 nm, see Figure 5.4a. The LCST was found to decrease from 75 °C to 55 °C with increasing PNMEP DP (Figure 5.4b). The LCST appears to plateau around 55 °C with only a 1 °C difference between $PNMEP_{397}$ and $PNMEP_{467}$. Similar LCSTs (72 to 53 °C) were reported by Deng et al. for PNMEP homopolymers with DPs of approximately 90 to 480.

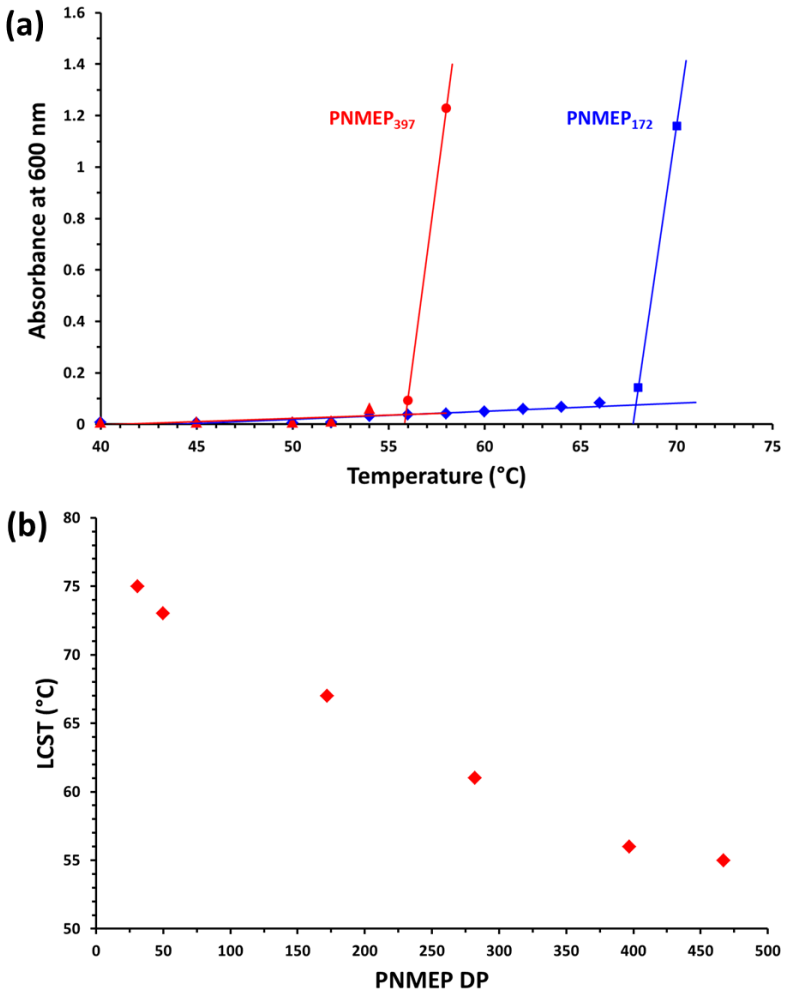

Figure 5.4 (a) Absorbance at 600 nm against temperature plot for 1.0% w/w aqueous solutions of $PNMEP_{172}$ and $PNMEP_{397}$ homopolymers to determine the LCST, (b) LCST against PNMEP DP for a series of $PNMEP_x$ homopolymers prepared via RAFT solution polymerisation.

5.3.2 Synthesis of $PGMA_{63}$-$PNMEP_x$ diblock copolymers via RAFT aqueous dispersion polymerisation

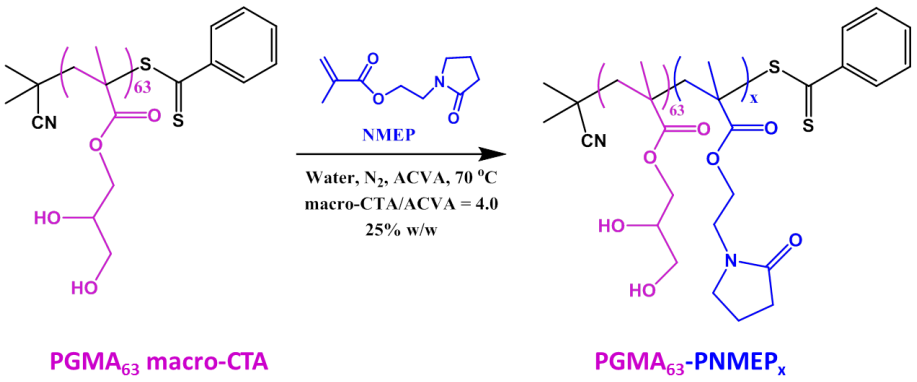

Scheme 5.1 Synthesis of $PGMA_{63}$-$PNMEP_x$ diblock copolymers via RAFT aqueous dispersion polymerisation at 70 °C.

$PGMA_{63}$-$PNMEP_x$ diblock copolymers were prepared at 25% w/w solids via the RAFT dispersion polymerisation of NMEP using a $PGMA_{63}$ macro-CTA at 70 °C (Scheme 5.1). The target PNMEP DP was varied from 100 to 6000 (Table 5.1). The synthesis was carried out above the LCST of PNMEP and therefore the PNMEP block would be weakly hydrophobic and insoluble in water at 70 °C. However, cooling of the diblock copolymers causes the PNMEP block to pass through its LCST leading to a completely water-soluble polymer at 20 °C. Conversions above 90 % were achieved when targeting PNMEP DPs up to 5000, with only 76% conversion achieved for a target DP of 6000.

Table 5.1 Target PNMEP DP, conversion, M_n and M_w/M_n for a series of $PGMA_{63}$-$PNMEP_x$ (G_{63}-N_x) diblock copolymers prepared at 25% w/w solids and the corresponding $PGMA_{63}$ macro-CTA.

	Block composition	Target PNMEP DP	Conversion[a] (%)	GPC	
				M_n[b] (g mol^{-1})	M_w/M_n[b]
1	G_{63}	-	67	14,100	1.20
2	G_{63}-N_{99}	100	99	27,200	1.16
3	G_{63}-N_{198}	200	99	39,300	1.18
4	G_{63}-N_{294}	300	98	51,900	1.19
5	G_{63}-N_{392}	400	98	62,900	1.22
6	G_{63}-N_{480}	500	96	70,100	1.24
7	G_{63}-N_{720}	750	96	94,200	1.30
8	G_{63}-N_{990}	1000	99	130,800	1.49
9	G_{63}-N_{1125}	1250	98	152,700	1.61
10	G_{63}-N_{1459}	1500	97	178,900	1.78
11	G_{63}-N_{1706}	1750	96	211,600	1.51
12	G_{63}-N_{1960}	2000	98	254,800	1.81
13	G_{63}-N_{2300}	2500	92	278,200	1.51
14	G_{63}-N_{2940}	3000	98	374,700	2.22
15	G_{63}-N_{3290}	3500	94	445,600	1.98
16	G_{63}-N_{3720}	4000	93	490,100	1.86
17	G_{63}-N_{4161}	4500	92	518,300	2.32
18	G_{63}-N_{4700}	5000	94	627,800	2.17
19	G_{63}-N_{4560}	6000	76	n.d.	n.d.

a. Monomer conversion determined by ^{1}H NMR spectroscopy in d_4-methanol
b. Determined by DMF GPC using a series of near-monodisperse PMMA calibration standards
(n.d. = not determined)

Each $PGMA_{63}$-$PNMEP_x$ diblock copolymer was analysed by DMF GPC to determine the molecular weight and dispersity of the sample. Figure 5.5 shows the GPC chromatograms for selected $PGMA_{63}$-$PNMEP_x$ diblock copolymers and the $PGMA_{63}$ macro-CTA. High blocking efficiencies are obtained for all diblock copolymers with minimal macro-CTA contamination. However, a high molecular

weight shoulder begins to appear when targeting PNMEP DPs of 400 or greater. This leads to an increase in dispersity from 1.18 for $PGMA_{63}$-$PNMEP_{198}$ to 2.17 for the highly asymmetric $PGMA_{63}$-$PNMEP_{4700}$. The high molecular shoulder was originally thought to be due to branching of the polymer chain, which is known for PNVP prepared via conventional free radical polymerisation.[2] However, this was found not to be the case and will be discussed later in Section 5.3.5. Figure 5.6 shows a linear increase in molecular weight with PNMEP DP. This linearity is followed up to a very high molecular weight of approximately 600 kg mol^{-1}. These high molecular weight polymers are thought to be the highest prepared via RAFT *aqueous dispersion* polymerisation. Davis and co-workers have reported the synthesis of high molecular weight polystyrene by using a poly(poly(ethylene glycol)methyl ether acrylate-*co*-*N*-hydroxyethyl acrylamide) macro-CTA by RAFT *emulsion* polymerisation with M_n values of up to one million g mol^{-1} reported with a low dispersity of 1.39.[18] Destarac and co-workers have also synthesised ultra-high molecular weight polymers using acrylamide-based monomers by low temperature RAFT *solution* polymerisation using a xanthate RAFT agent.[19]

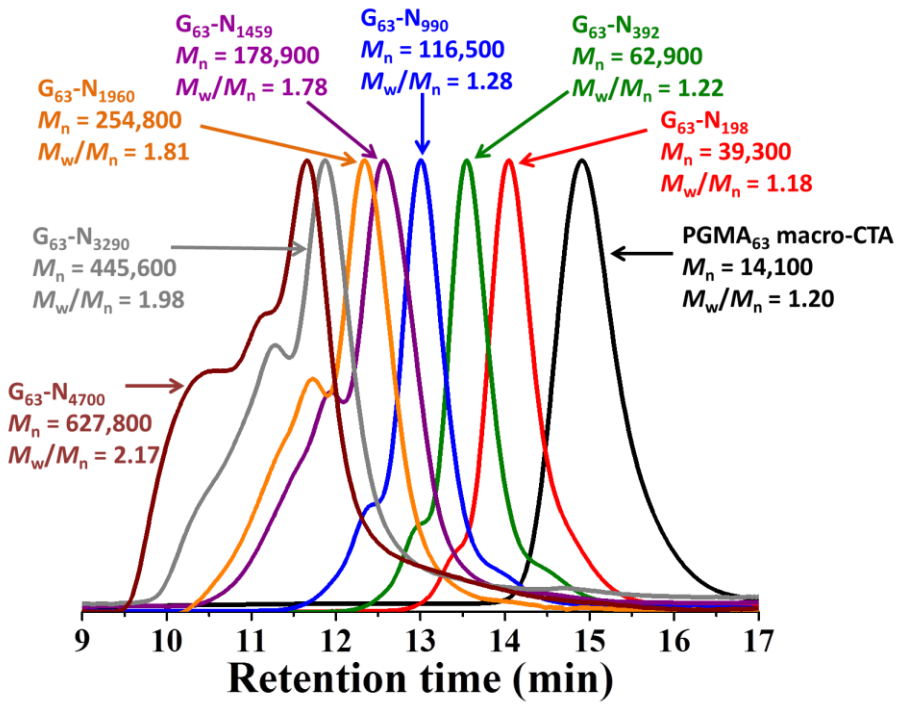

Figure 5.5 DMF GPC curves for $PGMA_{63}$-$PNMEP_x$ diblock copolymers and the $PGMA_{63}$ macro-CTA (where G = PGMA and N = PNMEP, against PMMA standards).

Figure 5.6 also shows the gradual increase in dispersity with PNMEP DP. When targeting PNMEP DPs of 1000 or less, relatively low dispersities of less than 1.50

are achieved indicating good RAFT control. Conversely, PNMEP DPs of greater than 1000 have significantly higher dispersities.

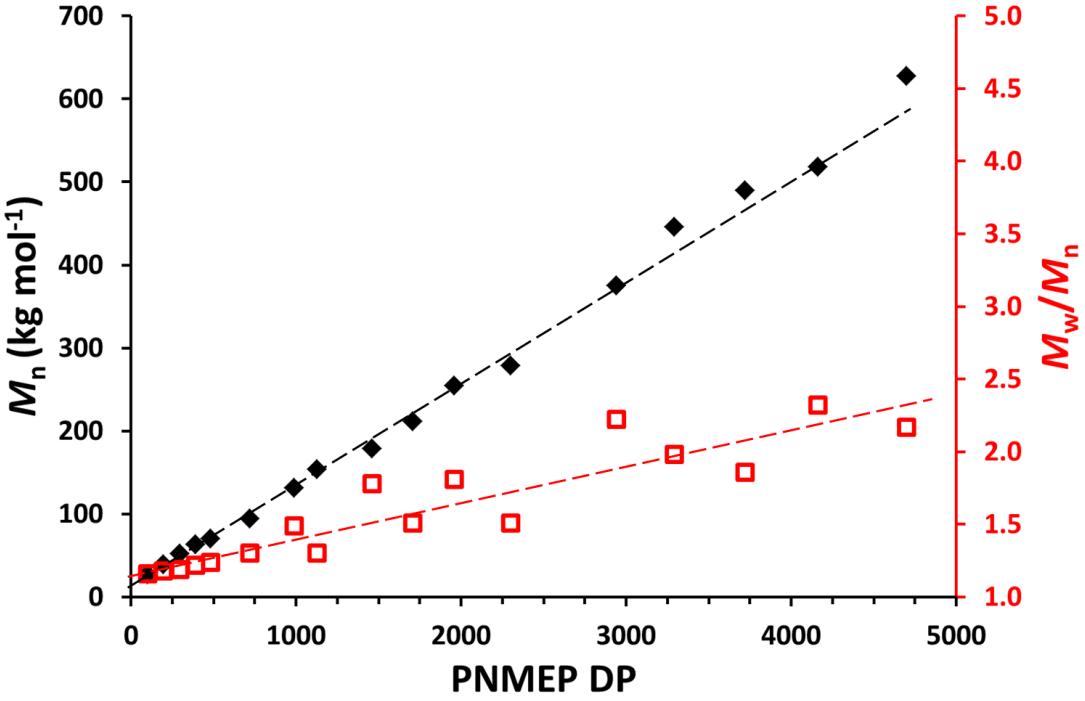

Figure 5.6 Molecular weight (M_n) and dispersity (M_w/M_n) against PNMEP DP for PGMA$_{63}$-PNMEP$_x$ diblock copolymers prepared at 25% w/w solids at 70 °C.

The synthesis of PGMA$_{63}$-PNMEP$_x$ diblock copolymers via RAFT aqueous dispersion polymerisation at 70 °C offers a convenient route to low viscosity high molecular weight PNMEP. At 70 °C, the PNMEP is above its LCST and therefore weakly hydrophobic while the water-soluble PGMA$_{63}$ block acts as a steric stabiliser resulting in particles. Visual inspection during the polymerisation indicated slightly turbid dispersions at 70 °C. However, cooling of the PGMA$_{63}$-PNMEP$_x$ dispersion to 20 °C causes the PNMEP chains to pass through their LCST resulting in a clear liquid with increased viscosity compared to that at 70 °C. DLS studies of the diblock copolymers at 70 °C report polydisperse particles with a diameter of approximately 1 μm. This is significantly larger than other RAFT dispersion polymerisations (typically 50 – 300 nm)[20,21] and suggests that the cores of the PGMA$_{63}$-PNMEP$_x$ diblock copolymers are highly hydrated. To see if this was the case, variable temperature ^{1}H NMR spectroscopy was utilised for PGMA$_{63}$-PNMEP$_{990}$. A 5.0% w/w solution in D_2O was prepared and the ^{1}H NMR spectrum was recorded in 5 °C increments between 25 °C and 70 °C (Figure 5.7). Using the signal at 2.5 ppm, corresponding to the methylene carbonyl protons in the pyrrolidone ring and

comparing it to an internal standard indicated a maximum degree of core hydration at 25-35 °C, which was normalised to 100%. As the $PGMA_{63}$-$PNMEP_{990}$ diblock copolymer is heated above its critical micellisation temperature of 45.6 °C as determined by turbidimetry (see Figure 5.8) the mean degree of hydration of the $PNMEP_{990}$ block was reduced from approximately 100% to 70%. This indicates that the core-forming PNMEP chains within the diblock copolymer particles are still extremely well-solvated at 70 °C when prepared.

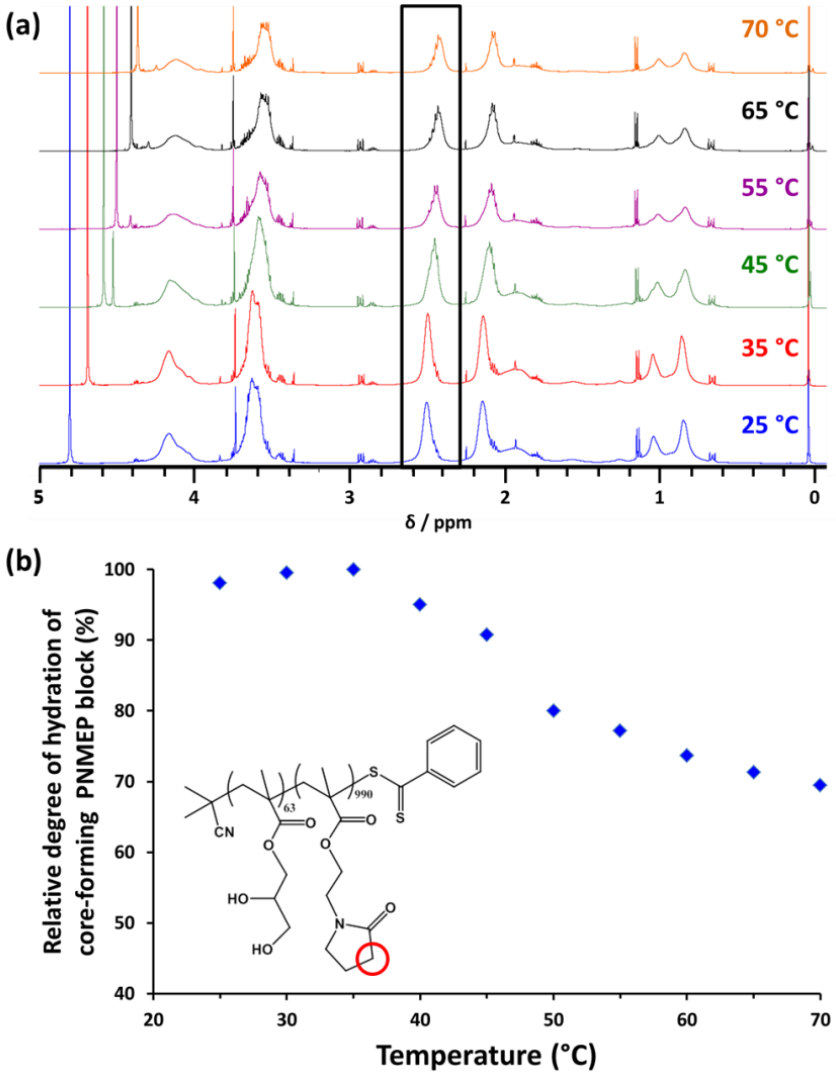

Figure 5.7 Variable temperature ^{1}H NMR for $PGMA_{63}$-$PNMEP_{990}$ at 5% w/w solids in D_2O. (a) NMR spectra recorded at 25 °C to 70 °C in 5 °C increments showing the change in hydration relative to an internal standard at 0 ppm. (b) Change in the relative degree of hydration of the core-forming PNMEP block (using the 2H signal at 2.5 ppm corresponding to the methylene carbonyl protons for PNMEP) against temperature.

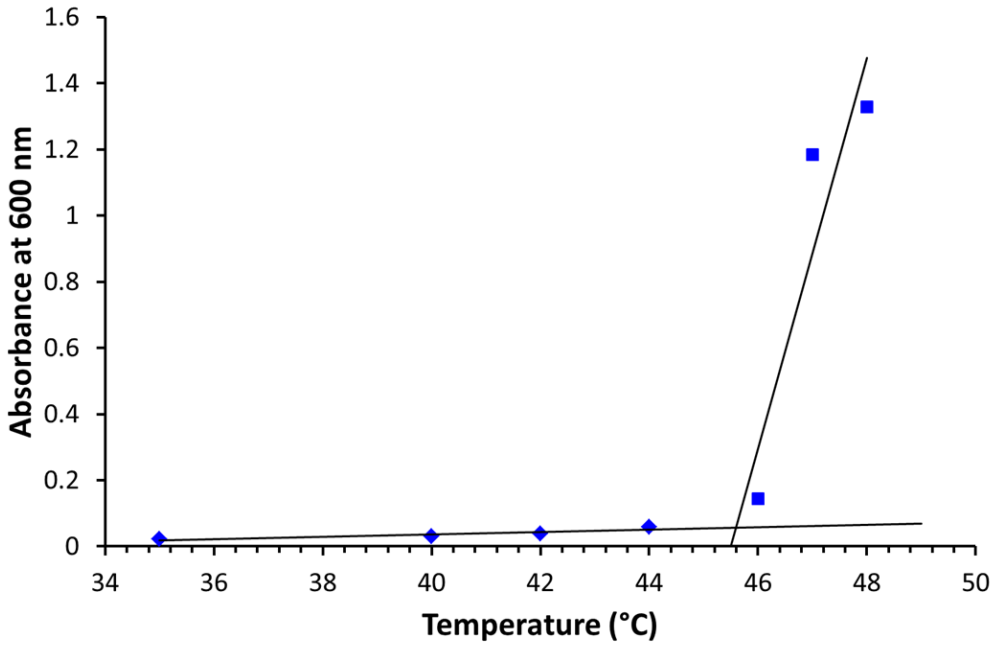

Figure 5.8 Visible absorbance at 600 nm against temperature plot recorded for a 5% w/w aqueous solution of $PGMA_{63}$-$PNMEP_{990}$ to determine its critical micellisation temperature (45.6 °C).

5.3.3 Comparison of the kinetics of the PNMEP homopolymerisation in ethanol with that of the RAFT aqueous dispersion polymerisation of NMEP using a $PGMA_{63}$ macro-CTA

Utilising a relatively short $PGMA_{63}$ macro-CTA has enabled the synthesis of very high molecular weight PNMEP via RAFT aqueous dispersion polymerisation. To determine the advantages of using a PGMA macro-CTA over a RAFT CTA some kinetic experiments were examined to compare the RAFT dispersion polymerisation of NMEP to the equivalent RAFT solution polymerisation.

A $PGMA_{63}$-$PNMEP_{500}$ diblock copolymer was synthesised via the RAFT aqueous dispersion polymerisation of NMEP at 25% w/w solids and 70 °C. Aliquots of the reaction solution were taken every 30 minutes for the first 4 h, and then every 1 h for 12 h. After 24 h the reaction was quenched. This RAFT aqueous *dispersion* polymerisation was compared to the RAFT *solution* polymerisation of a $PNMEP_{500}$ homopolymer in ethanol at 70 °C. A solids content of 27.7% w/w was selected to ensure that the two polymerisations had the same molar concentration of NMEP. Both polymerisations utilised a CTA or macro-CTA/initiator molar concentration of 4.0.

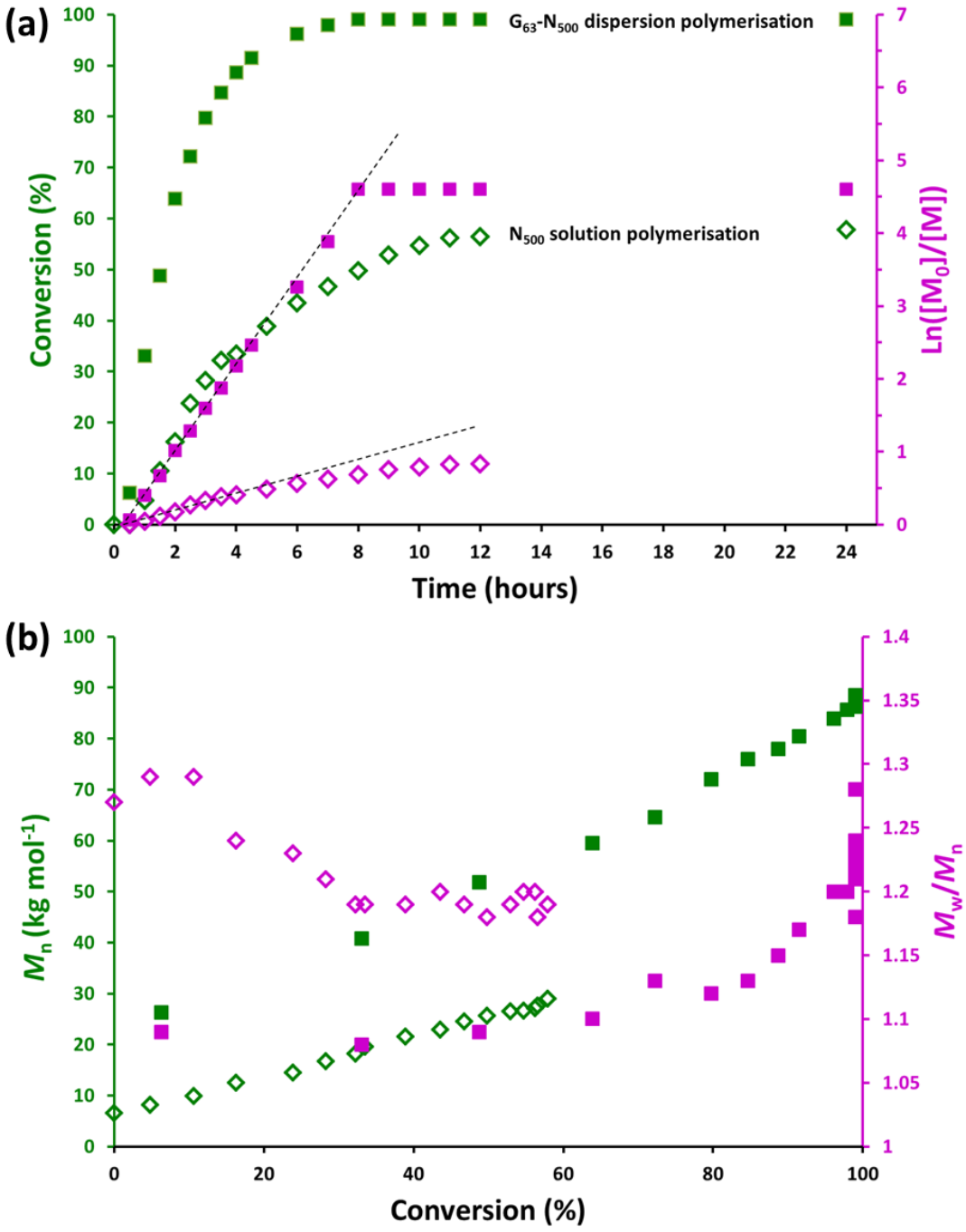

Figure 5.9 (a) Conversion and semi-logarithmic plots versus time for the RAFT aqueous dispersion polymerisation of $PGMA_{63}$-$PNMEP_{500}$ (filled squares) compared to the RAFT solution polymerisation of $PNMEP_{500}$ in ethanol (open diamonds) at 70 °C. Both reactions were conducted at the same molar concentration of NMEP. (b) Molecular weight (M_n) and dispersity (M_w/M_n) versus conversion plots for the same two syntheses (DMF eluent; vs. PMMA standards).

The RAFT dispersion polymerisation of NMEP from a water soluble $PGMA_{63}$ macro-CTA proceeded to 99% conversion after 8 h at 70 °C (Figure 5.9). The semi-logarithmic plot shows that the polymerisation follows pseudo-first-order kinetics up

to 99% conversion with a rate constant of 1.6 x 10^{-4} s^{-1} (Figure 5.9a). In contrast, the RAFT solution polymerisation of $PNMEP_{500}$ only reaches 50% conversion within 8 h, with a final conversion of 58% after 24 h. Pseudo-first-order kinetics are only followed for the first 5 h of the reaction, after which there is a decrease in the rate of polymerisation. The pseudo-first-order rate constant for the RAFT solution polymerisation of PNMEP is 3.5 x 10^{-5} s^{-1}. This shows an approximate five-fold rate enhancement for the dispersion polymerisation compared the equivalent RAFT solution polymerisation.

Both reactions were analysed by DMF GPC (Figure 5.9b). The RAFT dispersion polymerisation of $PGMA_{63}$-$PNMEP_{500}$ shows a linear increase in molecular weight with conversion up to 90 kg mol^{-1}. However, the dispersity of the diblock copolymer also increases with conversion. Resulting in a final dispersity of 1.28 after 24 h. The equivalent $PNMEP_{500}$ homopolymer prepared via RAFT solution polymerisation also shows a linear increase in molecular weight with conversion, resulting in a final M_n of approximately 30 kg mol^{-1} and dispersity of 1.19 at 58% conversion.

As a control experiment, the same $PGMA_{63}$-$PNMEP_{500}$ diblock copolymer was also prepared via RAFT solution polymerisation in ethanol. A macro-CTA/ACVA molar ratio of 4.0 was utilised at 70 °C using a solids content of 29.7% to ensure an equal molar concentration of NMEP. The reaction kinetics was not studied but ^{1}H NMR spectroscopy confirmed 67% conversion after 24 h. The final conversion is comparable to the synthesis of the PNMEP homopolymer in ethanol (58% vs. 67% conversion) with a slightly higher conversion achieved when using a $PGMA_{63}$ macro-CTA rather than a RAFT CTA. The RAFT solution polymerisation of a $PGMA_{63}$-$PNMEP_{500}$ diblock copolymer in ethanol is significantly slower than the equivalent RAFT aqueous dispersion polymerisation (67% in 24 h vs. 99% conversion in 8 h) under otherwise identical conditions. This difference could simply be due to solvent effects such as those reported by Jones et al.[22] Here, water was used as a co-solvent in the RAFT ethanolic dispersion polymerisation of benzyl methacrylate, leading to a significant rate enhancement. Similar behaviour has also been reported by Zhang[23] and Huo.[24] In addition to this, PISA typically leads to faster rates of polymerisation compared to solution polymerisation due to a locally high monomer concentration within the growing nanoparticles.[21,25,26]

Targeting DPs greater than 1000 can lead to slow polymerisations resulting in low final conversion. Therefore higher DPs are rarely targeted. To explore the $PGMA_{63}$-$PNMEP_x$ diblock copolymer synthesis further, a PNMEP DP of 2000 was targeted. The reaction kinetics were monitored and compared to the equivalent RAFT solution polymerisation, targeting $PNMEP_{2000}$. Figure 5.10a shows the conversion and semi-logarithmic plot for these two reactions. The RAFT aqueous dispersion polymerisation of NMEP when targeting $PGMA_{63}$-$PNMEP_{2000}$ at 70 °C and 25% w/w solids went to 92% conversion within 13 h. A final conversion of 95% was achieved after 24 h. In contrast, the $PNMEP_{2000}$ homopolymer synthesised via RAFT solution polymerisation in ethanol at 70 °C only achieved 46% conversion after 12 h with no increase in conversion between 12 and 24 h. The same molar concentration of NMEP was used for this RAFT solution polymerisation corresponding to 29.2% w/w solids. Despite the higher solids the solution polymerisation is significantly slower than the RAFT aqueous dispersion polymerisation utilising a $PGMA_{63}$ macro-CTA. An approximate four-fold rate enhancement is observed for the dispersion polymerisation over the solution polymerisation (rate constants of 6.4×10^{-5} s^{-1} and 1.7×10^{-5} s^{-1} respectively). The semi-logarithmic plot is linear to above 90% conversion for the RAFT dispersion polymerisation. In contrast, the initial linear semi-logarithmic rate for the equivalent solution polymerisation is only followed for the first 5 h, after which a reduction in the rate is observed. Figure 5.10b shows the DMF GPC analysis of the two polymerisations, which both show a linear increase in molecular weight with NMEP conversion. For the RAFT dispersion polymerisation of $PGMA_{63}$-$PNMEP_{2000}$ a linear increase in molecular weight is obtained up to approximately 300 kg mol^{-1}, conversely, only approximately 70 kg mol^{-1} was achieved for the solution polymerisation of NMEP. A reasonably low final dispersity of 1.28 was attained for the solution polymerisation of $PNMEP_{2000}$. However, the dispersity of the RAFT aqueous dispersion polymerisation begins to increase after 70% conversion resulting in a final dispersity of 1.47.

A $PGMA_{63}$-$PNMEP_{2000}$ diblock copolymer was also prepared via RAFT solution polymerisation in ethanol at 70 °C (macro-CTA/ACVA molar ratio of 4.0). A solids content of 29.7% w/w was once again utilised to ensure an equal molar concentration of NMEP. ^{1}H NMR spectroscopy indicated 65% NMEP conversion after 24 h. This is almost 20% higher than the equivalent $PNMEP_{2000}$ homopolymer synthesis

suggesting that using a relatively short PGMA macro-CTA rather than a CTA can lead to faster reactions with higher final conversions.

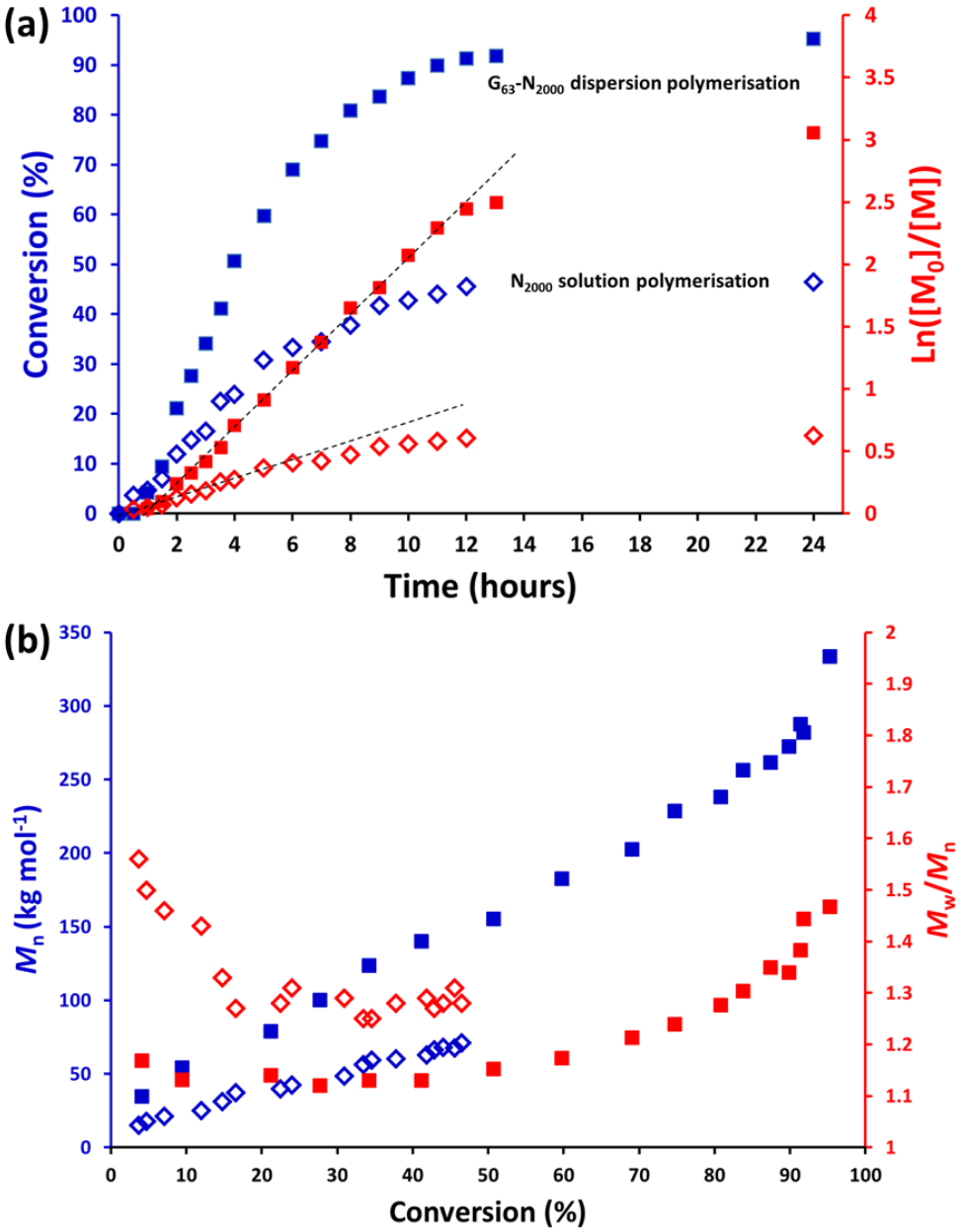

Figure 5.10 (a) Conversion and semi-logarithmic plots versus time for the RAFT aqueous dispersion polymerisation of $PGMA_{63}$-$PNMEP_{2000}$ (filled squares) compared to the RAFT solution polymerisation of $PNMEP_{2000}$ in ethanol (open diamonds) at 70 °C. Both reactions were conducted at the same molar concentration of NMEP. (b) Molecular weight (M_n) and dispersity (M_w/M_n) versus conversion plots for the same two syntheses (DMF eluent; vs. PMMA standards).

Overall the RAFT dispersion polymerisation of NMEP using a PGMA macro-CTA offers several advantages over the equivalent RAFT solution polymerisation. High conversions of greater than 90% can be achieved within 24 h at 70 °C, using a

macro-CTA/ACVA molar ratio of 4.0. The RAFT aqueous dispersion polymerisations of NMEP are significantly faster than that of the equivalent RAFT solution polymerisation.

5.3.4 Synthesis of $PMAA_{85}$-$PNMEP_x$ diblock copolymers

As discussed in Chapter 2, GMA is a relatively expensive specialty monomer. So a cheaper alternative hydrophilic macro-CTA would make the synthesis of high molecular weight PNMEP more attractive to industry. Therefore, a PMAA macro-CTA was synthesised via RAFT solution polymerisation in ethanol at 70 °C. ^{1}H NMR spectroscopy indicated a PMAA DP of 85 after purification. This $PMAA_{85}$ macro-CTA was chain-extended with varying amounts of PNMEP to see if high molecular weight PNMEP could be achieved. The target PNMEP DP was varied from 300 to 4000 (Table 5.2) and high conversions of at least 92% were achieved.

Table 5.2 Target PNMEP DP, conversions, molecular weights (M_n) and dispersities (M_w/M_n) for a series of $PMAA_{85}$-$PNMEP_x$ (M_{85}-N_x) diblock copolymers prepared at 25% w/w solids and the $PMAA_{85}$ macro-CTA.

	Block composition	Target PNMEP DP	Conversion[a] (%)	GPC	
				M_n[b] (g mol^{-1})	M_w/M_n[b]
1	M_{85}	-	84	8,600	1.21
2	M_{85}-N_{294}	300	98	51,100	1.27
3	M_{85}-N_{495}	500	98	73,500	1.35
4	M_{85}-N_{1000}	1000	>99	129,800	1.56
5	M_{85}-N_{1500}	1500	>99	169,700	1.75
6	M_{85}-N_{1940}	2000	97	226,600	2.32
7	M_{85}-N_{2758}	3000	92	331,700	2.05
8	M_{85}-N_{3760}	4000	94	481,600	2.35

a. Monomer conversion determined by ^{1}H NMR spectroscopy in d_4-methanol
b. Determined by DMF GPC using a series of near-monodisperse PMMA calibration standards after exhaustive methylation using trimethylsilyldiazomethane.

Each $PMAA_{85}$-$PNMEP_x$ diblock copolymer was methylated using trimethylsilyldiazomethane to enable GPC analysis.[27] Figure 5.11a shows the GPC chromatograms for the methylated $PMAA_{85}$-$PNMEP_x$ diblock copolymers. High blocking efficiencies are observed with minimal $PMAA_{85}$ macro-CTA contamination. A linear increase in molecular weight with PNMEP DP is observed up to approximately 480 kg mol^{-1}, as shown in Figure 5.11b. However, a growing high molecular weight shoulder is present in the chromatograms which results in an increase in dispersity with increasing PNMEP DP.

Similarly to the $PGMA_{63}$-$PNMEP_x$ diblock copolymers very high molecular weight PNMEP can be obtained using a $PMAA_{85}$ macro-CTA. Both macro-CTAs show a linear increase in molecular weight with PNMEP DP. Molecular weights up to approximately 600 kg mol^{-1} could be achieved using a $PGMA_{63}$ macro-CTA or approximately 480 kg mol^{-1} using a $PMMA_{85}$ macro-CTA.

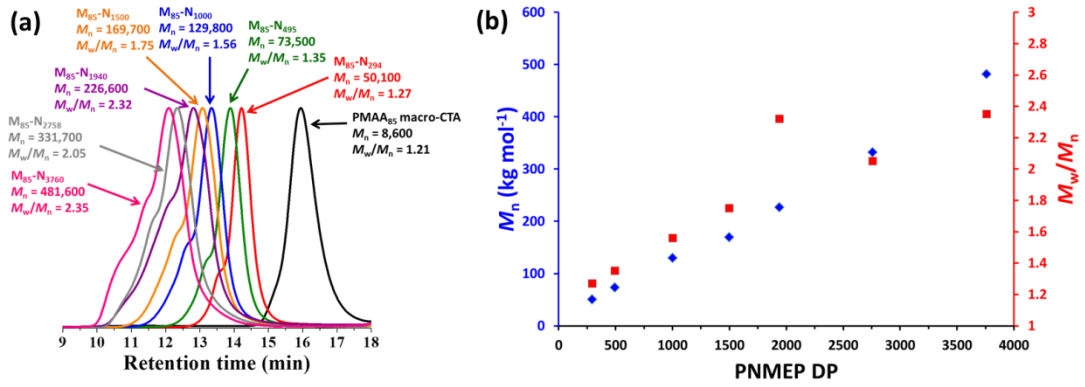

Figure 5.11 DMF GPC analysis of $PMAA_{85}$-$PNMEP_x$ diblock copolymers. (a) GPC chromatograms of the diblock copolymers and the corresponding $PMAA_{85}$ macro-CTA. (b) M_n and M_w/M_n against PNMEP DP.

5.3.5 How does the NMEP monomer purity affect the molecular weight distribution?

Towards the end of this study a higher purity (98%) batch of NMEP monomer became available. All previous experiments were carried out using 96% NMEP.

This higher purity monomer was utilised in the RAFT aqueous dispersion polymerisation of five $PGMA_{63}$-$PNMEP_x$ diblock copolymers. The target PNMEP DP was varied from 100 to 5000 (see Table 5.3). The diblock copolymers were compared to those prepared using the lower grade (96%) NMEP monomer.

Table 5.3 Target PNMEP DP, conversions, molecular weights (M_n) and dispersities (M_w/M_n) for a series of $PGMA_{63}$-$PNMEP_x$ (G_{63}-N_x) diblock copolymers prepared using 98% purity NMEP monomer at 25% w/w solids and 70 °C.

	Block composition	Target PNMEP DP	Conversion[a] (%)	GPC	
				M_n[b] (g mol^{-1})	M_w/M_n[b]
1	G_{63}-N_{99}	100	99	25,300	1.12
2	G_{63}-N_{495}	500	99	61,000	1.18
3	G_{63}-N_{977}	1000	98	103,200	1.19
4	G_{63}-N_{2955}	3000	99	243,700	1.37
5	G_{63}-N_{4900}	5000	98	346,900	1.46

a. Monomer conversion determined by ^{1}H NMR spectroscopy in d_4-methanol
b. Determined by DMF GPC using a series of near-monodisperse PMMA calibration standards

High conversions of 98% or greater were achieved as judged by ^{1}H NMR spectroscopy within 24 h at 70 °C. Each $PGMA_{63}$-$PNMEP_x$ diblock copolymer was analysed by DMF GPC. Figure 5.12a shows unimodal peaks for the series prepared with 98% purity NMEP. A shift to lower retention times with increasing PNMEP DP is observed together with increasing molecular weights. A linear increase in molecular weight with PNMEP DP is observed in Figure 5.12b. An increase in dispersity with PNMEP DP is observed however, this remains relatively low (M_w/M_n < 1.50) compared to the $PGMA_{63}$-$PNMEP_x$ diblock copolymers synthesised with the 96% purity monomer (M_w/M_n up to 2.32). Targeting a PNMEP DP of 5000 with the 98% NMEP led to a M_n of 346.9 kg mol^{-1} with a dispersity of 1.46 (Figure 5.13). In contrast, using the 96% purity NMEP monomer and targeting the same DP led to a significantly higher molecular weight of 627.8 kg mol^{-1} due to the presence of a high molecular weight shoulder. This also resulted in a higher dispersity of 2.17. This suggests that the high molecular weight shoulder is due to the presence of a dimethacrylate impurity in the PNMEP monomer, which is causing some light branching and not due to side reactions such as chain transfer to polymer.

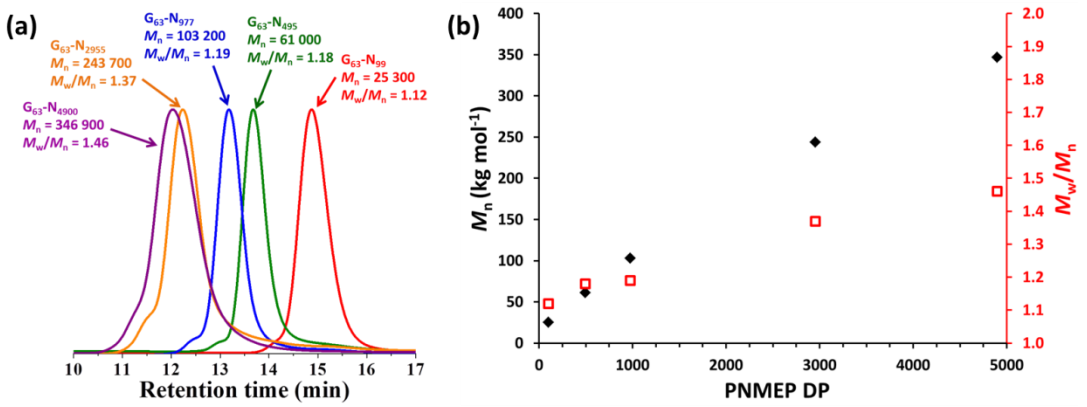

Figure 5.12 DMF GPC analysis of $PGMA_{63}$-$PNMEP_x$ (G_{63}-N_x) diblock copolymers prepared using 98% purity NMEP monomer at 25% w/w solids and 70 °C; (a) GPC chromatograms and (b) M_n and M_w/M_n versus PNMEP DP.

Finally, a $PMAA_{85}$-$PNMEP_{4000}$ diblock copolymer was targeted using the 98% purity NMEP. The RAFT aqueous dispersion polymerisation of NMEP went to 98% conversion after 24 h at 70 °C. After methylation the resulting $PMMA_{85}$-$PNMEP_{3920}$ diblock copolymer was analysed by GPC. Similarly to the $PGMA_{63}$-$PNMEP_x$ diblock copolymers, a reduction in the dispersity was observed from 2.35 (96% NMEP) to 1.73 (98% NMEP), see Figure 5.14.

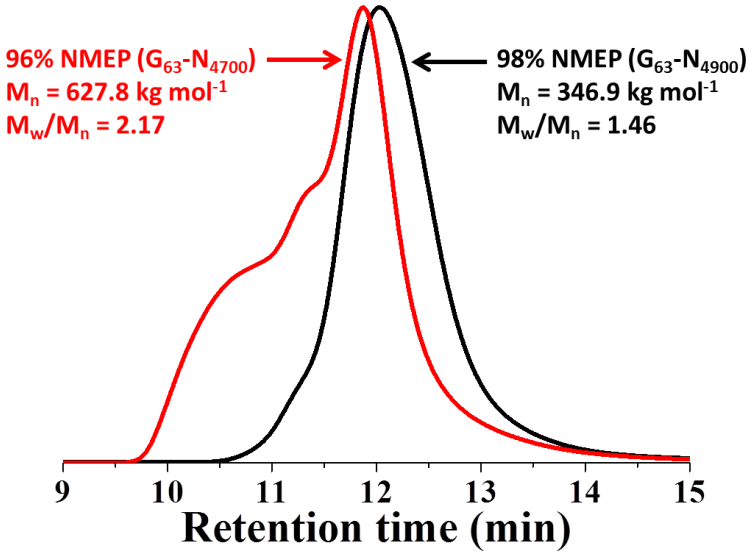

Figure 5.13 DMF GPC chromatograms recorded for $PGMA_{63}$-$PNMEP_x$ diblock copolymers when targeting a PNMEP DP of 5000, using either 98% purity NMEP (black) or 96 % purity NMEP (red).

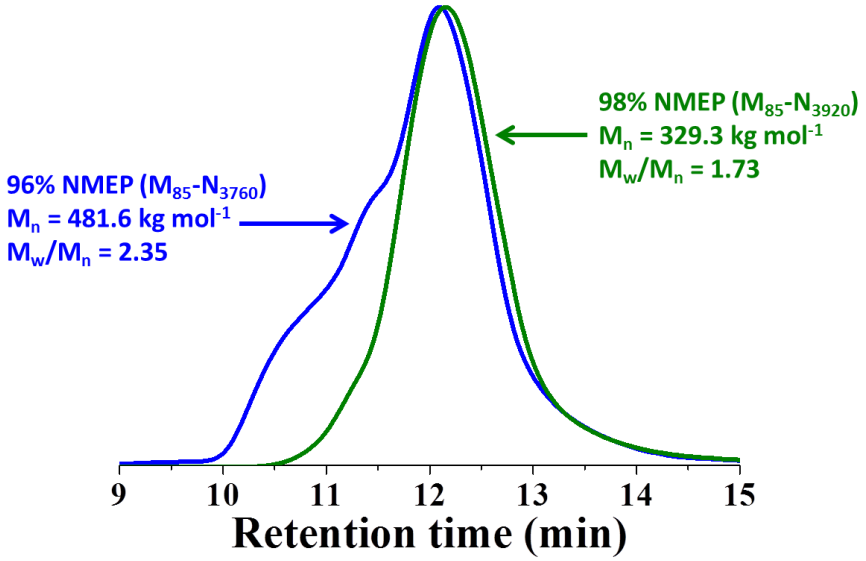

Figure 5.14 DMF GPC chromatograms recorded when targeting a $PMAA_{85}$-$PNMEP_{4000}$ diblock copolymer prepared using NMEP monomer of either 96 % (blue) or 98% (green) purity.

5.4 Conclusions

A series of $PNMEP_x$ homopolymers have been prepared via RAFT solution polymerisation in ethanol. LCSTs of the purified homopolymers varied from 75 °C to 55 °C on increasing the PNMEP DP from 31 to 467. $PGMA_{63}$-$PNMEP_x$ diblock copolymers were prepared via RAFT aqueous dispersion polymerisation at 70 °C. The target PNMEP DP was varied from 100 to 6000 at 25% w/w solids. Conversions

of at least 90% were achieved for all diblock copolymers up to a target PNMEP DP of 5000. DMF GPC analysis indicated a highly linear increase in molecular weight with PNMEP DP. Molecular weights of up to approximately 600 kg mol^{-1} were achieved, but a high molecular weight shoulder appeared when targeting PNMEP DPs of at least 1000. This resulted in an increase in the final diblock copolymer dispersity. Replacing the 96% purity NMEP monomer with a higher purity batch (98%) reduced the final dispersity from 2.17 to 1.46 when targeting a block composition of $PGMA_{63}$-$PNMEP_{5000}$. This suggested the presence of a dimethacrylate impurity in the lower purity NMEP batch. Synthesis of $PGMA_{63}$-$PNMEP_x$ at 70 °C, i.e. above the PNMEP LCST, enabled diblock copolymers to be prepared in the form of low-viscosity particles. Cooling the reaction solution below the LCST of the PNMEP block caused the PNMEP chains to become water-soluble, leading to an increase in solution viscosity as the particles dissolved. Kinetic experiments comparing the RAFT *solution* polymerisation of NMEP to the RAFT aqueous *dispersion* polymerisation of NMEP using a $PGMA_{63}$ macro-CTA confirmed that the dispersion polymerisation was significantly faster than the equivalent solution polymerisation, which enabled higher final conversions to be achieved.

Finally, the $PGMA_{63}$ macro-CTA was replaced with a cheaper $PMAA_{85}$ macro-CTA. A series of $PMAA_{85}$-$PNMEP_x$ diblock copolymers were prepared and the target PNMEP DP was systematically varied from 300 to 4000. Greater than 90% conversion was attained in all cases. GPC analysis indicated a linear increase in molecular weight with PNMEP DP. Like the $PGMA_{63}$-$PNMEP_x$ diblock copolymers, the final dispersity increased with the target PNMEP DP. However, using 98% purity NMEP led to a significant reduction in the final dispersity from 2.35 to 1.73 when targeting a $PMAA_{85}$-$PNMEP_{4000}$ diblock copolymer.

5.5 References

(1) Walter, R.; Keyssner, E.; Fritz, N. *Process of Producing N-Vinyl Compounds*, **1939**, US2153993A.
(2) Haaf, F.; Sanner, A.; Straub, F. *Polymer Journal* **1985**, *17*, 143.
(3) Sun, X.; Cao, Z.; Yeh, C.-K.; Sun, Y. *Colloids and Surfaces B: Biointerfaces* **2013**, *110*, 96.

(4) Sung, S. L. L.; Tordil, H. B.; Trinh, T.; Wendland, P. A. *Fabric softening compositions with dye transfer inhibitors for improved fabric appearance*, **2001**, EP19940901229.
(5) Chen, T. *Dental bleach*, **2004**, US20030129148 A1.
(6) Bajpai, S. K.; Sonkusley, J. *Journal of Applied Polymer Science* **2002**, *83*, 1717.
(7) Bailly, N.; Thomas, M.; Klumperman, B. *Biomacromolecules* **2012**, *13*, 4109.
(8) Devasia, R.; Bindu, R. L.; Borsali, R.; Mougin, N.; Gnanou, Y. *Macromolecular Symposia* **2005**, *229*, 8.
(9) Pound, G.; Eksteen, Z.; Pfukwa, R.; McKenzie, J. M.; Lange, R. F.; Klumperman, B. *Journal of Polymer Science Part A: Polymer Chemistry* **2008**, *46*, 6575.
(10) Guinaudeau, A.; Coutelier, O.; Sandeau, A.; Mazières, S.; Nguyen Thi, H. D.; Le Drogo, V.; Wilson, D. J.; Destarac, M. *Macromolecules* **2013**, *47*, 41.
(11) Zhao, X.; Coutelier, O.; Nguyen, H. H.; Delmas, C.; Destarac, M.; Marty, J.-D. *Polymer Chemistry* **2015**, *6*, 5233.
(12) Guinaudeau, A.; Mazieres, S.; Wilson, D. J.; Destarac, M. *Polymer Chemistry* **2012**, *3*, 81.
(13) Deng, J.; Shi, Y.; Jiang, W.; Peng, Y.; Lu, L.; Cai, Y. *Macromolecules* **2008**, *41*, 3007.
(14) Sun, J.; Peng, Y.; Chen, Y.; Liu, Y.; Deng, J.; Lu, L.; Cai, Y. *Macromolecules* **2010**, *43*, 4041.
(15) Zhang, J.; Zou, M.; Dong, J.; Li, X. *Colloid and Polymer Science* **2013**, *291*, 2653.
(16) Cunningham, V. J.; Derry, M. J.; Fielding, L. A.; Musa, O. M.; Armes, S. P. *Macromolecules* **2016**, *49*, 4520.
(17) Semsarilar, M.; Jones, E. R.; Blanazs, A.; Armes, S. P. *Advanced Materials* **2012**, *24*, 3378.
(18) Truong, N. P.; Dussert, M. V.; Whittaker, M. R.; Quinn, J. F.; Davis, T. P. *Polymer Chemistry* **2015**, *6*, 3865.
(19) Read, E.; Guinaudeau, A.; James Wilson, D.; Cadix, A.; Violleau, F.; Destarac, M. *Polymer Chemistry* **2014**, *5*, 2202.
(20) Li, Y.; Armes, S. P. *Angewandte Chemie International Edition* **2010**, *49*, 4042.
(21) Blanazs, A.; Ryan, A. J.; Armes, S. P. *Macromolecules* **2012**, *45*, 5099.
(22) Jones, E. R.; Semsarilar, M.; Wyman, P.; Boerakker, M.; Armes, S. P. *Polymer Chemistry* **2016**, *7*, 851.
(23) Zhang, X.; Rieger, J.; Charleux, B. *Polymer Chemistry* **2012**, *3*, 1502.
(24) Huo, F.; Wang, X.; Zhang, Y.; Zhang, X.; Xu, J.; Zhang, W. *Macromolecular Chemistry and Physics* **2013**, *214*, 902.
(25) Blanazs, A.; Madsen, J.; Battaglia, G.; Ryan, A. J.; Armes, S. P. *Journal of the American Chemical Society* **2011**, *133*, 16581.
(26) Warren, N. J.; Mykhaylyk, O. O.; Mahmood, D.; Ryan, A. J.; Armes, S. P. *Journal of the American Chemical Society* **2014**, *136*, 1023.
(27) Couvreur, L.; Lefay, C.; Belleney, J.; Charleux, B.; Guerret, O.; Magnet, S. *Macromolecules* **2003**, *36*, 8260.

Chapter 6

Conclusions and Outlook

RAFT polymerisation has been used to synthesise a series of amphiphilic block copolymers that undergo polymerisation-induced self-assembly (PISA) to form a range of nano-objects including spheres, worms and vesicles. Both Chapter 2 and Chapter 5 utilise a PGMA macro-CTA. This non-ionic, water-soluble steric stabiliser has been previously used for the RAFT aqueous dispersion polymerisation of HPMA to produce spheres, worms or vesicles. RAFT aqueous emulsion polymerisation (Chapter 2) produced well-defined PGMA-PBzMA spheres at up to 50% w/w solids. However, only spherical nanoparticles could be obtained, even when using a relatively short PGMA macro-CTA and targeting PBzMA DPs up to 1235. According to the literature, many other RAFT emulsion polymerisation formulations also yield only kinetically-trapped spheres, but the physical reason for this limitation is not clear. Several papers from the Lyon group have demonstrated that worms and vesicles can be achieved via RAFT aqueous emulsion polymerisation in a few isolated cases, but the reason(s) for their success is not at all clear. Given the relative ease with which RAFT aqueous dispersion polymerisation formulations can generate higher order morphologies, it seems likely that sufficiently high aqueous monomer solubility may be an important parameter. Reducing the ability of the steric stabilisation mechanism via hydrogen bonding interactions between stabiliser chains may also play a role in facilitating sphere-sphere fusion, which is the crucial first step to worm (and ultimately vesicle) formation. In principle, statistically copolymerising a more water-soluble comonomer (e.g. HPMA) with BzMA might enable access to higher order morphologies. Alternatively, targeting PGMA-PBzMA-PHPMA triblock copolymers via sequential monomer addition could lead to exotic morphologies via microphase separation. In this context, it is noteworthy that Mable et al. have recently reported that addition of BzMA to PGMA-PHPMA vesicles enabled PGMA-PHPMA-PBzMA *framboidal* vesicles to be obtained.[1] In Chapter 5, a $PGMA_{63}$ macro-CTA was utilised for the convenient synthesis of water-soluble $PGMA_{63}$-$PNMEP_x$ diblock copolymers. Taking advantage of the inverse temperature solubility behaviour of PNMEP in water (LCST ~ 55 °C), PISA synthesis at 70 °C enabled high molecular weight PNMEP to be synthesised in the form of low-viscosity particles, with spontaneous dissolution occurring on cooling from 70 °C to 20 °C. The $PGMA_{63}$ macro-CTA utilised in this study enabled the synthesis of PNMEP up to a target DP of 5000 while still achieving NMEP conversions above 90%. This is interesting, because using the same $PGMA_{63}$ macro-CTA for the RAFT

emulsion polymerisation of BzMA only enabled DPs of up to 1235 to be achieved efficiently (> 99 % BzMA conversion). In contrast, targeting DPs of 1500-2000 led to much lower BzMA conversions. This may in part be simply a testament to the much faster rate of polymerisation of NMEP compared to BzMA (as demonstrated in Chapter 3). However, other parameters could conceivably account for the differing upper limit DPs for these two aqueous PISA syntheses. Deeper scientific understanding is likely to be critical for the rational development of improved formulations.

Chapters 2 and 4 each utilise BzMA to generate the core-forming block via RAFT aqueous emulsion polymerisation or RAFT alcoholic dispersion polymerisation, respectively. High conversions (> 90%) were obtained for both formulations, but the latter polymerisations proceeded much more slowly than the former. These observations are consistent with a study by Ratcliffe et al., who demonstrated that RAFT emulsion polymerisation was faster than either RAFT aqueous dispersion polymerisation or RAFT solution polymerisation.[2] Nevertheless, these significant kinetic differences are not properly understood. The RAFT alcoholic dispersion polymerisation of BzMA typically take 12-24 h to reach high conversion, although Jones et al. have recently demonstrated that the addition of water can substantially enhance the rate of BzMA polymerisation.[3] The PGMA-PBzMA diblock copolymers only formed spheres, whereas spheres, worms and vesicles could be obtained for the PNMEP-PBzMA diblock copolymers. This suggests that the morphology limitation observed for RAFT emulsion polymerisation is not an intrinsic problem associated with the choice of PBzMA as the core-forming block. Similarly, the ability to form spheres, worms or vesicles via RAFT aqueous dispersion polymerisation when using a PGMA macro-CTA also indicates that the observation of kinetically-trapped spheres for the PGMA-PBzMA RAFT aqueous emulsion polymerisation formulation is most likely not related to the choice of the stabiliser block.

RAFT dispersion polymerisation of NMEP was the major focus of this thesis. It has been used to generate a core-forming block for RAFT dispersion polymerisation in *n*-dodecane (Chapter 3) and water (Chapter 5) as well as a steric stabiliser block for RAFT dispersion polymerisation in ethanol (Chapter 4). For the RAFT dispersion polymerisation of NMEP in *n*-alkanes, DPs of up to 1000 were targeted, with high conversions being achieved within 30 min at 20% w/w solids and 90 °C. In contrast,

the RAFT aqueous dispersion polymerisation of NMEP proceeded to more than 90% conversion when targeting a DP of 5000. However, this rate of polymerisation was significantly slower, with at least 12 h being required to reach 90% conversion at 25% w/w solids and 70 °C. Both dispersion polymerisations used the same macro-CTA/initiator molar ratio of 4.0, however different temperatures (90 °C vs. 70 °C) and copolymer concentration (20% w/w vs. 25% w/w) were utilised making a direct comparison difficult. But it is expected that some aspect of the solvent (*n*-dodecane vs. water) must be influencing the rate of polymerisation. Both polymerisations exhibit a linear increase in molecular weight with PNMEP DP. $PSMA_{14}$-$PNMEP_{245}$ was the highest molecular weight diblock copolymer that could be analysed by GPC (M_w/M_n = 2.85). Although relatively high dispersities were also obtained for the $PGMA_{63}$-$PNMEP_x$ syntheses, these corresponded to significantly higher PNMEP DPs (e.g. $PGMA_{63}$-$PNMEP_{4700}$ had an M_w/M_n of 2.17). One obvious explanation for the significant differences in rate of polymerisation and final dispersity is the degree of solvation of the growing particle cores. The PNMEP chains are very poorly solvated by *n*-dodecane, so the monomer-swollen particle cores should contain rather little solvent. This should lead to a relatively high local monomer concentration, which accounts for the relatively fast rate of NMEP polymerisation observed for this formulation. In contrast, variable temperature ^{1}H NMR studies indicate highly hydrated particle cores during the RAFT aqueous dispersion polymerisation of NMEP. The presence of water as well as NMEP in the growing particles reduces the effective local monomer concentration, which leads to a significantly slower rate of polymerisation. Moreover, branching/crosslinking is known to be more efficient for RAFT copolymerisations conducted at higher monomer concentrations.[4] Thus this hypothesis also accounts for the difference in final dispersities: broader molecular weight distributions are more readily obtained for the RAFT dispersion polymerisation of NMEP in *n*-dodecane even when targeting much lower DPs. In principle, the higher purity batch of NMEP monomer (98% vs. 96%) could be utilised for the RAFT dispersion polymerisation of NMEP in *n*-dodecane to reduce the final dispersity. Utilising the LCST behaviour of PNMEP for the synthesis of $PGMA_{63}$-$PNMEP_x$ diblock copolymers has enabled relatively high molecular weight PNMEP chains to be synthesised efficiently in a convenient low-viscosity form. In principle, this approach could also be applied to other thermoresponsive monomers such as *N*-isopropylacrylamide (NIPAM) to target high molecular weight polymers.

One underlying theme in this thesis is the use of spherical nanoparticles to stabilise Pickering emulsions (Chapter 2 and 3). In Chapter 2, a range of $PGMA_{63}$-$PBzMA_x$ spheres were used to stabilise oil-in-water emulsions. These spheres proved to be stable to the high-shear homogenisation conditions required for emulsification and the resulting mean droplet diameter had a pronounced concentration dependence, with lower copolymer concentrations forming larger droplets. This is consistent with Pickering stabilisation, rather than the amphiphilic copolymer chains simply acting as a soluble polymeric surfactant. In Chapter 3, 25 nm $PSMA_{14}$-$PNMEP_{49}$ spheres were utilised as a Pickering emulsifier. In this case, low shear rate (i.e. hand-shaking) led to the formation of water-in-oil Pickering emulsions, whereas higher shear rates (3500 rpm or greater) unexpectedly produced oil-in-water emulsions. Subsequent experiments confirmed that the *hydrophobic* $PSMA_{14}$-$PNMEP_{49}$ spheres were unstable with respect to high shear, undergoing *in situ* inversion to produce *hydrophilic* $PNMEP_{49}$-$PSMA_{14}$ spheres. Future studies could examine whether cross-linking of the PNMEP cores prevents such nanoparticle inversion. The $PSMA_{14}$-$PNMEP_x$ worms and vesicles could also be evaluated as Pickering emulsifiers. These higher order structures should lead to more stable nanoparticles that are less likely to undergo *in situ* inversion.

It is well-known that poly(*N*-vinylpyrrolidone) binds strongly to dyes, this has been utilised in laundry formulations for more than fifty years.[5] PNMEP also has a strong dipole moment, so it might be worth investigating selective dye binding to either PNMEP-based nanoparticles or water-soluble diblock copolymer chains. A final area of interest is the RAFT polymerisation of *N*-(2-acryloyloxy)ethyl pyrrolidone (NAEP). This acrylic analogue of NMEP has not yet been polymerised by living radical polymerisation under any conditions and is much less utilised for the RAFT synthesis of well-defined diblock copolymers. Given the relative scarcity of highly hydrophilic acrylic monomers, NAEP could provide access to a range of new PISA formulations as either a core-forming block in *n*-alkanes or as a steric stabiliser block in either aqueous or alcoholic media.

6.1 References

(1) Mable, C. J.; Warren, N. J.; Thompson, K. L.; Mykhaylyk, O. O.; Armes, S. P. *Chemical Science* **2015**, *6*, 6179.
(2) Ratcliffe, L. P. D.; Blanazs, A.; Williams, C. N.; Brown, S. L.; Armes, S. P. *Polymer Chemistry* **2014**, *5*, 3643.
(3) Jones, E. R.; Semsarilar, M.; Wyman, P.; Boerakker, M.; Armes, S. P. *Polymer Chemistry* **2016**, *7*, 851.
(4) Rosselgong, J.; Armes, S. P.; Barton, W. R.; Price, D. *Macromolecules* **2010**, *43*, 2145.
(5) Saraydin, D.; Karadağ, E. *Polymer Bulletin* **2000**, *44*, 501.

Chapter 7

Appendix

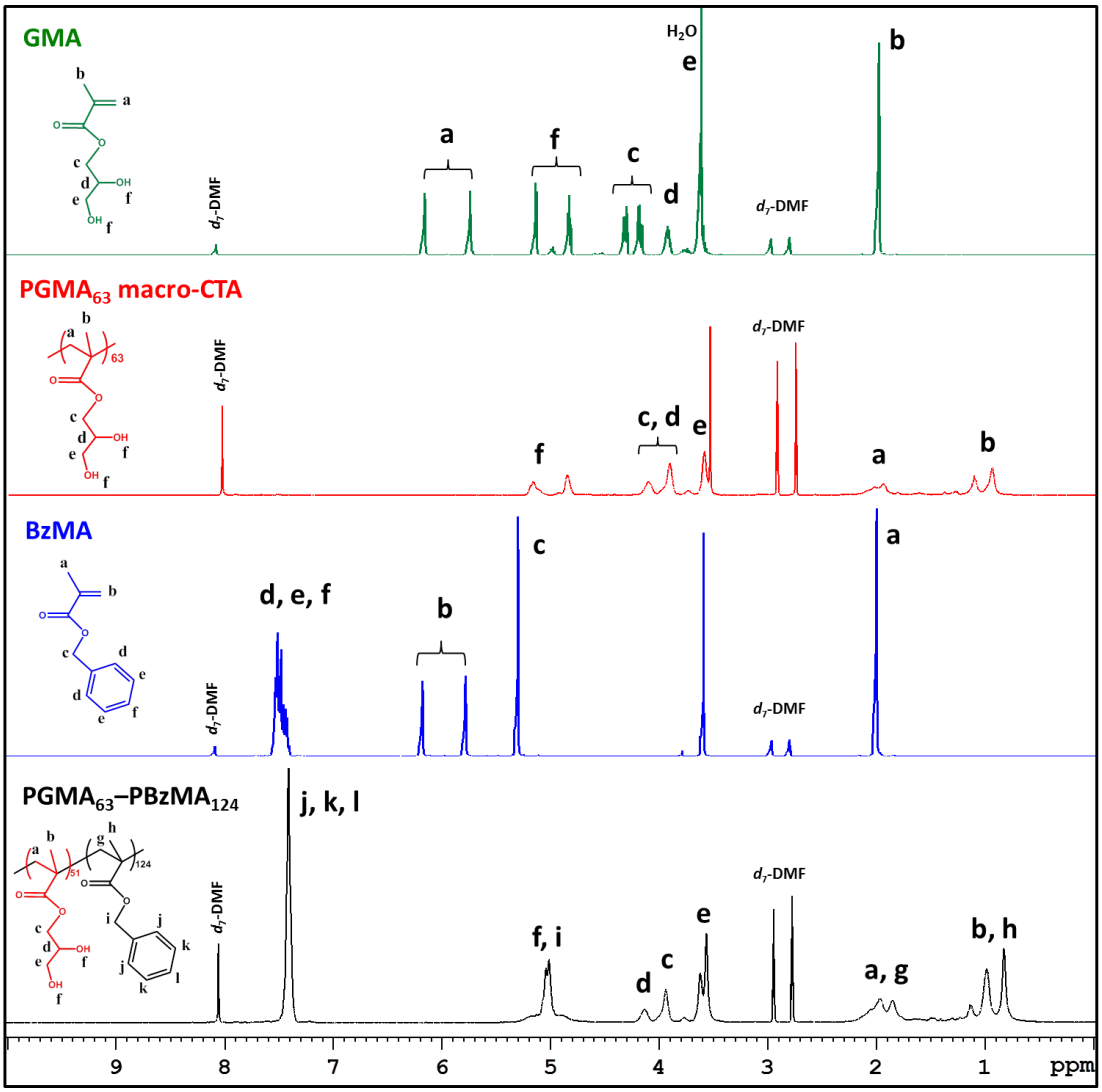

Figure 7.1 Assigned ^{1}H NMR spectra of both GMA and BzMA monomers, $PGMA_{63}$ macro-CTA and $PGMA_{63}$-$PBzMA_{124}$ diblock copolymer in d_7-DMF. $PGMA_{63}$-$PBzMA_{124}$ was freeze-dried prior to dilution in d_7-DMF.

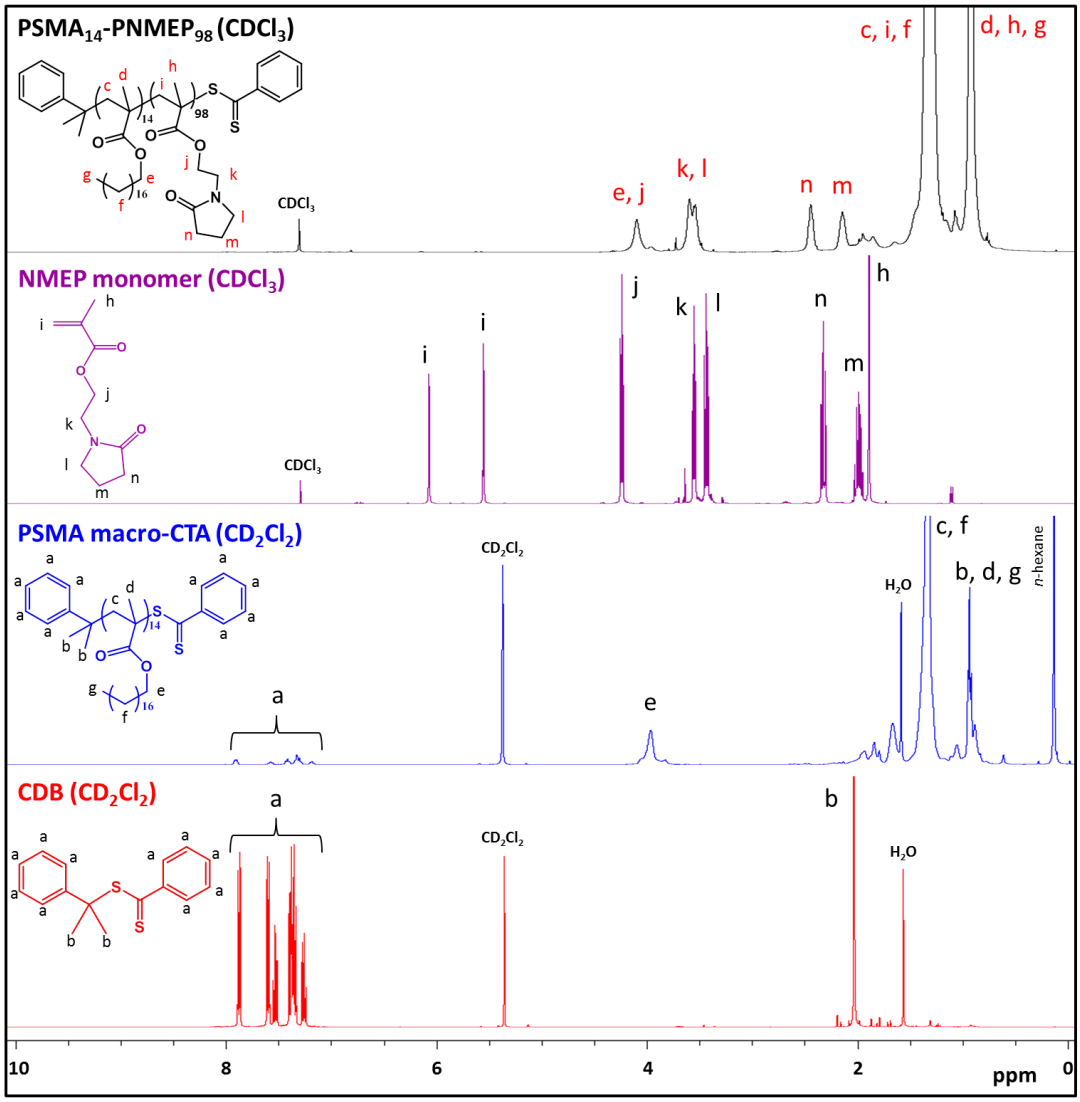

Figure 7.2 Assigned ^{1}H NMR spectra obtained for the CDB RAFT agent, $PSMA_{14}$ macro-CTA, NMEP monomer and $PSMA_{14}$-$PNMEP_{98}$ diblock copolymer.

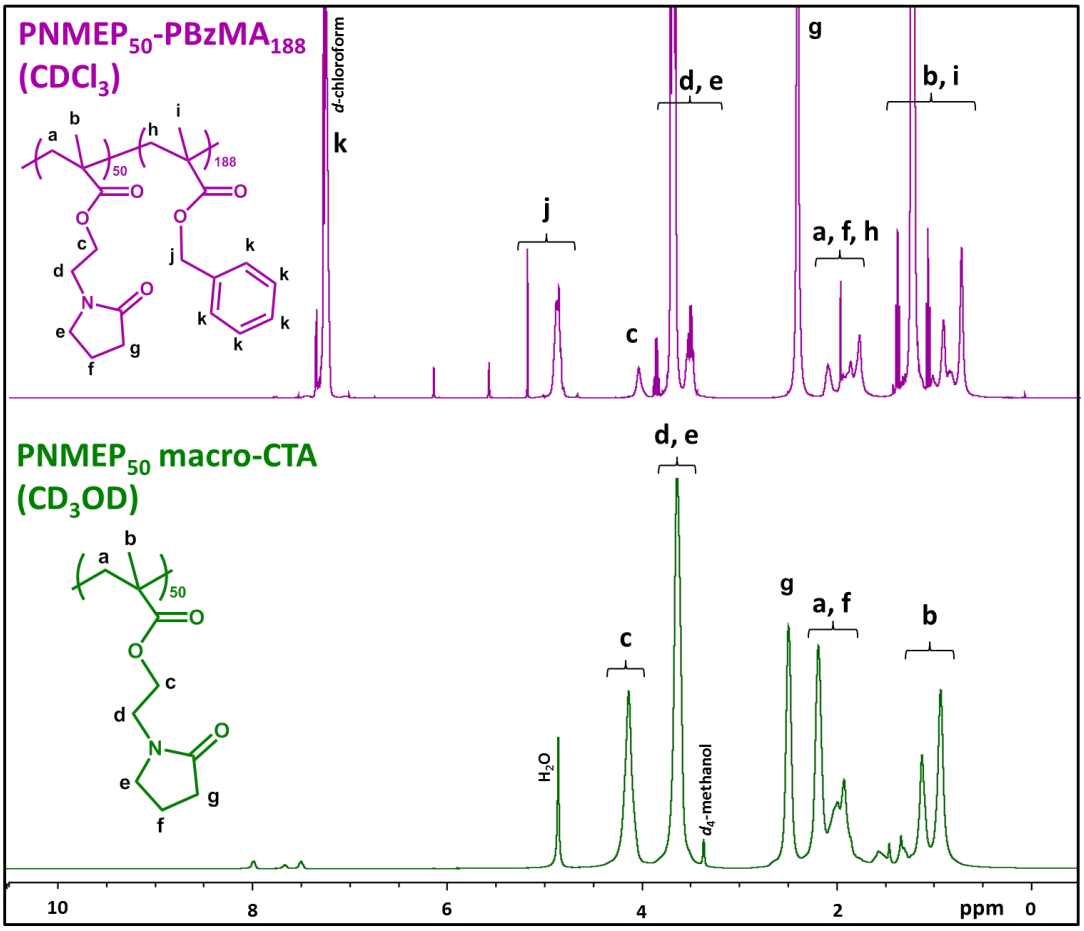

Figure 7.3 Assigned ^{1}H NMR spectra obtained for the PNMEP$_{50}$ macro-CTA in *d*$_4$-methanol and PNMEP$_{50}$-PBzMA$_{188}$ diblock copolymer in *d*-chloroform.

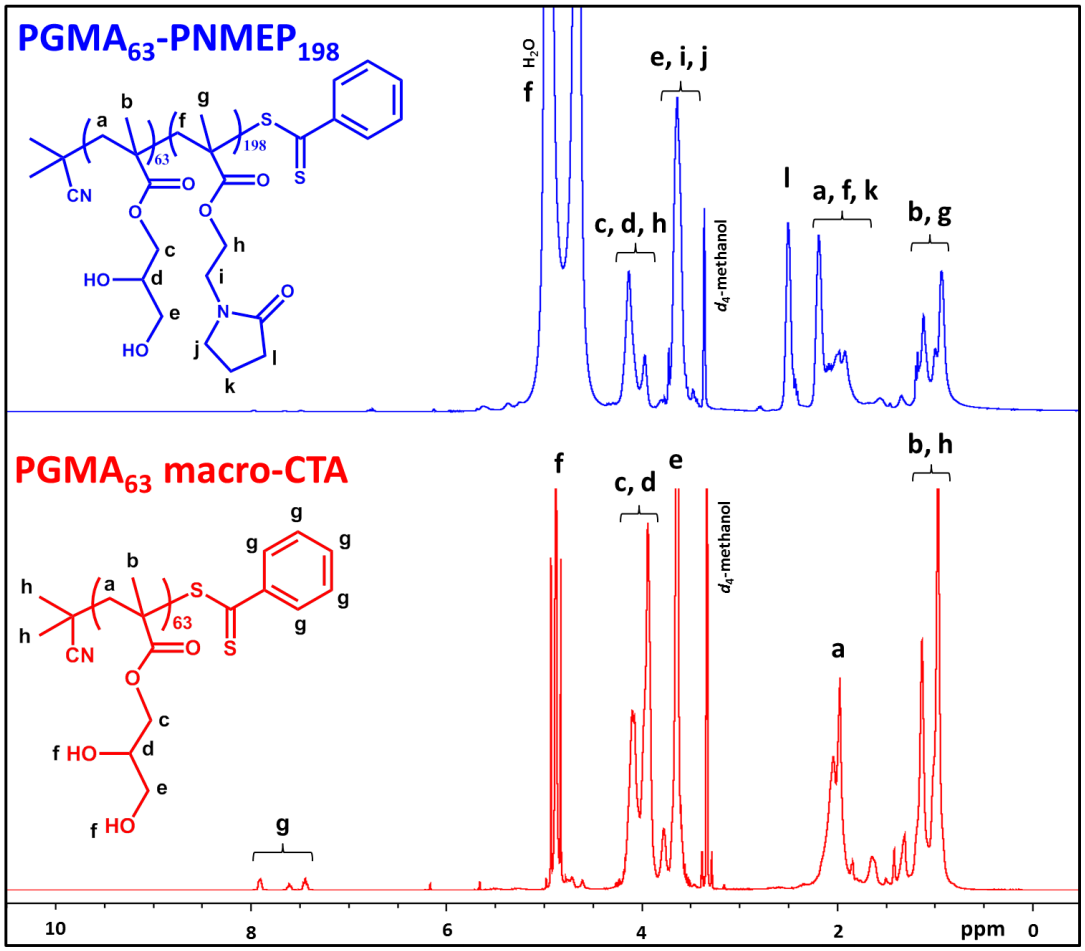

Figure 7.4 Assigned ^{1}H NMR spectra obtained for the $PGMA_{63}$ macro-CTA and $PGMA_{63}$-$PNMEP_{198}$ diblock copolymer in d_4-methanol.